The University Of Sheffield.

The role of extracellular vesicles in the oral cancer microenvironment

By: Mark Ofield

A thesis submitted in partial fulfilment of the requirements for the degree of

Doctor of Philosophy

The University of Sheffield

Faculty of Medicine, Dentistry and Health

School of Clinical Dentistry

February 2018

Figure 1 Effect of a PhD on the physical appearance of an average PhD student over 4 years. Note dramatic hair loss, decline in grooming and sunglasses hiding bags under the eyes.

Acknowledgements

There are many people without whom I wouldn't be writing this now. Firstly, I would like to thank my friends and family who put up with me during the 2 years I spent applying for PhDs lending a sympathetic ear when necessary or just not asking me about it depending on my mood. I am also grateful to my parents who put up with a son they thought had moved out moving back in again. It was thanks to your encouragement and teaching growing up that I discovered the curiosity and passion for science that drove me into a research career and without your generous financial support I would not have been able to gain the experience I needed to get the PhD studentship. To all of my grandparents who fed the enthusiasm with museum trips and scientific themed Christmas and birthday presents down the years I will always be grateful.

Special mention should go to Andy, Kate, Charlotte, Liz, Toby, and Genevieve amongst the people who make the Dental School such a fantastic place to work, also to Rachel especially for the final few months. You have provided more than your fair share of help, support, amazing memories and early trips to the pub to celebrate or commiserate over the four years. Thank you also to Brenka McCabe Jason Heath Chris Hill and Lizzy Martin for all your patience and technical expertise, I wouldn't have made it without you! I am grateful to Oana Peala for being a fantastic summer student I am sure your career will outstrip mine! Thanks also to Helen Colley, Amy Harding and the patients who donated cells over the years.

Lastly, I owe an extraordinary amount to Stuart Hunt and Daniel Lambert, without their vision and dedication this project would never have existed and without their extreme patience, advice and guidance it certainly would never have been finished.

So, thank you everyone who helped me find and, more importantly, stay in love with science. This is for all of you. Especially Grandpa.

Abstract

Background: The oral cancer microenvironment is an evolving landscape comprised of different cell types. As the disease progresses environmental conditions within this landscape change and its composition must evolve and adapt to this for the tumour to develop. Since the discovery of mRNA and miRNA in extracellular vesicles (EVs) much interest has focused on the contribution of EVs to cancer. Here the role of EVs in oral cancer progression is explored.

Methods: EVs were purified from the conditioned media of oral squamous carcinoma cells (OSCC) by serial centrifugation and size exclusion chromatography before characterisation with electron microscopy, western blotting and tuneable resistive pulse sensing. Next generation sequencing and mass spectrometry were used to identify the RNA and protein contents of these EVs. Bioinformatic approaches were used to correlate the contents with tumour stage of the producing cell. A fluorescence staining technique was used to image the transfer of EVs to cells of the tumour microenvironment *in vitro* and the impact of this uptake assessed in normal oral fibroblasts (NOF).

Results: EVs of between 50-200 nm were produced by cells throughout oral cancer progression. These EVs were positive for markers CD63 and TSP1 but negative for the golgi body marker GM130. Transcriptomic and proteomic techniques have identified miRNA families and proteins changing in abundance in EVs with tumour stage including miR-200, miR-34, nespirin 1 and syndecan 4. EVs were taken up by cells of the tumour microenvironment. This uptake caused no change to NOF proliferation but activated them into a cancer associated fibroblast phenotype.

Conclusions: EVs from OSCC are produced throughout tumorigenesis and their contents could reflect the status of the producing cell enabling them to act as diagnostic markers. EV uptake by NOFs caused them to become activated into a pro tumorigenic phenotype.

Contents

Acknowledgements III

Abstract IV

Contents V

List of Methods XII

List of Figures XIII

List of Tables XVIII

List of Abbreviations XIX

1. Introduction 1

1.1. Cancer 1

1.2. Oral Cancer 1

1.2.1. Introduction and statistics 1

1.2.2. Stages of oral cancer 2

1.3. Composition and conditions of the tumour microenvironment 3

1.3.1. Epithelial cells and keratinocytes 3

1.3.2. Fibroblasts 7

1.3.3. Endothelial cells 9

1.3.4. Immune cells 11

1.3.5. Changing conditions in the microenvironment 14

1.3.6. Discovery of extracellular vesicles 16

1.3.7. What's in a name? 17

1.3.8. Biogenesis of extracellular vesicles from MVB 21

1.3.9. Formation of microvesicles and large oncosomes 28

1.4. Packaging of EVs 32

1.4.1. Proteins 32
1.4.2. Nucleic acids 36
1.4.3. Lipids 37
1.5. Uptake of EVs 38
1.6. The role of EVs in normal processes 42
1.6.1. Role of EVs in disease states 44
1.6.2. Role of EVs in cancer 45
1.7. Future challenges 61
1.8. Hypothesis and Aims 65
2. Materials and methods 67
2.1. Materials 67
2.2. Cell lines and tissue culture 67
2.2.1. OSCC cell line panel 67
2.2.2. Stromal cell panel 68
2.2.3. Routine cell culture and maintenance 69
2.2.4. Cell counting and seeding 70
2.2.5. EV-depleted serum 70
2.2.6. Preparation of whole cell lysates. 70
2.2.7. Preparation of conditioned medium for tunable resistive pulse sensing 71
2.3. EV extraction and physical characterisation 71
2.3.1. ExoQuick extraction 71
2.3.2. Valadi et al, extraction 72
2.3.3. Théry et al, extraction 72
2.3.4. Hybrid protocol 72

2.3.5. Size exclusion chromatography 73
2.3.6. EV quantification by tuneable resistive pulse sensing 74
2.3.7. Electron Microscopy of EV samples 74
2.4. Protein Analysis 76
2.4.1. BCA Assay 76
2.4.2. SDS-PAGE 77
2.4.3. Western Blotting 79
2.4.4. iTRAQ 8 Plex 83
2.4.5. Label free spectrometry 86
2.5. RNA extraction and analysis 88
2.5.1. miRCURY RNA extraction kit 88
2.5.2. Measuring of RNA concentration using Agilent Bioanalyzer 88
2.5.3. Small RNA sequencing 89
2.5.4. Quantitive real-time PCR 90
2.6. Cell treatments and assays 93
2.6.1. Fluorescent imaging of EV mediated RNA transfer 93
2.6.2. Staining of extracellular EVs 93
2.6.3. Cell treatment, fixing and mounting 94
2.6.4. Proliferation and viability assays 95
2.6.5. Fibroblast activation 97
3. Optimisation of methods for purifying and storing EVs from the culture medium of oral cancer cell lines 99
3.1. Introduction 99
3.2. Aims and objectives 101
3.3. Depletion of bovine EVs from FBS 102

3.3.1. Centrifugation for 18 hours at 100,000 x *g* removes bovine EVs from FBS. 102

3.4. Comparison of EV purification methods 106

3.4.1. High protein concentrations are seen in pellets produced by ExoQuick reagent 107

3.4.2. Detection of EV markers in pellets from different extraction techniques 109

3.4.3. Size exclusion chromatography can be used to purify vesicles from large starting volumes of culture media 114

3.5. Storage of EVs 116

3.5.1. Intact vesicles are seen by TEM after freezing at -20ºC 116

3.5.2. Freezing to -20ºC and thawing on ice has no impact on EV samples particle count 118

3.6. Discussion 121

3.6.1. Future work 123

4. Characterisation of EVs produced by oral cancer cells 125

4.1. Introduction 125

4.2. Aims and objectives 126

4.3. EVs are produced by oral cancer cells representing different stages of tumourigenesis 127

4.4. Comparison of production rates of EVs from different stages of oral cancer 132

4.5. RNA can be purified from EVs produced by oral cancer cells 135

4.6. Protein markers of oral cancer extracellular EVs 138

4.7. Discussion 141

4.7.1. Future work 147
5. Next generation sequencing of the miRNA contents of oral cancer EVs ... 148
5.1. Introduction 148
5.2. Aims and Objectives 150
5.3. Small RNA sequencing quality and species distribution 150
5.4. Processing of IonTorrent data 153
5.5. Comparison of the miRNA contents of EVs produced by mild and severe dysplastic cells 157
5.6. Comparison of the miRNA contents of EVs from non-metastatic carcinoma and metastatic deposit cells 160
5.7. Comparison of the miRNA content of EVs from two oral dysplastic cell lines and an oral carcinoma cell line 163
5.8. Comparison of miRNA levels and target pathways in EVs from different tumour stages 166
5.9. Validation of IonTorrent sequencing data 170
5.9.1. Selection of targets 170
5.9.2. Validation by qPCR 172
5.10. Discussion 176
5.10.1. Future work 187
6. Proteomic analysis of the contents of oral cancer cell EVs 190
6.1. Introduction 190
6.2. Aims and Objectives 192
6.3. iTRAQ mass spectrometry of EV contents 192
6.4. Label free mass spectrometry of oral cancer EV contents 200
6.4.1. Mass spectrometry data processing 200

6.4.2. Comparison of protein contents of oral cancer EVs 201
6.4.3. Comparing the protein contents of EVs from mild and severe dysplastic cells 212
6.4.4. Comparison of the protein contents of EVs from non-metastatic carcinoma and metastatic deposit cells 216
6.4.5. Comparison of the protein contents of EVs from two oral dysplastic cell lines with those of oral carcinoma..... 220
6.5. Validation of mass spectrometry data..... 224
6.6. Oral cancer EVs are enriched in proteins from oral cancer associated pathways 227
6.7. Discussion 230
6.7.1. Future work..... 239
7. Effect of oral cancer EVs on cells of the tumour microenvironment 241
7.1. Introduction 241
7.2. Aims and objectives 242
7.3. EVs produced by oral cancer cells can be taken up by a range of cell types 242
7.4. Optimisation of fibroblast seeding densities in full serum and serum free conditions 248
7.5. EVs from cancer cells have a minimal impact on fibroblast turnover 250
7.6. Uptake of oral cancer derived EVs causes normal oral fibroblasts to display cancer associated fibroblast characteristics. 254
7.7. Discussion 265
7.7.1. Future work..... 269
8. Discussion..... 271

8.1. Method optimisation and characterization 271

8.2. Oral cancer cell derived vesicles deliver cargos to the surrounding cells of the tumour microenvironment 274

8.3. Next generation sequencing and label free mass spectrometry techniques reveal differences in vesicle contents which are linked to tumour stage 276

8.4. Oral cancer vesicles can promote pro-tumourigenic changes in normal oral fibroblasts..... 278

8.5. Limitations of the study..... 281

8.6. Further work 285

8.7. Conclusion..... 288

9. References..... 289

10. Appendix..... 324

10.1. Comparison of EVs purified by serial centrifugation and SEC 324

10.2. miRNA sequencing data table 325

10.3. Label free mass spectrometry data tables..... 328

List of Methods

Cell culture 67

Cell counting and seeding 70

EV depletion of bovine serum 70

Preparation of whole cell lysate 70

Preparation of conditioned medium 71

ExoQuick extraction 71

Valadi et al extraction 72

Théry et al extraction 72

Hybrid protocol 72

Size exclusion chromatography 73

Particle counting and sizing 74

Transmission electron microscopy 74

BCA assay 76

Western blotting 78

iTRAQ 8 plex 82

Label free mass spectrometry 85

RNA extraction 87

Small RNA sequencing 88

qPCR 89

Fluorescent imaging of EV uptake 93

Proliferation and viability assays 94

αSMA staining 97

List of Figures

Figure 1.1 Oral cancer microenvironment 5

Figure 1.2 Symmetric and asymmetric cell division 6

Figure 1.3 Oral cancer tumourigenesis 15

Figure 1.4 Mechanisms of EV release 20

Figure 1.5 ESCRT-dependent mechanisms of EV formation 22

Figure 1.6 ESCRT-independent mechanisms of EV formation 26

Figure 1.7 Microvesicle formation 31

Figure 3.1 Overnight centrifugation at 100000 x *g* reduces serum particle count 103

Figure 3.2 Size distribution profiles of bovine vesicles in DMEM 104

Figure 3.3 Overnight centrifugation at 100000 x *g* removes EV like structures from DMEM 105

Figure 3.4 Serial centrifugation protocols produce lower protein yields than precipitation reagents 108

Figure 3.5 EVs purified by all methods are positive for CD63 and TSP1 but not HSP70 110

Figure 3.6 Wash step reduces protein concentration but doesn't remove CD63 band 113

Figure 3.7 EVs elute at fractions 4-9 on homemade SEC column with protein eluting at fractions 10-12 115

Figure 3.8 Freezing to -20^{o}C and thawing on ice has no impact on EV morphology 117

Figure 3.9 Freezing to -20^{o}C and thawing on ice has no impact on EV sample particle count 119

Figure 3.10 Freezing to -20ºC and thawing on ice slightly alters EV particle distribution 120

Figure 3.11 Final workflow 124

Figure 4.1 EVs purified from OSCC culture medium exhibit different morphologies under TEM 129

Figure 4.2 EVs produced by OSCC have similar size distribution profiles 130

Figure 4.3 Average sizes of EVs produced by OSCC cells 133

Figure 4.4 Severe dysplastic cells produce double the EVs in 24 h 134

Figure 4.5 EVs from OSCC contain high numbers of RNA between 25 and 200 nucleotides long 136

Figure 4.6 EVs from severe dysplastic and metastatic deposit cells contain double the RNA of EVs from mild dysplastic and carcinoma cells 137

Figure 4.7 OSCC EVs are positive for TSP1 CD63 and Alix but negative for GM130 140

Figure 5.1 RNA distribution in OSCC by IonTorrent sequencing shows majority of RNA are categorized other with miRNA being less than 0.2% in all EV types 152

Figure 5.2 1000 RPM cut of reduces number of miRNA to around 100 per EV type 155

Figure 5.3 Euclidean heat map of OSCC RNA shows severe dysplasia and carcinoma cell derived vesicles have most similar contents 156

Figure 5.4 Volcano plot of miRNA in mild and severe dysplastic cell derived EVs 158

Figure 5.5 Top 10 most differentially regulated miRNA in mild and severe dysplastic cell derived EVs 159

Figure 5.6 Volcano plot of miRNA in non-metastatic carcinoma and metastatic deposit cell derived EVs 161

Figure 5.7 Top 10 most differentially regulated miRNA in non-metastatic carcinoma and metastatic deposit cell derived EVs 162

Figure 5.8 Volcano plot of miRNA in dysplastic and carcinoma cell derived EVs 164

Figure 5.9 Top 10 most differentially regulated miRNA in dysplastic and carcinoma cell derived EVs 165

Figure 5.10 Abundance of detected miRNA varies with EV type 168

Figure 5.11 Kegg pathway analysis of EV miRNA contents reveals no significant changes 169

Figure 5.12 Let-7a miR-199a-3p and miR-29a-3p are suitable validation candidates 171

Figure 5.13 Presence of all three validation candidates is confirmed by qPCR 174

Figure 6.1 Work flow for post processing of label free mass spectrometry data and range in protein number with EV type 202

Figure 6.2 Protein contents of OSCC EVs do not cluster by tumour stage 203

Figure 6.3 Binding and catalytic proteins are most abundant in OSCC EVs 205

Figure 6.4 EV proteins are predominately cell part of extracellular region in origin 206

Figure 6.5 EV proteins from organelles are predominantly from nucleus or cytoskeleton in origin 207

Figure 6.6 EV proteins from cell parts are predominantly intracellular or plasma membrane in origin 208

Figure 6.7 Nucleic acid binding is the most common function of OSCC EV proteins 209

Figure 6.8 Largest population of EVs is enriched in mild dysplastic cell derived EVs compared to severe dysplastic cell derived EVs 214

Figure 6.9 Top 10 differentially abundant proteins in mild and severe dysplastic cell derived EVs 215

Figure 6.10 Largest population of EVs is enriched in non-metastatic carcinoma cell derived EVs compared to metastatic deposit cell derived EVs 218

Figure 6.11 Top 10 differentially abundant proteins in non-metastatic carcinoma and metastatic deposit cell derived EVs 219

Figure 6.12 Majority of proteins enriched in carcinoma cell derived EVs compared to dysplastic cell derived EVs 222

Figure 6.13 Top 10 differentially abundant proteins carcinoma and dysplastic cell derived EVs 223

Figure 6.14 Validation of label free mass spectrometry by western blot confirms presence of some candidates 226

Figure 6.15 Integrin signalling, and other pathways are most abundantly represented in OSCC EV proteins 228

Figure 6.16 Integrin signalling, inflammation, apoptosis and cytoskeletal regulation pathways all represented in OSCC EVs 229

Figure 7.1 OSCC EVs can be taken up by other OSCC cells 244

Figure 7.2 OSCC EVs can be taken up by oral keratinocytes 245

Figure 7.3 OSCC EVs can be taken up by endothelial cells 246

Figure 7.4 OSCC EVs can be taken up by NOFs 247

Figure 7.5 NOF growth curves in presence and absence of serum 249

Figure 7.6 Treatment with increasing doses of OSCC EVs has no effect on NOF viability after 48 hours 251

Figure 7.7 Treatment with OSCC EVs produces no significant change in NOF proliferation after 48 hours 253

Figure 7.8 EV treatment of NOF803 cells produces increase in αSMA mRNA and protein and the formation of stress fibres 257

Figure 7.9 EV treatment of NOF316 cells produces no change in αSMA mRNA. except with the EVs from carcinoma and metastatic deposit cells, no change at the protein level but does produce stress fibres 259

Figure 7.10 EV treatment of NOF319 cells produces no change in αSMA mRNA. except with the EVs from carcinoma and metastatic deposit cells, no change at the protein level but does produce stress fibres 261

Figure 7.11 EV treatment of NOF335 cells only produces a change in mRNA levels when treated with EVs from severe dysplastic cells and produces no change in protein levels but does produce stress fibres 263

Figure 8.1 miRNA and protein enrichment in OSCC EVs changes with tumour stage 277

Figure 8.2 OSCC EV miRNA interact with regulatory members of TGFβ-1 pathway 280

Figure 10.1 EVs purified from OSCC conditioned medium by serial centrifugation and SEC are of a similar size and bear the same protein markers 325

List of Tables

Table 2.1 Details of patient fibroblasts 69

Table 2.2 1.0 mm acrylamide resolving gel 77

Table 2.3 1.0 mm acrylamide stacking gel 78

Table 2.4 Primary antibodies manufacturers clone numbers and dilutions 80

Table 2.5 Secondary antibodies manufacturers and dilutions 82

Table 2.6 TaqMan assays 92

Table 2.7 Sybr Green PCR primers 93

Table 3.1 EV marker antibodies 109

Table 4.1 Antibodies used to characterise EV 139

Table 5.1 Characteristics of EV RNA from IonTorrent samples 153

Table 6.1 Proteins down regulated in EVs of severe dysplastic cells compared to carcinoma cells 194

Table 6.2 Proteins upregulated in EVs of severe dysplastic cells compared to carcinoma cells 195

Table 6.3 Proteins upregulated in EVs of metastatic deposit cells compared to carcinoma cells 197

Table 6.4 Proteins downregulated in EVs of metastatic deposit cells compared to carcinoma cells 198

Table 6.5 Log2 of LFQ intensity scores for MS validation candidates 229

Table 10.1 List of miRNAs identified in all EVs by IonTorrent 326

Table 10.2 Proteins identified in dysplastic cell EVs 329

Table 10.3 Proteins identified in carcinoma and metastatic deposit cell EVs 335

List of Abbreviations

αSMA - Alpha smooth muscle actin

Alix – ALG-2 interacting protein X

BCA - Bicinchoninic acid

BSA - Bovine serum albumin

CAF - Cancer associated fibroblast

DNA – Deoxyribonucleic acid

EBV – Epstein Barr Virus

EEF2 – Eukaryotic elongation factor 2

EV/EVs – Extracellular vesicle/s

EVL - EV protein lysate

EPF – Epidermis growth factor

EMT - Epithelial to mesenchymal transition

ESCRT – Endosomal sorting complexes required for transport

FAP – Fibroblast activation protein

FSP1 – Fibroblast specific protein

GO – Gene ontology

HPV – Huma papilloma virus

HRP – Horseradish peroxidase

IL – Interleukin

iTRAQ – Isobaric tag for relative and absolute quantitation

Kegg – Kyoto encyclopaedia of genes and genomes

LFQ – Label free quantification

LGAL3BP – L-galectin 3 binding protein

mRNA – Messenger RNA

miRNA/miR – microRNA

MMP – Matrix metalloproteinase

MVB – Multivesicular body

MS- Mass spectrometry

NOF – Normal oral fibroblast

NF-κB – Nuclear factor kappa B

OSCC – Oral squamous cell carcinoma

RNA – Ribonucleic acid

RIPA - Radio immunoprecipitation assay

PBS – Phosphate buffered saline

PBST – Phosphate buffered saline – tween 20

qPCR – quantitative real time PCR

SEC - Size exclusion chromatography

TEM – Transmission electron microscopy

TGF-β – Transforming growth factor beta

TME – Tumour microenvironment

TNF-α – Tumour necrosis factor alpha

TRPS – Tuneable resistive pulse sensing

TSP1 – Thrombospondin 1

WCL – Whole cell lysate

1. Introduction

1.1. Cancer

Cancer is one of the modern world's biggest killers; in the UK it kills someone every four minutes. In 2014 Cancer Research UK released the worrying forecast that 1 in 2 people will have cancer at some point in their lifetime (Cancer Research UK., 2014). Often referred to as a disease of old age, cancer is significantly more common in people over the age of 60, and with improvements in modern medicine and lifestyle allowing people to live longer; so, cancer rates are rising. Medical dictionaries define cancer as a disease caused by an uncontrolled division of abnormal cells. These cells arise from a series of mutations caused either by carcinogens such as those found in tobacco smoke, alcohol and other chemicals, or by errors in replication, which naturally increase with age. Despite the rising number of cases, the mortality rates have been falling since the late 1970s with the advent of improved screening programmes and new generations of therapeutics. However oral cancer mortality rates are slowly on the rise, increasing by 10% in the last decade and 92% since the late 1970s (Cancer Research UK., 2014).

1.2. Oral Cancer

1.2.1. Introduction and statistics

Oral cancers are a subset of head and neck cancers: this collection of tumour types covers those arising from the tongue, throat and the mucosal layers of the oral cavity. Cancer Research UK figures released in 2014 place the number of cases at 6767 per year with the number of deaths at 2119 per year. These figures account for 2% and 1%

of all cancer cases and deaths in the UK. Of the 18-people diagnosed with this disease every day the majority are men, it is most prevalent in the 50-74 age group and five-year survival rates are currently at 50% (Cancer Research UK., 2014). As with many cancers the causes are linked to drinking alcohol, smoking tobacco and poor diet. More than two thirds of male cases and half of female cases are linked to tobacco use. The human papilloma virus (HPV), that also causes cervical cancer, has been associated with the risk of oral cancer and has recently become the focus of a vaccine programme in the UK (Waller, 2008).

1.2.2. Stages of oral cancer

Tumourigenesis is an increasingly well-defined process initiated following multiple genetic alterations caused by exposure to carcinogens in tobacco smoke, alcohol or viral infections as described by Knudson's two hit hypothesis (Knudson, 2001). In oral cancer these mutations, often transforming growth factor alpha (TGF-α) and epidermal growth factor receptor (EGFR) overexpression (Todd et al., 1997), set the afflicted cell on the path of tumorigenesis. This leads to cells acquiring some or all of the hallmarks of cancers as described by Hanahan and Weinberg (Hanahan and Weinberg, 2011, 2000). Cells which only develop the first three hallmarks: evasion of growth suppressors, sustained proliferative signalling and resisting cell death form benign or pre-malignant dysplasias. Dysplasias are defined as an abnormality of development or an epithelial anomaly of growth and differentiation (Reibel, 2003). Often referred to as premalignant lesions they are sometimes the first indication of an impending cancer in the oral cavity. Leukoplakias are a white plaque that forms on the oral mucosa and which cannot be identified as any other condition (Lodi et al., 2006);

similarly, erythroplakia (Reibel, 2003) is a red lesion which cannot be identified as any other condition. Dysplasias are the physical evidence of cells which have acquired those initial hallmarks of cancer allowing aberrant replication to establish itself within a population.

Continued exposure to these carcinogens causes increasing damage with Kirsten rat sarcoma viral oncogene homolog (KRas) mutations, adenomatous polyposis coli (APC), tumour protein 53 (P53) and anaphase promoting complex subunit Doc1 (Doc1) inactivation, the overexpression of c-myelocytomatosis viral oncogene (MYC) and downregulation of E-cadherin (Todd et al., 1997). This results in the progression from dysplasia to a malignant carcinoma with the cells acquiring the final three hallmarks of cancers: induction of angiogenesis, replicative immortality and invasion and metastasis. Carcinomas are a type of cancer that arises from epithelial cells and account for 90% of all oral cancers (Markopoulos, 2012).

1.3. Composition and conditions of the tumour microenvironment

A developing cancer can be thought of as a distinct organ comprising of multiple cell types each with distinct roles essential to the function of the whole. Constantly changing environmental pressures will drive the need of a tumour to recruit and manipulate normal cells like epithelial cells, fibroblasts, keratinocytes and macrophages into the developing mass termed the tumour microenvironment (TME) (figure 1.1).

1.3.1. Epithelial cells and keratinocytes

Epithelial cells and keratinocytes are the normal cells of the oral mucosa and are found as a stratified squamous epithelium with thin flat cells on the topmost apical layer

above layers of more regular cuboid cells. Some areas of oral epithelium are keratinized; like the dorsal surface of the tongue, palate and gingiva. Keratinized epithelium has a topmost layer of keratinocytes which are differentiated epithelial cells that are almost completely filled with keratin to produce a barrier (Collins and Dawes, 1987). Epithelial cells are often the cells from which oral cancer will arise, however the majority of them have too short a life span (14-24 days) to accumulate the necessary genetic changes to develop into a tumour (Squier and Kremer, 2001). An epithelial layer, whether keratinized or not, is constantly being replaced with cells dividing and becoming progressively more differentiated as they rise up the epithelial layers. Within an epithelium there exists a population of stem cells; these have a low proliferative rate and a high self-renewal capacity. This population is maintained by asymmetric division. Asymmetric division (figure 1.2) gives rise to a new stem cell and a more differentiated "normal" cell. In this way the number of stem cells remains at a constant level whilst a continuous supply of cells is fed into the differentiation pathway (Thomson et al., 1999). It is in this population of cells that tumorigenic mutations can occur.

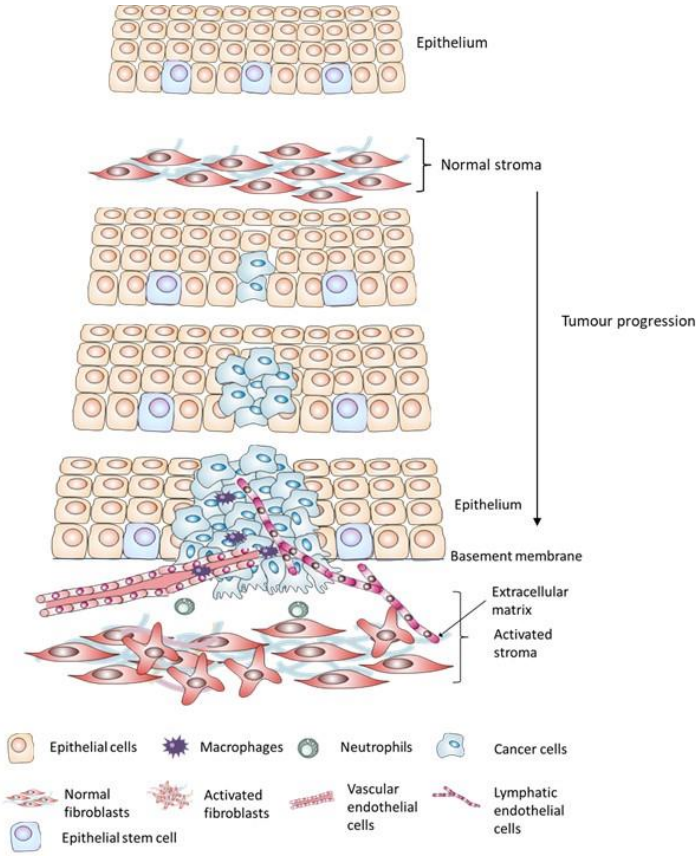

Figure 1.1 Changing oral cancer microenvironment from a healthy epithelial layer to a fully developed squamous cell carcinoma. Tumourigenic mutations are acquired by the stem cells and as the tumour progresses additional cell types are recruited into the surrounding area particularly macrophages and neutrophils. The surrounding stromal cells are altered by signals from the tumour cells forming activated or cancer associated fibroblasts which benefit a developing tumour. The final image in the set shows a fully developed tumour that has begun to metastasise. This tumour has established its own blood and lymphatics supply and has established an invasive front which is breaking through the basement membrane and is beginning to metastasise to secondary sites.

Symmetric and asymmetric division

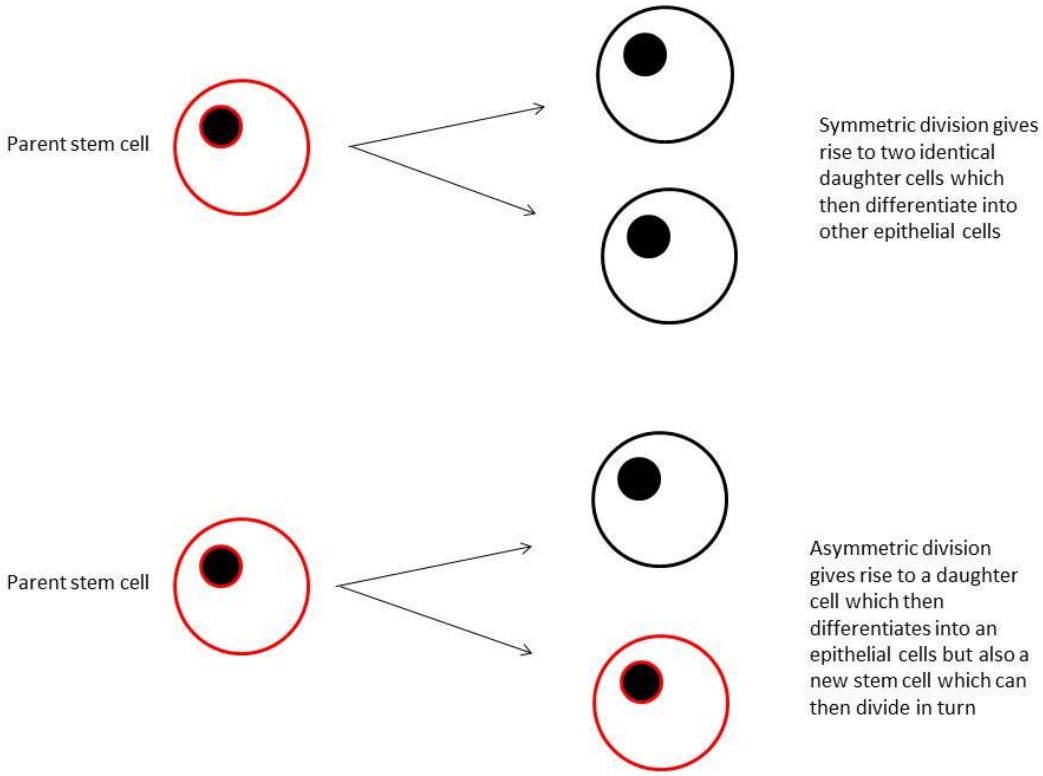

Figure 1.2 Symmetric division as undergone by normal cells and asymmetric division as undergone by epithelial stem cells. Symmetric division gives rise to two identical daughter cells whereas asymmetric division gives rise to a new epithelial cell and a new stem cell; it is this process that creates a pool of cells with a lower turnover rate in which carcinogenic mutations can accumulate.

1.3.2. Fibroblasts

Fibroblasts are the cells responsible for secreting the extracellular matrix and are abundant within the TME. The fibroblasts within a tumour however are very different to those found in normal tissue. In wounded tissue fibroblasts become activated to form myofibroblasts (Majno et al., 1971), a similar phenomenon is seen in cancer. Cancer-associated fibroblasts (CAFs) have a more spiny morphology and have been identified by a range of different markers including alpha smooth muscle actin (α-SMA) (Serini et al., 1998; Tomasek et al., 2002), platelet derived growth factor (PDGF) receptor α/β, tenascin-C, periostin, neural/glial antigen 2 (NG2), fibroblast specific protein (FSP) and fibroblast activation protein (FAP) (Prime et al., 2016; Togo et al., 2013). With so many different markers it is highly likely that there are actually a number of different sub-populations present in a tumour potentially with subtly different functions. The activation of fibroblasts to form CAFs is driven by the epithelial cells producing protein factors such as transforming growth factor beta (TGF-β), tumour necrosis factor alpha (TNF-α) and interleukin (IL)-1 α/β. Also implicated are the miRNAs miR-210, miR-21, miR-146a, miR-27, miR-155 and miR-200b (Pang et al., 2015; Tanaka et al., 2015; Yao et al., 2011).Interestingly it has also been observed that cigarette smoke, a major risk factor for oral cancer can regulate some of these miRNA (Pal et al., 2013). The relationship between fibroblasts and cancer cells is actually a reciprocal one, as once activated, the fibroblasts release a range of molecules including prostaglandin E, stromal cell derived factor 1, bone morphogenetic protein 4, activin A, matrix metalloproteinases, hepatocyte and keratinocyte growth factors and insulin like growth factor 2. This potent cocktail can drive cell growth (Castells et al., 2012; Olumi et al., 1999), metastasis, angiogenesis and immune escape (Leef and Thomas, 2013; Togo et al., 2013). They have also been seen to facilitate evasive resistance by giving alternative

angiogenesis pathways to tumours treated with VEGF inhibitors (Sun and Nelson, 2012).

Interestingly, CAFs have also been seen to release pro-inflammatory cytokines (Muppalla et al., 2013) indicating that CAFs have more in common with myofibroblasts than just morphology. Rudolf Virchow first postulated that inflammation accelerated cancer growth in 1863. Although some of his theories on cancer origins were shown to be incorrect by subsequent scientists, his thoughts on inflammation have become widely accepted as shown in recent reviews on the subject (Coussens and Werb, 2002; Ostrand-Rosenberg and Sinha, 2009).

Activated fibroblasts are not the only fibroblasts found in and around a tumour. Senescence is a state where cells are no longer capable of dividing but remain viable and metabolically-active. This self-imposed limit on replication is normally triggered in response to extreme cellular stress or to DNA damage and therefore acts as a tumour suppressing mechanism. However, fibroblast senescence has recently been shown to be induced by tobacco and alcohol and that this senescence actually precedes the dysplasia in a pre-malignant oral fibrosis condition (Pitiyage et al., 2011). This is a very interesting observation particularly when viewed alongside other data; co-culture experiments of senescent prostate or lung fibroblasts with their pre-malignant epithelial counterparts stimulates cell growth as well as invasion and migration (Bavik et al., 2006). One of the key contributions from senescent fibroblasts to the TME is the senescence-associated secretory phenotype or SASP. This is a combination of favourable protein factors including IL6 and matrix metalloproteases (MMPs), IL8, vascular endothelial growth factor (VEGF) and osteopontin (Coppé et al., 2008; Pazolli

et al., 2009). These factors contribute to a range of processes including epithelial cell proliferation, possibly leading to the dysplasias it precedes. Another beneficial aspect of the SASP is the induction of epithelial to mesenchymal transition (EMT) (Coppé et al., 2008). This is a phenomenon where epithelial cells transition from an adhesive phenotype to a more migratory phenotype similar to that seen in mesenchymal cells. It is often thought of as being the first step necessary for tumour metastasis. However, this theory has potentially been disproved with data emerging showing EMT is non-essential for metastasis (Zheng et al., 2015), but it remains to be seen if this will be true in other models.

1.3.3. Endothelial cells

The induction of angiogenesis is one of the extended hallmarks of cancer described by Hanahan and Weinberg in their 2011 sequel, the next generation (Hanahan and Weinberg, 2011). A study published in 2007 showed that oral cancer patients with the most heavily vascularised tumours had five-year survival rates of up to 50% lower than patients with poorly vascularised tumours (Miyahara et al., 2007). This clearly vital process is mediated by endothelial cells. In humans, the cells of the vascular endothelium exhibit different characteristics depending on their organ of origin (Langenkamp and Molema, 2009). In recent years, studies have shown that the endothelial cells seen in tumours exhibit further heterogeneity. A study from 2000 identified 13 novel protein markers for colon carcinoma endothelial cells (St Croix et al., 2000), similar differences have also been observed in ovarian cancer (Lu et al., 2007). An interesting molecular difference between tumour and non-tumour endothelial cells, is that tumour endothelial cells are more responsive to VEGF (Matsuda et al.,

2010). Additionally, they express high levels of the receptor for epidermal growth factor (EGF) (Amin et al., 2006). These molecular variations would combine to give tumour endothelial cells a doubly more responsive phenotype towards angiogenic factors, reflecting the need of tumour endothelial cells to handle the more demanding conditions of the tumorous pseudo organ.

A paper from 2003 describes how the endothelial cells from a renal carcinoma were resistant to vincristine (Bussolati et al., 2003). This trait is seen in hepatocellular carcinoma with both 5-fluoruracil and adriamycin (Akiyama et al., 2012; Xiong et al., 2009). This is an interesting development in the study of tumour angiogenesis, next to the tumour cells themselves the endothelial cells will be the fastest replicating cells within the microenvironment and highly vulnerable to many of the chemotherapy agents in use. That the endothelial cells have a way to offset this potential weakness to the tumour is fascinating. Many drugs will circulate around a tumour using the vasculature, meaning endothelial cells also represent the first contact of the tumour tissue with any cytotoxic compounds and being able to remove some of these from circulation without cost to themselves is a subtle advantage to the tumour.

Recent studies have demonstrated a role for endothelial cells in tumour development beyond angiogenesis. Several studies have implicated endothelial cells in cancer metastasis. Metastasis to the blood vessels require the tumour cells overcome two challenges, first they must cross a barrier. Secondly the cells must acquire a motile phenotype, either by cytoskeletal remodelling or because of chemotactic gradient. Endothelial cell expression of Akt-1 was seen to be pivotal to preventing the invasion of prostate cancer cells through an endothelial cell layer (Gao et al., 2018). It’s loss in

endothelial cells caused increased phosphorylation of β catenin and disruption of the tight junctions. Aa study in oral cancer demonstrated the endothelial cells were capable of secreting EFG which could induce epithelial to mesenchymal transition in head and neck cancer cells (Zhang., et al 2014). This transition gives the cells a more motile phenotype and is thought to be essential for metastasis. Another study in oral cancer show another endothelial cell secreted protein contributing to a different element of metastasis, interleukin 6 (IL6) secreted by endothelial cells establishes a chemotactic gradient enabling the movement of cancer cells towards the blood vessels (Kim et al., 2017).

1.3.4. Immune cells

Many of the cells of the innate immune system have been found in the microenvironment of different tumour types and it has been shown that these cells can have both pro and anti-tumour roles. Macrophages are phagocytic cells formed by differentiating monocytes. In normal tissues these cells are essential for the clearance of apoptotic cells and control of epithelial cell turnover (Geissmann et al., 2010; Medzhitov, 2008). In patients with oral cancer an increased number of macrophages within the TME correlates with significantly worse outcome (Liu et al., 2008). During differentiation monocytes can become either M1 like or M2 like macrophages and although both are found in tumours there are contradictory studies describing their respective roles. M1 macrophages have been shown to exhibit strong anti-tumour behaviours by some groups (Beatty et al., 2011; Fridlender et al., 2009). This subtype is more commonly associated with the early stages of tumour progression and the removal of macrophages from a tumour in mouse models of breast cancer by depletion of the

macrophage growth factor colony- stimulating factor 1significantly impedes the development of a cancer (Lin et al., 2001). They also release a variety of chemokine and cytokines which can promote tumour development (Yang et al., 2008). M2 macrophages are more common in later stage cancers and as a result are frequently shown to have a role in metastasis (Na et al., 2013; Yang et al., 2015).

It is interesting to note that M2 macrophages have well documented anti-inflammatory properties (Bouhlel et al., 2007) in contrast to the M1 macrophages which are known to be pro- inflammatory. Prolonged inflammation has come to be accepted as a favourable backdrop for the development of a tumour, being included as one of the next generation hallmarks in 2011 (Hanahan and Weinberg, 2011). This would suggest that the ratio of M1 to M2 macrophages in cancer is dependent on the stage of the cancer and the need for their other abilities to take precedence at any given stage in the cancer's life span.

The infiltration of neutrophils in head and neck squamous cell carcinomas has been associated with worse outcome (Trellakis et al., 2011), conversely however in gastric cancer high neutrophil count is associated with a favourable prognosis (Caruso et al., 2002). Neutrophils have been linked to genetic instability in a mouse model of tumour initiation via an inducible nitric oxide synthase (Sandhu et al., 2000). They have also been seen to increase tumour cell proliferation by transfer of neutrophil elastase to neighbouring tumour cells, the elastase enhances platelet derived growth factor signaling (Houghton et al., 2010). In a reciprocal exchange interleukin 8 produced by melanoma cells increases β2 integrin expression on the neutrophils. This changes the interaction between neutrophils and melanoma cells in a way which favours the

movement of the melanoma cells across the endothelium (Huh et al., 2010). In a breast cancer model interleukin 17 (IL-17) producing γδ T-cells cooperate with neutrophils to promote metastasis (Coffelt et al., 2015). First the T-cells release IL-17 this promotes the invasion of neutrophils into the tumour. These neutrophils then supress cytotoxic T lymphocytes which would normal inhibit metastasis (Coffelt et al., 2015).

Another class of immune cells, regulatory T cells have been implicated in the suppression of anti-tumour immune responses. In oral cancer increasing FOXP3 mRNA expression correlates with increasing malignancy (Schipmann S et al., 2014), this transcription factor helps to recruit the regulatory T cells into the cancer micro environment to supress the anti-tumour effects. CD-3 positive T-cells have also been implicated in oral cancer progression with a higher level of these cells in biopsies of oral dysplasias correlating with the prevention of transformation into a carcinoma (Öhman et al., 2015). Using a range of mouse models for oral cancer a study showed that different levels of different T-cells are associated with more or less aggressive tumours. Less aggressive slower growing tumours were associated with increased CD-8 positive T-cells whereas more aggressive metastatic tumours were associated with increased CD4 positive regulatory T-cells (Judd et al., 2012). This study neatly encapsulates the dynamic nature of the immune component of the tumour microenvironment. As the tumour progresses and its demands change the composition of the immune component will be altered with it.

1.3.5. Changing conditions in the microenvironment

Tumour formation is a very good example of the evolutionary phenomenon niche construction occurring on a cellular level. Niche construction is the process by which an organism shapes the niche it inhabits further tailoring it to suit its needs against those of potential rivals. The organisation of cells to form tissues within the human body is very highly conserved to allow adequate circulation and for the tissues to perform their biological role. By necessity, the growth and turnover of tissues is kept in check by homeostatic processes. The mutations that cause tumorigenesis disrupt this process causing a series of dramatic changes in the conditions of the surrounding tissue (figure 1.3). As soon as a cell has acquired sufficient mutations it begins to replicate incessantly. This replication causes an increase in the size of the tissue causing cells to grow further from their nearest blood vessels. Once cells are further than the 2 mm diffusion limit from a blood vessel they will begin to experience hypoxic conditions (Rouwkema et al., 2008). Another early change is caused by the innate immune system. Our immune system is programmed to recognise and remove transformed cells arising from replication errors, which should normally include cancer cells. Macrophages neutrophils and leukocytes in the vicinity of the developing tumour will be driving the establishment of localised inflammation.

Oral cancer tumourigenesis

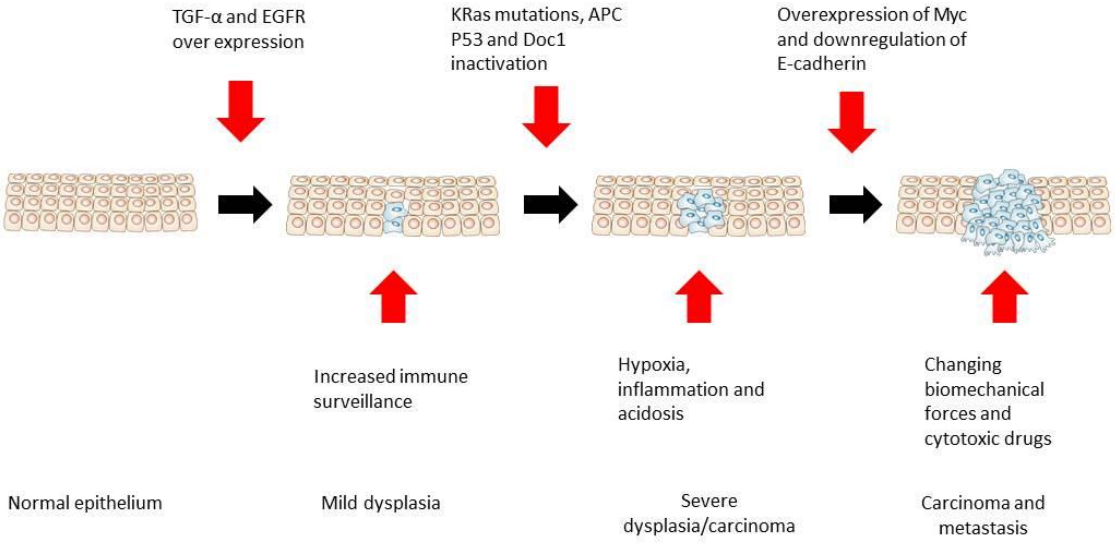

Figure 1.3 The progression of oral cancer with the carcinogenic mutations that cause the transition between the stages. As tumorigenesis of oral cancer progresses from normal epithelium through to a metastatic carcinoma the changing environmental pressures experienced by the growing cells are also indicated.

As a carcinoma progresses it will establish its own blood supply; however, despite this, many tumours will have a necrotic centre comprising cells that have starved to death. A large number of dead or dying cells will change the pH of the blood circulating in the surrounding vessels due to the breakdown products of the cells causing acidosis. Because tumours distort the ordered formation of tissues to such an extent they can also change the biomechanical forces experienced by the surrounding tissue (Dvorak., 2011). This effect is particularly apparent where tissue has a very physical role to perform such as that found in the mouth or oesophagus.

Once a tumour is advanced enough to be diagnosable it is hoped that a patient would be treated, which will often include either chemo or radiotherapy. Both therapeutic approaches will have a dramatic impact on the conditions of the tumour, as both are highly cytotoxic and will have the greatest impact on those cells that are rapidly replicating. In an established tumour this potentially results in a collapse of the tissue structure and vasculature along with an increase in the number of dead cells. These effects will again cause acidosis and hypoxia within the surrounding area (Chiche et al., 2010).

1.3.6. Discovery of extracellular vesicles

In 1987 Rosemary Johnston was studying the fate of the transferrin receptor during the maturation of sheep reticulocytes. Using immunogold labelling and transmission electron microscopy (TEM) she observed the receptor being removed from the membrane and trafficked to multivesicular bodies (MVB), which when they fused with the plasma membrane released transferrin containing vesicles from the cells

(Johnstone et al., 1987). This is widely considered as the starting point for a new field of research. However, the first mention of the term exosomes, that Johnstone is often credited with coining in this paper, was actually seen in a report from 1981. The study in question observed various cell lines releasing vesicles with 5'-nucleosidase activity. When visualised using TEM, these vesicles were between 500 to 1000 nm in size and often contained a second smaller population of vesicles of 40 nm in size (Trams et al., 1981). It was their suggestion that all of the vesicles should be termed exosomes.

It wasn't until the early 2000s that these vesicles were seriously considered as anything more than cellular waste removal systems. In 2006 and 2007 it was demonstrated that extracellular vesicles (EVs) contained both mRNA and miRNA which could be transferred between cells (Ratajczak et al., 2006; Valadi et al., 2007). A few years later another landmark was reached, the discovery that melanoma and ovarian cells produced significantly more EVs than healthy cells (Logozzi et al., 2009; Taylor and Gercel-Taylor, 2008). Since then research in this area has bloomed with increasing numbers of groups working to elucidate the roles EVs play in both healthy and diseased tissues. EVs have been isolated and investigated from an increasing range of biological fluids and the culture medium of various cell lines.

1.3.7. What's in a name?

Names and definitions are an important part of any scientific field but are doubly important to an emerging field as it takes shape. The International Society for Extracellular Vesicles (ISEV) has endeavoured to grapple with this issue in various position papers and meetings (Gould and Raposo, 2013; Hill et al., 2013; Witwer et al.,

2013). Currently there are as many as four major classes of EVs being studied: exosomes, microvesicles, apoptotic extracellular vesicles and large oncosomes.

The vesicles Johnstone and her colleagues observed came to be known as exosomes and these were distinguished from other EVs by their formation in MVB inside the cell (figure 1.4). The majority of studies on PubMed (4334) are focused on exosomes. These are normally described as being between 30-100 nm in size. A second class of EVs is seen to bud off directly from the plasma membrane that have been termed microvesicles and range from 100-1000 nm in size (Akers et al., 2013). The overlapping size ranges of these different EVs present one of the biggest challenges for the field, as current techniques for extracting them from cell culture media or biological fluids are incapable of distinguishing between EVs of the different classes. This is because existing methods are only capable of separating the EVs by their size or density. Perhaps one of biggest problems with this is many of the protein markers for different subclasses of EVs have been determined by studies using size or density-based separation methods where there will undoubtedly have been some crossover of EVs types inevitably making the definitions of some groups inconsistent with what they are actually studying. A further complication is that there are numerous papers which still use older terminology, some of which relates to the producing cells or tissues to distinguish the EVs such as oncosomes (Di Vizio et al., 2009) or prostasomes (Aalberts et al., 2012). It is almost certain that the majority of groups are working on preparations containing a mixture of the different subclasses within a density and/or size range created by their chosen extraction protocol.

Apoptotic bodies are vesicles released by apoptotic cells as they break down (Kerr et al., 1972, Gregory and Pound., 2011). Similarly, to exosomes these have previously been viewed as waste disposal systems however it has been demonstrated that they actually play a part in the signalling process of apoptosis (Hawkins and Devitt, 2013). The final class of EVs is relatively new; large oncosomes are around 1-10 μm in size and bleb from the plasma membrane of cancer cells and are thought to function in very different ways to the other smaller EVs (Di Vizio et al., 2012; Meehan et al., 2016; Minciacchi et al., 2015; Morello et al., 2013).

Regardless of the terms used to describe them, or the challenges with defining them, these EVs are now a pivotal part of the future of cancer treatment with a vast range of possibilities as a source of biomarkers, therapy vehicles or a previously unknown signalling system to understand and exploit.

Mechanisms of EV release

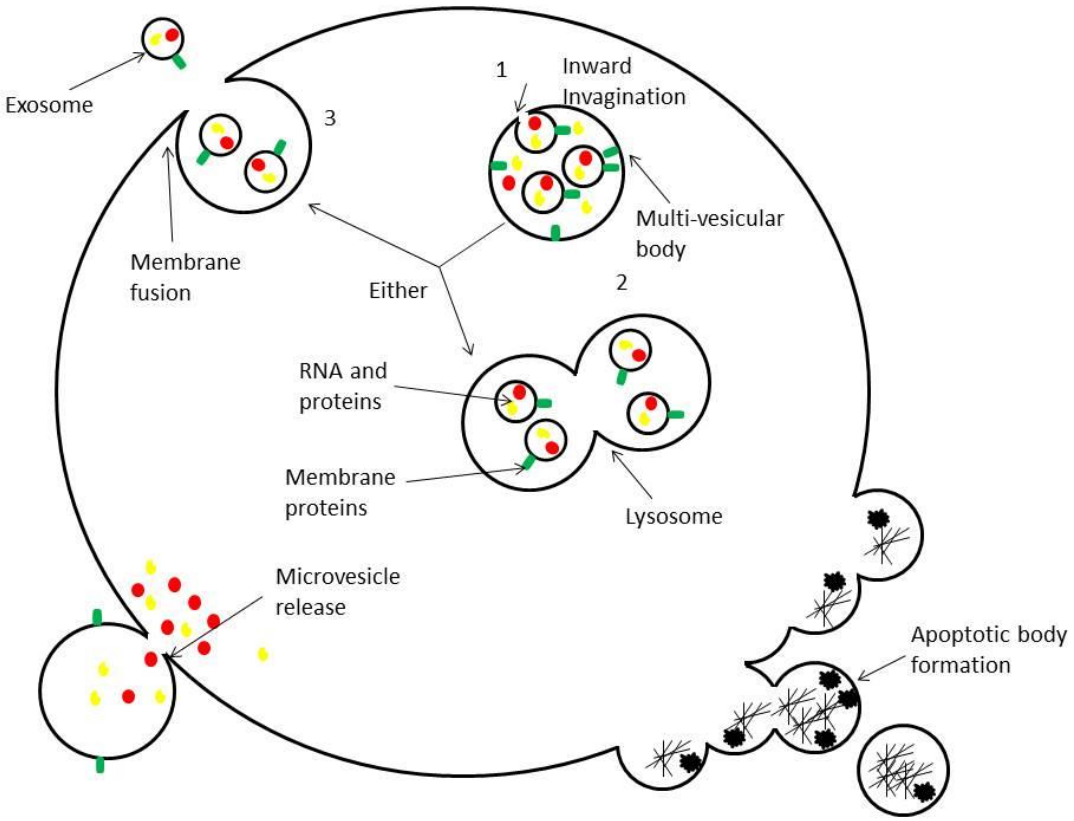

Figure 1.4 Mechanisms of EV release. Exosomes are shown forming in MVBs by inward invagination of the late endosomal membrane (1). They are then trafficked either to the lysosome and degraded (2) or to the plasma membrane where they undergo fusion releasing the intact internal vesicles in to the extracellular spaces. In addition, some EVs can bud directly from the plasma membrane in the form of apoptotic bodies and microvesicles.

1.3.8. Biogenesis of extracellular vesicles from MVB

The formation of the vesicles derived from MVB is still not clearly understood. Whilst the process has been visualised using electron microscopy and the stages are well known, the individual mediators and regulators are not. Johnstone's early work showed that the process involved invagination of the limiting membrane that resulted in a structure that budded into the lumen of the late endosome (Johnstone et al., 1989). This allows the forming exosome to capture proteins and nucleic acids from the cytoplasm. Initially the orientation of the membrane relative to the plasma membrane was unclear. It was later shown that the membrane underwent two inversions, the first upon endocytic internalization, and the second as the intraluminal vesicles budded off into the late endosomal lumen (Février and Raposo, 2004; Lakkaraju and Rodriguez-Boulan, 2008). The second inversion is an essential one as it allows exosomes to present membrane proteins in the same orientation as the cellular membrane therefore retaining activity in the extracellular space. Vesicles are not directed to a lysosomal compartment as usual but are directed by a range of proteins and endocytic components to fusion with the plasma membrane and the extracellular space. Currently the mechanisms that drive and facilitate this process are divided into endosomal sorting complex required for transport (ESCRT) dependent (figure 1.5) and ESCRT independent mechanisms (figure 1.6).

ESCRT-dependent mechanisms of EV formation

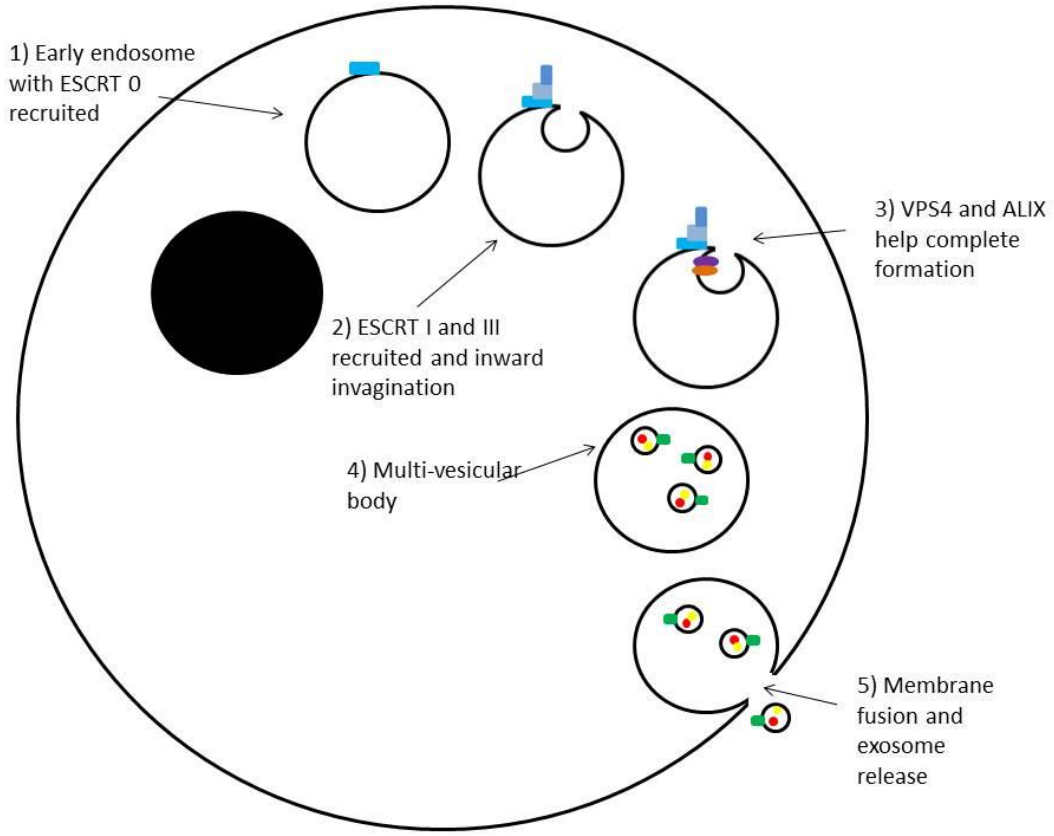

Figure 1.5 ESCRT-dependent formation of vesicles in MVBs begins the sequential recruitment of the ESCRT complex components to the site of invagination (1&2). The next steps are the closure of the "neck" by the combined action of VSP4 Alix and ESCRT-III forming the complete vesicles within the MVB (3&4) which can then be trafficked to the plasma membrane and released (5). There are still many gaps in our understanding of this mechanism as it relates to vesicles that are released from the cell.

1.3.8.1. ESCRT - dependent mechanisms

ESCRT is the endosomal sorting complex required for transport, a well characterised complex with integral roles in intracellular transport and vesicle formation. There are four ESCRT complexes - 0-III each of these has been, or is being, studied in the context of exosome production. Several groups have focused on individual members of these complexes following their detection in proteomic studies of vesicles. HRS, an ESCRT-0 member has been established as a requirement for exosome production in several cell models (Colombo et al., 2013; Gross et al., 2012; Hoshino et al., 2013; Tamai et al., 2010), Depletion of another ESCRT-0 component STAM1 also reduced exosome production (Colombo et al., 2013). With the involvement of two of the complex members it is highly likely that depletion of the remaining components will show similar results.

To date only one ESCRT-I component has been implicated, with TSG101 depletion reducing exosome secretion in various cells (Colombo et al., 2013; Abrami et al., 2013; Baietti et al., 2012). However, this had no impact in oli-neu oligodendroglial cells, which revealed the existence of an ESCRT independent system for the first time (Trajkovic et al., 2008). It is here the picture becomes less clear whilst ESCRT II and III components are seen in proteomic studies of exosome contents, more detailed experiments are showing conflicting results from different research groups. In their shRNA screen of ESCRT proteins in HeLa-CIITA cells one group saw no impact of ESCRT-II proteins on exosome production and ESCRT-III data was inconclusive (Colombo et al., 2013). However, (CHMP4 an ESCRT-III member) has been shown to play a part in exosome secretion in MCF-7 cells (Abrami et al., 2013). It is possible that ESCRT-II maybe the odd complex out and plays no role in the production and secretion

of exosomes, but this is highly unlikely. During canonical vesicle budding in the MVBs the four ESCRT complexes are recruited in sequence to the site of invagination. ESCRT-0 initiates the process and each complex interacts with the other to form ESCRT-III within the neck formed by the membrane invagination. ESCRT-III then draws closed the two sides of the neck and is broken down itself by a VPS4 VTA1 complex (Henne et al., 2011). While it is a possibility that vesicles which become exosomes exhibit some differences to this process; it is more likely that they are formed via an identical process but exhibit different protein surface markers changing their eventual traffic destination. Currently there is no evidence to support either hypothesis.

Alix is a protein that associates with ESCRT-III and has been implicated in conflicting roles. Depletion of Alix in HeLa-CIITA cells showed no clear effect on exosome production, whereas in primary dendritic cells from various donors its silencing decreased exosome production in half of the cells tested (Colombo et al., 2013). This data raises an interesting possibility that the mechanisms producing exosomes are different in healthy and diseased cells. It has also been observed that Alix silencing decreased production of exosomes but increased the production of vesicles generated from outward budding of the plasma membrane (Bissig and Gruenberg, 2014). Further contradictions are seen surrounding the VPS4 protein which is involved in the final steps of intraluminal vesicle formation. This protein has multiple isoforms which appears to be complicating the picture. In HeLa-CIITA cells silencing of the B isoform increased secretion of exosomes, (Colombo et al., 2013). However, in MCF-7 cells when silencing both isoforms independently and in combination, and an effect was only observed when they were silenced in concert which was a decrease in secretion (Abrami et al., 2013). The authors of the first study postulated that silencing of the B

isoform could lead to compensation by the A isoform or an alternative role for the B isoform in HeLa cells. It is worth noting that because these vesicles are often released as a stress response, experiments relying on silencing of a particular protein need to be planned and interpreted with caution as observed effects may not be the direct result of silencing alone.

ESCRT-independent mechanisms of EV formation

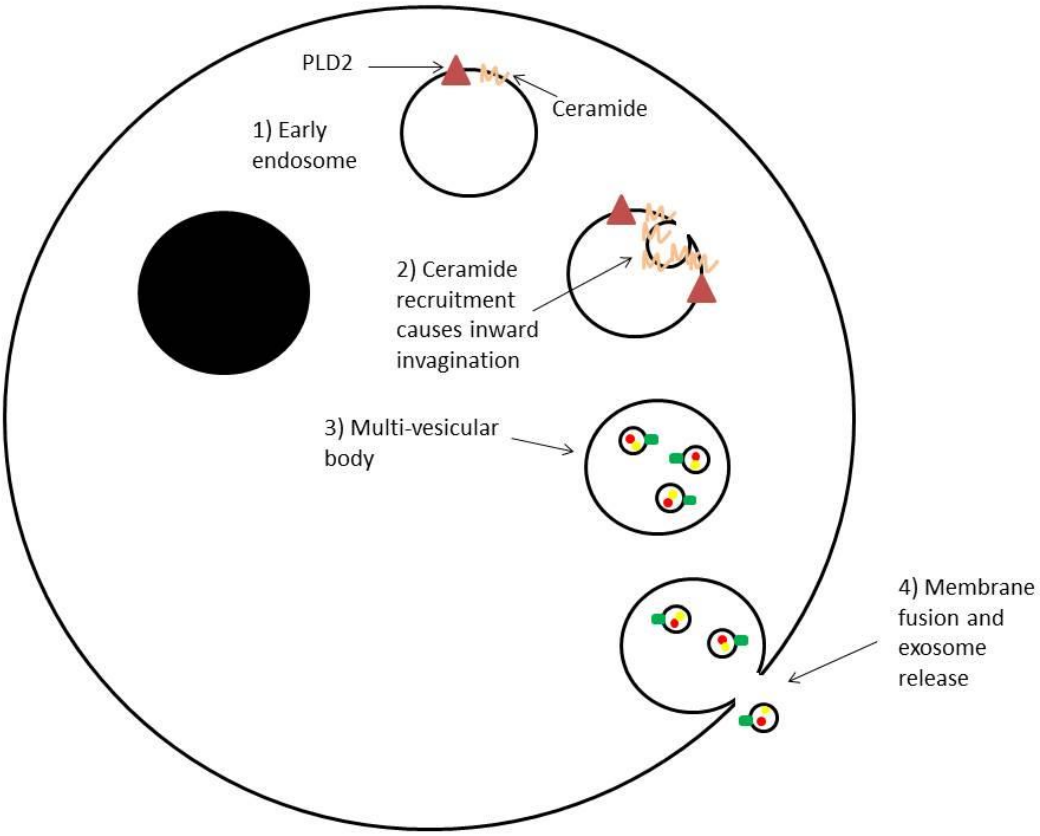

Figure 1.6 ESCRT-independent formation of vesicles and their subsequent release. The process is initiated by changes in lipid membrane composition at the site of invagination with an increase in PLD2 and ceramide concentration (1) the properties of the membrane are altered driving inward curvature at this point it is assumed that proteins like VAMP and SNAREs will be involved in completing the formation of the vesicles within the MVBs (2 & 3). After their formation the MVBs can fuse with the plasma membrane and release their contents from the cells.

1.3.8.2. ESCRT - independent mechanisms

ESCRT - independent mechanisms for exosome production are less well characterised, but mammalian cells lacking key ESCRT components can still form MVB and exosomes (Stuffers et al., 2009). These mechanisms are thought to rely on lipids and are frequently studied using disruption of lipid biogenesis. In oligodendroglial cells, inhibiting neutral sphingomyelinase reduces production of ceramide. Ceramide is hypothesised to induce the characteristic curvature of the membrane in MVBs that leads to exosomes (Trajkovic et al., 2008). Like ceramide, cholesterol is abundant in exosomes and an important component of MVB. In the same oligodendroglial cells its accumulation, mediated either by drugs or genetic mutation, causes an increase in vesicle secretion (Strauss et al., 2010). Another candidate is phospholipase D2 (PLD2) which is enriched in exosomes and has been shown in two different cell lines to be required for exosome biogenesis (Baietti et al., 2012; Laulagnier et al., 2004). It is believed to play a similar role to, or work in concert, with ceramide in facilitating inward curvature of the membrane in the early stages of exosome formation. Studies of ESCRT independent pathways for the biogenesis of exosomes are hampered by the major contributions of key lipids. Because cellular membrane is comprised of the same components, albeit in different proportions, it is highly likely that disrupting the synthesis of one of these components alters the plasma membrane stability possibly leading to an increase in the numbers of vesicles formed by direct budding of the plasma membrane. Until a reliable method for separating the classes of vesicle is available this problem will remain.

The same issue is highlighted by a study which focuses on the regulation of exosome secretion. RAB-27a, a member of the abundant GTPase family, has been

shown to be the leading regulator of exosome secretion. However, it's silencing in mouse tumour cells revealed the presence of different subpopulations of vesicles obtained from the standard extraction protocols (Bobrie et al., 2012). Its silencing led to reduced levels of some of the accepted markers of exosomes but not others. They demonstrated neatly using electron microscopy and sucrose density gradients that this was caused by the presence of different populations with diverse physical properties and possibly different origins (Bobrie et al., 2012). This issue is one facing all researchers in this field, with extraction protocols currently unable to separate vesicles of different origins the possibility of the different subpopulations of vesicles playing different roles cannot be eliminated. The RAB family of GTPases has numerous members implicated in control of exosome secretion including 2B, 5A, 9A, 11, 35, and both 27A and B they are thought to function by blocking the release of vesicles from the cell (Kowal et al., 2014). However, there is still work required to clarify this and to clarify the proportion of the effects caused by changing exosome secretion as opposed to other secretion mediated by RAB proteins. SNARE proteins like VAMP-7 and 8 as well as SNAP-23 have been shown to play a role in calcium ion - mediated fusion of other secretory bodies with the plasma membrane (Puri and Roche, 2008; Rao et al., 2004; Tiwari et al., 2008) and targeting of these in combination with or independently of RAB proteins could help with solving this problem.

1.3.9. Formation of microvesicles and large oncosomes

Both these EV subtypes form from the outer plasma membrane of a cell as opposed to the internal membranes. Whilst some of the processes are similar there are some subtle differences. Many of the conditions required for the formation of EVs from

the outer membrane come under the control of the enzymes responsible for regulating the fluid state of membranes (Singer and Nicolson, 1972). These changes are thought to be induced by changing calcium ion levels which are required by scramblase and floppase type enzymes. Once these are activated they begin to modify the lipid arrangement within the plasma membrane (Piccin et al., 2007), a major change is the externalisation of phosphatidylserine (PS) (Lima et al., 2009). Cholesterol is another major player in this process as shown by its depletion impairing the production of EVs from monocytes (Del Conde et al., 2005). This is likely to be linked to the recruitment or formation of lipid raft domains which are seen to be abundant in these microvesicles. These changes to the lipid composition make the membrane more amenable to the curvature necessary to form EVs (figure 1.7).

It is at this juncture that proteins are likely to play their part. One such protein could be Ras homolog gene family, member A (RhoA) a small GTPase which together with some downstream kinases have been identified as regulators of microvesicle release (Li et al., 2012). Other proteins including ADP ribosylation factor 6 (ARF6) (Muralidharan-Chari et al., 2009), calpain a cytoskeletal regulator which is calcium-dependent (Crespin et al., 2009), and Ras homolog gene family, member C (RhoC) (Cussac et al., 1996) have all been studied in the context of microvesicle release. However, there is a distinct issue facing scientists when trying to elucidate the mechanisms responsible for forming these vesicles subtypes, that of reliably ensuring a pure preparation of a single subtype. In the experiments that have identified RhoA as a potential regulator of microvesicle release the vesicles were isolated by serial centrifugation culminating in a spin at 100,000 x *g* speeds at which a mixed population of vesicles will be pelleted (Li et al., 2012). The study that linked ARF-6 to

microvesicle formation by contrast performed experiments on a population of vesicles pelleted at 10,000 x *g* as well as the 100,000 x *g* population (Muralidharan-Chari et al., 2009). Whilst this is a commonly seen approach to separate “microvesicles” and “exosomes” it is still slightly flawed as there will inevitably be some crossover of subtypes in the two different pellets. Unfortunately, at this stage a better approach to solving this problem has yet to be found by the EV community but it does highlight the extreme importance of a robust system of definitions being adhered to.

The term oncosome has been used by a variety of groups to distinguish EVs derived from cancerous cell or biofluids. More recently the term large oncosomes has been used to describe a potentially new subset of EVs. These large oncosomes are around 1-10 μm in size and released from the outer membrane of cancer cells (Di Vizio et al., 2012; Minciacchi et al., 2015; Morello et al., 2013). Formation of these large EVs is thought to be linked to the amoeboid phenotype; this is adopted by invading cancer cells to overcome problems with breaking down surrounding matrices (Wolf et al., 2003). Cells with this phenotype have a membrane highly prone to blebbing which is under the control of RhoA and Rho-associated protein kinase (ROCK), both of which are linked to microvesicle formation (Oppel et al., 2011). This blebbing is the precursor to formation of large oncosomes. After treatment with EGF prostate cancer cells were seen under live microscopy to enter an amoeboid state and release these blebs as intact vesicles (Di Vizio et al., 2009). Because they are formed from the membrane of cells in an amoeboid phenotype their formation is likely to be dependent on proteins that regulate both mechanisms such as diaphanous related formin 3 (DIAPH3) (Hager et al., 2012) and ARF6, which is highly abundant in large oncosomes (Di Vizio et al., 2012).

Microvesicle formation

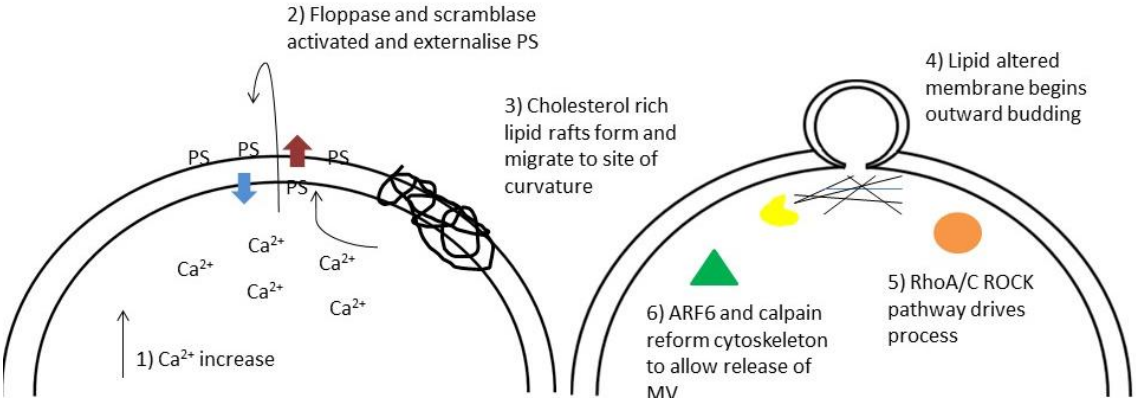

Figure 1.7 A possible mechanism of microvesicle formation with the initial changes in lipid membrane composition driven by calcium-dependent floppase and scramblase enzymes (1-3) allowing the outward budding which is then probably chaperoned by a number of proteins under the control of RhoA/C ROCK and ARF6 signalling (5-6). The final steps involve cytoskeletal remodelling mediated by calpain to remove the vesicle and reform the lipid bilayer behind it.

1.4. Packaging of EVs

1.4.1. Proteins

From their initial discovery there has been increasing evidence indicating the presence of some guiding system behind the packing of these EVs. But while there are several steps in their biogenesis at which such a system could be involved we are still some way from a definitive understanding of such a system. The studying of it is complicated by the fact cells can produce multiple distinct populations of EVs at any given point in their life cycle. For example, the colon cancer cell line LIM1863 releases two distinct populations of EVs; one that bears markers of the apical membrane and trafficking systems while the other carries markers of the basolateral membrane and trafficking systems (Tauro et al., 2013). It is likely that similar systems exist in other cells and given the 3D cell spheroid model system used in this study it is highly possible that a contact-based mechanism could play a role in determining vesicle contents although as yet there has been no evidence for such a mechanism. This work also highlights one of the weaknesses common to much of the work done in this area; many laboratories work with cells in a 2D culture system and as such the cells and by extension the EVs are likely to show differences between *in vivo* and *in vitro* conditions. However even 3D culture models will have their limitations, most cells exist in vivo in close proximity to or even contact with other cells, 3D culture with multiple cell types would obviously not be a practical system to study EVs.

Whatever the subclass of EVs their biogenesis begins with changes in the membrane. Lipid rafts are good candidates for sorting these regions and the membrane proteins within them. GM1, Lyn, flotillin-1 and stomatin all of which have been

associated with lipid raft domains have been detected in EVs (de Gassart et al., 2003). The study went on to demonstrate that the Lyn found in the EVs is further processed post-sorting by caspase-3. The fact post-translational modification is occurring in the EVs is compelling evidence for the presence of a deliberate packing process. Lipid rafts are known to associate with numerous protein types and the idea that rafts change the membrane properties allowing the curvature characteristic of vesicle formation would suggest that whole rafts are incorporated into EVs bringing with them their anchored proteins (de Gassart et al., 2003).

Post-translational modification of proteins by ubiquitination is a common method for cells to divert proteins into degradation processes (Hicke., 2001). After ubiquitination the proteins are packaged into EVs formed in MVBs with the help of the ESCRT complexes. Some of these EVs will follow the normal degradation pathway and be trafficked to the lysosome while others could be released from the cell as exosomes. Research on the ubiquitination status of EV proteins shows that major histocompatibility complex class II (MHC-II) complexes are not ubiquitinated, (Gauvreau et al., 2009) suggesting that two mechanisms for loading these proteins into MVBs exist. Further work has shown that in immature dendritic cells a ubiquitin-dependent method is used, and the receptors are degraded. After the cells have been activated however, a ubiquitin independent method is used, and the cells release EVs bearing the MHC-II complex that can interact with T cells (Buschow et al., 2009). In dendritic cells at least, the ubiquitination status of a protein appears to be sufficient to determine the fate of the vesicle containing that protein.

However, this is not the case for all proteins or all cells. Epstein Barr virus (EBV) protein LMP2A is highly ubiquitinated in exosomes (Ikeda and Longnecker, 2007) and the Nedd4 family interacting protein 1 which aids in the ubiquitination of proteins that cannot be bound by certain ubiquitin ligases is required for the Nedd4 family proteins to be present in exosomes (Putz et al., 2008). In cases such as these where the proteins are ubiquitinated prior to loading into MVBs it is likely that a second signal is present either on the protein to determine which vesicle type it is packaged into or on the surface of the vesicle that distinguishes those that head to the lysosome from those which are released.

A candidate for this second signal is phosphorylation, another common protein modification which has also been implicated in selecting proteins destined for EVs. In Alzheimer's disease the tau protein is aberrantly phosphorylated and then added to EVs which facilitates its spread (Saman et al., 2012). This would suggest that there are other parts to this system, possibly proteins that bind preferentially to the aberrantly phosphorylated tau protein to manipulate it into place within the EVs. A recent study has identified another fascinating possibility: They observed the common vesicle markers CD63 and CD81 co-localizing on the cell membrane with complex N linked glycans and then demonstrated that the same N linked glycans were necessary for the presence of a CD81 associated protein and subsequently the presence of CD81 in these EVs (Liang et al., 2014). The hypothesis they put forward, that the glycans identify discrete membrane domains that give rise to EVs, links well with the earlier work on lipid rafts. Proteins could then be directed to these domains by glycosylation or other modifications and either integrated into the membrane or anchored to it prior to the inward curvature.

Several less conventional processes for the sorting of individual proteins have also been reported to date. The degradation of the AP2 adaptor complex drives the binding of heatshock protein 70 (HSC70) and Alix, both commonly found in EVs, to a site on the transferrin receptor prior to it being sorted into EVs (Géminard et al., 2004). Interestingly this study actually identifies a peptide sequence on the transferrin receptor with which both proteins can interact, and this sequence encompasses the internalisation sequence for this receptor. In B cells the sorting of CD23, another membrane protein, into exosomes was shown to be dependent on both CD23 sheddase and a disintegrin and metalloproteinase domain-containing protein 10 (ADAM10). These enzymes act together to cleave the CD23 from the membrane prior to its entry to the endosomal sorting pathway (Mathews et al., 2010).

A recent study has identified the KRas mitogen activated protein kinase kinase (MEK) signalling pathway as being responsible for regulating the sorting of argonaute 2 (Ago2) into exosomes from colon cancer cells (McKenzie et al., 2016). Ago2 is a critical component of the RNA induced silencing complex (RISC) and can bind to RNA. Ago2 sorting into exosomes regulates in turn the levels of three candidate miRNA sequences (McKenzie et al., 2016). Whilst neither KRas or MEK are the actual mediators of the sorting the fact they are involved in its regulation is highly significant for cancer research as mutations to either or both genes are common to many cancers suggesting by extension a mechanism by which vesicle packaging can be altered in cancerous cells compared to normal cells.

1.4.2. Nucleic acids

Like protein sorting, despite the circumstantial evidence for a sorting process for nucleic acids into EVs the details of such a process are still scarce. A limited study using differing serial centrifugation protocols to separate the different subclasses of EVs by size alone identified differences in the RNA profiles of the subclasses. Their data, whilst allowing for the limitations of the method, is interesting. They showed that apoptotic bodies contained large quantities of ribosomal RNA whereas exosomes contained very little and microvesicles contained little or no RNA (Crescitelli et al., 2013). These differences not only indicate the presence of a sorting mechanism but also offer hope for distinguishing between the EV subclasses in the future. Although they went on to note that the EVs displayed significant variation in size and appearance under electron microscopy even within the same size brackets. This would suggest either that cells are producing different types of each subclass at any given point in time or that the size of EVs is not strictly controlled during their release. A similar study carried out on EVs produced by a panel of prostate cancer cell lines showed that the genomic DNA content varied between cell lines and within subpopulations (Lázaro-Ibáñez et al., 2014).

It has been hypothesised by several groups that a signalling motif exists in RNA destined for EVs that are released from the cell; this hypothesis was recently proved for miRNA. The group used microarray analysis to identify miRNA enriched in EVs compared to the whole cell and then performed sequence alignment to identify conserved regions to each set. They were able to identify two four base pair motifs (GGAG and CCCU) that were common to the miRNAs enriched in the EVs alongside several longer motifs that were common to miRNA enriched in the cells (Villarroya-Beltri et al., 2013). Using site directed mutagenesis they were able to subsequently

reverse the enrichment of miR-601. They went on to demonstrate that the ribonuclear protein hnRNPA2B1 could recognize this motif and was responsible for packing these miRNA into the EVs when sumoylated (Villarroya-Beltri et al., 2013). This is a huge landmark for the field of EV research, it has given us the first part of a system that we can exploit for medical purposes or use to help map the rest of the system in detail for the first time.

An alternative mechanism was proposed by another group. This group approached the sorting from a homeostatic approach, demonstrating that an abundance of the target for a given miRNA leads to its depletion in MVBs and exosomes whereas overexpression of the miRNA itself leads to it being enriched in MVBs and exosomes (Squadrito et al., 2014). This suggests that EVs actually do function as a form of waste disposal, albeit one that mostly functions in response to stress caused by artificially driven overproduction rather than during maturation as was seen with the transferrin receptor.

1.4.3. Lipids

Whilst their formation and size differ, the lipid membrane composition of these EVs is similar and often reflects the producing cell. The cholesterol to phospholipid ratio of the vesicular membrane is similar to that of the plasma membrane (Vidal et al., 1989), however there are some major differences. The lipid bilayer of these EVs is typically enriched for cholesterol, sphingomyelin, ceramide (Laulagnier et al., 2004; Trajkovic et al., 2008) and PS but interestingly not lysobisphosphatidic acid which is typical of the intraluminal vesicles of MVB where exosomes are formed (Brouwers et

al., 2013; Karine Laulagnier et al., 2004; Llorente et al., 2013; Wubbolts et al., 2003). The particular distribution of the lipids in the vesicle membrane is highly characteristic of lipid rafts and these domains have been linked to the production of exosomes (Matsuo et al., 2004). Another study used the membrane analysis techniques fluorescence anisotropy, nuclear magnetic resonance and electron spin resonance to compare the physical properties of EV membrane with plasma membrane. They discovered that despite the similarities in major contents, the membrane of these EVs has different properties; it appears to be more fluid with a very rapid "flip-flop" between the membranes (Brouwers et al., 2013).

As the life cycle of a cell progresses its needs change and it is reasonable to assume that the EVs produced will change accordingly. A study that followed exosome production by maturing reticulocytes showed that their physical properties changed throughout the maturation period. By the end of the seven-day period the cells produced fewer exosomes that were around 10% larger than earlier days (Carayon et al., 2011). They also observed differences in the lipid composition of the exosomes, with those produced at day 2 having a four times higher ratio of cholesterol esters to free cholesterol when compared to those from day 4 and 7 (Carayon et al., 2011). It is possible that similar changes occur in other models, but this has not yet been reported.

1.5. Uptake of EVs

There are a variety of well-established mechanisms by which materials from the extracellular spaces can be internalised across the plasma membrane of a cell. Interestingly the uptake of EVs appears to make use of nearly all of these. Endocytosis

is a well-studied process that involves the cell engulfing the molecule in an energy intensive process. Because it relies on the expenditure of energy its involvement with EV uptake can be simply tested by incubating the cells at 4^{o}C (Christianson et al., 2013; Escrevente et al., 2011), which shows that internalization of EVs is dramatically reduced by this step. There are different types of endocytosis, one of these is clathrin mediated. Clathrin is a well-characterised protein that forms a triskelion shape made up of three heavy and three light chains. These chains assemble together to form a coated pit which deform the cells membrane until it collapses into a vesicular bud. The vesicular bud will then pinch off; now inside the cell it is uncoated and fuses with the endosome releasing its contents (Kirchhausen, 2000). Blocking of this process either by treatment with chlorpromazine (Escrevente et al., 2011) or inhibition of dynamin2 (Vallee et al., 1993) was shown to reduce the uptake of EVs. There are also clatherin-independent pathways; one of these relies on caveolae. Caveolae are small depression in the outer membrane formed by the protein caveolin-1 (Doherty and McMahon, 2009). the silencing of this protein was shown to impair the uptake of EVs in one experiment (Nanbo et al., 2013) but in another set up was seen to increase the uptake of EVs (Svensson et al., 2013). The reasons for this duality are unclear, whilst it indicates the potential for some flexibility in this system, it also could suggest that in some cells the silencing of caveolin-1 causes changes to the membrane composition, possibly lessening its rigidity, that make the uptake of EVs more efficient.

Macropinocytosis is another endocytic pathway, albeit a dramatically different one. The membrane forms large distinctive protrusions from the cell surface these can then surround an area of the extracellular space which is then internalized either by direct fusion with the plasma membrane or by fusion with another protrusion (Swanson,

2008). As with the other mechanisms researchers have blocked this process by the inhibition of Na+/H+ exchange or by small molecule inhibitors of ras-related C3 botulinum toxin substrate (rac-1) 1) (Fitzner et al., 2011) both of which have reduced EV uptake by microglia. However, there are other studies using different inhibitors that have found no impact on EV uptake (Christianson et al., 2013; Feng et al., 2010; Nanbo et al., 2013).

Phagocytosis is a highly specialised form of endocytosis that is normally associated with the internalisation of large objects like bacteria by macrophages. However, an interesting study with leukaemia cell-derived EVs showed that they could only be taken up by macrophages and not other cells suggesting this is occurring by phagocytosis (Feng et al., 2010). Further experiments using inhibitors of phosphoinositol 3 kinase (PI3K) (Feng et al., 2010), to stop phagocytosis, and EVs stained with the pH sensitive dye pHrodo, which can visualise them inside the acidic phagosomes, (Montecalvo et al., 2012) confirm a role of phagocytosis in uptake of EVs.

Because of the fluid properties of membrane, it is also possible that EVs can be taken up by direct fusion with the plasma membrane. Direct fusion between two lipid bilayers can occur readily in an aqueous environment and this process can be visualised by fluorescent lipid dequenching. Experiments using this technique have shown the possibility of some EV uptake via this pathway (Parolini et al., 2009) it is likely that this mechanism owes much to the lipid raft like membrane composition of EVs (Valapala and Vishwanatha, 2011). What is clear however is that this is a pH-dependent process which is likely to limit its capacity under physiological conditions (Parolini et al., 2009).

It is apparent from the range of research being done that there is no one pathway responsible for EV uptake. There is good, albeit at times contradictory, evidence for each of them being involved in EV uptake. There are a few reasons why this isn't a simple question to answer. The first lies in the limitations of the tools available to researchers to study this. Uptake of EVs can be visualised using a range of lipophilic or carboxyfluorescein succinimidyl ester (CFSE) dyes which whilst very stable can potentially introduce artefacts. The lipophilic PKH dyes in particular will form micelles in organic material. Another possible approach to visualising EV uptake is to use fluorescence tagged versions of marker proteins, whilst these are highly specific there are two uncertainties. First there is an uncertainty over whether every EV in your sample will carry that protein and second there is the uncertainty over whether the addition of a bulky fluorophore will change the behaviour of the tagged protein. Currently without super resolution adaptation the physical resolution of fluorescence microscopy is also inadequate to resolve an individual vesicle meaning that unless they aggregate, or the dye diffuses throughout the receptor cell the quantification of the uptake will not be accurate.

Aside from the technical difficulties there are two different but overlapping problems introduced by the nature of the EVs themselves. It is possible that different populations of EVs are taken up preferentially by different routes depending on the cell type they are docking with. This is probably mediated by protein/protein or protein/ lipid interactions between the EV and the target cell. If this is the case then manual transfer of EVs between 2D culture models is going to create a few issues. Firstly, any EV sample will contain multiple subtypes and secondly, they may not be delivered in either a physiologically relevant dose or to an appropriate cell type leading to the cells

taking them up in ways they wouldn't normally do so or less efficiently than other cells.

1.6. The role of EVs in normal processes

To date EVs have been found in a range of biological fluids including: urine (Sato et al., 1990), saliva (Palanisamy et al., 2010), synovial fluid (György et al., 2012), cerebrospinal fluid (Marzesco et al., 2005; Street et al., 2012), bronchialveolar fluid (Admyre et al., 2003), nasal fluid (Lässer et al., 2011), uterine fluid (Al-Dossary et al., 2013; Griffiths et al., 2008), amniotic fluid (Keller et al., 2007), breast milk (Lässer et al., 2011b), blood (Chargaff and West 1946; Wolf, 1967) and seminal plasma (Saez et al., 2003). The fact that EVs have been discovered in such a wide range of fluids in healthy individuals indicates a variety of roles in normal processes. The EVs in urine like those initially found in blood were suggested to be involved in the disposal of unwanted proteins and lipids from the cell (van Balkom et al., 2011) but it is also possible that they can signal along the nephrons (Knepper and Pisitkun, 2007).

In saliva EVs have been shown to contain tissue factor and can initiate blood clotting of vesicle free plasma (Berckmans et al., 2011), which led to the interesting suggestion that these EVs could be an evolutionary keepsake where licking a wound initiates the healing process. EVs from synovial fluid have been shown to carry functional integrins which can mediate anchorage to cell surface adhesion molecules and possibly deliver autoantigens (Skriner et al., 2006). In the male reproductive system proteins are transferred by EVs to the immature sperm cells during their transit through the epididymis (Sullivan et al., 2005). There are many hypothesised roles in mother-foetal communication and placental organization currently being explored; immuno-

competent EVs have been discovered in breast milk raising the possibility of a role in conferring viral resistance (Admyre et al., 2007).

EVs have long been studied in the context of coagulation and the increased formation of platelet-derived EVs have been shown to enhance thrombin generation and induce thrombosis in different experimental conditions (Chen et al., 2013; Suades et al., 2012). The immune system seems to make extensive use of EVs with mature dendritic cell derived EVs being potent inducers of antigen specific immune responses (Segura et al., 2005). A similar role has been observed with keratinocyte derived EVs in mice (Kotzerke et al., 2013); while T-regulatory cells produce EVs that contain miRNA capable of suppressing pathogenic T-helper cells (Okoye et al., 2014). In recent years it has also become apparent that EVs are an important aspect of the interactions between a foetus and a mother during pregnancy (Arck and Hecher, 2013; Chua et al., 1991) with dysregulation in this process linked to preeclampsia and miscarriages. In lung injury EVs derived from marrow cells can modulate the expression of prosurfactant B in marrow cells starting the repair of this process (Aliotta et al., 2007).

Bone calcification is another area in which EVs have been investigated for many years, our current understanding suggests that these EVs originate from the plasma membrane of mineral forming cells and can then go on to induce calcification during endochondral bone formation (Golub, 2009). These EVs contain and can transfer bone morphogenetic protein, VEGF and bone sialoprotein (Nahar et al., 2008). EVs from hepatocytes have also been shown to transfer proteins in liver (Conde-Vancells et al., 2010, 2008). This signalling has been shown to function both in the cases of liver damage (Royo et al., 2013) and in normal cellular proliferation (Lee et al., 2008).

1.6.1. Role of EVs in disease states

With such a wide and varied number of roles within the human body it is inevitable that EV signalling and its dysregulation will play a part in different disease states.

1.6.1.1. Cardiac disease

Following a myocardial infarction, EVs from cardiac progenitor cells have been shown, by transfer of conditioned media from cardiac progenitor cells with and without EVs, to limit the damage by inhibiting cardiomyocyte apoptosis thereby improving the heart's ability to function (Barile et al., 2014). They also play a role in mediating the cytoprotective action of mesenchymal stromal cells in response to hypoxia induced pulmonary hypertension (Lee et al., 2012). However, during myocardial ischemia EVs are produced bearing the hypoxia inducible factor-1α (HIF-1α) which initiates the production of TNF-α by macrophages which is damaging to the cardiomyocytes (Yu et al., 2012).

1.6.1.2. Neurological diseases

In neurological pathologies EVs have been implicated in a variety of roles. Most recently they have been shown as a mechanism for the release of prions (Arellano-Anaya et al., 2015). The EVs released by prion infected cells have been shown to have distinctive structural differences when compared to normal EVs with an increased number of membranes and a larger diameter (Coleman et al., 2012). EVs have also been linked to Alzheimer's disease, astrocytes release highly pro-apoptotic EVs(Wang et al., 2012) driving the later phase of the disease, but they have also been shown to have a role in clearing the amyloid-β fibrils (Yuyama et al., 2012). In Parkinson's disease EVs

have been shown to transfer α-synuclein helping to spread the disease through the central nervous system (CNS) (Boelens et al., 2014) and a similar phenomenon is seen in amyotrophic lateral sclerosis with the transfer of superoxide dismutase -1 (SOD1) (Gomes et al., 2007).

Multiple sclerosis (MS) is another neurological condition where EVs involvement is well studied. In MS EVs can both disrupt the blood brain barrier which allows the migration of inflammatory cells into the CNS and induce the migration of those inflammatory cells (Jy et al., 2004; Sheremata et al., 2006). Additionally, these EVs are found in the plasma of patients during relapses offering a potential prognostic marker (Sheremata et al., 2006). There is also some evidence beginning to appear that links EVs to strokes, with a raised level of EV release from activated endothelial cells being correlated with ischemic events and neurological damage in patients (Lee et al., 2012).

1.6.2. Role of EVs in cancer

1.6.2.1. Anti-tumorigenic effects

EVs appear to be similarly duplicitous and flexible in their functions in cancer development with research revealing both pro and anti-tumorigenic properties and traits. This is to be expected if cells are producing different types of EVs at different stages of their life cycle and in response to different stimuli or changing conditions in the surrounding environment.

1.6.2.1.1. Immune activating effects

In vitro studies have shown that EVs produced by melanoma cell lines contain antigens which can exert a potent effect on dendritic cells upon their uptake causing

CD8+ T cell dependent anti-tumour effects in established murine tumours (Wolfers et al., 2001). This discovery has actually led to a dendritic cell-based immunotherapy model being investigated. It is however extremely peculiar that a cancer cell would produce EVs capable of mobilising the immune system against them in such a way and it is doubtful that these EVs are constitutively secreted. A likely explanation for this could be they are released for a short window during which dendritic cells attract the T cells into the tumour microenvironment to support angiogenesis and once there they produce a signal to stop the production of those EVs to stop them exerting an anti-tumour effect.

1.6.2.1.2. Induction of apoptosis

The other major anti-tumorigenic role of these EVs is induction of tumour cell apoptosis. Pancreatic tumour cells produce EVs that are reported to increase Bax expression whilst decreasing BCL-2 expression, driving tumour cells towards the mitochondrial apoptotic pathway (Ristorcelli et al., 2009). Another anti-survival effect of this interaction is decreased expression of the intra-nuclear target of the Notch-1 signalling pathway and activation of the apoptotic pathway (Ristorcelli et al., 2009). The production of EVs capable of decreasing their own proliferation is an extremely puzzling trait for a cancer cell to possess, however it is possible that these EVs aren't intended to target other tumour cells *in vivo*, but to target cells of the immune system but with the absence of these targets *in vitro* are being taken up by the tumour cells.

1.6.2.1.3. Therapy vehicles

There are other more indirect ways in which EVs can have anti-tumorigenic effects. One of these is as a drug delivery vehicle, EVs being lipid enclosed and potentially generated from a patient's cells, are an attractive prospect for a drug delivery vehicle and this review (Tominaga et al., 2015) gives a nice summary of the range of compounds that are currently being studied or have already been successfully loaded into EVs. One of the more interesting studies has been performed with curcumin, experiments that deliver this drug encapsulated in EVs show it to have a significantly improved absorption and bioavailability over unencapsulated curcumin (Sun et al., 2010). This approach is now in clinical trials and has yielded promising results in pancreatic cancer patients (Gupta et al., 2013). This approach, the direct loading of drugs into EVs is one of two avenues for therapeutic delivery involving EVs.

The second is an older one based around the immunogenic capacity of exosomes released from dendritic cells, a field summarised well by the review of Chaput et al. (2006). It is based around the ability of dendritic cells when challenged by tumour antigens to produce EVs that can stimulate the induction of cytotoxic T cells against the tumour (Zitvogel et al., 1998). One of the great advantages to this approach is that the treatment is uniquely tailored to an individual patient using their own cells to generate a personalised vaccine against their own tumour removing immunogenicity issues and optimizing efficiency. This concept has been proved on a scale suitable for medical application and has led to clinical trials in both melanoma and lung cancer patients with mixed results (Escudier et al., 2005; Morse et al., 2005).

1.6.2.1.4. Biomarkers

A simple search on PubMed for EVs and biomarkers reveals that there are nearly 2000 papers on the subject and 1500 of these have been published since 2009. Whilst this rapid expansion owes much to improving technology it is also partly a result of the changing environment in cancer therapy today to place a greater emphasis on personalised treatment. Because EVs are produced by cancer cells and are found in biological fluids they have huge potential as both diagnostic and prognostic markers. In oral cancer for instance the availability of EVs in saliva offers the tantalising prospect of a "liquid biopsy" where a simple saliva sample could replace the invasive excision of tissue for analysis. A recent study showed that saliva from oral cancer patients contained a higher number of EVs and that there is a limited degree of molecular differences between the EVs of healthy individuals and cancer patients (Zlotogorski-Hurvitz et al., 2016). The findings of this paper are limited by the techniques they used – namely ELISA and western blotting but other studies have begun to use mass spectrometry techniques to screen the contents of salivary EVs (Kawahara et al., 2016; Winck et al., 2015).

There are numerous similar studies using the same kind of screening of EVs from biological fluids summarised in several recent reviews (Ciardiello et al., 2016; Kinoshita et al., 2016). In the last few years a company in the US, Exosome Diagnostics, has completed clinical trials of an EV based diagnostic kit for certain brain cancers and is aiming to bring them to clinics in America in the next 12 months, the company also intends to expand its repertoire of kits into other cancers.

1.6.2.2. Pro-tumorigenic effects

Alongside these anti-tumour effects EVs have been seen to play a role in many of the hallmarks of cancer described by Hanahan and Weinberg (Hanahan and Weinberg, 2011, 2000).

1.6.2.2.1. Angiogenesis

Angiogenesis is the development of new blood vessels within the growing tumorous mass. A paper from 2002 demonstrated that EVs rich in sphingomyelin released from cancer cells could promote angiogenesis (Kim et al., 2002). More recent papers suggest that both protein and RNA species within the EVs could also play a part. Cell lines derived from both renal cancer and leukaemia have been shown to produce EVs that promote angiogenesis in endothelial cells (Chen et al., 2014; Mineo et al., 2012). The renal cancer cell derived EVs increased VEGF expression at both the mRNA and protein levels by down regulating hepatocyte cell adhesion molecule (hepaCAM), suggesting that the EVs contain a miRNA for the hepaCAM mRNA (Chen et al., 2014). The leukaemia derived EVs promoted angiogenesis via the activation of the proto-oncogene tyrosine protein kinase (Src) possibly indicating the presence of a Src binding kinase in these EVs (Mineo et al., 2012).

Cancers are characterised by rapid replication, this accelerated growth frequently leads to hypoxia as the growing cancer becomes too large for local vasculature to maintain. In a recent study researchers cultured hypoxia resistant multiple myeloma cells in a state of permanent hypoxia, they found that these cells produced a greater number of EVs than the parent cell line in similar conditions (Umezu et al., 2014). They

went on to demonstrate that these EVs contained significant quantities of miR-135b, which targets the factor inhibiting hypoxia inducible factor 1 (FIH-1) and was shown to suppress this protein in endothelial cells. This action resulted in an increase in the formation of endothelial tubes (Umezu et al., 2014). A particularly fascinating paper released in 2008 describes a novel way in which EVs can contribute to angiogenesis. In a glioma model they demonstrated that the EVs can transfer an oncogenic mutated version of the EGFR, this mutant version is associated with aggressive brain tumours but only a small percentage of cells may express this receptor (Al-Nedawi et al., 2008) those cells that do express it are shown to transfer it via EVs to those that don't. The arrival of this oncogenic receptor changes the regulation of genes under its control promoting angiogenesis. Given that this problem is common to many, if not all cancer types, it is likely that similarly capable EVs can be produced by other cancer cell lines under these conditions. However, it is worth noting that there are some studies that show EVs inhibiting angiogenesis. One study showed that miR-29a and miR-29c transferred by EVs inhibited angiogenesis in a gastric cancer model (Zhang et al., 2016). The weakness of this study is that it uses overexpression of miR-29a and c in HEK293T cells to produce EVs carrying miR-29a and miR-29c which are then transferred to gastric cancer cells. Whilst there may be some of these RNA species in non-engineered EVs in the TME it may not be present in sufficient quantities to drive these changes.

1.6.2.2.2. Immune evasion and suppression

As discussed previously, cancer cell EVs provide a range of tactics for immune activation. Perhaps characteristically, other tumour vesicle types have been shown to have immuno-suppressive roles; melanoma and colorectal cancer cell derived EVs

contain the death ligands: factor related apoptosis ligand (FasL) and TNF related apoptosis inducing ligand (TRAIL) which can trigger the apoptotic death of activated T cells (Andreola et al., 2002; Huber et al., 2005). Ovarian tumour derived EVs can also impair T cell receptor signalling through down regulation of CD3-ζ chain expression impairing T cell mediated immune functions (Taylor et al., 2003). In mice with OVA-expressing tumours the immune responses could be suppressed by MHC class II bearing EVs produced by the tumour cells (Yang et al., 2012).

Lymphoblastoid cell lines were also shown to produce "killer" EVs containing the Fas ligand and bearing the MHC class II allowing them to reduce T cell responses by inducing apoptosis in these cells (Klinker et al., 2014). A subtler approach is adopted by prostate cancer cell lines, which produce EVs bearing ligands for the NKG2D receptor on their surface allowing them to down-regulate NKG2D and its cytotoxic response in natural killer cells and CD8+ T Cells in a dose dependent fashion (Lundholm et al., 2014). In cervical cancer, EVs are produced bearing ectonucleotidases, which hydrolyse adenosine phosphates to release adenosine, these can then suppress the proliferation and activation of cytotoxic CD8+ T cells *in vitro* by production of large amounts of adenosine (de Lourdes Mora-García et al., 2016). Another recent paper demonstrates a similar ability in leukaemia but again one mediated by a different mechanism; in this case EVs produced by leukaemia cells carry both the tax oncoprotein and a range of miRNA which activate nuclear factor kappa B (NF-κB) and cause an increase in the induction of apoptotic markers (El-Saghir et al., 2016). The range of mechanisms used by cancer cell derived EVs to reach the same objective is a real insight into the extent of cancers exploitation of this system.

1.6.2.2.3. Suppression of apoptosis

Like immune evasion the bypassing or prevention of apoptosis is another necessary step for a developing tumour. Extracellular survivin is a potent apoptosis inhibitor and has been shown to be released in EVs produced by HeLa cells following irradiation to trigger a stress response (Khan et al., 2009). Bladder cancer cell lines were shown to produce EVs capable of inhibiting apoptosis in a more complex fashion, they upregulated synthesis of B cell lymphoma 2 (Bcl-2) and cyclin D1 whilst reducing the levels of Bax and caspase 3 suggesting a mixture of mRNA and miRNA for the affected proteins being present in the EVs (Yang et al., 2013). It is worth considering that these responses are likely to be triggered by stress stimuli like hypoxia and that the production of proteins such as survivin will be critical to the survival of the producing cell. The release of this hard-won advantage into the extracellular space in EVs seems like a waste of work by the cell; however, the picture is not as simple as one cell, or a small group, of them fighting to avoid apoptosis. Cancer cells will produce a range of different EVs creating a communal pool for all cells in the surrounding area to access. Some of these EVs will be “reserved” or targeted for certain cells. This would represent a premade source of survivin or other urgently required molecules for all cells to utilise.

When EVs released from CD133+ breast cancer cells are taken up by receptor positive cells the proliferation of these cells is increased and apoptosis following doxorubicin treatment is suppressed. However, the same effect was not observed after uptake of CD133- cells indicating a change in packaging of EVs in the different breast cancer cell lines (Shi et al., 2015). Recent data appears to show that this aspect of EVs contribution to cancer is driven by exchanging EVs between the stromal and cancer cells. Experiments with an osteosarcoma model show EVs from mesenchymal stem

cells that have been exposed to stress caused osteosarcoma cells to become more resistant to apoptosis. Further experiments showed that these EVs transfer miRNA which regulate the expression of PTK2 a versatile non-receptor tyrosine kinase with roles in cell cycle progression proliferation and apoptosis (Vallabhaneni et al., 2016). There are other examples of the signalling going in the opposite direction, EVs produced by various cancer cell lines have all been shown to activate the mitogen activated protein kinase (MAPK) pathway in monocytes which improves their survival in inflammatory conditions (Song et al., 2016). What these recent revelations suggest is that there is a reciprocal relationship between the stromal cells and the cancer cells to keep each other alive in the face of changing conditions to support the long-term development of tumour.

1.6.2.2.4. Activation of stromal cells

EV exchange between the cancerous and non-cancerous cells of a TME is not just used to keep cells alive. Cancer cells have been shown to produce EVs that activate or differentiate the surrounding non-cancerous stromal cells. In the case of fibroblasts this activation is particularly useful to the developing tumour. A single dose of EVs from prostate cancer cells was able to transform bone marrow mesenchymal stem cells or patient fibroblasts into myofibroblasts (Chowdhury et al., 2015; Webber et al., 2015). These αSMA positive cells were seen to secrete high levels of VEGF-A, HGF and MMP1,3 and 13, which enable fibroblasts to drive tumour angiogenesis, proliferation and invasion respectively (Chowdhury et al., 2015). It was demonstrated that a fraction of the total cellular TGFβ was localized to the EVs (Chowdhury et al., 2015) which enabled them to drive the myofibroblastic differentiation upon uptake.

When cells were treated with a similar dose of soluble TGFβ however the cells were seen to differentiate into morphologically similar myofibroblasts, but those cells were unable to promote angiogenesis or tumour proliferation (Webber et al., 2015) in the same way as those activated by EV delivered TGFβ. This suggests that the delivery of TGFβ to cells via EVs is either targeted to a specific subset of the fibroblast population or that because the TGFβ is delivered alongside other components its activity in the receptor cell is modified thereby allowing it to secret the beneficial proteins in sufficient quantities. It was previously demonstrated that the TGFβ is neither detectable in EVs from every prostate cancer cell line nor is it enclosed within the EVs but bound to their surface by betaglycan (Webber et al., 2010). In a more recent publication it was shown that the ability of the EV tethered TGFβ to activate fibroblasts requires the presence of heparan sulphate chains on the surface of the EVs (Webber et al., 2015). What is interesting about this data is it illustrates the importance and potential complexity of the relatively unstudied EV surface interaction with other cells and proteins. With the large variation of heparan sulphate additions possible it is likely that different chains result in a slightly different effect of the protein on the target.

Recently, large oncosomes have also been shown to activate prostate fibroblasts through AKT1 kinase activity which is specific to this class of EVs in the plasma of prostate patients (Minciacchi et al., 2017). The uptake of these large oncosomes by fibroblasts causes the AKT1 kinase to activate the MYC pathway allowing the reprogramming of the cells. In a pancreatic cancer model a similar activation of fibroblasts on EV uptake was shown to be mediated by EV delivered miR-155 (Pang et al., 2015). The fact this ability appears to be common to EVs produced by different

tumour types each of which uses different mechanisms to produce the same effect reflects how beneficial the activated fibroblasts are to the developing tumour.

1.6.2.2.5. Invasion and metastasis

Metastasis is a complex series of events that contribute to cancer cells being able to invade tissues as far as the bloodstream or lymphatic vessels and then travel to a new site and propagate again. This process can be broken down into a number of required phases many of which EVs have been shown to facilitate. The first step is the breakdown of the extracellular matrix freeing space for cells to move. Both cancer cells and neighbouring stromal cells have been shown to produce EVs that contain high levels of various protease enzymes involved in the degradation of cell-cell and cell-matrix junctions (Shimoda and Khokha, 2013). These include the matrix metalloproteinase MMP14 which is normally a membrane-bound protein, research has shown this can be released from the cells on vesicle membranes allowing them to access membranes the cell cannot reach (Hakulinen et al., 2008).

Following the breakdown of cellular junctions, the cancer cells need to be able to cross the weakened extracellular matrix requiring dramatic reorganization of the cytoskeleton, something that EVs produced by breast cancer cells have been observed doing (Wang et al., 2014). In another study in breast cancer, EVs containing miR-200 family microRNA were shown to transfer these to non-metastatic cells which led to them acquiring metastatic potential (Le et al., 2014). The miR-200 family regulates epithelial-mesenchymal transition (Yuan et al., 2014) a process where epithelial cells become less adherent and more capable of migration and one that is considered to be an

essential part of the metastatic process. Experiments in bladder cancer have identified several other miRNAs that are abundant in the EVs produced by the cells including miR-23B, miR-224 and miR-291. Further investigations have shown that blocking vesicle release by inactivation of Rab27B blocked the acquisition of metastatic properties (Ostenfeld et al., 2014). The interesting thing about this experiment is that the miRNA in question are tumour suppressing. The group's hypothesis is that in order to progress to metastasis the tumour must remove these using the vesicle export system. Obviously, this doesn't explain how EVs generated by breast cancer cells can drive the generation of metastatic traits. However, what it does reveal is the intricacies of this system, EVs containing these unwanted molecules must end up somewhere, the question of where they are going and how they are directed there is an important one for the future.

An alternative strategy has been demonstrated in a different breast cancer model, working with cancer models in orthotopic mice a group has shown that fibroblasts release EVs that cause the mobilization of Wnt-planar cell polarity signalling in the cancer cells driving metastasis (Luga et al., 2012). This is a fascinating revelation particularly as it was identified in a live animal model, but it is unlikely to be the whole story. It is highly probable that before fibroblasts release such EVs they must be reprogrammed by the cancer cells, possibly by EVs which they have produced first. A more recent paper has identified something similar in a pancreatic cancer model. However, in this model they used CAFs in culture as opposed to an animal model. They showed that these EVs containing a complex of annexin 6 LDL receptor related protein and thrombospondin 1 (TSP1) which can only form in the CAFs is necessary for the cancer cells to develop the invasive properties (Leca et al., 2016).

EVs inherent stability in the bloodstream means they can reach distant targets. This means they can potentially travel ahead of detached cancer cells and prepare the ground for their arrival. This is the “seed and soil” theory of metastasis and it is still a controversial one. Experiments in mice models have shown that EVs released by melanoma cells are targeted to the lymph nodes and trigger changes in extracellular matrix deposition and vascular proliferation, along with changes that help recruit the melanoma cells (Hood et al., 2011). Such EVs are likely to be common to other cancers too particularly those with preferential metastatic destinations like breast and prostate cancers. A recent study showed this to be partially true in metastatic osteosarcoma cells, they produced EVs which not only preferentially localised to the lungs, a major site of osteosarcoma metastases, but were also capable of increasing metastatic behaviour in poorly metastatic clones (Macklin et al., 2016). These EVs contain a range of proteins with roles in processes essential for metastasis (Macklin et al., 2016)**.** Another group has also focused on the protein contents of EVs in relation to metastasis identifying EGF-like repeat and discoidin I-like domain-containing protein 3 (EDIL3) as being critical for the acquisition of invasive properties of breast cancer cells and accelerating lung metastasis *in vivo* (Lee et al., 2016).

1.6.2.2.6. Drug resistance

The final major role these EVs can serve in cancers is supporting drug resistance. This can be acquired through a variety of mechanisms and EVs have been shown to both directly play a role in the resistance and act to transfer this resistance through the tumour environment. Studies in platinum resistant ovarian cancer cells have shown that

in response to cisplatin treatment cells dramatically increase their production and release of EVs and the EVs contain high concentrations of cisplatin (Safaei et al., 2005). It is assumed that these EVs are designed to take the cisplatin on a one-way trip possibly to be removed in the urine. Such a mechanism could be present in other cancer cells as a response to other drugs but has not yet been seen. Another method of EVs aiding in resistance is seen with the antibody-based Herceptin (trastuzumab). Human epidermal growth factor receptor 2 (HER-2) overexpressing tumour cell lines have been shown to release EVs with a full length and active form of the HER-2 molecule on their surface capable of binding the trastuzumab in place of the target cells (Ciravolo et al., 2012). Although it hasn't been seen with other similar treatments, all antibody-based therapies will be vulnerable to a similar mechanism.

Vesicle transfer has been shown to confer resistance across a population in several models to date. In prostate cancer docetaxel resistant cells can transfer resistance to both docetaxel and doxorubicin sensitive cells. This is thought to be via transfer of the multidrug resistance protein 1 (MDR-1)/P-glycoprotein (P-GP) transporter (Corcoran et al., 2012). Vesicle mediated transfer of docetaxel resistance has also been studied in breast cancer models with one group implicating the transfer of miRNAs notably miR-100 miR-222 and miR-30a. Interestingly one of the pathways these miRNAs are involved in is membrane vesiculation (G. Chen et al., 2014; Mineo et al., 2012). The implication of this is that increased vesicle production is involved in the resistance to the drug in a similar fashion to ovarian cancer cells and cisplatin. The same group has also identified the vesicle-mediated transfer of P-GP transporter to sensitive cells as a mechanism of conferring resistance (Lv et al., 2014) P-GP is a membrane protein transporter capable of transporting drugs rapidly out of the cell.

Transfer of resistance is not just limited to cancer-to-cancer cell transfers. Normal cells have been shown to gift cancer cells with resistance through vesicular transfer of miRNA and proteins. In a model using multiple myeloma cells and bone marrow stromal cells EVs produced by the stromal cells promoted several pathways including p38, p53, protein kinase B (AKT) and c-Jun N-terminal kinase, all of which are linked to survival (Wang et al., 2014). The group offers three possible explanations for this effect: the presence of ligands for anti-apoptotic pathways on the surface of the EVs, the presence of whole receptors for these pathways in EVs, or the direct transfer of transcription factors miRNA or mRNA for pro-survival genes by EVs. This latter method is used by mesenchymal stem cells to transfer functional anti-miR-9 to glioblastoma cells (Munoz et al., 2013), which causes the miR-9 suppression of P-GP to be reversed allowing the transporters to export temozolomide.

In situations like this where the surrounding normal cells are delivering essential components to cancer cells it is likely that a currently unseen transfer occurs from the cancer cells to the normal cells first. This transfer would change vesicle production in the normal cell altering the contents and any targeting on the surface along with the number produced to meet the demands of the cancer cells. It is also probable that the components being transferred by normal cells are produced in higher quantities or are not possible for the cancer cells to produce themselves. A recent publication reveals data that shows transformed fibroblasts can be resistant to gemcitabine and can transfer this resistance to the cancer cells by increasing zinc finger protein SNAI1 (Snail) expression (Richards et al., 2016). CAFs are dramatically altered in comparison to normal fibroblasts and part of this alteration may include changes to vesicle secretion as is seen in the differentiation of stem cells monocytes and colon cancer cells. In a model of

differentiating stem cells and monocytes where the differentiated cells were seen to release EVs containing 14-3-3 proteins which could activate dermal fibroblasts (Median and Ghahray., 2010). Experiments in colon cancer cell lines showed treatment with sodium butyrate increased EV release (Lucchetti et al., 2017) and these EVs had different phenotypic effects on recipient cells. A study published this year identified the transfer of miR-21 from CAFs and cancer associated adipocytes. The miR-21 transferred can confer paclitaxel resistance on binding to apoptotic protease activating factor 1 (APAF1) (Au Yeung et al., 2016). As with the CAFs it is likely that the cancer associated adipocytes are altered from their normal form in ways that change EV production.

1.6.2.2.7. Extracellular vesicles and oral cancer

To date there is a limited number of studies focusing on the EVs produced or found in oral cancer. One focus of these studies is the diagnostic/prognostic potential of the EVs, having identified miR-1246 and miR-21 as potential markers of oral cancer (Takeshita et al., 2013; Tanaka et al., 2013). These biomarker discovery studies have also focused on saliva as a source of EVs (Iwai et al., 2016; Yap et al., 2016 Kawahara et al., 2016 and Winck et al., 2015) with saliva being an abundant and available biofluid in contact with oral cancer it is a logical source of EV based biomarkers. A group in China has investigated the role of what they term circulating microparticles in promoting angiogenesis in oral cancer (Ren et al., 2016), these are pelleted at 50,000 x *g* from the blood of patients with oral cancer. Whilst these are unlikely to all be from a cancerous cell they were capable of promoting human umbilical vein endothelial cells to form tubules and proliferate. A study demonstrated that EVs from oral cancer cells

could activate MAPK/ERK and JNK-1/2 pathways *in vitro* which promoted proliferation and migration of oral cancer cells (Sento et al., 2016). Perhaps the most interesting discovery in this paper is that fact that the ability of EVs to drive these changes could be blocked by continuous heparin treatment of the cells. The treatment with heparin delayed the uptake of the EVs significantly for four hours after which time the vesicle uptake resumed as normal. Heparan sulphate proteoglycans (HSPGs) are thought to function as receptors for cancer cell derived EVs on the target cells (Christianson et al., 2013) making it a desirable focus of research for potential clinical applications.

1.7. Future challenges

Research into EV signalling over the past decade has begun to create a map of interactions occurring in both normal conditions and during disease. New interactions between EVs and cells are being frequently identified and what is obvious is that these EVs represent an extremely powerful and versatile system involved in a huge number of processes, including unexpected ones like interspecies communication (Mu et al., 2014). Our increasing understanding of EV-mediated signalling in the cancer microenvironment offers a new range of therapeutic options and strategies to be explored. If the signalling can be disrupted then some of the advantages it brings to a cancer will be lost, either enabling the patients' immune system to clear out the cancer or increasing the efficacy of existing chemotherapeutics. There is also the possibility of utilising vesicle signalling to deliver drugs and several promising combinations are being explored *in vitro*. One group has developed a technique that enables them to create EVs with specific contents and targets that can deliver therapeutic siRNA against

Alzheimer's disease in mice with high specificity and low immunogenicity (Alvarez-Erviti et al., 2011; Cooper et al., 2014). Although in its infancy the potential of this system is huge and could become a key therapeutic strategy within the next decade. There is also interest in using EVs as a source of biomarkers both for diagnosis and prognosis with EVs found in urine or blood replacing more invasive biopsies. Exosome Diagnostics are currently working on introducing a microfluidics platform to remove EVs from biofluids and analyse them quickly and cheaply. This platform could be endlessly adaptable with EVs capable of giving information on various cancer types as well as neurological disorders.

There are still several key challenges facing the field in the next few years. Firstly, finding a robust extraction technique that is capable of separating or distinguishing the vesicle subclasses. This would allow standardisation of both research techniques and terminology. It is currently expected that the exosome subclass has the greatest biological impact and some research has seemed to support this with the finding that the larger microvesicles contain no RNA (Crescitelli et al., 2013). However, the research is still hampered by current extraction techniques and the overlapping size ranges of the EVs. It is also important that universal quantification and purity scales are introduced, there are a growing number of groups using innovative transfer experiments to elucidate the effects EVs from one cell type can have on another cell type but without such quantification and purity measurements there is still the question of the dose of EVs being biologically relevant and pure. A group in Cardiff has proposed using the ratio of protein per particle as an indication of purity (Webber and Clayton, 2013). This method offers a simple way to obtain the purity of the EVs but does only allow for protein-based contamination of the extractions.

Although EV-based therapy methods are currently undergoing clinical trials there are very few papers that include information on the number of EVs used to treat cells or animals with many groups only using a weight of protein to give any indication of the amount of EVs used. This is a deeply flawed measurement as EV preparations are very variable in purity and not all the protein present in the majority of preparations will be EV associated.

Another key area for the next decade of EV research is to try and unravel the composition of the total population of EVs in a given microenvironment and the impact this can have. There are also questions surrounding the availability of the EVs: are all EVs available for all cells or are some like those containing drugs prevented from entering cells by some mechanism? Already an increasing amount of work is being done on 3D multiple cell type models more like the *in vivo* environment and this approach is going to become essential to understanding the complexity of vesicular signalling, particularly in cancer research. As more details on the mechanisms that target proteins and RNA to these EVs appears there will be an increase in the possible uses of EVs as a therapy delivery system.

Four years ago, an editorial piece was submitted to the Bioessays journal (Sverdlov, 2012) entitled Amedeo Avogadro's cry: What is 1 μg of exosomes? In it the author raised several key points that the EV field needed to address, notably the need for a more robust system for quantifying exosomes than by weight of protein but also the idea that miRNA transfer by EVs causing behavioural changes may not be as simple as first thought. The basis for his argument is that simple calculations of the number of

miRNA present in a tissue and the number of miRNA that could physically be within a vesicle means there are anywhere between 10^{10}- 10^{240} combinations of miRNA cargoes in EVs. Because our current understanding of EVs has them existing as a heterogeneous population it is statistically very unlikely therefore that a large enough pool of EVs with the required miRNA to produce an effect will exist or be separable from the mass of other EVs in experiments.

Despite the weaknesses and outstanding questions posed by our current understanding of the field, there have been many important and exciting revelations to date. Vesicle signalling has been shown to be a sophisticated and powerful mechanism that all cells can make use of. It has been shown to drive progression of phenotypic change allowing regulation of complex processes requiring the interaction of multiple cell types. It has been shown to deliver information in multiple directions with high specificity. With a potentially infinite number of combinations of cargoes and surface components the circulating EV population can be viewed like a communal Swiss army knife, with different attachments contributed by different cell types at different points in their life cycle. Each of the subsets or combinations of them can be used to perform a particular task in response to external stimuli or changing conditions. Being readily available, this pool offers a lifeline in the form of a faster response to potentially fatal changes like hypoxia, it allows advantageous mutations occurring in a single cell to be rapidly shared amongst a growing population of cancer cells and it offers new routes from therapeutic intervention and diagnostic tools.

1.8. Hypothesis and Aims

The hypothesis for this study is that EV signalling between oral squamous cell carcinoma (OSCC) cells and surrounding stromal tissues contributes to oral cancer progression. To test this hypothesis the project will focus on four separate areas or questions. Firstly, are vesicles released by oral cancer cells and do the physical characteristics of these vesicles with respect to production rates, morphology or markers change with tumour stage? Methods for the isolation and characterisation of EVs from the culture media of oral cancer cells will be optimised and used to count and size any vesicles produced by cells representative of different stages of oral cancer. Transmission electron microscopy will be used to compare the morphology of any vesicles produced. Western blotting for proteins marker identified in the literature will be carried out to characterize both the potential origins of the vesicles as well as to place them in context of vesicles purified in other published studies.

Secondly, what are the genomic and proteomic contents of these vesicles and is there any variation in these contents with tumour stage? Next generation sequencing and mass spectrometry techniques in combination with bioinformatics tools will be used to identify the miRNA and protein contents of these vesicles and explore any changes with disease stage.

Can the EVs produced by oral cancer cells be taken up by neighbouring cells of the tumour microenvironment and lastly are the EVs capable of inducing any changes in those cells? To study this signalling a fluorescence microscopy-based technique will be used to visualise the uptake of oral cancer derived EVs by other cells of the tumour microenvironment. Functional assays for behaviours beneficial to progression of a

tumour will then be used to determine if the OSCC EVs are capable of effecting these processes.

2. Materials and methods

2.1. Materials

All chemicals were routinely purchased from ThermoFisher or Sigma. Cell culture medium and supplements were purchased from Sigma, unless otherwise stated.

2.2. Cell lines and tissue culture

All cell lines were frozen or brought mycoplasma free and media from cell lines was routinely sent for mycoplasma testing throughout the project to ensure they remained mycoplasma free.

2.2.1. OSCC cell line panel

A panel of cell lines was assembled from those previously purchased from ATCC and held in the lab (H357) or gifted by Professor Keith Hunter. These cells were representative of the stages of oral, specifically tongue, cancer: mild and severe dysplasia, carcinoma and a metastatic deposit from a lymph node.

H357 was established from OSCC of the tongue from a 74-year-old male patient who smoked between the ages of 17 and 20. The carcinoma was a STNMP stage 1, well differentiated, node negative tumour. This cell line was maintained in Dulbecco's Modified Eagles Medium (DMEM) supplemented with 10% (v/v) FBS, 2 mM L-glutamine, 100 I.U./mL penicillin and 50 to 100 μg/mL streptomycin. Cells were passaged at 70-80% confluency.

The following cell lines were maintained in KGM medium (DMEM: F12 (3:1 v/v)), 10% FBS, 2 mM L-glutamine, 100 I.U./mL penicillin and 50 to 100 μg/mL

streptomycin.1.8 mM Adenine, $1.45x10^{3}$ mM Hydrocortisone, 10 ng/ml epidermal growth factor, 10^{-10} M cholera toxin and 5 μg/ml insulin and passaged at 70-80% confluency.

D20 was established from a leukoplakia (a white lesion of the oral mucosa) situated on the lateral tongue of a 50-year-old non-smoking male and was found to be immortal after over a hundred passages.

D35 was established from an erythroleukoplakia (a red and white non-homogenous lesion of the oral mucosa) situated on the lateral tongue of 68-year-old male smoker and was found to be immortal after over a hundred passages

B22 was established from the lymph node metastasis of an 88-year-old smoking male. The tumour originated in the tongue, was stage four, and well differentiated with invasion of multiple nodes.

2.2.2. Stromal cell panel

OKF6 (ATCC) is a normal oral keratinocyte cell line that was immortalized by the over-expression of hTERT (Dickson et al., 2000). This cell line was grown in defined serum free keratinocyte growth medium (Gibco).

HMEC1 (ATCC) is a human dermal microvascular endothelial cell line isolated from human foreskins and immortalized by the addition of a pSVT vector containing the Simian virus 40A gene product large T antigen. This cell line was grown in MCDB

131 medium (Gibco) supplemented with 2 mM L-glutamine, $1.45x10^3$ mM Hydrocortisone and 10 ng/ml epidermal growth factor.

Normal oral fibroblasts (NOFs) were donated by healthy volunteers or NHS patients according to University of Sheffield Ethics Approval 3463 or NHS Ethical Approval 09/H1308/66, respectively (table 2.1). NOFs were cultured in DMEM supplemented with 10% (v/v) FBS, and 200mM L-glutamine. Cells were passaged at 70-80% confluency.

Name	Gender	Age	Site	Smoking status	Ethics type
DENF008	F	18	buccal	NS	University
NOF803	M	45	buccal	NS	University
NOF804	F	34	buccal	NS	University
NOF805	F	28	buccal	S	University
NOF806	F	26	buccal	S	University
NOF316	F	22	gingival	NS	NHS
NOF319	M	73	gingival	NS	NHS
NOF335	M	47	gingival	S	NHS

Table 2.1 Details of patient fibroblasts used during this project detailing age gender smoking status and site of the extraction.

2.2.3. Routine cell culture and maintenance

All cells were cultured in a 37ºC, 5% CO_2 environment. Cell culture was carried out inside a class 2 tissue culture hood to ensure sterility. Cells were cultured in

appropriate sized flasks or plates according to experimental demands. Upon reaching 70-80% confluency the medium was removed, and cells washed twice with PBS before being treated with trypsin EDTA solution at 37ºC for 5 min. Trypsin was neutralised by the addition of the appropriate FBS containing medium before centrifugation at 1000 x *g* for 5 min in a bench-top centrifuge (Harrier 18/80). The resultant pellet was re-suspended in the appropriate medium before reseeding at the required density.

2.2.4. Cell counting and seeding

Where a particular number of cells was required for an experiment, cells were counted using a haemocytometer before reseeding. 10 µl of cell suspension was placed on a haemocytometer slide and the cells counted under a microscope. Cells with anomalous morphologies or those outside of the grid squares were not counted; the final averaged count was multiplied by 10,000 to give the number of cells per ml of suspension.

2.2.5. EV-depleted serum

For experiments requiring EV to be harvested from the culture medium, vesicle-depleted serum was used when making the culture medium to avoid contamination with bovine vesicles. Serum was depleted of vesicle contaminants by centrifugation at 100,000 x *g*, overnight at 4ºC in a Beckman TLA100.3 angled rotor followed by filter sterilisation with a 0.2 µm syringe filter.

2.2.6. Preparation of whole cell lysates.

Cells were cultured, as previously described, either in 6 well plates or T75 flasks

to confluency before being placed on ice. Culture medium was removed, and the cells washed twice with PBS before the addition of 1 ml 1x RIPA buffer containing complete mini EDTA-free easy protease inhibitors (Roche). After 5 min cells were scraped and the resulting suspension transferred to a microcentrifuge tube and clarified by centrifugation at 8000 x g for 10 min at 4^{o}C (Heraeus Fresco 17). The supernatant was transferred to a fresh tube and stored at -80^{o}C.

2.2.7. Preparation of conditioned medium for tunable resistive pulse sensing

To determine the vesicle production rate of each cell line the following protocol was developed. One million cells were seeded in a T25 flask and left to adhere overnight. The medium was then removed, and the cells washed three times with PBS before 2 ml of medium supplemented with 10% (v/v) EV depleted FBS was added and the cells incubated for 24 h. The conditioned medium was centrifuged as follows: 300 x g 10 min, 3,000 x g 15 min and 10,000 x g 40 min. The medium was diluted 1/10 with filtered PBST and filtered through a 0.2 µm centrifugal filter unit (Millipore) prior to analysis.

2.3. EV extraction and physical characterisation

2.3.1. ExoQuick extraction

Conditioned medium was centrifuged at 3000 x *g* for 15 minutes to remove cell debris, the supernatant was incubated overnight at 4^{o}C with ExoQuick precipitation reagent at a ratio of 1:5 (v/v). The mixture was centrifuged for 30 min at 1500 x g and the supernatant removed. The pellet was washed with PBS and centrifuged at 1500 x g

for 5 min to remove any excess precipitation reagent before being re-suspended in PBS.

2.3.2. Valadi et al, extraction

The method of Valadi et al. (2007) was performed as follows. Conditioned medium was centrifuged at 300 x g for 10 min to remove whole cells. Cell debris and large EVs were removed from the supernatant by centrifugation at 16,500 x g for 15 min followed by filtration with a 0.22 µm filter. Small EVs were pelleted by centrifugation at 100,000 x g for 90 min in a Beckman TLA100.3 angled rotor. The pelleted EVs were then re-suspended in PBS.

2.3.3. Théry et al, extraction

The method of Théry et al. (2006) was performed as follows. Conditioned medium was centrifuged at 300 x g for 10 min to remove whole cells. Cell debris was removed from the supernatant by centrifugation at 3,000 x g for 15 min. Large EVs and small debris were removed by centrifugation at 10,000 x g for 40 min. Small EVs were pelleted by centrifugation at 100,000 x g for 90 min in a Beckman TLA100.3 angled rotor and then re-suspended in PBS.

2.3.4. Hybrid protocol

A hybrid protocol was created to isolate EVs from small volumes of conditioned medium (up to 30 ml). The protocol uses a serial centrifugation approach adapted from that described by Théry et al. (2006) and Valadi et al. (2007) with all steps being carried out at 4^{o}C. The medium was first centrifuged at 300 x g for 10 min to remove whole cells, the supernatant was then centrifuged for 15 min at 3,000 x g to remove cell debris. The supernatant was then re-centrifuged at 10,000 x g for 40 min (Beckman Coulter

Avanti J26 with a JA 12 conical rotor) and the supernatant filtered through a 0.2 µm filter to remove any additional cell debris or large EVs before ultracentrifugation. The filtered supernatant was centrifuged at 100,000 x g for 90 min in a Beckman TLA100.3 angled rotor to pellet the small EVs. The pellet was then washed by the addition of 1 ml of PBS and a second spin at 100,000 x g for 90 min to remove soluble protein contaminants before re-suspending in the appropriate buffer. EVs were typically resuspended in PBS for storage at -20ºC and subsequent use in transfer experiments or RNA extraction, lysis buffer (RIPA Buffer containing 1x Complete mini Protease inhibitors (Roche) and storage at -80ºC for western blots, or 2% PFA and storage at 4ºC for electron microscopy.

2.3.5. Size exclusion chromatography

To isolate EVs from larger volumes of conditioned medium (above 30 ml) that would yield the required amount of protein and RNA for mass spectrometry and small RNA sequencing, size exclusion chromatography (SEC) was used as an alternative method. Conditioned medium was prepared as previously described. The medium was processed by the following serial centrifugation steps: 300 x *g* for 10 min to remove detached cells 3,000 x *g* for 15 min to remove cell debris and 10,000 x *g* for 40 min to remove large EVs. The supernatant was concentrated down to a volume of <1 ml using a Vivaspin 20 (100 kDa MW cut off) centrifugal device at 6,000 x *g*. A SEC column was prepared by allowing 15 ml of Sepharose CL-2B (GE) slurry to settle under gravity in an Econopack column (Biorad). A top bed support was placed on the Sepharose column and the ethanol removed by washing with 2 bed volumes of PBS. The concentrated medium was allowed to enter the Sepharose before the addition of PBS + 0.03% (v/v)

Tween-20 (PBST) to elute the column and twelve 0.5 ml fractions were taken.

2.3.5.1. Analysis of SEC fractions

SEC fractions were analysed for EV and soluble protein concentration by TRPS using the qNano instrument (Izon) and BCA assays, respectively. For both small RNA sequencing and mass spectrometry analysis a high yield of pure EVs was required. To achieve this, SEC fractions containing abundant EVs, but low soluble protein were pooled and EVs pelleted by centrifugation at 100,000 x g for 90 min at 4ºC.

2.3.6. EV quantification by tuneable resistive pulse sensing

EV concentration and size distribution were determined by tuneable resistive pulse sensing (TRPS) using a qNano instrument. Calibration was performed using CPC100B calibration particles (Izon) with a modal diameter of 114 nm diluted 1/2000 (v/v) in PBST. EV samples were diluted 1/10 (v/v) in PBST and then filtered through a 0.2 μm centrifugal unit. EV and calibration samples were analysed with the same NP100 nanopore with the same settings for voltage, nanopore stretch and pressure. Settings were chosen that gave an optimum separation of particles from the background noise and a constant flow rate of particles. Runs were recorded for 200 particles or 2 min whichever came first.

2.3.7. Electron Microscopy of EV samples

2.3.7.1. Preparation of solutions

2.3.7.1.1. 2% and 4% W/V Paraformaldehyde

2 or 4 g of paraformaldehyde powder (BDH Chemicals) were dissolved in 90 ml

of 0.1 M sodium phosphate buffer by heating to 65^{o}C whilst stirring. If necessary drops of 1 M NaOH were added until the solution became clear. The solution was made up to 100 ml with 0.1 M sodium phosphate buffer cooled and filtered. Aliquots were stored at -20^{o}C.

2.3.7.1.2. 4% W/V Uranyl Acetate

2 g of uranyl acetate powder (Agar Scientific) was dissolved in 50 ml distilled water and stored in the dark at 4^{o}C.

2.3.7.1.3. Uranyl Oxalate

4% (w/v) uranyl acetate was mixed with 0.15 M Oxalic acid (Sigma) (0.945 g in 50 ml distilled water) in a 1:1 ratio and stored in the dark at 4^{o}C.

2.3.7.1.4. Methyl Cellulose

196 ml of distilled water was heated to 90°C and 4 g methyl cellulose added (Sigma, 25 centipoise, M-6385) whilst stirring. This suspension was rapidly cooled on ice whilst stirring until the solution had reached 10°C. The solution was left overnight at 4°C with the stirrer on low then left to “ripen” for 3 days at 4°C. The solution was made to final volume of 200 ml in distilled water before centrifugation for 95 min at 100,000 × *g*, 4°C and the supernatant stored for up to 3 months at 4°C.

2.3.7.2. Fixation

Samples were prepared for electron microscopy using the following method as described by Théry et al. (2006) taking care at all stages to keep the grids wet on the membrane side and dry on the opposite side. EV pellets were re-suspended in 50 µl 2% paraformaldehyde (PFA) fixative and placed on ice. For each sample three 8 µl drops of the PFA suspended EVs were placed onto a square of parafilm in a petri dish and a 200 mesh formvar coated grid was placed membrane side down on each drop using a pair of forceps. Grids were then left for 20 min in a dry environment to allow adsorption. The grids were then washed once in PBS by floating them membrane side down on a 100 µl drop on the parafilm before being transferred to a 50 µl drop of 1% glutaraldehyde for 5 min.

2.3.7.3. Contrasting

Following the treatment with glutaraldehyde the grids were given 8 washes of 2 min each in distilled water by flotation on drops on parafilm. After the wash steps the grids were contrasted and embedded first in a 50 µl drop of pH 7 uranyl-oxalate solutions for 5 min and then for 10 min in a 50 µl drop of 9:1 (v/v) 2% methylcellulose: 4% Uranyl acetate solution on ice. The grids were then gently blotted on Whatman no.1 filter paper to remove the excess liquid before being allowed to air dry prior to storage. The grids were imaged using a Tecani Spirit G2 at 80 kV.

2.4. Protein Analysis

2.4.1. BCA Assay

Protein concentration was estimated by micro BCA assay using the following technique. Bovine serum albumin (BSA) standards of known concentration (0 to 1

mg/ml) were prepared in the same buffer as samples were made in. All samples were tested in duplicate with 10 µl of each sample and standard added to a microplate. 200 µl of assay reagent (consisting of A and B solutions in a 50:1 ratio) was added to each well. The plate was sealed with a plastic film cover added and incubated for 30 min at 37ºC. Following the incubation, the absorbance was measured at 540 nm on a Tecan M200 plate reader. A standard curve was created by plotting absorbance values against BSA concentrations and a polynomial equation used to determine the concentration of samples.

2.4.2. SDS-PAGE

12% Acrylamide gels were cast between glass plates using the following quantities to produce two gels.

dH_2O	4.3 ml
40% Acrylamide (37.5:1 acrylamide: bis-acrylamide)	3.0 ml
pH 6.8 Tris Page SDS buffer	2.5 ml
10% Ammonium persulfate	350 µl
Temed	5 µl

Table 2.2: Reagents for two 1.0 mm acrylamide resolving gels

The resolving gel was overlaid with isopropanol and allowed to polymerise.

dH_2O	4.725 ml
40% Acrylamide (37.5:1 acrylamide: bis-acrylamide)	975 µl
pH 6.8 Tris Page SDS buffer	2.1 ml
10% Ammonium persulfate	100 µl
Temed	17 µl

Table 2.3: Reagents for two 1.0 mm acrylamide stacking gels.

The stacking gel was poured on top of the set resolving gel and a sample comb was inserted before allowing the gel to polymerise for 10 min. The comb was then removed and each well washed out with copious amounts of distilled water.

Samples volumes were equalised to the lowest concentration 20 µl with 1X RIPA buffer (containing protease inhibitors) before the addition of 5 µl 5X loading buffer (National Diagnostic). The samples were then heated at 95^{o}C for 5 min. Samples were separated using either 12% polyacrylamide SDS-PAGE or precast 4-18% gradient gels (Biorad) in Biorad tanks filled with 1X Running buffer (88 g Glycine, 10% W/V SDS and 32 g Tris Base in 1 L dH2O). 20 µl of sample was loaded in each well alongside Precision Plus prestained protein ladder (Biorad) in the outside wells. Separation was performed at 150 V until the dye front had reached the bottom of the glass plates.

2.4.3. Western Blotting

2.4.3.1. iBlot transfer

Proteins separated by SDS-PAGE were transferred using the iblot system (Life Technologies). The gel was placed on top of the nitrocellulose membrane of the iblot cathode. This was covered with filter paper pre-soaked in distilled water taking care to remove all air bubbles. The stack was completed by the addition of the anode and a sponge. Proteins were transferred at 23 V for 6 min.

2.4.3.2. Biorad turbo blot transfer

Following SDS-PAGE the gel was placed on the nitrocellulose membrane of a pre-prepared stack. The sandwich was assembled by the addition of the top layers and bubbles removed. Proteins were transferred using an appropriate programme for the thickness of gel. For 1.0 mm gel this was 28 V for 7 min and for 1.5 mm gels this was 28 V for 10 min.

2.4.3.3. Blocking and antibody incubation

The nitrocellulose membrane was blocked in 5% (w/v) skimmed milk in TBST (8 g NaCl 0.2 g KCl 3 g Tris base in 1l dH2O and 0.1% Tween-20) for 1 h on a rocker shaker. The membrane was incubated overnight on a rocker shaker with primary antibody (table 2.4), diluted in blocking buffer, at 4^{o}C. Following incubation with the primary antibody, the membrane was washed three times in TBST for 15 min and incubated with the appropriate secondary antibody (table 2.5) diluted in blocking buffer for 1 h at room temperature. The membrane was washed three times with TBST for 5 min and placed in cling film. The two parts of ECL substrate (Pierce) were mixed in a 1:1 ratio and 500 µl of the solution was added to the membrane. The excess was removed after a few seconds and the cling film was sealed before placing the membrane

either in an x-ray cassette for exposure to an x-ray film and developing with an automated processor (Xograph Compact X4) or imaged using a Licor scanner (Model no 3600) on high quality 12 min scan.

Antibody (clone)	Blocking buffer	Dilution	Manufacturer (Antibody number)
Alix (1A12) mouse monoclonal	5% milk in TBST	1:200	Santa Cruz (sc-53540)
Annexin V (C-20) goat polyclonal	5% milk in TBST	1:200	Santa Cruz (sc-1929)
ADP ribosylation factor 6 (ARF6) (3A-1) mouse monoclonal	5% milk in TBST	1:200	Santa Cruz (sc-7971)
CD63 (H-193) rabbit polyclonal	5% milk in TBST	1:200	Santa Cruz (sc15363) (This antibody was discontinued in 2016)
CD63 (EPR5702) rabbit monoclonal	5% milk in TBST	1:500	Abcam (ab134045) (This antibody was brought in 2016 to replace the discontinued Santa Cruz antibody)

Heat shock protein 70 (HSP70) (3A3) mouse monoclonal	5% milk in TBST	1:200	Santa Cruz (sc-32239)
Thrombospondin 1 (TSP1) (A6.1) mouse monoclonal	5% milk in TBST	1:200	Santa Cruz (sc-59887)
Vesicle associated membrane protein 3 (VAMP3) (N12) goat polyclonal	5% milk in TBST	1:200	Santa Cruz (sc-18208)
Alpha smooth muscle actin (αSMA) (IA4) mouse monoclonal	5% milk and 2.5% bovine serum albumin (BSA) in TBST	1:500	Sigma (A2547)
Horseradish peroxidase conjugated glyceraldehyde 3 phosphate dehydrogenase (GAPDH) (EPR6254) rabbit monoclonal	2.5% BSA in TBST	1:20000	Abcam (abc181602)
Galectin 3 binding protein (GAL3BP) mouse polyclonal	2.5% BSA and 5% milk in TBST	1:500	Abcam (ab67353)

Major vault protein (MVP) (1032) Rabbit monoclonal	2.5% BSA and 5% milk in TBST	1:1000	Abcam (ab2376)
Eukaryotic elongation factor 2 (EEF) (EP880Y) rabbit monoclonal	2.5% BSA and 5% milk in TBST	1:10000	Abcam (ab75748)
Integrin alpha six (ITA6) (EPR18124) rabbit monoclonal	2.5% BSA and 5% milk in TBST	1:1000	Abcam (ab181551)

Table 2.4 Details of manufacturers, dilutions and blocking buffers for all primary antibodies used in western blotting experiments

Antibody	Blocking buffer	Dilution	Manufacturer
Anti-mouse	5% milk in TBST	1:3000	Cell Signalling (New England Biosciences)
Anti-rabbit	5% milk in TBST	1:3000	Cell Signalling (New England Biosciences)
Anti-goat	5% milk in TBST	1:3000	Promocell

Table 2.5 Details of HRP conjugated secondary antibodies, blocking buffer, dilutions and manufacturers used in western blot experiments

2.4.4. iTRAQ 8 Plex

2.4.4.1. Sample collection

Conditioned medium was harvested from three confluent T175 flasks and EVs isolated by SEC. Fractions 6-9 were pooled and EVs pelleted by centrifugation at 100,000 x g for 90 min. The pellet was then lysed in 50 µl of 1 M triethylammonium bicarbonate (TEAB) (Sigma), pH 8.5 with 0.05% (w/v) SDS buffer and 0.05% (v/v) Triton x 100 detergent on ice for 20 min. Samples were centrifuged at 10,000 x g for 20 min at 4^{o}C and protein concentration was determined by BCA assay.

2.4.4.2. Isobaric tag labelling

Samples were normalised to the lowest concentration in 25 µl TEAB buffer. Following this reduction of cysteine residues was carried out by addition of 2.5 µl 50 mM tris (2-carboxyethyl) phosphine. After vortexing and briefly pulsing the samples in a microfuge they were incubated at 60^{o}C for one hour to break any disulphide bonds in the proteins. To prevent them from reforming, the samples were allowed to cool to room temperature before alkylation with 1.25 µl of methyl methanethiosulphonate and incubation for 10 min at room temperature. Tryptic digestion was carried out by adding 0.25 µg of porcine trypsin to the samples and overnight incubation at 37^{o}C. Samples were then labelled with iTRAQ reagents (ABSciex) as follows B22 with 117, D35 in two technical replicates with 118 and 119, and H357 with 121. The labelled samples were then combined, vacuum evaporated and stored at -20^{o}C.

2.4.4.3. High resolution hydrophilic interaction chromatography (HILIC)

Initial fractionation was carried out by Hypercarb™ separation on a Dionex

UltiMate 3000 Autosampler linked to a flow manager and pump system (Thermo Scientific, UK). Samples were re-suspended in 120 µL Buffer A (3% ACN, 0.1% TFA) and loaded onto a Hypercarb™ Porous Graphitic Carbon LC reversed phase analytical column (Cat no. 35003-052130, ThermoFisher Scientific, UK) with the following dimensions, 50 mm length, 2.1 mm diameter, particle size of 3 µm and a 250 Å pore size. The flow rate for loading and gradient separation was 0.2 mL/min. A gradient was established using Buffer A and Buffer B (97% ACN, 0.1% TFA) in the following proportions 0% B (0-5 minutes), 0-5% B (5-6 minutes), 5-35% B (6-51 minutes), 35-45% B (51-56 minutes), 45-90% B (56-61 minutes), 90% B (61-66 minutes) followed by re-equilibration at 0% B. Peptide fractions were dried by centrifugal evaporation using a Scanvac vacuum centrifuge (Labogene, Denmark) connected to a Vacuubrand Vacuum Pump (Vacuubrand, Germany). The fractions were then recombined into 6 samples to run on the LC-MS/MS.

2.4.4.4. Reverse phase liquid chromatography (RPLC) and liquid chromatography tandem mass spectrometry (LC MS/MS) mass spectrometric analysis

LC MS/MS was performed by nano-flow liquid chromatography (U3000 RSLCnano, Thermo Scientific) coupled to a hybrid quadrupole-orbitrap mass spectrometer (Q Exactive HF, Thermo Scientific). iTRAQ labelled-peptides were separated on an Easy-Spray C_{18} column (75 µm x 50 cm) using a 2-step gradient from 97% solvent A (0.1% formic acid in water) to 10% solvent B (0.08% formic acid in 80% acetronitrile) over 5 min then 10% to 50% B over 75 min at 300 nL/min. The mass spectrometer was used in data dependent acquisition mode with 10 product ion scans

(resolution 15000, automatic gain control 5^4, maximum injection time 20 ms, isolation window 1.2 Da, normalised collision energy 32, intensity threshold 2.5^5) per full MS scan (resolution 60000, automatic gain control 3^6, maximum injection time 100 ms).

2.4.4.5. Protein identification and relative quantification

iTRAQ ratios used for relative quantification were determined by applying an in-house data analysis pipeline (Ow et al., 2009). Firstly, the raw data was converted to generic MGF peaklists via the mascot.dll embedded script (version 1.6 release no. 25) in Analyst QS v. 1.1 (Applied Biosystems, Sciex; Matrix Science) with the option of averaging the MS/MS spectra removed. The spectra charge deconvolution was disabled around the iTRAQ reporter region (113−119 and 121 *m*/*z*). Centroided data were interrogated for identifications using an in-house Phenyx algorithm cluster (binary version 2.6; Genebio Geneva) at the ChELSI Institute, University of Sheffield. The 8-plex data were interrogated using the latest UniProt Human database with the following modifications set 8-plex iTRAQ mass shifts (+304 Da, K and N-term), methylthiol (+46 Da, C) and oxidation of methionine (+16 Da, M).

Stringent mass tolerances of 0.4 Da on both MS and MS/MS were used along with peptide level filters of a *z*-score of 5.0 and a *p*-value significance of 0.0001 to filter the hits. Phenyx protein scores were set using a total *z*-score of 20. MS/MS peptides that met these criteria were then used as the basis for calculations. In order to confirm relative quantification, the iTRAQ reporter intensities for these peptides were referenced directly to the centroided data provided in the MGF peaklists. Appropriate isotopic and median corrections were applied to the reporter ions intensities to compensate for systematic errors in the sample loading. Students tests with Bonferroni's

multiple test correction was performed on the corrected values to compare between the different vesicle sources.

2.4.5. Label free spectrometry

2.4.5.1. Sample collection

Conditioned medium was harvested from three confluent T175 flasks and EVs isolated by SEC. Fractions 6-9 were pooled and EVs pelleted by centrifugation at 100,000 x g for 90 min. The pellet was then resuspended in 50 µl of 50 mM ammonium bicarbonate buffer prepared with HPLC grade water (Thermofisher) containing 0.1% RapiGest (Waters). Sample protein concentration was determined by BCA assay.

2.4.5.2. Preparation of samples

Samples were normalised to the lowest concentration in 25 µl 50 mM ammonium bicarbonate buffer. Following this reduction of cysteine residues was carried out by addition of 2.5 µl 50 mM tris (2-carboxyethyl) phosphine. After vortexing and briefly pulsing the samples in a microfuge they were incubated at 60^{o}C for one hour, to break any disulphide bonds in the proteins. To prevent them from reforming the samples were allowed to cool to room temperature before alkylation with 1.25 µl of methyl methanethiosulphonate and incubation for 10 min at room temperature. Tryptic digest was carried out using sequencing grade trypsin (Promega) which was resuspended in HPLC grade 50 mM ammonium bicarbonate and diluted to an 8 ng/µl working solution. Each sample had 5 µl of this solution added to give a final ratio of trypsin to protein of 1:50 (for these samples this was 40 ng of trypsin to 2000 ng of protein). Samples were incubated with the trypsin overnight at 37^{o}C.

2.4.5.3. RPLC and mass spectrometric analysis

Samples were run using a reverse phase chromatography column with a 2 µm particle size giving pores of 100 Å. The column was run with a flow rate of 0.3µl/min increasing the concentration of buffer B 80% Acetonitrile, 0.1% v/v formic acid in water from 3% to 90% of the column volume. This creates a potential retention time of between 5 and 105 min for proteins on the column. Fractions were analysed individually using a 105-minute data dependent acquisition (DDA) method on a QExactive HF. The full MS scan was from 375-1500 m/z was acquired in the Orbitrap at a resolution of 120,000 in profile mode. Subsequent fragmentation was Top 10 in the HCD cell, with detection of ions in the Orbitrap using centroid mode, resolution 30,000. The following MS method parameters were used: MS1, Automatic Gain Control (AGC) target 1^6 with a maximum injection time (IT) of 60 ms. MS2, Automatic Gain Control (AGC) target 1^5, maximum injection time (IT) of 60 ms and isolation window 2 Da. The intensity threshold was 3.3^4, normalized collision energy 27, charge exclusion was set to unassigned, 1, exclude isotopes was on, apex trigger deactivated. The peptide match setting was preferred with dynamic exclusion of 20 seconds.

2.4.5.4. Processing data

Initial data processing was carried out by MaxQuant v1.5.3.30. Samples were aligned against a human protein database. The following group specific parameters were used: Type Standard Multiplicity 1 no labels. Trypsin digestion and label free analysis were selected. Using the global parameters, the methylthio addition was added to allow for the changes caused to the protein structure by the reduction and alkylation reactions detailed in the processing steps. Following this processing with MaxQuant data was

imported into Perseus v1.5.2.6 for further analysis. Once imported into Perseus contaminants were removed from the list of samples, technical replicates were combined, and the label free values converted to a Log2x score.

2.5. RNA extraction and analysis

2.5.1. miRCURY RNA extraction kit

RNA was extracted from cells and EVs using the miRCURY RNA extraction kit (Exiqon). Cells or EV pellets were resuspended in 350 µl of lysis buffer and incubated at room temperature for 5 min. The lysate was then transferred to an RNAse free microcentrifuge tube to which 200 µl of 100% ethanol was added. The tube was vortexed for 10 seconds and the lysate/ethanol mixture was added to a spin column. Lysate was centrifuged through the column at 3,500 x *g* for 1 min and the flow through discarded. The column was then treated with 10 µl of DNase1 in 70 µl of DTT buffer (Qiagen). The DNase and buffer mixture were applied directly to the membrane and left for 15 min at room temperature. Following DNase treatment, the column was washed three times with 400 µl of wash buffer and centrifuged for 1 min at 14,000 x *g*. After the final wash the column was centrifuged for 2 min at 14,000 x *g* to dry the filter. The column was then placed into an elution tube and 50 µl of elution buffer added directly to the filter. RNA was eluted by centrifugation for 2 min at 200 x *g* and then 1 min at 14,000 x *g*. Extracted RNA was typically quantified on a NanoDrop spectrophotometer (Nanodrop 1000, Thermoscientific) and stored at -80^{o}C.

2.5.2. Measuring of RNA concentration using Agilent Bioanalyzer

Prior to small RNA sequencing analysis RNA concentration was determined by

Bioanalyzer (Agilent). Reagents were allowed to equilibrate to room temperature for 30 min, 9 µl of gel dye mix was added to the Picochip and the plunger depressed for 60 s before being released. 9 µl of RNA conditioning solution and 5 µl of marker were added to the appropriate wells. 1 µl of ladder and sample were added to the appropriate wells and the chip inserted into the instrument.

2.5.3. Small RNA sequencing

EVs were purified by SEC and RNA extracted using the miRCURY kit. RNA samples were submitted to Edinburgh Universities Clinical Research Facility for small RNA sequencing. The RNA samples were analysed by Agilent Bioanalyzer using the RNA 6000 Pico kit to assess the quality and integrity of total RNA and then quantified using a Qubit 2.0 fluorometer and the Qubit RNA HS assay kit. These processes enabled a standardised amount of RNA to be prepared for each sample. RNA was hybridized and ligated before being reverse transcribed into cDNA. The cDNA was purified using magnetic beads and then amplified with appropriate Ion torrent adaptors and barcodes for 18 cycles of PCR before being purified. The library yields were quantified and assessed for quality using the Qubit 2.0 fluorimeter and a Bioanalyzer running the appropriate DNA kits. Libraries were combined in equimolar amounts for template preparation before sequencing on the Ion Proton instrument with a P1 v3 chip. Additionally, a smallRNA analysis plug in was run, this aligns microRNA reads against databases of known mature miRNA and unmapped reads against the whole genome to identify other RNA molecules.

2.5.4. Quantitive real-time PCR

2.5.4.1. TaqMan qPCR

2.5.4.1.1. cDNA Synthesis

cDNA was prepared from extracted RNA using a TaqMan reverse transcription kit (Applied Bioscience). Reverse transcription master mix was first assembled on ice (0.15 µl of 100mM dNTPs, 1.00 µl MultiScribe™ Reverse Transcriptase 50 U/µl, 1.50 µl 10x Reverse Transcription Buffer, 0.19 µl RNase Inhibitor 20 U/µl and 4.16µl Nuclease free water.) This was then combined with between 1 and 10 ng of RNA in a 7 µl:5 µl ratio in a PCR tube for each reaction, 3 µl of 5X RT primer was then added to the tube before a 5 min incubation on ice. Samples were then treated to the following programme in a thermal cycler: 30 min at 16^{o}C, 30 min at 42^{o}C, and 5 min at 85^{o}C. The cDNA produced was stored at -20^{o}C prior to being used for qPCR.

2.5.4.1.2. Preamplification of RNA samples

Because some of the sequences were present in very low quantities a preamplification work flow (Applied Biosystems) was used with some of the miRNA sequencing validation PCRs. The first step was a Megaplex™ RT reaction, for each sample 0.8µl of 10X Megaplex™ RT primers, 0.2 µl 100 mM dNTPS, 1.5 µl of 50 U/µl Multiscribe™ Reverse transcriptase, 0.8 µl 10X RT buffer, 0.9µl of 25mM $MgCl_2$, 0.1µl of 20U/µl RNase inhibitor and 0.2µl of nuclease free water was combined in an RNase free tube. The tubes were inverted and 4.5µl of the master mix added to 3 µl of normalised RNA for each sample. Tubes were incubated on ice for 5 min before being run with the following programme in a PCR machine, 40 cycles of 16^{o}C for 2 min 42^{o}C for 1 minute and 50^{o}C for 1 second. Samples were incubated at 85^{o}C for 5 min.

Immediately following the RT reaction samples were prepared for the pre-amplification step. For each sample 12.5 µl of 2X PreAmp master mix was combined with 2.5 µl of 10x PreAmp primers and 7.5 µl of nuclease free water. The primers used were the Human Pool A Megaplex™ RT primers. After inverting the tubes and 5 min incubation on ice the RT reaction was run in a PCR machine with the following settings 95ºC for 10 min 55ºC for 2 min and 72ºC for 2 min. Followed by 12 cycles of 95ºC for 15 seconds and 60ºC for 4 min, 10 min incubation at 99.9ºC was used to inactivate the enzyme. Samples were stored at -20ºC prior to use in qPCR reactions.

2.5.4.1.3. qPCR

cDNA samples were analysed using a TaqMan RTqPCR kit (Life Technologies). Sufficient master mix was assembled to allow for each sample and a non-cDNA containing control to be run in duplicate. Master mix was assembled using the following proportions per well: 0.5 µl TaqMan Small RNA assay 20x (table 2.6), containing the primers and fluorescent probes specific for sequence of the species required), 5µl of TaqMan universal PCR Master mix II (2x) (with no Uracil-N-glycosylase(UNG)) and 4µl of nuclease free water. 0.5 µl of cDNA was then added to 9.5µl of master mix per well of 96 well qPCR plate for each reaction.

After the addition of the cDNA the plate was sealed and briefly centrifuged for 2 min at 1000 x *g* (Sorval Legend XT) before loading into the qPCR machine (7900 HT Fast Real Time PCR system). Plates were then run with the following programme using the FAM fluorophore and a standard run mode: 2 min at 50ºC to ensure no UNG activity, 10 min at 95ºC to activate the polymerase enzyme and the 40 cycles of 95ºC

for 15 seconds to denature the strands and 60ºC for 60 seconds to extend and anneal the strands.

Target	Thermo fisher assay ID
Let-7a-5p	000377
miR-199a-3p	002304
miR-29b-3p	000413

Table 2.6 ID numbers for TaqMan small RNA assays used to validate IonTorrent sequencing data

2.5.4.2. Sybr Green qPCR

2.5.4.2.1. cDNA Synthesis

cDNA was prepared from extracted RNA using a High capacity reverse transcription kit (Applied Bioscience). Reverse transcription master mix was first assembled on ice (0.8µl of 100mM dNTPs, 1.00µl MultiScribe™ Reverse Transcriptase 50 U/µl, 2.0 µl 10x Reverse Transcription Buffer, 1.0µl RNase Inhibitor 20 U/µl 2.0µl 10x RT random primers and 3.2µl Nuclease free water.) This was then combined with between 1 and 10 ng of RNA in a 10 µl:5µl ratio in a PCR tube for each reaction. Samples were then treated to the following programme in a thermal cycler: 10 min at 25ºC, 120 min at 37ºC, and 5 min at 85ºC. The cDNA produced was stored at -20ºC prior to being used for qPCR.

2.5.4.2.2. qPCR

cDNA samples were analysed using a SYBR Green RTqPCR kit (Life Technologies). Sufficient master mix was assembled to allow for each sample and a non-cDNA containing control to be run in duplicate. Master Mix was assembled using the following proportions per well: 0.25 µl of forward primer and 0.25 µl of reverse primer 5 µl of SYBR Green universal PCR Master Mix II (2x) and 4 µl of nuclease free

water. 0.5µl of cDNA was then added to 9.5 µl of master mix per well of 96 well qPCR plate for each reaction. Primers listed in table 2.7.

After the addition of the cDNA the plate was sealed and briefly centrifuged for 2 min at 1000 x *g* (Sorval Legend XT) before loading into the qPCR machine (7900 HT Fast Real Time PCR system). Plates were then run with the following programme 95ºC for 10 min and then 40 cycles of 95ºC for 10 seconds to denature the strands and 60ºC for 15 seconds to extend and 72ºC for 20 seconds to anneal the strands and acquire the signal.

Primer	Sequence
U6 Forward	5’ CTCGCTTCGGCAGCACA 3’
U6 Reverse	5’ AACGTTCACGAATTTGCGT 3’
αSMA Forward	5’ GAAGAAGAGGACAGCATG 3’
αSMA Reverse	5’ TCCCATTCCCACCATCAC 3’

Table 2.7 List of SYBR green primer sequences for U6 as a house keeping control and αSMA. All primers were ordered from Sigma Aldrich.

2.6. Cell treatments and assays

2.6.1. Fluorescent imaging of EV mediated RNA transfer

2.6.2. Staining of extracellular EVs

EVs were extracted from the culture medium of cell lines as described previously (section 2.3.4) and resuspended in 300 µl of PBS. The resuspended exosomes were treated with two different stains using the following method. Cyto RNASelect (Life Technologies) was used to stain EV RNA, this cell permeable dye binds nucleic acids but fluoresces strongly when bound to RNA with an absorption/emission maxima 490/530 nm, however when bound to DNA only emits weak fluorescence. A 1 mM

working solution was made up in dimethyl sulfoxide (DMSO) and 1µl of this added to the EVs for a final concentration of 0.1 mM. A cell permeable far red 5-Carboxyfluorescein diacetate succinimidyl ester isomer (Life Technologies), which binds covalently to primary amines in membrane proteins, was used to stain the exosome membranes. The powder was rehydrated in 200 µl of DMSO to make a 1 mM working solution and 1 µl of this was added to the RNA stained vesicle solution. The stained exosome solutions were wrapped in foil to protect them from light and incubated at 37ºC for 30 min. Following this excess or unincorporated dye was removed using a MW 3000 exosome spin column (Life Technologies). The column was first rehydrated by the addition of 650 µl of PBS and a 15 min room temperature incubation, before the addition of sample to the column it was centrifuged for 2 min at 750 x g to remove any remaining interstitial fluid. Samples were loaded on the column and treated to a second spin to remove the excess dye. Vehicle controls were prepared by treating a 300 µl aliquot of PBS to the same protocol.

2.6.3. Cell treatment, fixing and mounting

Cells were plated on sterile coverslips in a 24 well plate using 20,000 cells in vesicle free media. These cells were left to adhere overnight before the addition of the stained EVs. After this addition the cells were left for 1 hour in an incubator to allow uptake of the EVs. Following this the media was removed and cells washed twice with PBS. The washed cells were fixed in 4% paraformaldehyde (PFA) for 10 min after which the PBS was removed and the cover slips washed again in PBS. Slips were mounted on clean glass slides using 8 µl of ProLong Gold Antifade with DAPI (Life Technologies) per cover slip and left to dry overnight. Completed slides were then

imaged with a Zeiss Axioplan 2 fluorescence microscope.

2.6.4. Proliferation and viability assays

2.6.4.1. Cell seeding density optimisation

In order to optimise the seeding of cells in 96 well microplates for growth experiments cells were seeded in wells of a 96 well plate at varying densities alongside appropriate blanks in 90 µl of media. Cells were allowed to grow for 24 48 and 72 h. At each time point cells were imaged again and then 10 µl of presto blue added and left to incubate for an hour protected from light. Wells were then read using a Fluorstar plate reader with absorbance at 570 nm. Following this the presto blue containing medium was removed and replaced with fresh medium. The absorbance values were normalised and then used to indicate the growth of the cells.

2.6.4.2. Live/dead cell staining

Cells were seeded at values determined by the density optimisation experiments in triplicate in black walled clear bottom 96 well plates (Corning) in serum free media. After serum starving for 24 h the media on the wells to be treated with EVs or a vehicle control was replaced with the appropriate media supplemented with 2% serum to minimise any growth promoting impact from the medium. The cells were then treated with either 1000, 5000, 10000 or 200000 EVs per cell or the same volume of vesicle free PBS per well for 24 and 48 h. The maximum ratio of 20000 EVs per cell cells was determined from reverse calculating the number of EVs to cells used in the fluorescent imaging of uptake experiments. Appropriate controls were prepared using phenol red free DMEM supplemented with 10% FBS and by using cells treated with 70% methanol

for 30 min to give wells where all or nearly all of the cells were alive or dead. Relative numbers of live and dead cells were determined using a Life Technologies live dead staining kit. This kit comprises of ethidium homodimer- 1 (EthD-1), which enters cells via the damaged membranes of dead cells and undergoes a 40-fold enhancement of fluorescence when bound to nucleic acids, and calcein AM which is retained by live cells and converted to the intensely fluorescent calcein by intracellular esterases.

After optimising dye concentration, cell number and incubation times. A solution of 4 µm EthD-1 and 2 µm calcein AM was assembled from the supplied stock solutions; the media on the cells was replaced with 100 µl of sterile PBS and a 100 µl of the dual stain solution was added to each well for 30 min. The plate was then read on a Tecan M200 plate reader at 485/530 nm and 530/615 nm excitation/emission. Fluorescence values were used to calculate the relative number of live and dead cells compared to the control wells.

2.6.4.3. BRDU ELISA

Changes in cell proliferation following treatment with EVs was assessed using a BRDU ELISA kit (Roche) this kit incorporates a labelled derivative of thymidine into DNA during proliferation which can then be detected by an antibody conjugated to an enzyme with a substrate that can produce a coloured product. Cells were seeded at values determined by optimisation experiments in triplicate with both a blank and background wells in a 96 well plate and left to adhere overnight. The cells were then changed to 100 µl serum free media overnight and treated with 20000 EVs/cell from the four cancer cell lines or the same volume of serum free medium the following morning.

Treated cells were left to incubate for 48 h, at which point they were treated with 10 µl of BRDU labelling solution and the plate wrapped in foil to protect it from light and returned to the incubator for 4 h. After 4 h the media was removed by tapping the plate on top of a pad of paper towels. Cells were then fixed by the addition of 200 µl of fixdenat to the wells and incubation for 30 min at room temperature. During this incubation anti-BRDU-POD was diluted 1:100 in antibody dilution solution. The fixative was removed by tapping off in the same was as before. Wells were then treated with 100 µl of the anti-BRDU solution for 90 min at room temperature. After which time the solution was removed and the wells washed three times with 1XPBS following the final wash step 100 µl of substrate solution was added to the wells and left to develop for 15 min. After 15 min 25 µl of 1M H_2SO_4 was added to each well and the absorbance measured using a Fluorstar plate reader at a wavelength of 450nm.

2.6.5. Fibroblast activation

2.6.5.1. Treatment of fibroblasts

Fibroblasts were seeded at either 8000 per well in a 24 well plate or 250000 cells per well in a six well plate they were then serum starved for 24 h to synchronize the cells and prevent activating effects from the serum. After 24 h they were treated with either 20000 EVs from a cancer cell line 5 ng/ml TGFβ1 (R&D Systems UK) or the same volume of serum free medium. Protein and RNA was harvested and used for western blots or qPCR with αSMA antibodies or TaqMan primers.

2.6.5.2. Imaging fibroblast activation by immunofluorescence staining of alpha smooth muscle actin (αSMA)

Eight thousand fibroblasts were seeded onto a sterile cover slip in a well of a 24 well plate and allowed to adhere overnight. The cells were then serum starved for 24 h to minimise any impact of the serum before treatment with twenty thousand EVs per cell from one of the cancer cell lines for a further 24 h. After vesicle treatment the media was removed, and the cells were fixed by the addition of 100% methanol for 20 min at room temperature. The cells were then permeabilized by washing with 4 mM sodium deoxycholate before incubating them in 1 ml of sodium deoxycholate for 10 min at room temperature. This buffer was then removed before the addition of 1 ml blocking buffer of 2.5% BSA in 1x PBS, the plate was placed on a rocker at room temperature for 1 hour. Following this incubation, a FITC conjugated antibody for αSMA (mouse monoclonal antibody to αSMA (IA4) Sigma) was diluted 1 in 1000 in blocking buffer and added to the wells, the plate was wrapped in foil to protect the antibody from light and returned to the shaker for an hour. Finally, the cover slips were washed three times in PBS and mounted using prolong gold Antifade mounting medium (Life Technologies) which was left to cure for at least 24 h before being imaged using a Zeiss Axioplan fluorescent microscope.

3. Optimisation of methods for purifying and storing EVs from the culture medium of oral cancer cell lines

3.1. Introduction

Cell culture media are routinely supplemented with foetal bovine serum (FBS) and whilst this acts as a good source of growth factors and nutrients allowing the cells to be maintained *in vitro*, it also introduces animal-derived contaminants that must be considered during experimental design. In the case of experiments involving EVs, FBS is a source of unwanted bovine EVs, which could interfere with downstream analysis of cell culture-derived EVs. Two methods papers (Théry et al., 2006 and Witwer et al., 2013) stressed the necessity of either using EV depleted serum, or serum-free conditions if the cells could be grown without serum, when harvesting EVs from cell culture media. Recent studies have demonstrated how important this depletion step is when performing analysis of RNA contents of EVs as some RNA found in FBS is evolutionarily conserved and is indistinguishable from human transcripts (Shelke et al., 2014; Wei et al., 2016). Depleting the serum of EVs is particularly important when working with cell lines like the ones used in this project which cannot be grown in serum-free conditions without affecting cell viability.

Depleting serum of contaminating EVs can be performed by centrifugation of either the serum or the medium containing the serum at 100,000 x *g* for at least 18 h (Hill et al., 2013). Alternatively, EV-depleted serum can be purchased commercially. A recent article has raised considerable concerns that existing protocols for EV depletion are not sufficient to prevent contamination with bovine RNA species. The authors go as

far as to suggest some early findings that were considered breakthroughs in the field, including some of their own work, could in fact just be the results of persisting bovine contamination in culture as most bovine miRNA are 100% identical to their human homologs because of a high degree of conservation among mammals (Tosar et al., 2017). The authors have also identified several other possible sources of this contamination, including growth factors, extraction kit spin columns and ambiguous mapping. This is a particular problem with miR-1246 miR-4448, miR-3960, miR-1248, miR-1290, miR-574-5p and miR-644b-5p, these species are similar or identical to regions within ncRNA like RNU2. The suggestion being that the quantitation of these miRNA is affected by the presence of fragments of the longer ncRNA within the library (Tosar et al., 2017). The article concludes with the bleak tone that while current EV depletion approaches may not be good enough, the standard to which we should aspire, completely RNA free culture, is beyond our ability to achieve at this time.

EV purification has traditionally been achieved by serial centrifugation of either culture media or biofluids. There are numerous subtle variations on this methodology in the literature with additions of wash and filtration steps. Since the early 2000s biotechnology companies have begun to produce precipitation reagents aimed at reducing the time taken to harvest EVs. Work by Clayton and Webber (2013) elegantly demonstrated the extent of contamination with co-precipitated proteins when using different extraction techniques. The contamination was highest when using a precipitation reagent and lowest when using sucrose density gradient centrifugation. In 2014 a paper was published demonstrating that size exclusion chromatography could be used to purify EVs from platelets (Böing et al., 2014). The same group went on to work with Izon to develop the qEV column, a column of Sepharose CL2b with a top and

bottom bed support and a bed depth of 10 cm. Using these columns, it is possible to separate EVs from soluble proteins. The columns are also used to process samples with large starting volumes of biofluid or culture medium.

Literature searches indicate no firm consensus from the field on methods for the storage of EVs. A recent International Society for Extracellular Vesicles (ISEV) position paper stresses the importance of selecting appropriate storage buffers to prevent pH changes during storage and freeze thawing cycles (Lener et al., 2015). It also mentions that EV integrity is preserved better at -20^{o}C and -80^{o}C than at 4^{o}C. However, it only cites 4 different publications (Kalra et al., 2013; Lener et al., 2015; Lőrincz et al., 2014; Sokolova et al., 2011) as evidence for this, indicating just how little published evidence there is for appropriate storage protocols.

3.2. Aims and objectives

The aims of this chapter were to determine the most appropriate techniques for the purification of EVs produced by oral cancer cells for use in our laboratory. Once optimised these protocols would be used to produce EV samples for all experimental work performed as part of this PhD. During this optimisation, methods for depleting FBS of bovine EVs were compared along with different methods for purifying EVs from both low and high volumes of starting material. As future experiments would possibly require the long-term storage of EVs the impact of freeze-thawing stored EVs was also assessed.

3.3. Depletion of bovine EVs from FBS

3.3.1. Centrifugation for 18 hours at 100,000 x *g* removes bovine EVs from FBS.

The particle counts of commercially available EV-free serum and EV-depleted serum made in house were compared to undepleted serum to determine which method was most effective. EV-depleted serum was purchased from SBI (catalogue number EXO-FBS-50A-1) and used to make a standard DMEM culture medium (DMEM supplemented with 10% (v/v) FBS, 1% (v/v) L-Glutamine and 1% (v/v) Penicillin/Streptomycin). FBS purchased from Gibco was centrifuged at 100,000 x *g* for 18 h before being filter sterilised with a 0.22 µm filter and used to supplement DMEM culture medium with the same additives. To compare the success of EV depletion methods samples were analysed by TRPS using an NP100 nanopore (qNano, Izon).

Both the commercial serum and the in-house EV-depleted serum show a reduction of particle counts from $8.5x10^9$ to $1.4x10^9$ and $1.65x10^9$ respectively (figure 3.1). Interestingly neither method reduces the particle count to zero. There was no significant difference in particle counts between the commercially purchased serum and the serum depleted of EVs in house. All the samples exhibit similar size profiles (figure 3.2) with the majority of EVs below 100 nm in diameter. There are a few larger particles detected in the EV-depleted serum containing samples, particularly those depleted in house (figure 3.2 B&C), possibly as a result of aggregation occurring during the depletion techniques. As the qNano is not capable of determining the identity of particles passing through the nanopore, electron microscopy was used to visualise the particles present in the media.

Overnight centrifugation at 100000 x g reduces serum particle count

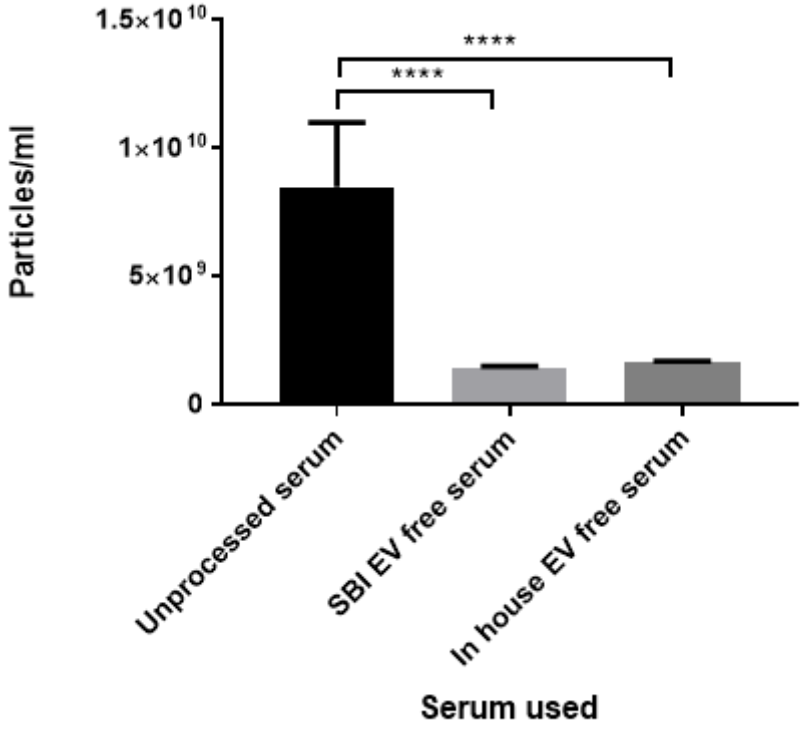

Figure 3.1 Particle concentrations of tissue culture DMEM made with FBS from three different sources. Unprocessed serum, EV free serum purchased from SBI Biosciences and serum depleted in house by 100,000 x g centrifugation overnight (18 h). The serum was diluted to a final concentration of 10% (v/v) in DMEM used for tissue culture. Supplemented DMEM was diluted 1 in 5 with filtered PBS containing 0.03% Tween-20 and run through a 0.22 μm centrifugal filter unit. Samples were then analysed by TRPS using an NP100 nanopore. The in-house and the SBI EV free serum were both seen to have significantly fewer particles when tested using a One-way Anova with Tukeys multiple test correction. n=2 technical replicates error bars representing SEM. **** = P <0.0001.

Size distribution profiles of bovine vesicles in DMEM

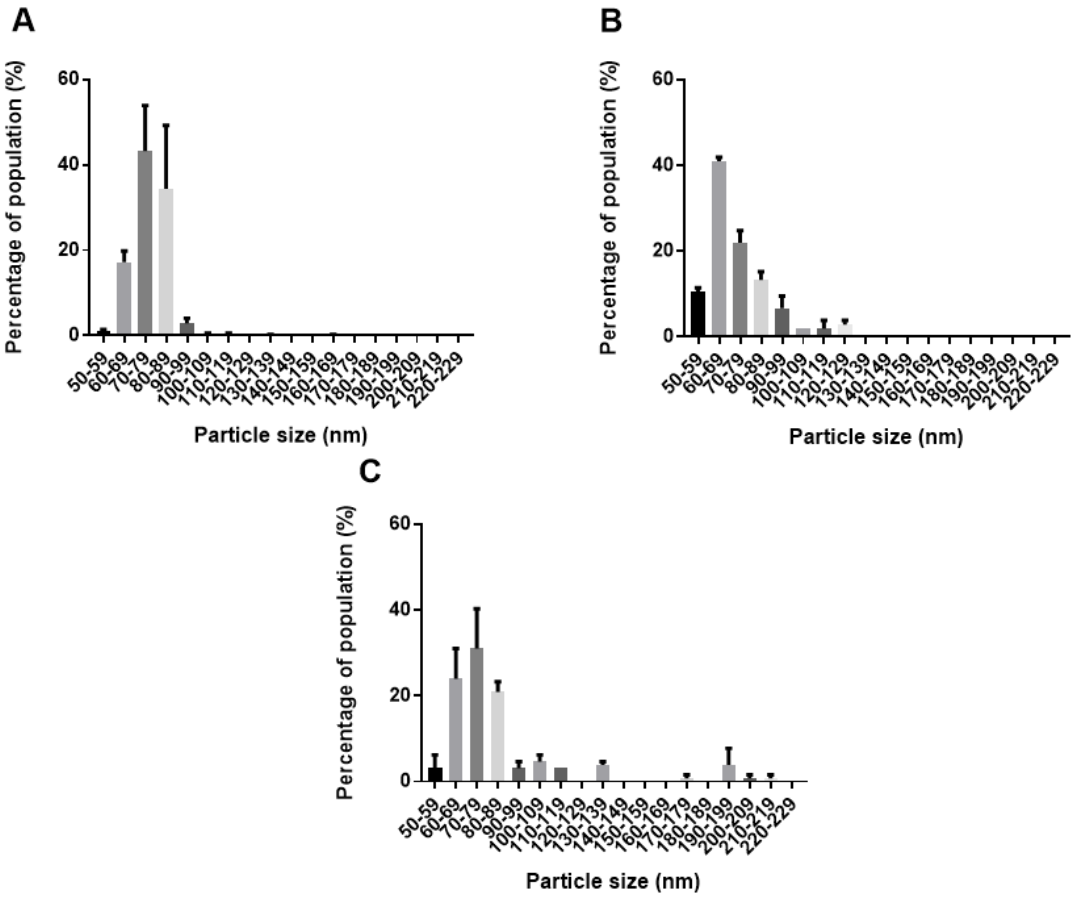

Figure 3.2 Size distribution profiles of tissue culture DMEM made with FBS from three different sources. Unprocessed serum (A), EV free serum purchased from SBI Biosciences (B) and serum depleted in house by 100,000 x g centrifugation overnight (18 h) (C). The serum was diluted 1 in 10 with DMEM used for tissue culture, the DMEM plus FBS was then diluted 1 in 5 with filtered PBS containing 0.03% Tween 20 and run through a 220 μm centrifugal filter unit. Samples were then analysed using an NP100 nanopore on Izons qNano. EVs are predominantly smaller than 100 nm in size for all three types of serum. Where the serum depleted in house was used, a few larger objects are detected around the 200 nm mark. n=2 technical replicates error bars representing SEM.

Overnight centrifugation at 100000 x g removes EV like structures from DMEM

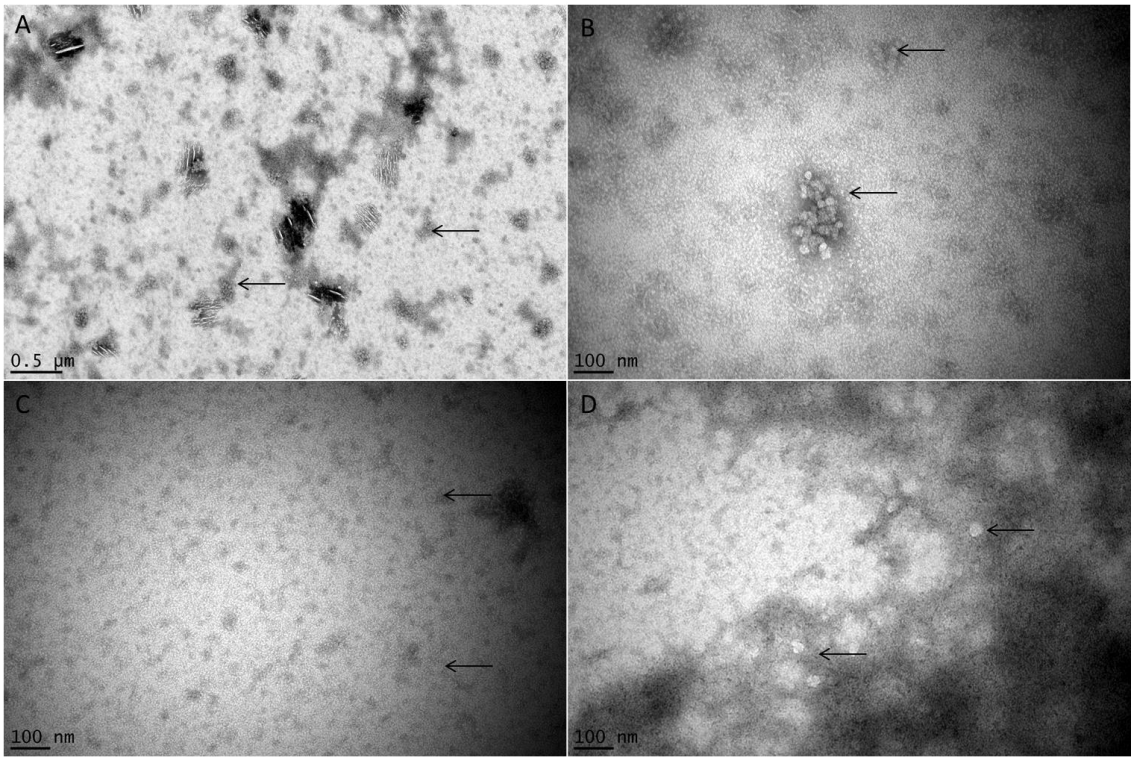

Figure 3.3 TEM images of DMEM supplemented with different serum types negatively stained with uranyl formate. DMEM made with undepleted serum (image A) at low magnification several clusters of vesicle like structures can be observed (marked with arrows). Image B is at a higher magnification and shows one of these clusters can be seen in the centre of the image comprised of multiple EVs. DMEM made with SBI Biosciences serum (Image C) and serum depleted of EVs in house (Image D) lack the clusters of small EVs observed in the DMEM with unprocessed serum but a few larger (60-80 nm) vesicle like structures are observed (marked with arrows) which is consistent with both the different particle concentrations and size distribution profiles seen with qNano. Representative images from 2 experiments.

As expected from the particle concentrations seen with the qNano, EVs are readily visible in the DMEM supplemented with unprocessed serum even at low magnifications (figure 3.3 A & B). These EVs appear to be quite small (less than 100 nm in size) and cluster together in large clumps which are distinctly visible at lower magnification. This is again consistent with the size profiles observed by the qNano, and the presence of the clusters indicates the capability of these EVs to aggregate even when they have not been subjected to the g forces experienced during the depletion steps. The large dense black structure seen in image A are salt crystals formed during the staining process. Images of DMEM containing the depleted sera do not show the clusters of small EVs present in the unprocessed samples (figure 3.3 C& D). There are a few larger vesicle like structures present which are around 80 nm in size in the serum depleted in house. This is consistent with the size distribution data from the qNano which showed 80 nm to be the modal size of particles in this sample. Similar structures were found in the SBI serum albeit slightly smaller in size which is again consistent with the data from the qNano. As depleting the serum of EVs in house was similarly efficient to the methods used by SBI biosciences this method was used for future experiments.

3.4. Comparison of EV purification methods

Three different EV purification methods were compared in order to determine which was the most efficient in our hands: ExoQuick reagent (SBI), a serial centrifugation method from Théry et al (referred to as the Théry method) (Théry et al., 2006) and a method with a filtration step from a paper published in 2007 (referred to as the Valadi method) (Valadi et al., 2007). The two serial centrifugation methods or

derivatives of them are widely used in the literature to purify EVs from cell culture media and using Clayton and Webber's particle to protein ratio measurement for purity have been shown to produce pure EVs with low protein contamination (Webber and Clayton, 2013).

3.4.1. High protein concentrations are seen in pellets produced by ExoQuick reagent

EV pellets produced by each of the extraction techniques were initially analysed by a BCA assay to determine the protein concentration (figure 3.4). The protein yields for the precipitation reagent are between two and three-fold higher than those seen for the serial centrifugation techniques potentially indicating a large quantity of co-precipitated protein impurities in this preparation. It is also interesting that the protein yields were more variable in extractions carried out using this reagent than either of the two centrifugation protocols tested. The Valadi method produces a lower yield of protein than the Théry method, but because this method utilises a filtration step excluding anything above 220 nm in size from the sample, it would suggest that the difference between the two is still contaminating proteins rather than EV proteins.

Serial centrifugation protocols produce lower protein yields than precipitation reagents

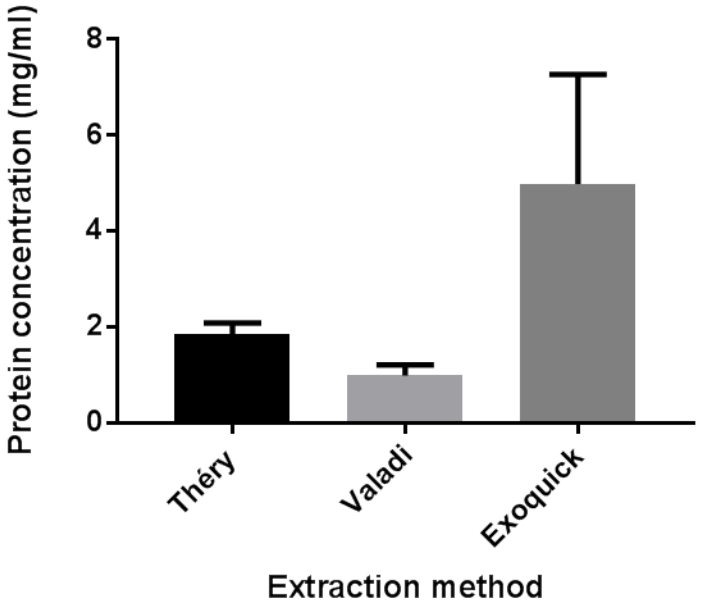

Figure 3.4 Protein concentration of vesicle pellets from three different vesicle purification techniques. Conditioned medium from confluent H357 cells was treated to one of three different extraction techniques and the final pellet resuspended in 1x RIPA buffer containing protease inhibitors. A BCA assay was used to determine the protein concentration of the resulting suspension. Protein concentration is around two-fold higher in the lysate produced by the ExoQuick method than in those produced by the serial centrifugation methods. Lysates produced by the Valadi method have marginally less protein in them than those produced by the Théry method. n=2 biological replicates error bars representing SEM. Results were non-significant with both a Student's Test and One-way Anova with Tukeys multiple test correction.

3.4.2. Detection of EV markers in pellets from different extraction techniques

To determine if the protein detected by the BCA assay was from lysed EVs, or just precipitated during the extraction, protein from the different extractions was normalised to the sample with the lowest concentration and 5 µg loaded into a well of a 12% polyacrylamide/SDS gel alongside 5 µg of protein lysate from whole cells. After transferring to a nitrocellulose membrane samples were treated with a panel of antibodies for proteins which had previously been detected in different EVs to determine which were present in the EVs purified by our techniques (Akers et al., 2013).

Antibody	**Marker for**	**Reference**
CD63	Exosomes	Escola et al., 1998
HSP70	Exosomes	Greening et al., 2015
ALIX	Exosomes	Lässer et al., 2012
TSP1	Apoptotic Bodies	van Engeland et al., 1998
ANNEXIN V	Apoptotic Bodies	van Engeland et al., 1998
VAMP3	Micro-vesicles	Muralidharan-Chari et al., 2009
ARF6	Micro-vesicles	Muralidharan-Chari et al., 2009

Table 3.1 List of antibodies used on pellets purified by the extraction techniques. The antibodies are markers for the three major subclasses of EVs identified in the literature. These were used to determine which previously identified markers were present on EVs purified from these cells using our protocol.

EVs purified by all methods are positive for CD63 and TSP1 but not HSP70

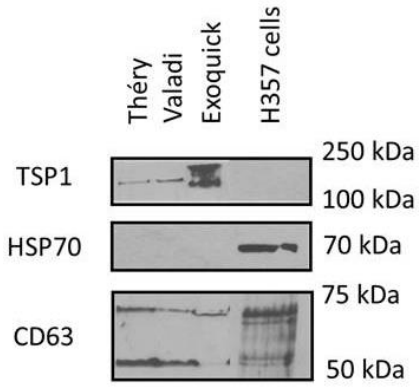

Figure 3.5 Detection of vesicle markers in pellets produced by three vesicle extraction techniques. Conditioned media was treated to one of three different extraction techniques and the final pellet resuspended in 1x RIPA buffer containing protease inhibitors. Whole cell lysate was produced by lysing 500000 H357 cells in 1x RIPA buffer and protease inhibitors. Following a BCA assay 5 µg of protein was run per lane of 12% acrylamide gel before transferring to a nitrocellulose membrane. Antibodies were diluted at 1:200 in 5% milk in TBST and incubated overnight at 4ºC. Secondary antibodies were used at 1:3000 in 5% milk in TBST and incubated for 1 hour. Bands for CD63 were in both the cells and in EVs purified by all extraction methods. TSP1 was in the EVs purified by all of the extraction methods but was not detected in the whole cell lysates. The reverse was seen for HSP70. Representative blot from 2 experiments.

Only three antibodies from the panel produced visible bands in the vesicle and cell samples these were HSP70 which was detectable only in the cells, TSP1 which was only detected in the EVs and CD63 which was detected in the both cells and EVs (figure 3.5). CD63 is a tetraspanin protein commonly referred to as a marker for exosomes and can be heavily glycosylated. The glycosylation most likely accounts the multiple bands seen for this protein, the ExoQuick method purifies samples with a greater proportion of the heavy form of the protein than the serial centrifugation approaches. The detection of CD63 in these samples would suggest that EVs are being successfully purified from the conditioned medium of H357 cells with these techniques.

TSP1 is thought of as a marker of apoptotic bodies and microvesicles. A double band was observed for TSP1 in the ExoQuick purified samples the second of which is approximately double the weight of the first. However, there is no record in the literature of multiple forms or dimers of this protein occurring, it would also be unlikely that a dimer would remain intact in the denaturing conditions of the SDS gel. The second band is close to the interface between the stacking and the resolving gels suggesting the upper band could be contaminants stuck in the stacking gel. Because of this uncertainty over the markers and the higher yields of protein generated using this method no further work was done using the ExoQuick reagent. HSP70 was detected in the cell lysates but not in the EVs purified by any of the methods suggesting it is unsuitable as a marker for EVs purified from these cells with these methods. Additionally, because CD63 was detectable in both the serial centrifugation methods but the Valadi method produced the lower protein yield, suggesting the filtration step reduced contamination, a hybrid final protocol was used in subsequent experiments (see section 2.3.4).

3.4.2.1. Wash step reduces protein concentration but doesn't remove EV markers

Clayton and Webber's work illustrated the efficacy of a wash step in further reducing protein contamination of EV samples (Webber and Clayton, 2013). Before adding one to our own protocol, media from three confluent T75 flasks of H357s were treated to the purification protocol detailed in section 2.3.4 both with and without a wash step the resultant pellets were lysed and BCA assays run to compare the final protein concentration. The wash step reduced the protein concentration in the sample from 4.3 mg/ml to 0.5 mg/ml whilst still retaining the band for CD63 indicating the presence of EVs in the sample (figure 3.6), interestingly the wash step appears to remove the larger form of CD63 seen in the unwashed sample suggesting that this is a co-precipitated contaminant of the extraction. On the strength of this evidence a single 90 min wash step was added to the combined protocol for subsequent use.

Wash step reduces protein concentration but doesn't remove CD63 band

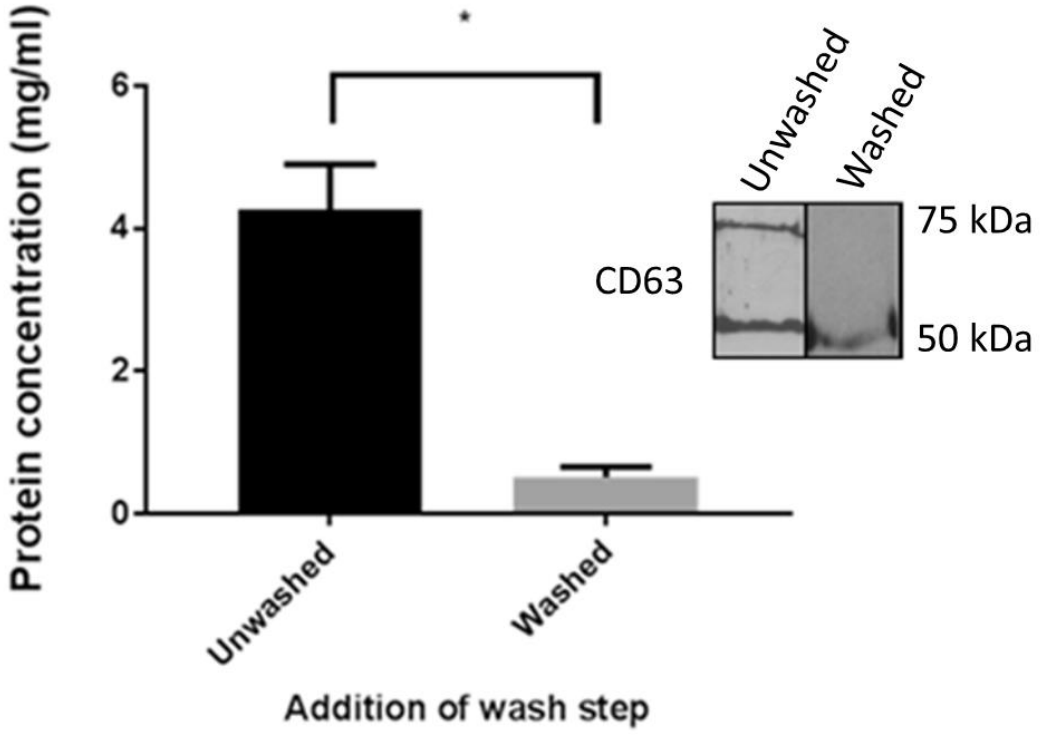

Figure 3.6 Effect of introducing a wash step on protein yield and detection of EV markers in pellet produced by final hybrid protocol. Conditioned medium was treated to the final extraction protocol. Three preparations were resuspended in 1x RIPA buffer containing protease inhibitors following the first 100,000 x g step. Three separate preparations were treated to a wash step using 1 ml of PBS and spun for 90 min at 100,000 x g the pellet was then resuspended in 100 ul of 1x RIPA buffer containing protease inhibitors. BCA assays were performed on the lysates. Protein concentration is reduced significantly by the wash step as determined by a two tailed unpaired students t test. 10 µg of EV lysate from the wash step was run on a 12% acrylamide gel and probed with CD63 primary antibody overnight after transferring to a nitrocellulose membrane. Following treatment with a HRP conjugated secondary antibody bands were detected in both the unwashed and the washed samples indicating the presence of CD63 in the pellet, representative blot from 3 experiments. n=3 biological replicates error bars representing SEM * = P <0.05 students T-test

3.4.3. Size exclusion chromatography can be used to purify vesicles from large starting volumes of culture media

Because of the limited capacity of our ultracentrifuge rotor an alternative method would be required for processing volumes of conditioned media above 30 ml. Such large volumes would be required for generating the yields of EV protein and RNA necessary for proteomic and transcriptomic analysis of their contents. Conditioned media from 3 confluent T175s of each of the cancer cells lines was concentrated from 60 ml to >1 ml using a Vivaspin 100 kDa MW cut off column and the concentrated media loaded on to a column of 15 ml Sepharose CL2B that had been allowed to settle under gravity for at least four hours. This gave a bed depth of 10 cm, the same depth used by the commercial columns. Twelve 0.5 ml fractions were taken from the column and the fractions used for a BCA assay to determine protein concentration and run through a NP150 nanopore on the qNano using appropriate stretch voltages and pressure settings to determine particle counts. Comparison of the particle count and the protein concentration of each fraction was used to generate an elution profile for the home-made columns. EVs eluted between fractions 4 and 9 in all cell lines peaking at fraction 8, the majority of the protein was eluted in fraction 12 indicating a good separation between EVs and protein is achieved by the column (figure 3.7).

EV's elute at fractions 4-9 on homemade SEC column with protein eluting at fractions 10-12

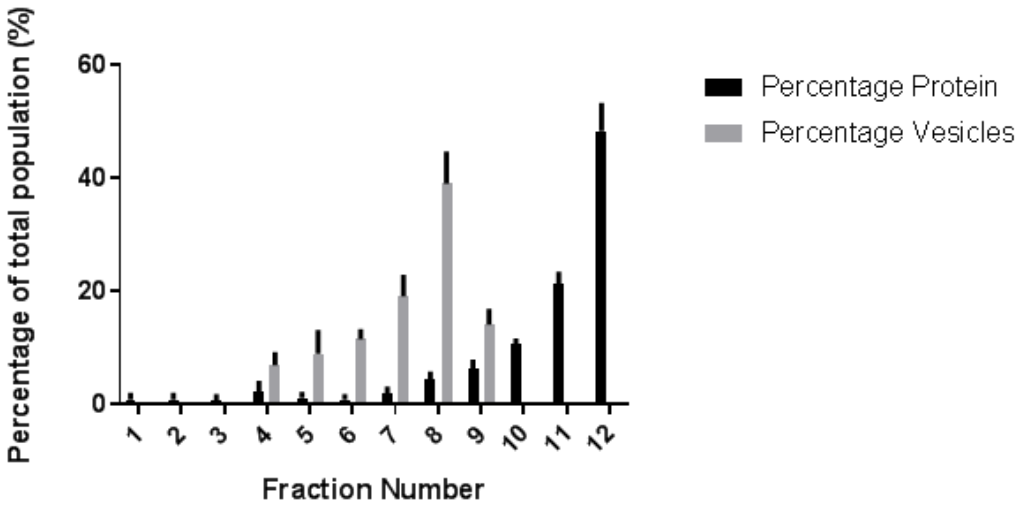

Figure 3.7 Elution profile of homemade Sepharose column. 60 ml of conditioned media was cleared of dead cells and cell debris before being concentrated down to >1 ml in volume using a 100 kDa MW cut off filter unit. The concentrated media was applied to the top of a fresh Sepharose CL2B column with a bed volume of 10 ml. Twelve 0.5 ml fractions were collected using PBS with 0.03% Tween 20. Fractions collected were analysed for protein concentration using a BCA assay and vesicle number using a qNano TRPS instrument with an NP150 nanopore. The combined data from four different cell lines was used to create a combined elution profile for the home-made columns. EVs are in fractions four through nine, with the peak being fraction eight. The majority of the protein elutes from the column in fractions ten to twelve. n=4 biological replicates error bars representing SEM.

3.5. Storage of EVs

3.5.1. Intact vesicles are seen by TEM after freezing at -20^{o}C

Because of the long duration of the intended experiments in this project EVs would have to be stored regularly. With this in mind EVs from the same serial centrifugation preparation were used to prepare grids for TEM before and after freezing to -20^{o}C and thawing on ice to determine if this had any impact on the integrity of the EVs. Under electron microscopy intact EVs are seen both before and after the freeze thaw cycle strongly suggesting this does no damage to the EVs structural integrity (figure 3.8). The EVs in both images have similar size ranges (80-150 nm) but do exhibit subtly different morphologies, with those that have been frozen showing a more compressed shape. However, it is uncertain if this is caused by the freezing, or as is more likely the fixation. Similar shapes have been seen by other groups using protocols that contain a fixation step, this morphology is however missing when EVs are fixed using cryo EM techniques.

Freezing to -20ºC and thawing on ice has no impact on EV morphology

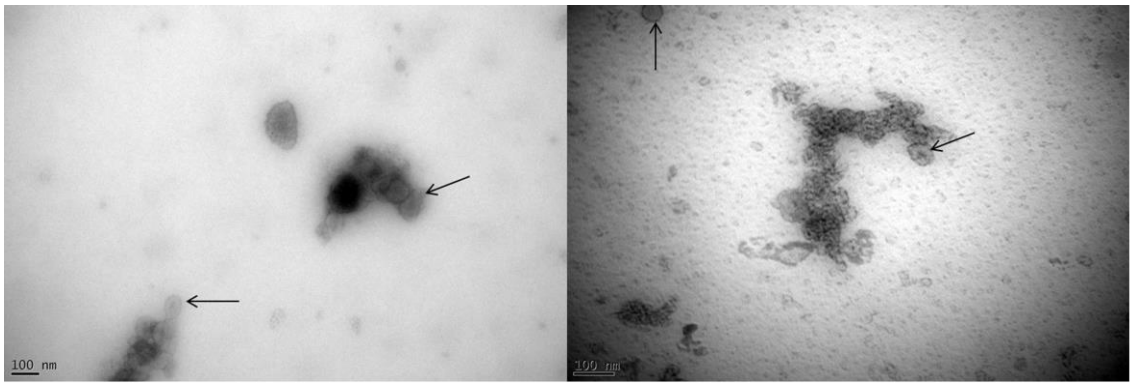

Figure 3.8 Transmission electron microscopy of EVs before and after freezing. EVs were extracted from the culture medium of confluent H357 cells using serial centrifugation and resuspended in PBS. The final suspension was split into two fractions and one of these was frozen at -20ºC and thawed on ice. Both were then fixed in 2% paraformaldehyde and then adsorbed on to formvar coated EM grids and negatively stained using uranyl acetate and uranyl oxalate before imaging with a Tecani Spirit G2 microscope. EVs (marked by arrows) were clearly visible both before (left hand image) and after (right hand image) freeze thawing with intact membrane structures and similar sizes. Representative images from 3 experiments.

3.5.2. Freezing to -20°C and thawing on ice has no impact on EV samples particle count

Alongside TEM samples were prepared in a similar fashion and used for analysis with the qNano. Samples split into two 50 µl fractions, one of which was frozen at -20°C before thawing on ice. Samples were diluted 1 in 10 and ran through an NP100 nanopore with appropriate stretch, voltage and pressure settings. The particle counts seen by the qNano were very similar before and after the freeze thawing suggesting that there is no damage caused to the EVs during the freeze thawing cycles (figure 3.9). There is however a difference in the size distribution profiles of the particles (figure 3.10). Before freezing the mode size is 110 – 120 nm but after a freeze thaw cycle this has shifted to 70-90 nm. Taken together this evidence suggests that EVs can be stored at -20°C and thawed on ice without a loss of structural integrity or a reduction in numbers. Where required EVs would be stored at -20°C in future experiments but with care taken to minimise the number of freeze thaw cycles a sample was subjected to.

Freezing to -20ºC and thawing on ice has no impact on EV sample particle count

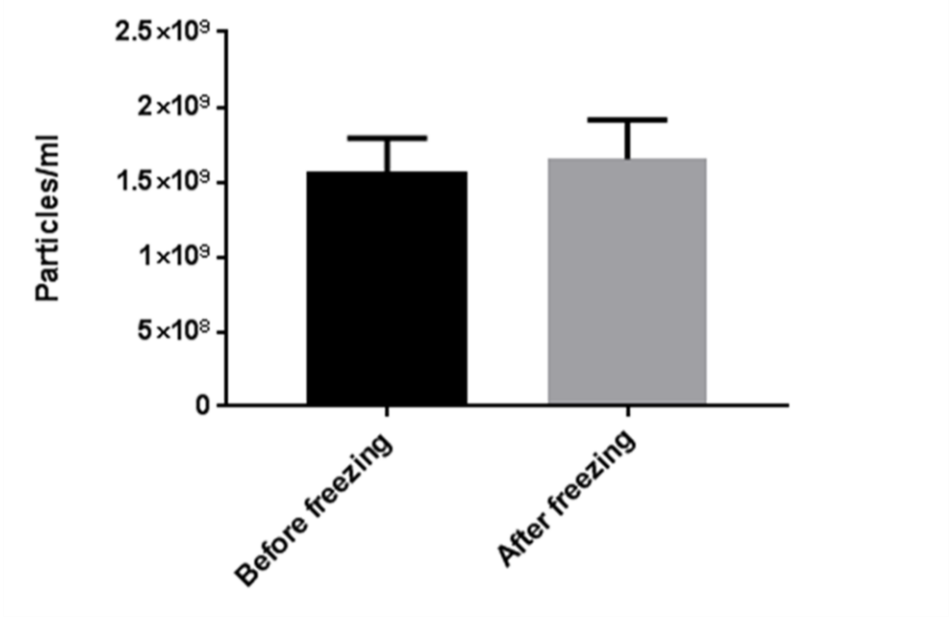

Figure 3.9 Particle counts of EV samples pre and post freezing. EVs were extracted from the culture medium of confluent OSCC cells using serial centrifugation and resuspended in PBS with 0.03% Tween 20. This final suspension was split into two fractions one of these was frozen at -20ºC and thawed on ice. Both fractions were then run through the qNano using an NP100 nanopore with appropriate settings. Particle counts were determined against CPC100B calibration beads. The freeze thaw cycle has no detectable impact on the number of particles in the sample difference was non-significant when tested with a student's T-test. n=4 biological replicates error bars representing SEM

Freezing to -20ºC and thawing on ice slightly alters EV particle distribution

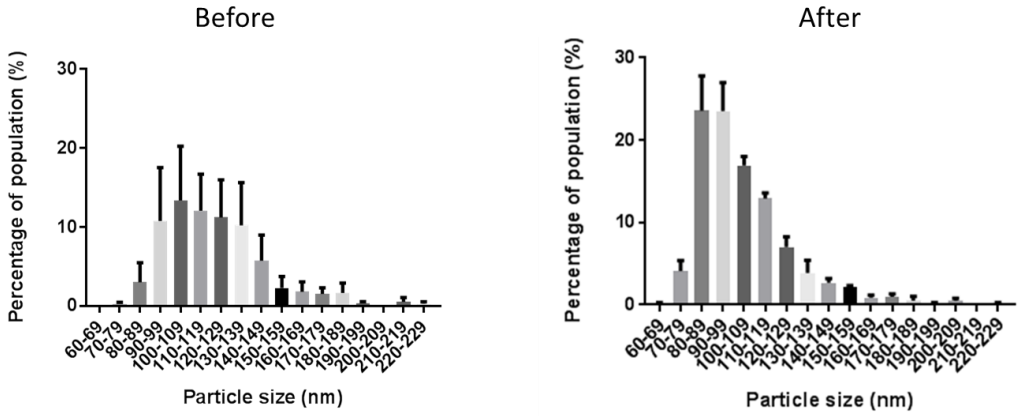

Figure 3.10 Size distribution profiles of EV samples pre and post freezing. EVs were extracted from the culture medium of confluent OSCC cells using serial centrifugation and resuspended in PBS with 0.03% Tween 20. This final suspension was split into two fractions one of these was frozen at -20ºC and thawed on ice. Both fractions were then run through the qNano using an NP100 nanopore with appropriate settings. Size distribution profiles were created using the data from the qNano. The freeze thawing process is shown to have shifted the size distribution with more smaller particles detected. This could be due to the breakup of vesicle aggregates into single EVs during the freeze thawing. n=4 biological replicates error bars representing SEM.

3.6. Discussion

In this chapter overnight centrifugation has been shown to deplete FBS of bovine EVs comparably to commercially depleted serum with around 75% of the EVs present in undepleted FBS removed by both protocols which is consistent with data from other groups (Shelke et al., 2014). Two different protocols for extracting EVs from both large and small volumes of conditioned media have been developed from a combination of established methods used by other groups. Antibodies for a range of proteins which have previously been detected in EVs were used to determine which markers were present in our EVs with whole cell lysate included as a control. Of this panel of antibodies only CD63 and TSP1 were present in our EVs. CD63 is widely reported to be a marker of EVs in the literature and is heavily glycosylated. Its expected weight is 26 kDa but is seen in all our samples to be present in two bands one at 50 kDa a second at 75 kDa potentially caused by variable glycosylation, that similar bands were in the whole cell lysate and in the vesicle samples suggests this glycosylation is a feature of the oral cancer from which this cell line was established. TSP1 has been considered as a marker of apoptotic bodies its presence in EVs purified by all three techniques suggests either that there is some contamination with apoptotic bodies, which is unlikely as these cells were grown in normal culture conditions and this protein was not detected in the cells, or it is present on other vesicle classes as suggested by entries in the database Exocarta (Chan et al., 2015).

EVs produced from these methods have been determined to have a reasonable degree of purity by methods available to us in the laboratory. Unfortunately, a direct comparison with the particle protein ratios determined by Clayton and Webber was not possible with this data for two reasons. Firstly, experiments were performed in my first

year prior to the arrival of the qNano in our laboratory. Secondly Clayton and Webber used a Nanosight instrument for the determination of particle count in their samples, whilst the two instruments perform the same function the different technologies used mean the particle counts are not easily comparable. The late arrival of the qNano in our laboratory also prevented a more detailed comparison of the three extraction techniques in terms of particles purified being carried out. As using protein concentration alone is inadequate to quantify the EVs it is still possible that the ExoQuick reagent was purifying more particles than the serial centrifugation methods. The elution profile of our homemade columns was similar to that published by Izon and their collaborators (Böing et al., 2014) with EV elution peaking at fractions 7 and 8.

Storage of EVs was also assessed using a combination of methods and EVs were seen to remain intact via TEM after freezing to -20^{o}C and thawing whilst TRPS shows no reduction in the number of particles in the sample. There were however differences in the size profile of the EVs before and after freezing. These shifts are possibly caused by dissociation of aggregated EVs during the freeze thawing, this would also explain the marginally increased particle counts following freeze thawing. The qNano is not able to distinguish clusters of EVs as individual particles and it will instead see them as a single larger particle. EVs were seen to cluster together under TEM, which may be caused by the final centrifugation step of the extraction process, but there was no consistent or quantifiable decrease in size of the EVs seen under TEM post freeze thawing. Another possibility is that some precipitation of the phosphate salts has occurred during the thawing process giving rise to small particles detectable by the qNano. This data compliments that published in previous papers, whilst our work hasn't touched on multiple freeze thaw cycles (Sokolova et al., 2011) or functional assays of

the EVs (Kalra et al., 2013) it has combined TEM and TRPS which will show any changes in pure particle number more accurately than the paper published in 2014 (Lőrincz et al., 2014), this combination of techniques has not previously been used in this context.

For experiments in subsequent chapters, all culture media required to be EV free will be supplemented with FBS treated with a 100,000 x *g* centrifugation overnight to remove bovine EVs as described in this chapter. The final serial centrifugation developed in this chapter (figure 3.11) will be used routinely for work performed in other chapters with vesicles stored at -20^{o}C in appropriate buffers for downstream experiments for future use. For generating the EV to produce sufficient RNA and protein for the next generation sequencing and mass spectrometry the size exclusion protocol developed in this chapter will be used instead of the serial centrifugation protocol.

3.6.1. Future work

Further work for this chapter should begin by confirming the functional integrity of EVs pre and post freezing. This would rely on the identification of a functional trait of the EVs which could be robustly quantified such as delivery of a particular protein or RNA. Work should also be done to study the effect of multiple freeze thaw cycles on EV numbers size and activity. It would also be instructive to perform a more in-depth comparison of the EVs purified from the different extraction techniques. This should include average diameters, size ranges, protein and RNA contents as well as functional activity. An alternative direction to take this research would be to follow the lead of other groups in the literature and perform parallel experiments on the products of the 10000 x *g* and 100,000 x *g* pellets of the serial centrifugation process.

Final workflow

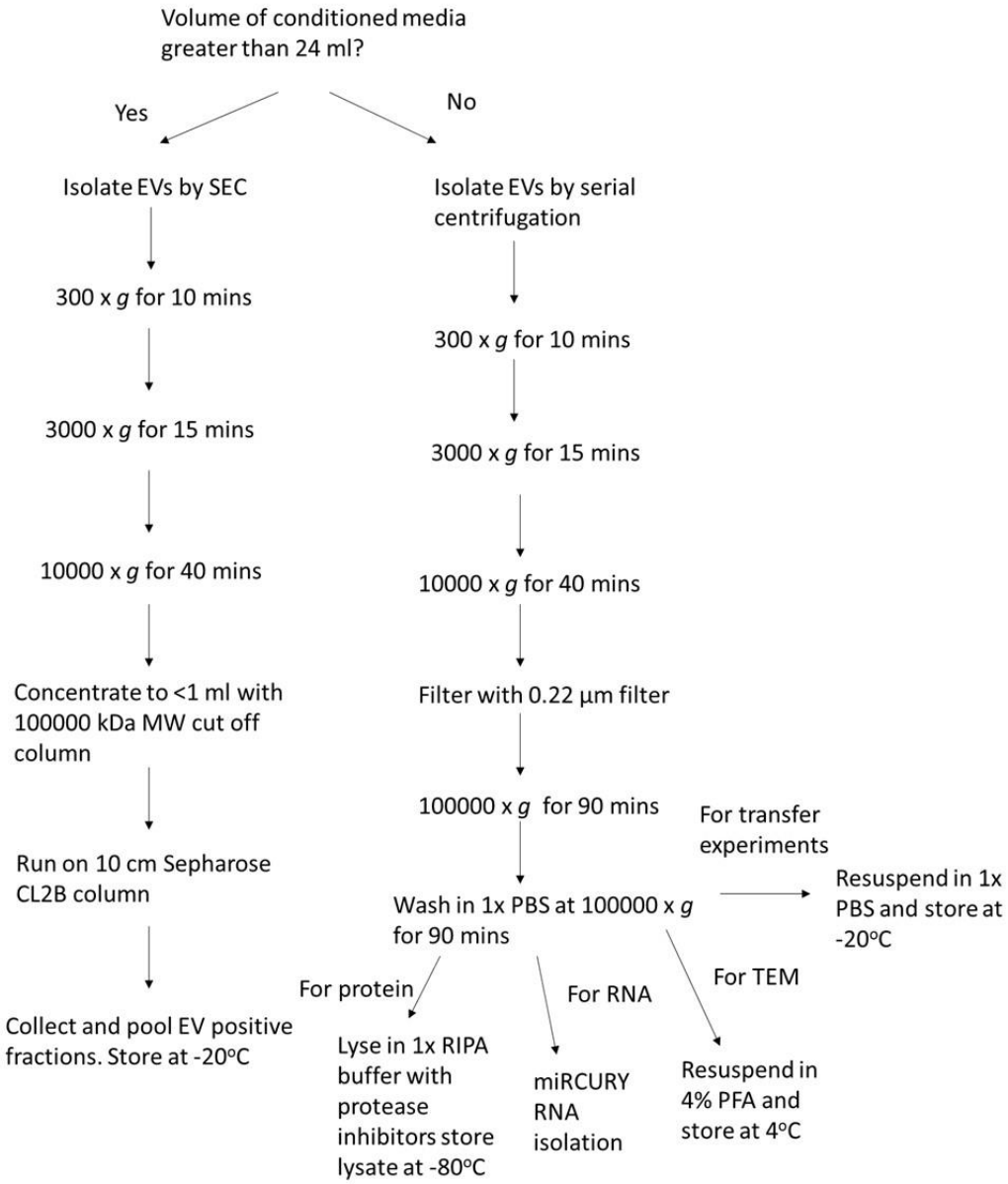

Figure 3.11 Schematic outlining routine workflow for EV purification which will be used for future chapters. Volume of starting medium will determine the choice of purification technique with volumes larger than 24 ml purified by size exclusion. The choice of resuspension buffer and storage will depend on intended downstream experiments with the purified EVs.

4. Characterisation of EVs produced by oral cancer cells

4.1. Introduction

Oral cancer, like other solid tumours, progresses through a defined process of tumourigenesis from dysplasia to carcinoma and finally, potentially, metastasis. To date there is a dearth of studies that explore how tumourigenesis effects EV production, although it is often speculated that circulating EVs in biofluids could be used as prognostic markers for disease progression as discussed in this review (Torrano et al., 2016). A study using an inducible mouse embryonic fibroblast model identified an interesting change upon the induction of an oncogenic transformation. The number of EVs released remained similar but the EVs released from the transformed cells contained a signalling protein (Kreger et al., 2016). This protein, focal adhesion kinase, allowed the EVs to promote the survival of untransformed fibroblasts and enhance their proliferation under anchorage independent conditions. This indicates a change in EV signalling caused directly by the induction of tumourigenesis.

However, this model has its limitations the induction of tumourigenesis is artificial and simplified by comparison to a real tumour. A study comparing oligodendroglioma cells and astrocytes, an example of natural tumour progression, (Schiera et al., 2013) suggests that a change in vesicle production occurs as a mechanism for the release of a histone protein H10. However, although they were able to demonstrate the transformed cells released vesicles containing this protein, they were not able to detect a change in vesicle production. It is also known that HPV can cause an increase in EV production in infected cells as a mechanism for spreading viral RNA (Ahmed et al., 2014). Although this viral transformation of cells is relevant in the

progression of some oral cancers many cases are not caused by an oncolytic virus but by other carcinogens.

EV production rates and size ranges can be measured using an instrument like the qNano or Nanosight and changes in these numbers between cancer stages can be easily identified. Whilst TEM has its limitations when studying EVs, particularly with regards to fixation induced changes in morphology, when membrane stabilising reagents are included in the protocol it remains a useful and accessible method for visualising the EVs. TEM experiments can be used to validate the size ranges observed with particle counting instruments alongside identifying any dramatic changes in morphology of the EVs. Thanks to databases like Exocarta and the work of numerous groups within the field there are a wide variety of protein markers for EVs that can help to distinguish the origin and status of the vesicle.

4.2. Aims and objectives

The aims of this chapter were to use the protocols developed in the previous chapter to isolate EVs from the culture media of oral cancer cell lines representing different stages of the disease. The physical properties of these EVs were characterised by a combination of TEM and TRPS to determine the size ranges and rates of production for the different cell lines. The Agilent Bioanalyzer and western blotting were used to identify RNA populations present in and any protein markers carried by the EVs produced.

4.3. EVs are produced by oral cancer cells representing different stages of tumourigenesis

Four cell lines were assembled representing various stages of oral cancer progression from the same primary site. D20 is a cell line established from a leukoplakia (a white lesion of the oral mucosa) situated on the lateral tongue of a 50-year-old non-smoking male and which was found to be immortal after over a hundred passages. This cell line is representative of an early stage of the tumourigenic process in oral cancer and progressed into a carcinoma within five years in this patient. D35 is a cell line established from an erythroleukoplakia (a red and white non-homogenous lesion of the oral mucosa) situated on the lateral tongue of 68-year-old male smoker and which was found to be immortal after over a hundred passages. This cell line represents a more severe dysplasia which is in the process of acquiring the mutations that will see it progress into a carcinoma and progressed to a carcinoma in situ shortly after the cell line was established. H357 is a cell line established from squamous cell carcinoma of the tongue from a 74-year-old male patient who smoked between the age of 17 and 20. The carcinoma was a STNMP stage 1, well differentiated, node negative tumour. Finally, B22 is a cell line established from the lymph node metastasis of an 88-year-old male smokers cancer of the tongue. The tumour was stage four well differentiated with invasion of multiple nodes. This cell line represents a local metastatic deposit of the lymph nodes.

To determine if EVs were being produced by these cell lines the conditioned media was subjected to the purification protocol developed in the previous chapter and the resulting sample adsorbed on to a TEM grid. Vesicle like structures can be clearly seen under the electron microscope (figure 4.1). For the mild dysplasia on the left (D20;

figure 4.1A) multiple EVs can be seen with a clearly defined outer membrane and an electron sparse lumen. These EVs range between 50 and 120 nm in size and are not observed to cluster. On the right (figure 4.1B) a single vesicle can be seen in the centre of the image, this is a larger vesicle, 150 nm in size, with a more electron dense cytosol than the EVs of the left-hand image, although this may be an artefact of the staining.

For EVs from the severe dysplastic cells (D35; figure 4.1C&D) similar sizes were observed (around 150 nm) and have very clearly defined membrane bilayers. In the left-hand image (figure 4.1C) there is some evidence of the 3D shape of the vesicle with a concave depression in the centre. Those in the right-hand image are more 2D in nature (figure 4.1D) indicating the variability of the fixation process. This image is the only one which shows evidence of a classic lipid bilayer like structure to the membrane, the other images do show some internal membrane like structure, but this is more central and possibly artefactual in nature.

Similar morphological variation was seen in the EVs from the carcinoma cell line (H357; figure 4.1E&F) however unlike the severe dysplasia derived EVs they were observed most frequently in clusters like those seen in the centre of both images. Smaller clusters were also observed in the EVs produced by the metastatic deposit cell line (B22; figure 4.1G) although the EVs are a similar size to those seen from other cell types. The vesicle in the centre of the right hand (figure 4.1H) image displays an unusual morphology not seen in the EVs produced by other cell types. This vesicle is around 160 nm in size and has an extremely electron dense region within the lumen suggesting the presence of more complex lipid or protein structures.

EVs purified from OSCC culture media medium exhibit different morphologies under TEM

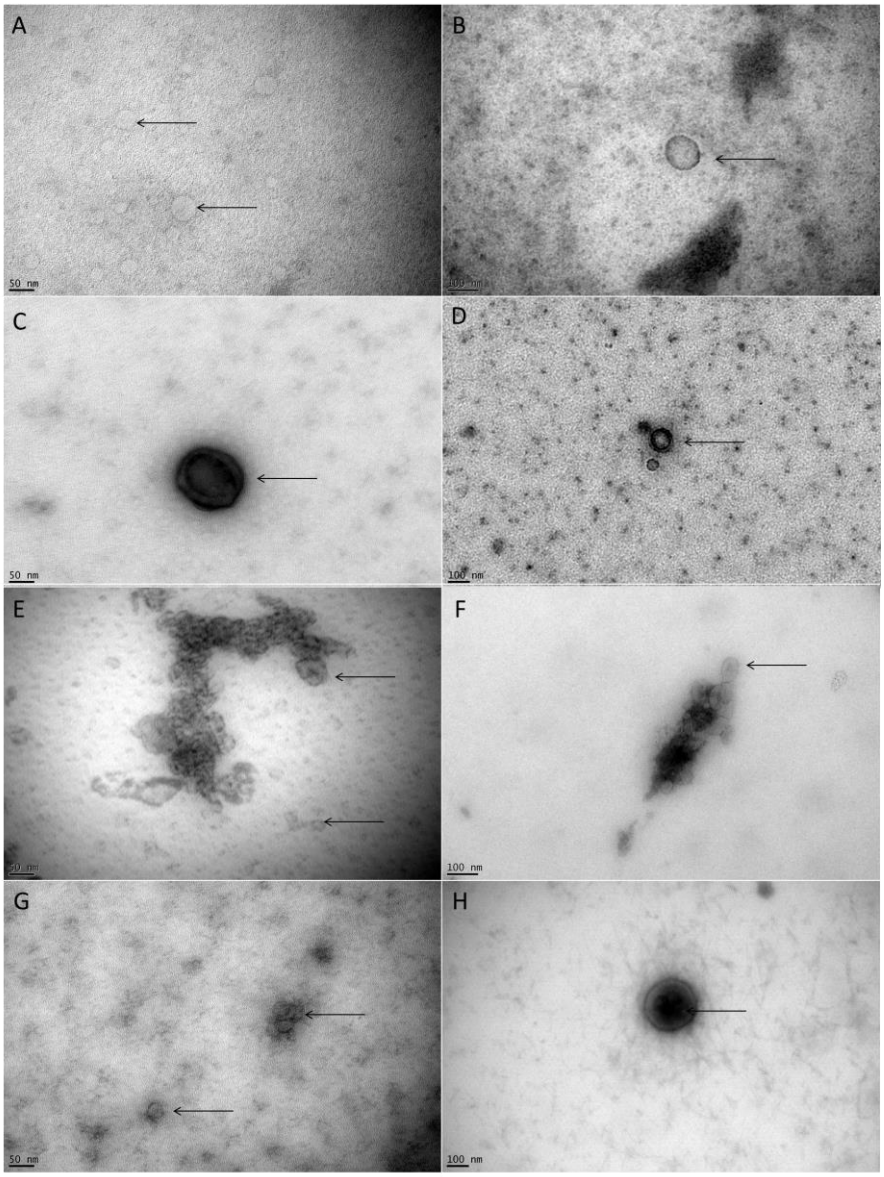

Figure 4.1 TEM of EVs released by oral cancer cell lines from different stages of oral cancer. From mild dysplasia (A&B), severe dysplasia (C&D) a non-metastatic carcinoma (E&F) and cells from a metastatic deposit (G&H). Conditioned media from oral cancer cells was treated to the serial centrifugation protocol as previously described. The resultant sample was adsorbed onto a formvar coated 200 mesh TEM grid and negatively stained with uranyl acetate and uranyl oxalate. Vesicle like structures (marked with arrows) are clearly visible in all images ranging from 50-200 nm in size. Representative images from 2 experiments.

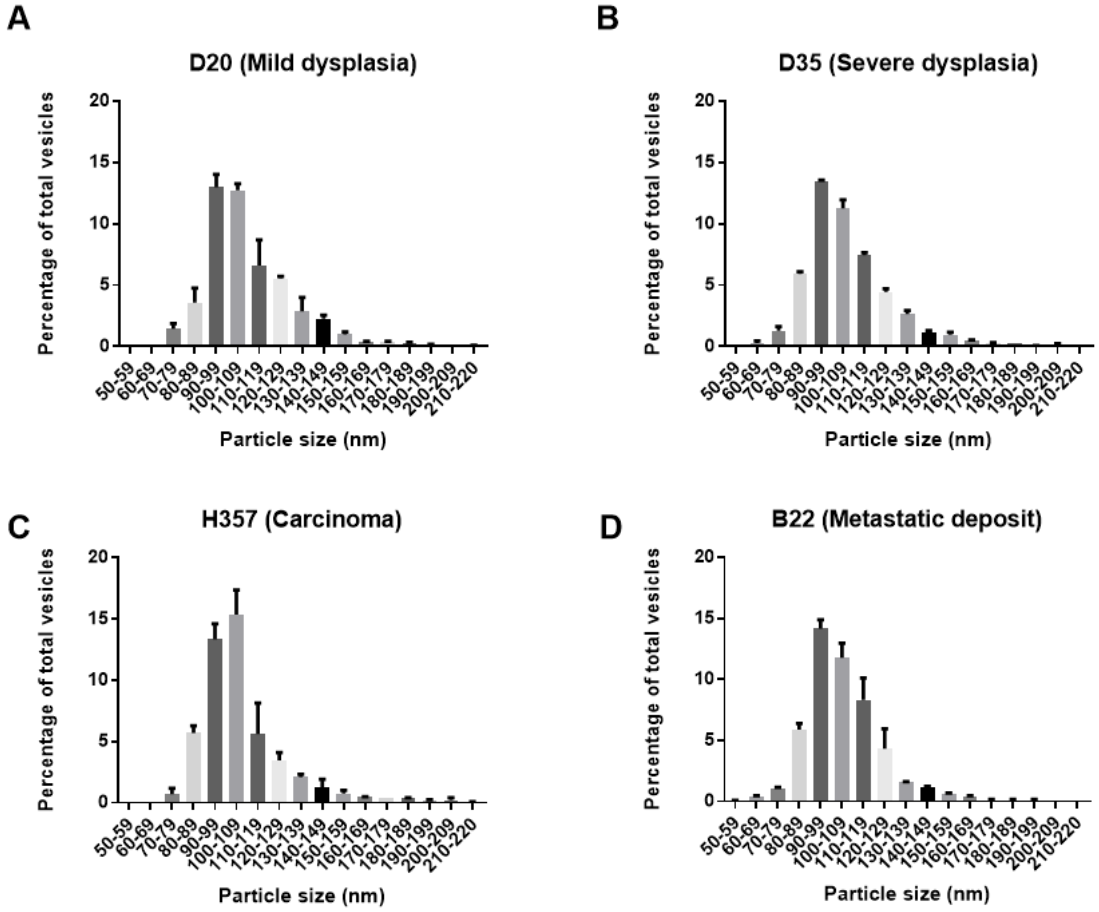

Figure 4.2 Size distribution profiles of EVs produced by oral cancer cell lines from different stages of oral cancer. From mild dysplasia (A), severe dysplasia (B) a non-metastatic carcinoma (C) and cells from a metastatic deposit (D). EVs were extracted from the culture medium of 500000 cancer cells using the protocol developed in the previous chapter as far as the filtration step to minimise the loss of EVs during the higher speed spins and get as close to the total EVs produced for this cell line as possible. Samples were run through an NP100 nanopore using appropriate stretch voltage and pressure settings and the data used to generate a size distribution profile. Detected EVs range in size from 60-210 nm with the modal size being 90-110 nm. n=3 biological replicates error bars representing SEM.

Alongside the electron microscopy conditioned culture media was prepared to use for TRPS analysis with the qNano to quantify the production of EVs by these cell lines using methods detailed in 2.3.6. The size distribution profiles (figure 4.2) generated were consistent with the sizes seen under TEM, with a marked similarity for all the cell lines EVs, only the metastatic cells (figure 4.2 D) produced EVs with a marginally larger modal size of 100-110 nm as opposed to 90-100 nm for the other cell lines. The data acquired shows that EVs from the different cell lines used in this project share similar physical properties. They are similar in size with only EVs from the carcinoma cells showing a slightly different size profile in that it has no EVs smaller than 70 nm and a larger modal size of 100-109 nm. Because of the physical characteristics selected for by the extraction protocol it was expected that the EVs would share similar size ranges with very few particles around the 200 nm mark thanks to the filtration step. Interestingly when the mean diameter of the EVs is compared (figure 4.3) a trend of increasing size with cancer stage is observed with the mean diameter increasing from 99-126 nm. EVs from the metastatic deposit cells were seen to be significantly larger than those of the severe dysplastic cells with a one-way Anova using Tukeys multiple test correction.

Images from the TEM grids show that EVs also share similar morphological properties. In general, the EVs show a well-defined outer membrane which is electron dense with a lumen that is electron poor. There are a few exceptions to this, notably where only a single EV is in the image frame, where the lumen is extremely electron rich. This would normally indicate a large quantity of lipids which stain well with these negative stains, but it is likely to also be an artefact of

the staining or the software trying to normalise the staining against the background with a small area of well stained grid in frame.

4.4. Comparison of production rates of EVs from different stages of oral cancer

The same samples that were used to generate the size distribution profiles for each of the cell line-derived EVs were also used to generate production figures per cell in 24 hours (figure 4.4). The rates of EV production were consistent for 3 of the cell lines, the mild dysplastic, the carcinoma and metastatic cells produced around 1500 EVs per cell in 24 hours but the severe dysplastic cells produced more than double that at around 4000 per cell in 24 hours. This difference was statistically significant by a one-way Anova with Tukeys multiple correction test.

Average sizes of EVs produced by OSCC cells

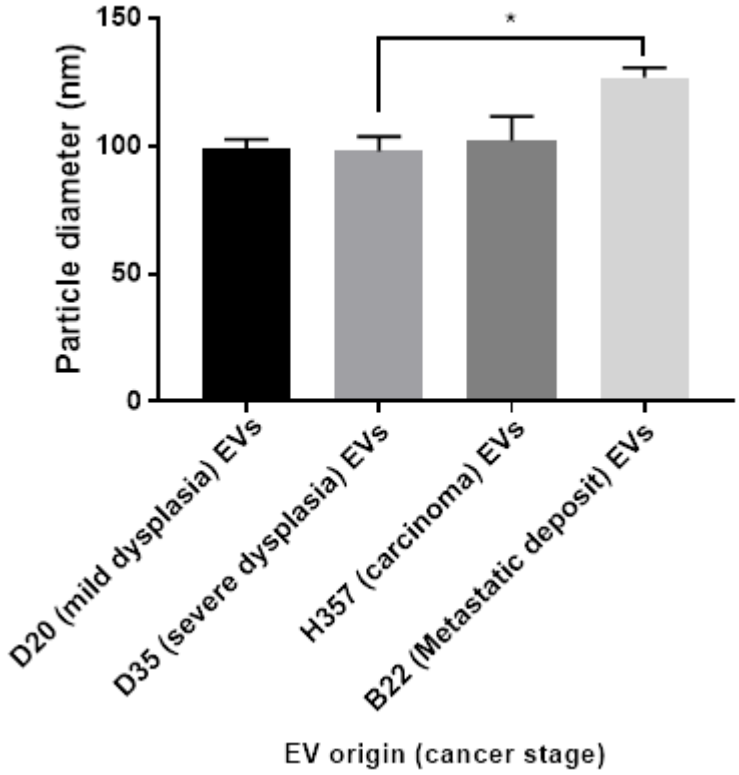

Figure 4.3 Mean diameter of EVs purified from the conditioned media of confluent OSCC cells by serial centrifugation. The EVs were resuspended in PBST before diluting 1in10 and running through a 0.22 µm centrifugal filter cartridge and measuring on an NP100 nanopore with appropriate stretch voltage and pressure settings. Values were compared to CPC100b calibration beads and the mean diameter calculated. General trend suggests and increase in average size with cancer stage, only the difference between the D35 (severe dysplastic) cell EVs and the B22 (metastatic deposit) cell EVs was seen to be significant by one-way Anova with Tukeys multiple test correction. Error bars representing SEM for n=3 biological repeats. * = $P < 0.05$.

Severe dysplastic cells produce double the EVs in 24 h

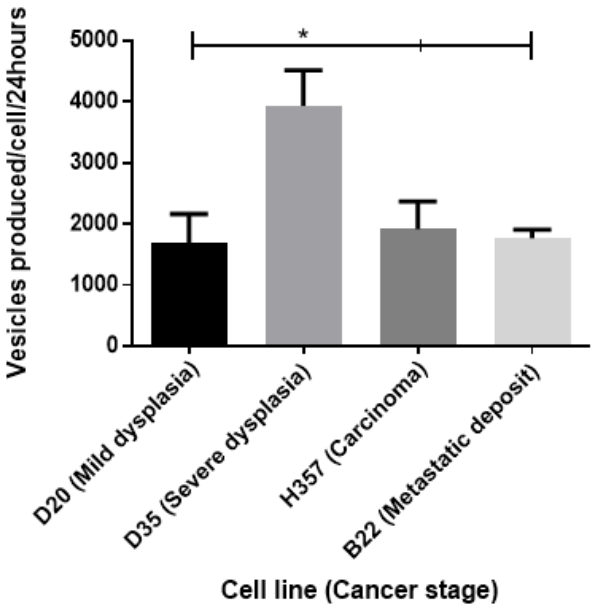

Figure 4.4 EV production rates of oral cancer cell lines. EVs were extracted from the culture medium of 500000 cells of each of the cell lines using the protocol developed in the previous chapter as far as the filtration step to minimise the loss of EVs during the higher speed spins and get as close to the total EVs produced for this cell line as possible. Samples were run through an NP100 nanopore using appropriate stretch voltage and pressure settings and the concentration of the samples used to generate a production figure per cell in a 24 period. The production was seen to be consistent with around 1500 EVs produced per cell in 24 hours for all bar the severe dysplastic cells where it is nearly 4000 EVs per cell in 24 hours. This difference was shown to be significant (p=>0.05) by a one-way Anova with Tukeys multiple correction test. n=3 biological replicates error bars representing SEM.

4.5. RNA can be purified from EVs produced by oral cancer cells

The Bioanalyzer (Agilent) was able to detect RNA in EVs produced by each of the oral cancer cell lines (figure 4.5). The bulk of the detected RNA falls between around 25 and 200 nucleotides, this spans the size ranges of miRNA and some smaller mRNA species, the RNA types most commonly associated with EVs. The mild dysplastic EVs show a peak of 20 FU at around 1000 nucleotides; the instrument has labelled some of this as contamination with 18s rRNA, a structural component of the small subunit of the eukaryotic ribosome. There are small peaks for this subclass of rRNA detected in each of the samples with similar small peaks for 28s rRNA present in EVs produced by the severe dysplastic and carcinoma cells. The severe dysplastic EVs contained the lowest signal for RNA, between 0-20 FU and the mild dysplastic EVs contained the highest, between 0-80 FU. 834.5 pg/µl and 1602.5 pg/µl of RNA was present in EVs purified by size exclusion chromatography from the culture media of the mild dysplastic and carcinoma cell lines (figure 4.6). This rises to around 6382 pg/µl and 4606 pg/µl in the severe dysplastic and metastatic deposit cell lines respectively (figure 4.6). These figures which were generated from separate biological replicates appear to contradict each other with the severe dysplastic vesicles having the lowest RNA content in the first experiments and the highest in the second. This would suggest that the protocols used to harvest RNA from the EVs have a poor repeatability.

EVs from OSCC contain high numbers of RNA between 25 and 200 nucleotides long

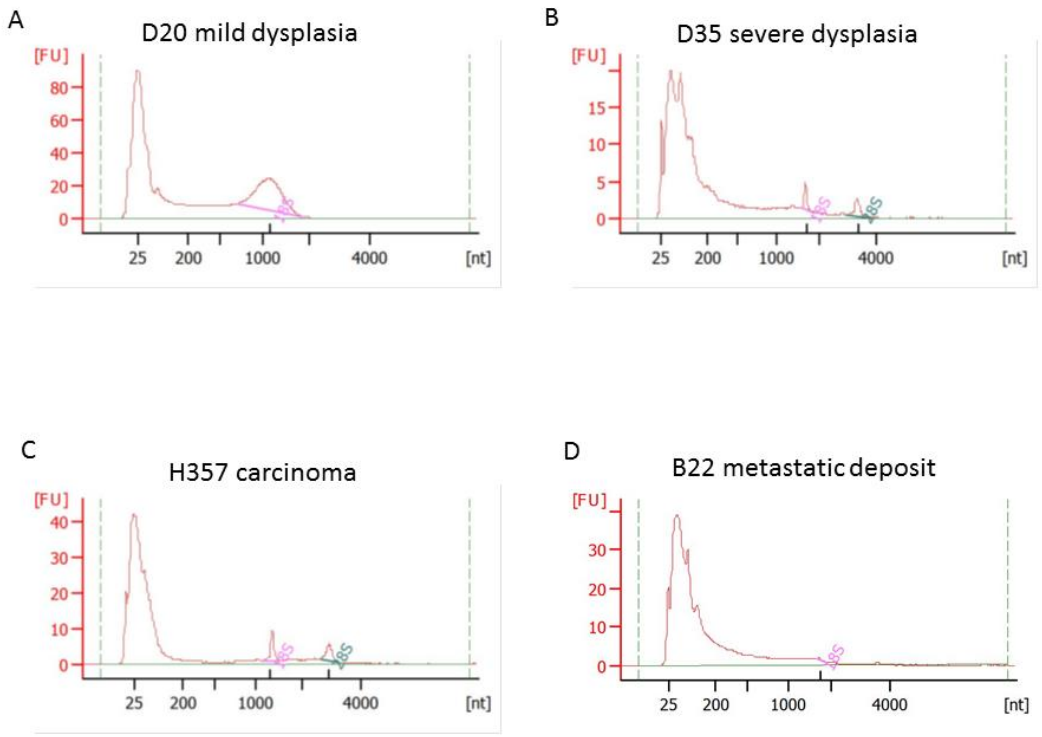

Figure 4.5 Bioanalyzer profiles of RNA isolated from EVs produced by oral cancer cells from different stages of oral cancer using size exclusion chromatography. A) Mild dysplasia, B) Severe dysplasia, C) a non-metastatic carcinoma and a metastatic deposit D). Fractions 4-9 were pooled and centrifuged at 100,000 x g for 90 min. The pellet was treated with the miRCURY miRNA isolation kit and run on a total RNA Picochip. All samples show a similar output with a large peak between 25 and 200 nucleotides representing miRNA and other small RNA species. Only the EVs from the mild dysplastic (A) cells contain substantial numbers of the larger RNA species shown by the peak at 1000 nucleotides. There is some contamination with rRNA in each sample with peaks for the 18s and 28s rRNA in all the samples. Outputs are representative from 2 experiments.

EVs from severe dysplastic and metastatic deposit cells contain double the RNA of EVs from mild dysplastic and carcinoma cells

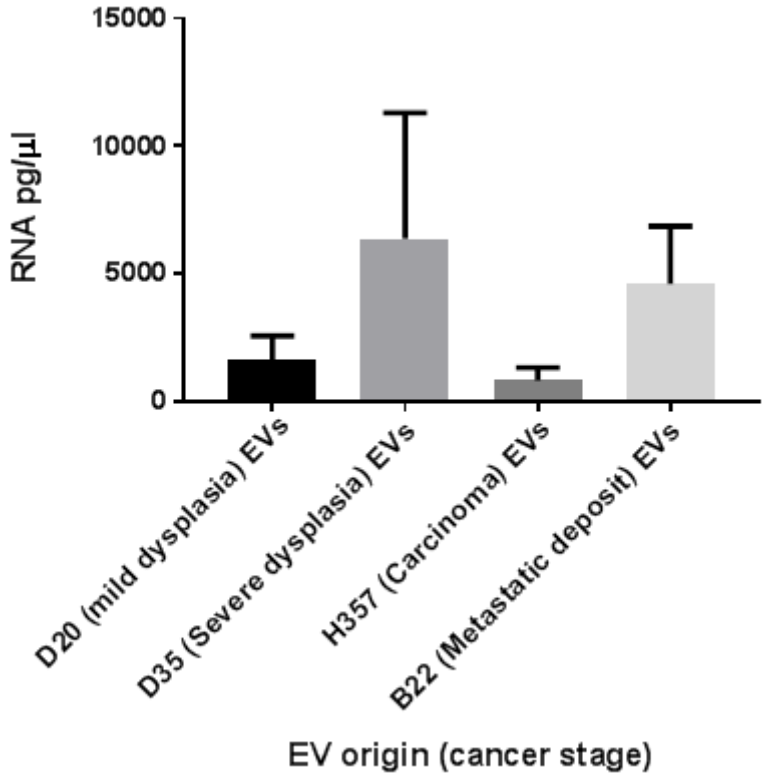

Figure 4.6 RNA yields from EVs produced by oral cancer cells purified using size exclusion chromatography. Fractions 4-9 were pooled and centrifuged at 100,000 x g for 90 min. The pellet was treated with the miRCURY miRNA isolation kit and run on a total RNA Picochip. RNA yields were expressed in pg/µl, yields from the D20 and H357 cell derived EVs were consistently around 1000 pg/µl with much more variability in yield of the EVs from D35 and B22 cells. D35 cell derived EVs have the highest yield of the four cell lines. n=2 biological replicates error bars representing SEM. Results were non-significant with both a Student's T test and One-way Anova with Tukeys multiple test correction.

4.6. Protein markers of oral cancer extracellular EVs

EVs are frequently characterised by particular protein markers to determine their origin within the cells, either MVBs or the plasma membrane, and subsequently attempt to identify the vesicle sub class to which they belong. The same antibodies used in the previous chapter with the addition of GM130 a golgi body marker, the presence of which would indicate cellular contamination, CD81 and tumour susceptibility protein 101 (TSG101) which are markers used in other studies of small EVs (Kowal et al., 2016). Protein lysates from both the producing cell and their EVs were analysed by western blot using the antibodies listed below (table 4.1). Bands were detected for CD63 TSP1 GM130 Alix and TSG101 (figure 4.7). No bands were detected for HSP70, Annexin V, VAMP3, ARF6 or CD81 in any of the samples. This could be due to them not being present or not present in sufficient quantities for detection with antibodies in these cells and their EVs. Something which could be confirmed by the use of a positive control for these proteins.

Antibody	Marker for	Citation
CD63 (Abcam antibody)	Exosomes	Escola et al., 1998
HSP70	Exosomes	Greening et al., 2015
ALIX	Exosomes	Lässer et al., 2012
TSP1	Apoptotic Bodies	van Engeland et al., 1998
ANNEXIN V	Apoptotic Bodies	van Engeland et al., 1998
VAMP3	Micro-vesicles	Muralidharan-Chari et al., 2009
ARF6	Micro-vesicles	Muralidharan-Chari et al., 2009
CD81	Exosomes	Lässer et al., 2012
TSG101	Exosomes	Lässer et al., 2012
GM130	Golgi body	Lässer et al., 2012

Table 4.1 Table of antibodies used in this chapter to characterise the EVs produced by oral cancer cells

OSCC EVs are positive for TSP1 CD63 and Alix but negative for GM130

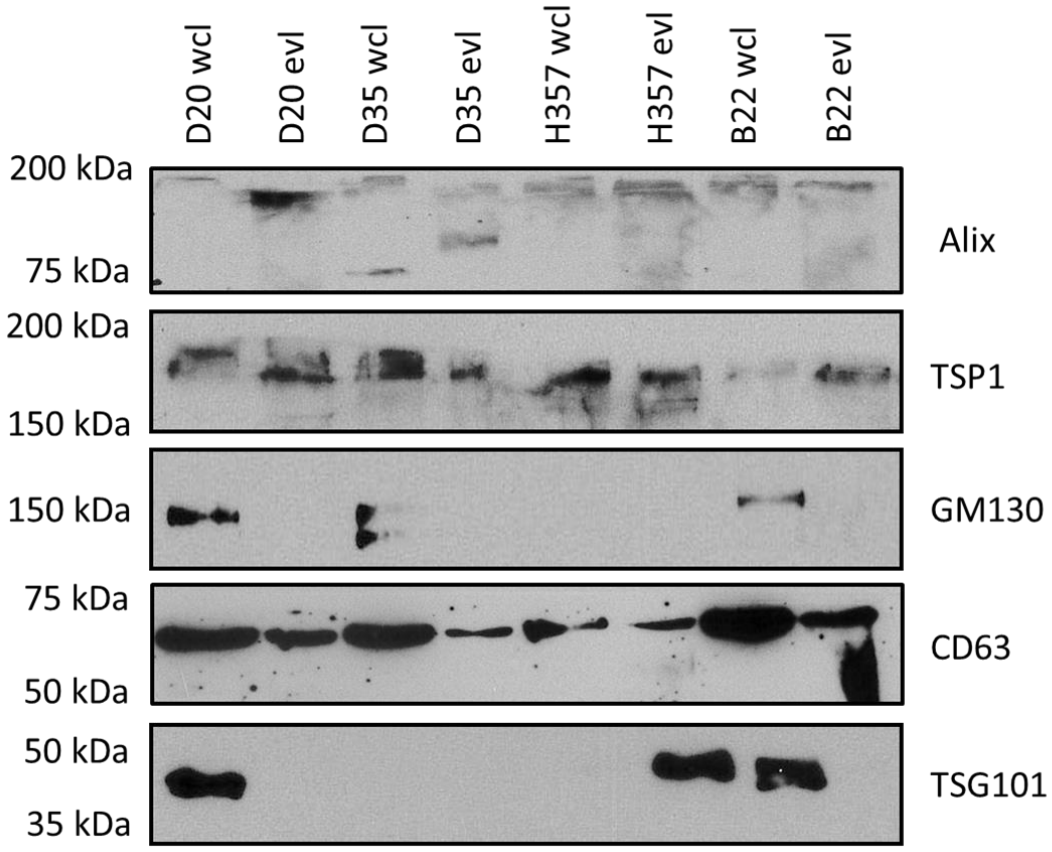

Figure 4.7 Western blots of vesicle markers present in the EVs purified from the conditioned media of oral cancer cells alongside the lysate of the producing cells. Whole cell lysate was produced from each of the cancer cell lines as previously described. EVs were purified using size exclusion chromatography. These were then normalised to 10 μg of protein and run on a 12% acrylamide gel. After transferring to a nitrocellulose membrane, they were blocked and incubated overnight with the primary antibodies. Blots were developed by incubation with appropriate HRP conjugated secondary antibodies and then exposed to ECL substrate and X-ray film and developed on a Xograph X4. No bands were observed for CD81 VAMP3 ARF6 Annexin V or HSP70 in any of the samples. Bands were observed in all whole cell lysate (WCL) and EV lysate (EVL) samples for CD63 TSP1 and Alix. Bands for TSG101 were in D20 and B22 WCL and H357 EVs. GM130 was detected in WCL of D20 D35 and B22 cells. Blots shown are representative from at least three experiments.

4.7. Discussion

In this chapter EVs were shown to be produced by four oral cancer- or pre-cancer-derived cell lines representative of different stages of the disease. These vesicles were shown to have similar size ranges by two different techniques and share similar morphologies when visualised via TEM. These size ranges and morphologies are consistent with those in many other studies. The mean measurements however do increase with cancer stage, something which hasn't been reported in the literature to date. However, there is evidence of vesicle size increasing with reticulocyte maturation (Carayon et al., 2011) a process which, like tumourigenesis, leads to differently differentiated cells.

Very little data exists on how tumour progression effects EV production, our data shows that the production rates for three cell lines are very consistent with only the severe dysplastic cells producing significantly more. Possible explanations for this lies in the details of this cell line, the patient from which these were established was a smoker whereas the other dysplastic cell line was established from a non-smoker, this patients disease also progressed to a carcinoma shortly after the establishment of the cell line. Both of these could provide a biological explanation for this observation either in combination or alone. However, it is worth noting that the patient donors for both the carcinoma and metastatic deposit cell line were smokers (although the carcinoma patient had only smoked between the ages of 17 and 20). This suggests that is more likely to be a combination of the two factors or the severity of the dysplasia alone that is responsible for the increased production rates. There is also a distinct difference in the genomic landscape of the cells. All cell lines have P53 mutations however each has a different mutation. The mild dysplastic cells have a G to A base change at codon 248

causing an arginine to glutamine amino acid change the mild dysplastic cell line has a t insertion at codon 200 which gives rise to a frameshift mutation. The carcinoma cell line also has a base change but at codon 110 from G to A, the metastatic cells exhibit a fourth different mutation, a 19 bp deletion. It is also possible that the increased EV production is an artefact caused by an accelerated doubling time of the severe dysplastic cells relative to the other lines in the OSCC panel, this could be tested for by comparing the growth rates of the cell lines in the same conditions and producing a figure for vesicles produced per cell per doubling time.

One limitation to our data is that whilst the cell lines cover the same primary site they are not from the same patient. Similar work would need to be carried out in samples from more patients encompassing a wider variety of gender (all of our patients were male) age and smoking status to ensure these observations were not just caused by patient variability. There are two other distinct limitations in these cells as a model of tumour progression, first is 2D culture on plastic does not truly represent the complexity of the tumour with a number of cellular processes demonstrating differences when co culture or 3D conditions. The second is the observed immortality of the dysplastic cell lines which sheds doubt on how representative they are of an early stage of a tumour. However, whilst 3D culture would have been a more realistic representation of the tumour environment it would not have been possible to purify EVs from individual cells in the same way from a 3D culture model.

It was the discovery that EVs could transfer RNA species between other cells which caused the fields rapid expansion. The majority of these papers focus either on

the coding mRNA or the non-coding miRNA, many of these have benefitted from the increasing availability of next generation sequencing technology (Jenjaroenpun et al., 2013; Lunavat et al., 2015). Our data has shown that there is RNA present in the EVs produced by oral cancer cells although the variability in RNA yields between replicates make it difficult to make meaningful comparisons. Several groups have made use of the same Bioanalyzer platform used in this study to analyse vesicle RNA contents and it is instructive to compare their findings with ours. A group in Sweden performed Bioanalyzer assays on samples from whole cell RNA, microvesicles pelleted at 16500 x *g* and exosomes pelleted at 100,000 x *g* (Lunavat et al., 2015). Similarly, to this data they saw their 100,000 x *g* exosome pellets had an abundance of small RNA species between 25 and 200 nucleotides. Another group (Jenjaroenpun et al., 2013) has performed similar experiments comparing the outputs from breast cancer cells and the EVs they produced, their EVs exhibited similar profiles to ours with large peaks for the smaller nucleotides and small rRNA peaks, where these EVs appear to differ is they contain a large number of nucleotides up to 1000 nucleotides in size. The cellular RNA has more in common with that from the EVs purified from the 16500 x *g* centrifugation step (Lunavat et al., 2015) with large rRNA peaks which mask any signal from smaller rRNA species.

Data from the western blots strongly suggests that our EVs, or a sizeable proportion of them, originate from within MVBs of the parent cells and could perhaps be termed exosomes. Alix is a 97 kDa adaptor protein involved in sorting cargo proteins in MVBs into the intraluminal vesicles. While bands for Alix were detected in all WCL and EVL samples, they were not at the normal size of 97 kDa but were visible at around the 200 kDa mark suggesting the protein is present as a dimer (figure 4.6). Alix

functions in the MVBs of cells as a dimer (Hurley and Odorizzi, 2012; Pires et al., 2009) which binds to the ESCRT III component CHMP4. However, the dimer form of the protein should be reduced to the monomer by the loading buffer and SDS within the gel although it is possible that its packaging into EVs is as part of a complex with CHMP4 which protects it from the reducing conditions. Its presence in the vesicle samples strongly suggests the EVs produced by the oral cancer cells and isolated by our protocol originate in the MVB of the cells.

CD63 is a tetraspanin protein long established as a marker of EVs (Escola et al., 1998; Zitvogel et al., 1998) its molecular weight is normally 26 kDa. There are bands for this protein in all cell and EV samples on this blot (figure 4.6), however the weights of these bands are all over 50 kDa. The protein itself is heavily and variably glycosylated with three N linked glycosylation sites, cancer cells can exhibit different glycosylation to healthy cells (Horejsí and Vlcek, 1991; Metzelaar et al., 1991). It maybe that the form in these cells are very heavily glycosylated explaining the higher sized bands than expected. The Abcam data sheet for the antibody indicates a predicted range of between of between 30 and 65 kDa and suggests that the canonical weight is only detected in non-reducing conditions. The glycosylation of this protein in vesicles could be confirmed by treating with PNGase. It is still possible that the protein detected by this antibody is not CD63, however with the monoclonal antibody which was used in this chapter it is unlikely to be the case. CD63 has been shown to have a role in the intracellular vesicle signalling process (van Niel et al., 2011) which is why it is frequently used as a vesicle marker. Its detection in these EVs could indicate the presence of a population of vesicles arising from MVBs.

The absence of bands for GM130, a marker of the golgi body, in the EVs indicates the EVs are not contaminated with cellular debris and are unlikely to be produced by apoptotic processes. GM130 is a 130 kDa golgi matrix protein, the antibody for this was included to determine that the vesicles purified contained no cellular contaminants or were not themselves cellular debris. This protein was detected only in the whole cell lysates of D20 D35 and B22 cells but not in the EV samples from any of the cells. This is an important indication that the purification process is not purifying cellular fragments or co precipitating any cellular debris. Its absence in H357 whole cell lysate was unexpected but given the weak bands in other samples it may be that the signal was too weak to be detected in this sample. The double band in the lysate of the D35 cells is also unusual, whilst the protein has a splice variant it is shorter by 382 amino acids than the 1002 amino acid full length variant the size difference between the two isoforms would be expected to be bigger than that seen on the blot. This band could be explained by a mutated or modified form present in the D35 cells.

The EVs were also positive for the protein thrombospondin 1 (TSP1) which has been seen to associate with EVs isolated from the saliva of a healthy patient (Gonzalez-Begne et al., 2009) as well as oral cancer cells (Chan et al., 2015) suggesting it is possibly enriched in oral cancer. TSP1 is a highly adhesive glycoprotein which binds to fibrinogen, fibronectin, laminin, type V collagen and integrins alpha 5 and beta 1 it has no transmembrane components indicating it should be present inside the EVs although it could also be bound to matrix associated proteins on the EV surface. The protein was detected in all whole cell and EV lysate samples and has been shown to have roles in tumourigenesis and angiogenesis both of which might be highly significant given the

origin of these EVs. Without a loading control however it is not possible to quantify any differences between the amounts present in the samples however the strength of the bands suggests that it is enriched in the EV samples compared to the cells.

TSG101 is a 43 kDa protein which is involved with ubiquitination and can be recognized by the ESCRT-1 complex (Kostelansky et al., 2006; Teo et al., 2006) during the loading of vesicles. Its presence in so few of the samples was unexpected; it has also been used consistently as a vesicle marker and has been identified as being enriched in "light small EVs" a class of EVs they suggest can be separated from the tetraspanin enriched EVs purely by its physical properties (Kowal et al., 2016). Its presence in the H357 EVs could suggest that there is a similar subpopulation of EVs produced by these cells that is distinct from the CD63 positive population. It should also be noted that this protein is not detected in the parent cell lysate for H357 indicating it is possibly selectively enriched in the EVs. The bands for this protein were of similar sizes and intensity but it is possible that it is not expressed in the other cell lines or not expressed sufficiently to be detected. Alternatively, it could be expressed in a mutated form, one which removes its ability to negatively regulate cell growth (Morita et al., 2007) and which is not detectable by this antibody.

Taken together this chapter indicates that EV production is a constant throughout oral cancer development, possibly increasing during the final stages of establishing a carcinoma. EVs are produced with a similar size range throughout tumourigenesis with an increase in mean size observed as the cells progress through tumourigenesis. The EVs purified by our protocol are positive for two MVB associated proteins and negative for a golgi marker confirming the presence of a population of EVs derived from the

MVB of the producing cells in the final sample. Given that the size ranges observed for the samples are larger than those normally associated with exosomes it is possible that there are potentially larger EVs derived from other pathways in the final samples. This would explain the mixed morphologies present under TEM, particularly the larger EVs observed alone with the more electron dense lumens (figure 4.1 B, C&H).

4.7.1. Future work

Future work for this chapter should focus initially on performing the same experiments in a wider range of cell lines. This should include multiple samples from the same tumour stages as well as samples from patients of different genders and smoking status. This would go someway to overcoming the studies currently underpowered sample size and would help to confirm if trends identified in our samples such as an increasing mean diameter or producing rate with cancer stage is true of oral cancer in general or just in the cells used in this study. The western blot experiments detailed in this chapter have also raised some questions that were unable to be addressed during the time span of the project. The CD63 antibody consistently detected bands that were different to the cannonical weight for the protein, the impact of glycoslyation on this should be tested by comparing EV samples treated with PNGase against untreated samples. Another approach would be to use targeted mass spectrometry for the EV markers used in the western blots possibly with an iTRAQ experiment comparing the levels of those proteins against the producing cells. As with the other experiments these should ideally be performed in a wider range of cells lines than the four used in this study. If ethical permission could be obtained it would be interesting to compare the results obtained in this chapter with samples from either the saliva or cells isolated from the biopsies of oral cancer patients.

5. Next generation sequencing of the miRNA contents of oral cancer EVs

5.1. Introduction

The discovery that EVs contained miRNA was a catalyst for the fields rapid expansion. These versatile nucleic acid molecules hinted at the potential for EVs to do more than act as cellular recycling bins. Small RNA species like miRNA have been shown to play roles in various cellular processes and disease states, particularly in cancer (Palanichamy and Rao, 2014; Yuan et al., 2014). The presence of miRNA and mRNA in exosomes was reported in 2006 and 2007 (Ratajczak et al., 2006; Valadi et al., 2007). Subsequently the RNA contents of the different EV classes have been shown to vary (Crescitelli et al., 2013), with little or no RNA present in larger EVs pelleted at 12,200 x *g*. These EVs and similar ones pelleted at medium speeds are often thought of as microvesicles. A paper in 2012 focusing on immune cell-derived EVs demonstrated that the most abundant small RNA species in the EVs were not miRNA but other less well studied species, namely vault RNA, Y-RNA and specific t-RNAs (Hoen et al., 2012). Whilst these RNA species are not protein coding some of them have been observed to have regulatory functions in cells (Hoen et al., 2012).

The RNA contents of EVs have been shown to play potentially important roles during tumour progression. Early in tumourigenesis cells evade normal growth regulation pathways and then, when they grow beyond the 2 mm diffusion limit of O_2 from the local vasculature, begin to develop their own blood supply. EVs have also been shown to contribute to dysregulation of normal growth controls; in an osteosarcoma model EVs from mesenchymal stem cells exposed to stress caused osteosarcoma cells

to become more resistant to apoptosis via the EV mediated transfer of miRNA which regulate the expression of PTK2, a versatile non-receptor tyrosine kinase with roles in cell cycle progression, proliferation and apoptosis (Vallabhaneni et al., 2016). EV RNA regulates or facilitates angiogenesis in different tumour types. In renal cancer, EVs increased VEGF expression at both the mRNA and protein levels by down regulating hepaCAM, suggesting that the EVs contain a miRNA for the hepaCAM transcript (Zhang et al., 2013). In myeloma, EVs carrying miR-135b promote the formation of endothelial tubes during hypoxic conditions (Umezu et al., 2014). Another mechanism is seen in leukaemia where EVs carry a range of miRNA which activate NF-κB and cause an increase in the induction of angiogenic markers (El-Saghir et al., 2016).

Metastasis and the acquisition of drug resistance are two processes which can occur late in tumourigenesis and are most strongly associated with cancer becoming lethal. Both have been shown to be regulated by miRNA within EVs. In breast cancer EVs containing miR-200 family microRNA, a family that is highly dysregulated in cancer, were shown to transfer these miRNA to non-metastatic cells which in turn led to them acquiring metastatic potential (Le et al., 2014). The miR-200 family regulates epithelial-mesenchymal transition (D. Yuan et al., 2014), a process in which epithelial cells become less adherent and more capable of migration, considered a necessary part of the metastatic process. In a breast cancer model of docetaxel resistance one group showed that the transfer of miRNAs, notably miR-100 miR-222 and miR-30a, in EVs could facilitate this resistance (Chen et al., 2014).

Because of the ease with which miRNA can be detected and identified from low amounts of RNA there is a significant focus on their application as biomarkers for

cancers. Coupled to the stability of EVs in biofluids this has led to many studies on the ability of EV RNA to act as biomarkers. Oral cancer is relatively unique in having a readily accessible biofluid that could be enriched for products produced by its component cells, salivary miRNA is likely to be encapsulated in EVs and there are already studies exploring these, miR-139a-5p and miR-31 (Duz et al., 2016; Liu et al., 2012) are currently being proposed as salivary biomarkers for oral cancer. Next generation sequencing platforms, such as IonTorrent, provide a technique where the total RNA contents of a vesicle population can be profiled. This list of contents can then be interrogated to identify mediators of any observed biological effects or to track changes in contents with disease progression. Which could identify potential prognostic or diagnostic markers which can be looked for in patient samples.

5.2. Aims and Objectives

The aims of this chapter were to identify and characterize the RNA contents of the EVs produced by oral cancer cells. EVs were purified using size exclusion chromatography with pooled RNA positive fractions being spun down at 100,000 x g overnight. RNA extraction was carried out using the miRCURY extraction kit. Purified miRNA was sent to Edinburgh University for analysis on their Ion Torrent system. Analysis was carried out by a range of different bioinformatics techniques. Small RNA sequencing data was validated using TaqMan PCR

5.3. Small RNA sequencing quality and species distribution

EV samples were purified from the conditioned media of six confluent T175 flasks per cell line using the size exclusion protocol. Following the Bioanalyzer

measurements of RNA concentration the samples were sent for IonTorrent sequencing. Different RNA species were present in the samples (figure 5.1). The largest proportion of the samples, between 60 and 75% in each case, is classified as “other RNA” this will include vault RNA, Y RNA as well as unidentified fragments. The next most abundant class of RNA is mRNA in all samples, with around 20-25% of the total RNA in each case. The remaining fraction of the samples is comprised of non-coding RNA, including small nuclear and nucleolar RNA as well as long non-coding RNA. The most widely studied type of RNA in EVs is miRNA but this class was poorly represented in all our samples both as the primary transcript and the mature final version account for less than 0.5% of the total RNA in each sample.

Quality control measurements from the small RNA sequencing experiment (table 5.1) shows that a higher number of reads was gained from the RNA contained with the in the dysplastic cell derived EVs than the carcinoma or metastatic deposit derived EVs, $10x10^6$ and $9x10^6$ respectively compared to $4x10^6$ and $5x10^6$. Whilst this figure varies the mean read length, the filtered reads and the aligned reads figures are more similar. With an average read length of between 20-22 base pairs for each sample and between $2.7x10^6$ and $4.5x10^6$ filtered reads and between $2.5x10^6$ and $3.9x10^6$ aligned reads per vesicle samples. The trend observed in the total reads of more reads in the dysplastic cell derived EVs is lost when the reads are aligned. The fifth column details the percentage of mapped reads which for all bar the severe dysplastic derived EVs is above 91% but in this sample drops to 58.57%. In the final three columns the miRNA contents of these reads are detailed, in both the D20 and the B22 EVs miRNA accounts for less than 0.5% of the mapped RNA reads; in the D35 and H357 samples this rises to 3.86% and 1.21% respectively.

RNA distribution in OSCC by IonTorrent sequencing shows majority of RNA are categorized other with miRNA being less than 0.2% in all EV types

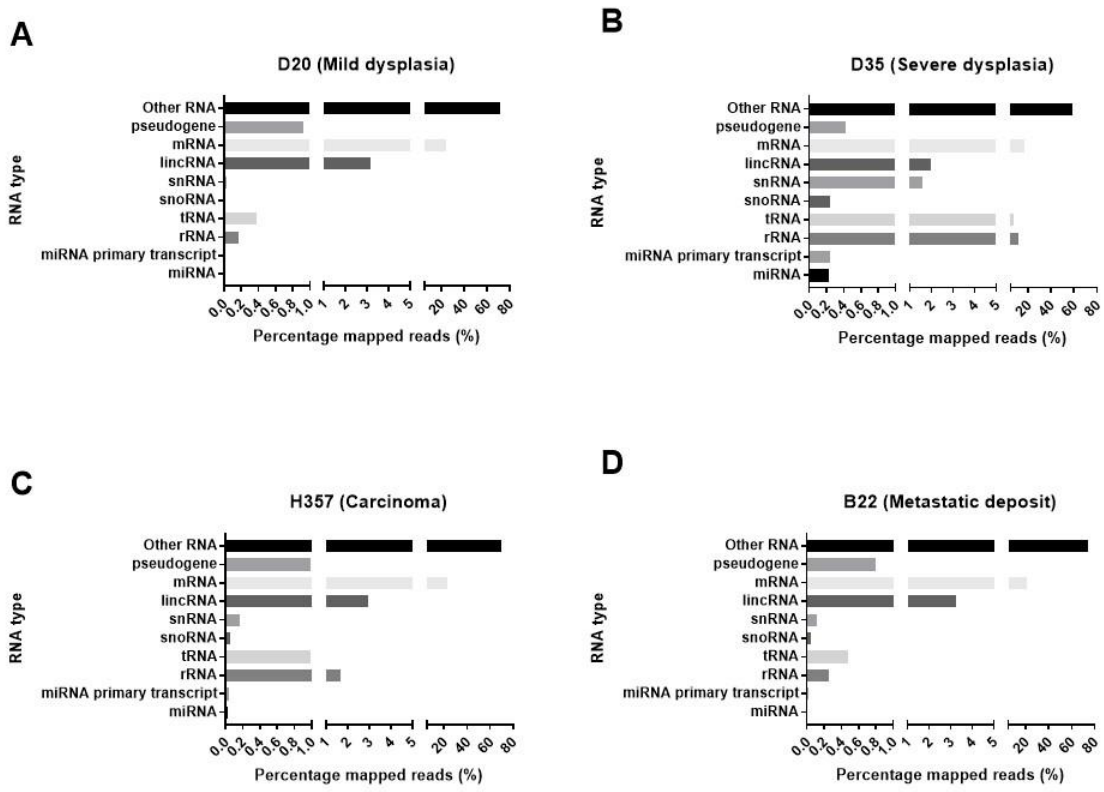

Figure 5.1 Distribution of RNA types within the samples sent for ion torrent sequencing. The largest component of the samples was classified as other RNA which includes vault RNA Y RNA and any unidentified fragments at around 60-75%. The next largest is mRNA with around 20-25% of the total RNA.

EV origin	Total reads	Mean read length (BP)	Reads passing filters	Aligned reads	Percentage mapped reads	miRNA reads	Percentage miRNA reads	miRNA detected with at least 10 reads
D20 (mild dysplasia)	10,123,202	20	4,265,363	3,982,359	93.37	17,683	0.41	138
D35 (severe dysplasia)	9,983,848	21	4,502,722	2,637,110	58.57	173,994	3.86	270
H357 (carcinoma)	4,390,352	22	2,743,519	2,502,136	91.20	33,216	1.21	174
B22 (metastasis	5,006,112	20	3,145,916	2,882,198	91.26	14,896	0.47	132

Table 5.1 Characteristics of RNA identified by IonTorrent smallRNA sequencing of EVs produced by oral cancer cell lines. Over $4x10^6$ total reads were identified in each of the EV samples, of these between $2\text{-}3x10^6$ were successfully aligned to the human genome. The table also shows the proportion of those reads which were determined to be miRNA as being between 0.4 and 3.8% in each of the vesicle types.

5.4. Processing of IonTorrent data

Following the Ion Torrent processing the number of miRNA reads ranged from 14896-173994. To normalise for this large variation the reads score for each sample was converted to reads per million mapped reads. 200-300 miRNA per vesicle type were identified by the Ion Torrent sequencing experiments (figure 5.2). Using 10 and 100 reads per million mapped reads does not reduce the number of miRNA significantly. Imposing a minimum of 1000 reads per million mapped reads as a threshold reduced this to less than 100 miRNAs per vesicle type.

Following this, Euclidean clustering was used to construct a heat map for the 107 miRNA species common to all the vesicle types. This heat map (figure 5.3) shows that

with respect to the miRNA contents the EVs cluster independently of tumour stage, with the EVs from the mild dysplastic (D20) and metastatic deposit cells (B22) showing the most similarity. EVs from the severe dysplastic cells were most dissimilar as they branch independently to any of other vesicle types, these EVs have 10-fold more miRNA reads than any of the other vesicle types which may contribute to this difference in the clustering (table 5.1). miR-23a was the most abundant miRNA in all the samples.

1000 RPM cut of reduces number of miRNA to around 100 per EV type

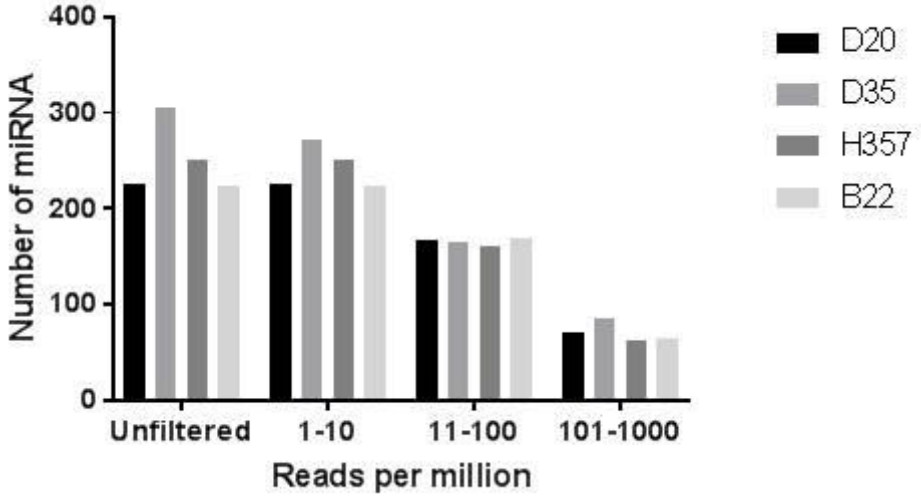

Figure 5.2 Following Ion Torrent sequencing and mapping to miRBase between 200 and 300 miRNA were identified for each cell line, cut of levels were imposed to remove sequences that weren't frequently identified. Several of these sequences were only read between 1 and 10 times per million mapped reads; around half of them were read between 11-100 times per million mapped reads. Neither of these values represent a significant proportion of the total reads, 1000 reads per million is often used as a cut of value in other similar studies, this cut of value reduced the number of miRNA sequences to between 50 and 100 more abundant sequences.

Euclidean heat map of OSCC RNA shows severe dysplasia and carcinoma cell derived vesicles have most similar contents

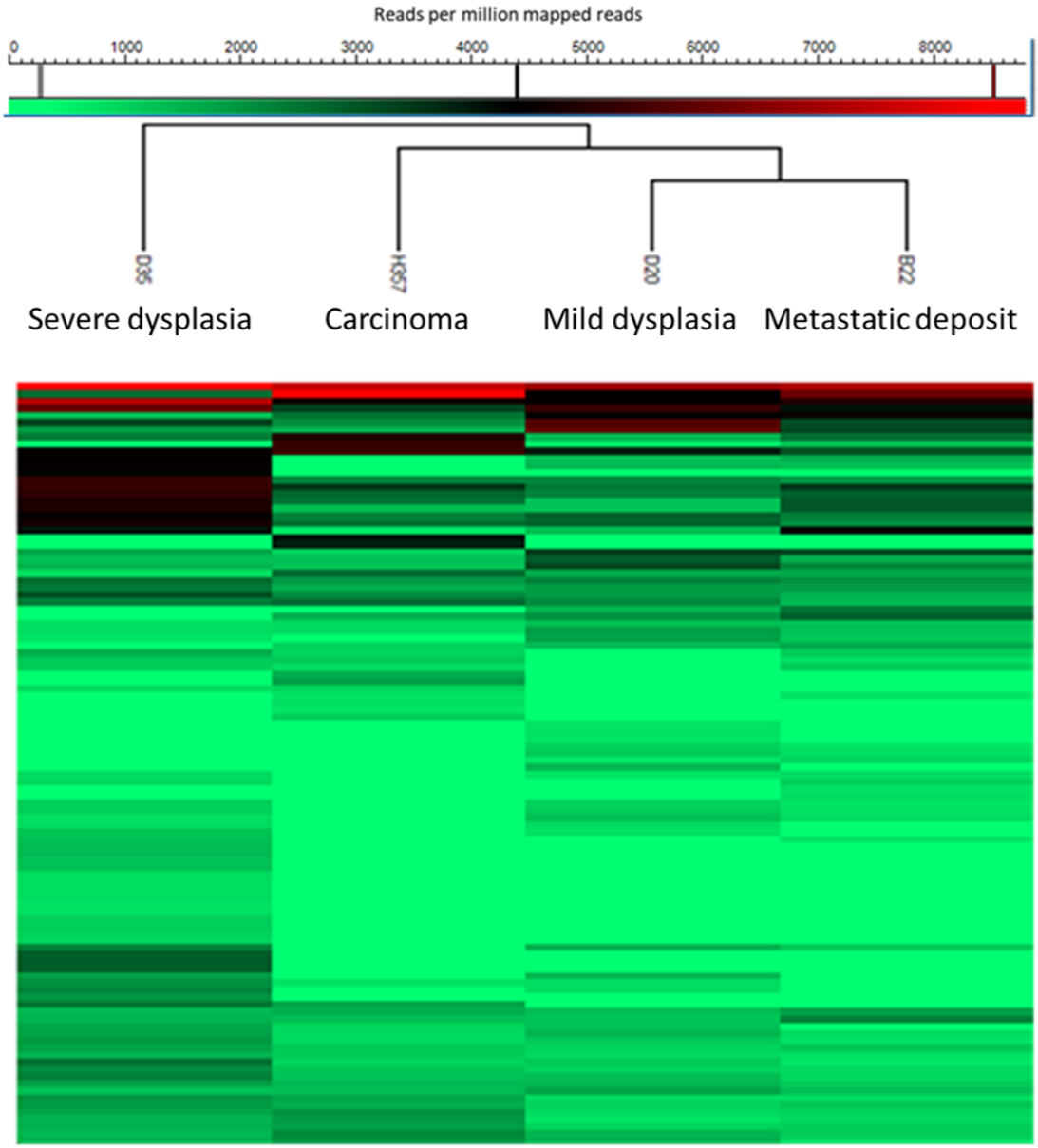

Figure 5.3 Euclidean clustering was performed on those miRNA with more than 1000 reads per million mapped reads using Perseus. The EVs didn't cluster by tumour stage. With the EVs of the mild dysplastic and metastatic deposit cells clustering together on the far right, the EVs of the carcinoma cells are separated from these two by one branch and on the far left are the EVs of the severe dysplastic cells.

5.5. Comparison of the miRNA contents of EVs produced by mild and severe dysplastic cells

As a means of expanding on the comparisons drawn by the heat map the miRNA contents of the two dysplastic cell lines were compared in a volcano plot (figure 5.4). Very few of the miRNA are significantly detected in EVs. The majority of the miRNA were non-significantly detected with a p value of less than 0.05. There are only two distinct populations revealed by this graph, the majority of miRNA have between a 0 and 5 log fold difference in levels between the two vesicle types which is not significant. Five miRNA were significantly detected in the severe dysplastic EVs, these include 2 members of the miR-199 and the miR-34 superfamilies of miRNA. The two significantly detected miRNA in the mild dysplastic EVs were miR-1307-3p and miR-1285-1-5p the latter being the most abundant. A large group of miRNA were common to both samples, this group includes several members of the large let-7 superfamily along with miR-23a-3p and miR-27b-3p.

Of those miRNA which were more abundant in the mild dysplastic EVs, both the 3 and 5p forms of miR-1285-1 along with miR-635-3p, 590-5p and 1307-3p were between 5 and 10-fold more abundant in the mild dysplastic cell EVs (figure 5.5). In the severe dysplastic cell derived EVs further enrichment for whole families was seen as three members of the miR-199 family and two each of the miR-200 and miR-34 family are enriched albeit not all of these are significant, also enriched 10-fold in the severe dysplastic EVs were miR-503-5p and miR-708-5p (figure 5.5). The two members of the miR-34 family were the most abundant miRNA in the severe dysplastic EVs.

Volcano plot of miRNA in mild and severe dysplastic cell derived EVs

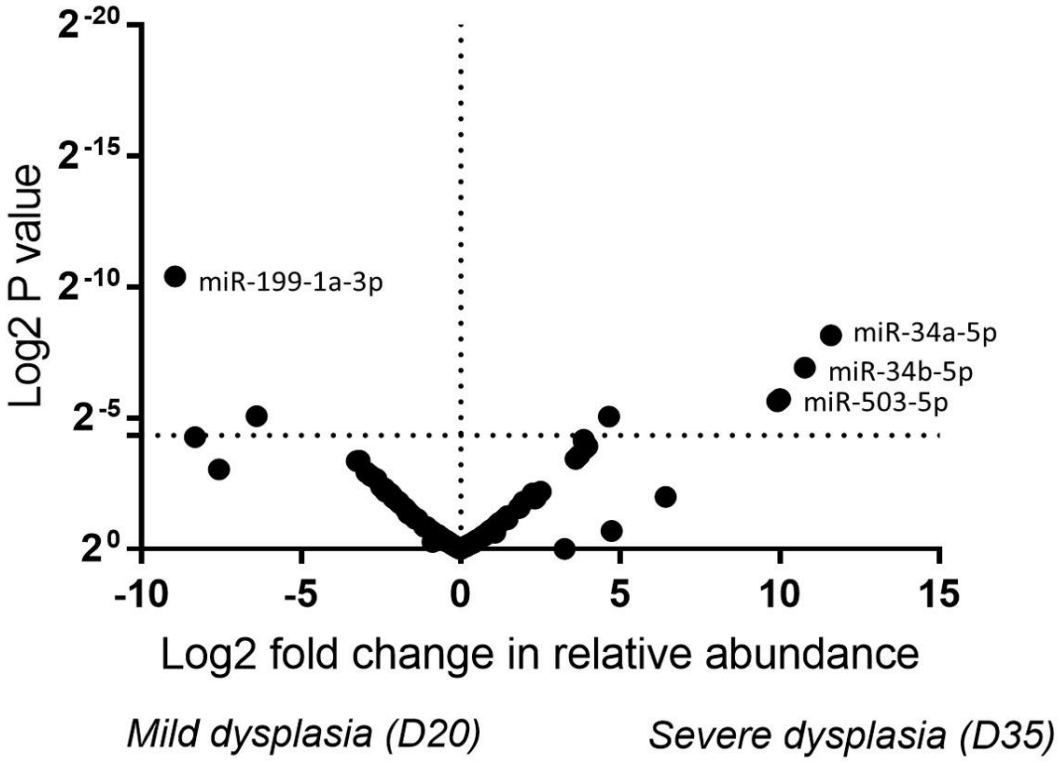

Figure 5.4 Volcano plot of miRNA identified in EVs from mild dysplastic and severe dysplastic cells. The majority of the miRNA detected were detected with between 0 and 5 log fold difference in amounts but at non-significant levels. Only two miRNA were significantly detected in the mild dysplastic cell derived EVs miR-1285-1-5p and miR-1307-1-3p with five significantly detected in the severe dysplastic cell derived EVs including miR-199a-1-3p and miR-503-5p as well as miR-34b-5p and 34b-5p. $p <= 0.05$.

Top 10 most differentially regulated miRNA in mild and severe dysplastic cell derived EVs

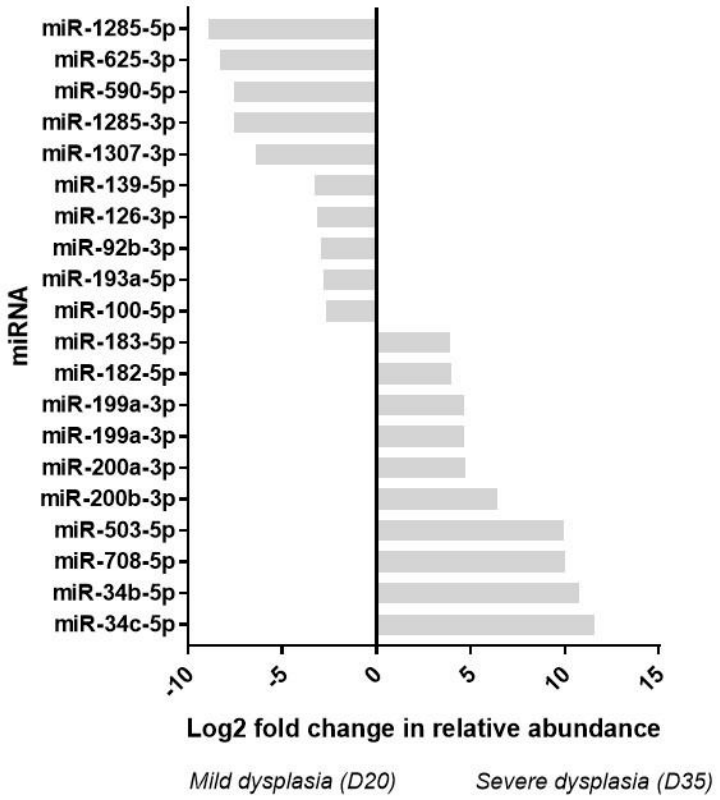

Figure 5.5 Log2 fold change of the 10 most differentially abundant miRNA in the mild dysplastic and severe dysplastic cell derived EVs. The miR-200 miR-199 and miR-34 families are more abundant in the EVs of the severe dysplastic cells.

5.6. Comparison of the miRNA contents of EVs from non-metastatic carcinoma and metastatic deposit cells

In a similar fashion to the EVs from the two dysplastic cell lines the miRNA contents of the non-metastatic carcinoma and the metastatic deposit were compared. As with the volcano plot for the EVs from the two different dysplastic cell lines the majority of the miRNA in the non-metastatic and metastatic cell derived EVs (figure 5.6) have a log fold change of between 0 and 5 whilst having a non-significant difference between them. The only four significantly detected miRNA are all in the non-metastatic carcinoma cell derived EVs, all of which were from the miR-200 family. The miR-34 and let-7 families are abundant in both vesicle types. Of the 10 most differentially abundant miRNA (figure 5.7) those in the metastatic deposit are all between 2 and 6-fold more abundant whereas those in the carcinoma exhibit fold changes of between 2-10-fold. In the EVs of the metastatic deposit cells miR-199a-2-3p was most abundant with a log fold change of 6. Also enriched in these EVs are miR-144-3p and miR-378a-3p. The most abundant miRNA in the non-metastatic cells with a log fold change of 10 are the miR-200 family members miR-200a-3p miR-200b-3p and miR-200c-3p along with miR-41-3p.

Volcano plot of miRNA in non-metastatic carcinoma and metastatic deposit cell derived

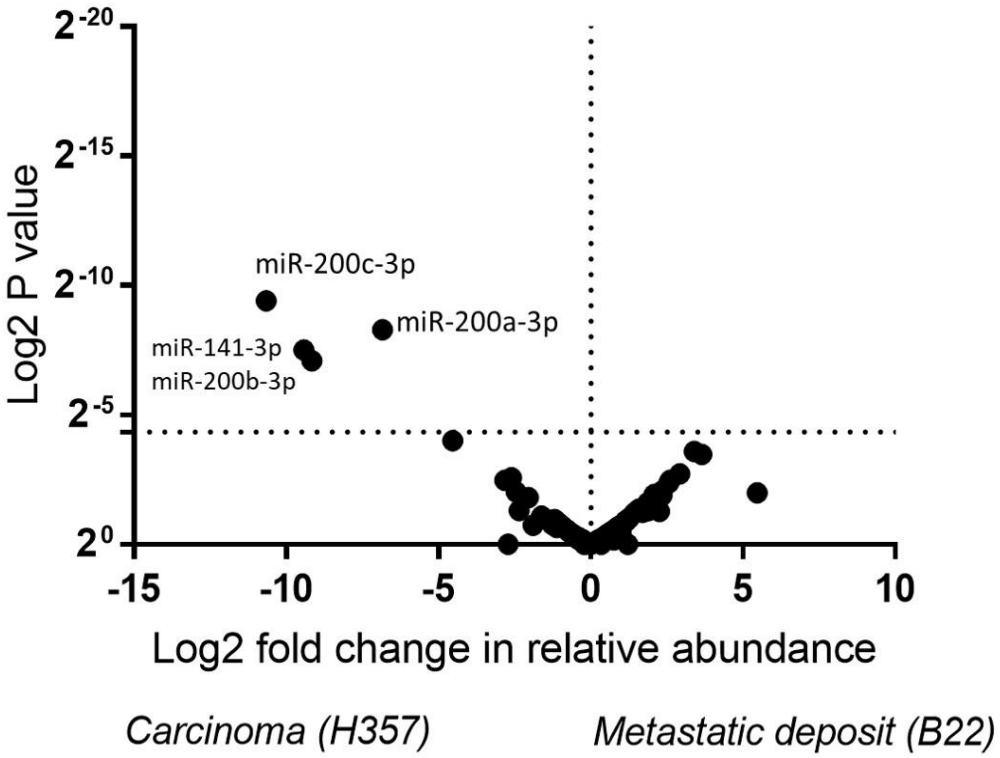

Figure 5.6 Volcano plot of miRNA identified in EVs from non-metastatic and metastatic cells. The majority of the miRNA detected were detected with between 0 and 5 log fold difference in amounts but at non-significant levels. Only four miRNA have a significant difference in abundance and all of these were in the non-metastatic cell derived EVs. These were the 3p forms for miR-200a miR-200b and miR-200c as well as miR-141-3p. $p <= 0.05$.

Top 10 most differentially regulated miRNA in non-metastatic carcinoma and metastatic deposit cell derived EVs

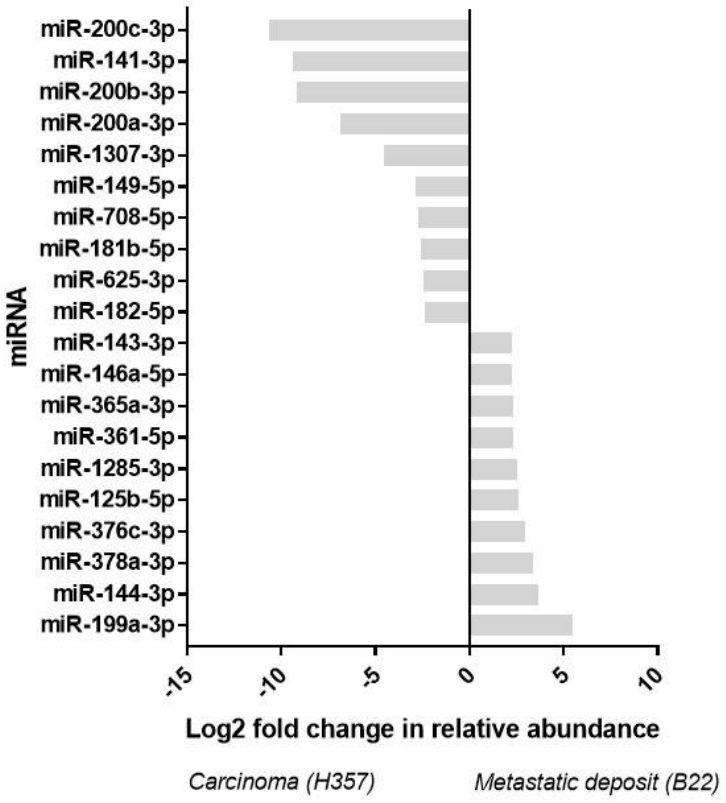

Figure 5.7 Log2 fold change of the 10 most differentially abundant miRNA in the carcinoma and metastatic deposit cell derived EVs. The most abundant miRNA in the metastatic deposit cell EVs is miR-199a-2-3p and the most abundant miRNA in the non-metastatic cell EVs are both 3p forms of miR-200 family members.

5.7. Comparison of the miRNA content of EVs from two oral dysplastic cell lines and an oral carcinoma cell line

Because the cell lines used in this project originate from the same primary site it is appropriate to combine the miRNA content of the EVs from the two dysplastic EVs into one set to compare these to those detected in the carcinoma cell derived EVs using the same techniques as used for the other comparisons. The volcano plot in figure 5.8 is different from that seen with previous comparisons, a far larger number of miRNA were significantly abundant in the different vesicle types. In the dysplastic EVs four miRNA are highly significant ($p = <0.0001$); these are miR-34c-5p miR-34b-3p and 5p along with miR-199b-3p. A further four are also significant but with a higher p value these include miR-199a-3p and miR-34a-3p. Six miRNA are significantly abundant in the carcinoma cell derived EVs these include miR-200a b and c 3p. As with the other comparisons a large proportion of the miRNA are common to both dysplastic cell and carcinoma cell derived EVs. The shared miRNA include 8 members of the let-7 family along with miR-29a and b 3p. In the dysplastic EVs the miR-199 and miR-34 family are between 4 and 14-fold more abundant than in the carcinoma EVs (figure 5.9). Similar enrichment of families is seen in the carcinoma cell derived EVs with three members of the miR-200 family between 5 and 10-fold more abundant in these EVs than in those of the dysplastic cells. Both miR-181a and b 5p are also slightly enriched in the carcinoma cell derived EVs with between 2 and 4-fold greater abundance than in the dysplastic EVs (figure 5.9).

Volcano plot of miRNA in dysplastic and carcinoma cell derived EVs

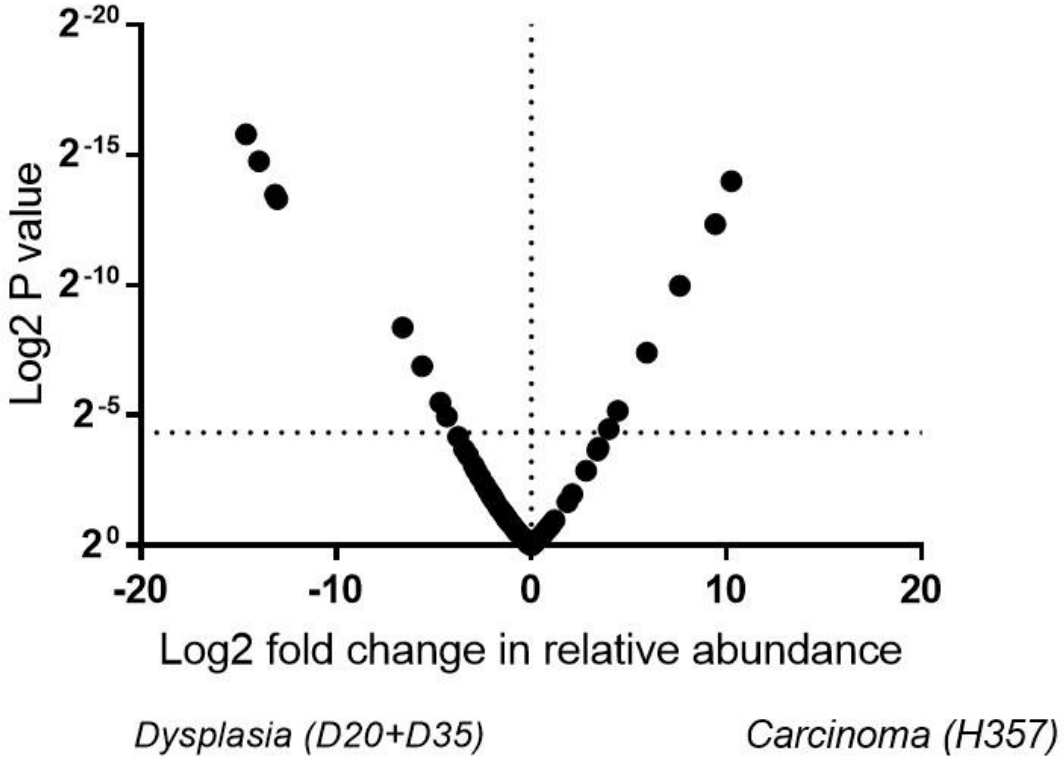

Figure 5.8 Volcano plot of miRNA identified in EVs from dysplastic and carcinoma cells. The majority of the miRNA detected were detected with between 0 and 5 log fold difference in amounts but at non-significant levels. Large numbers of miRNA were significantly abundant in EVs from the dysplastic cells, the most significant were miR-34 and miR-199 family members. The significantly abundant miRNA in the carcinoma cell EVs include miR-200 family members. p <=0.05.

Top 10 most differentially regulated miRNA in dysplastic and carcinoma cell derived EVs

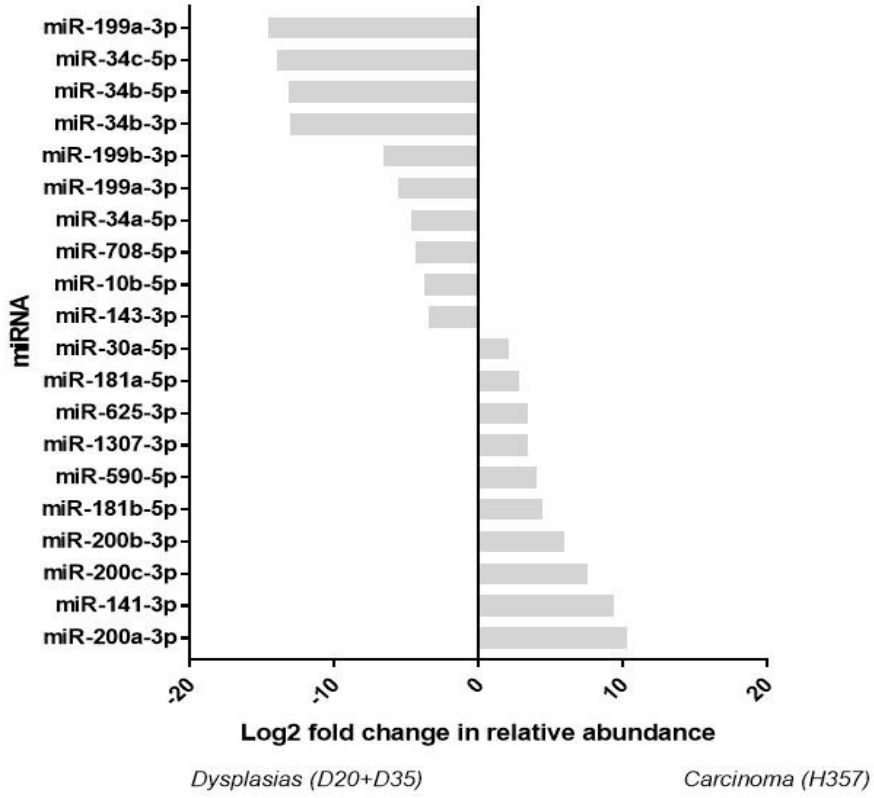

Figure 5.9 Log2 fold change of the 10 most differentially abundant miRNA for the 10 most abundant miRNA in the dysplastic cell and carcinoma cell derived EVs. This reveals the miR-199a family are enriched in the dysplastic EVs and the miR-200 family members are enriched in the carcinoma cell derived EVs.

5.8. Comparison of miRNA levels and target pathways in EVs from different tumour stages

Following the differential expression analysis between the vesicle types, those miRNAs which were common to all of the vesicle types were identified. Out of the 108 miRNA with more than a thousand reads per million mapped reads (RPM) 44 were common to all four EVs types. Several of the miRNA have changing levels across the different tumour stages (figure 5.10), miR-181a-5p is more abundant in both carcinoma and metastatic cell derived EVs when compared to the dysplastic EVs with an increase of between 3 and 5-fold. The levels of miR-31-5p halve in carcinoma and metastatic cell derived EVs compared to the dysplastic cell derived EVs. Both the 3p and 5p forms of miR-126 are twice as abundant in the EVs of the mild dysplastic cells compared to the other three vesicle types, whereas miR-27a-3p is twice as abundant in the EVs of the severe dysplastic cells when compared to the other three types. There are several miRNA which are present in much higher levels in the severe dysplastic cell EVs which might be caused by the 10-fold higher level of detected reads in this sample. As with the other analyses miR-23a-3p was the most abundant in all EVs types.

Using the miRBase tool DIANA the miRNA were mapped to the KEGG pathways in which their target proteins are found (figure 5.11). The majority of miRNA of interest are predicted to target multiple pathways, all bar three of the pathways are represented by at least 50 miRNA in all of the vesicle types. Because of the similar numbers of miRNA representing each pathway it is difficult to determine if there are any variations in the distribution. Among the pathways targeted by the miRNA in EVs are the MAPK, PI3K-AKT and WNT signalling pathways as well as focal adhesion and regulation of actin cytoskeleton. As expected the pathways all appear to be more heavily represented

in the EVs of the severe dysplastic cells however there are 15 more miRNA with over 1000 RPM in these EVs than any of the other vesicle types with 85 miRNA, those of the mild dysplasia had 70 the carcinoma 63 and the metastatic deposit cells 68. Putting these numbers alongside those seen in the graph reveals that for all the pathways bar fatty acid synthesis over 60% of the miRNA present in the EVs target that pathway.

Abundance of detected miRNA varies with EV type

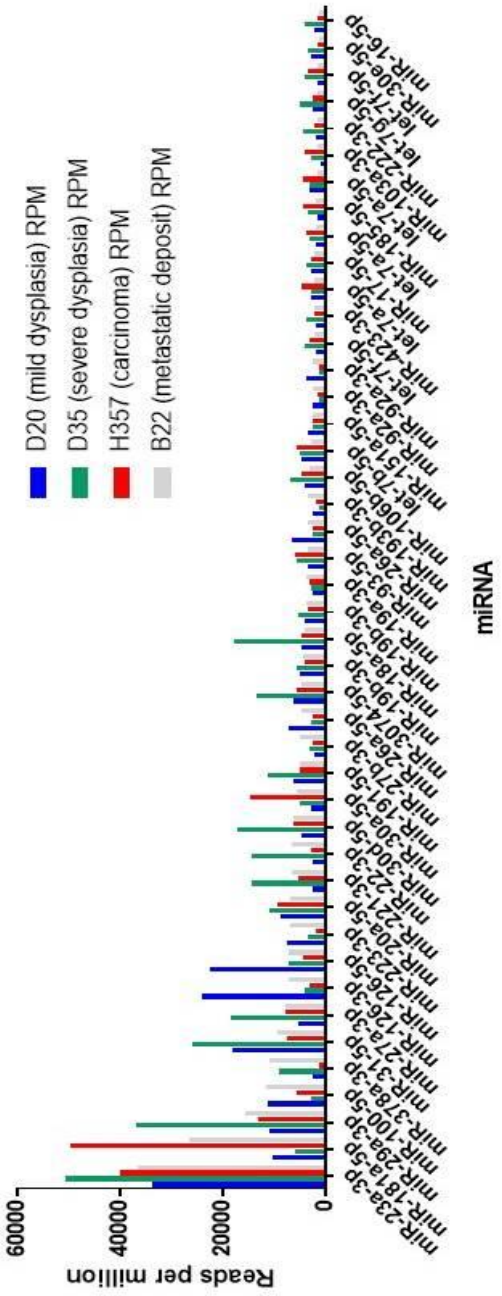

Figure 5.10 Comparison of the abundance of the miRNA common to all EVs types. 108 miRNA with more than 1000 reads per million mapped reads (RPM) were filtered to find those common to all of the vesicle types. Forty-four miRNA were present in EVs from each of the tumour stages, the amounts of several miRNA vary with tumour stage notably miR181a-5p.

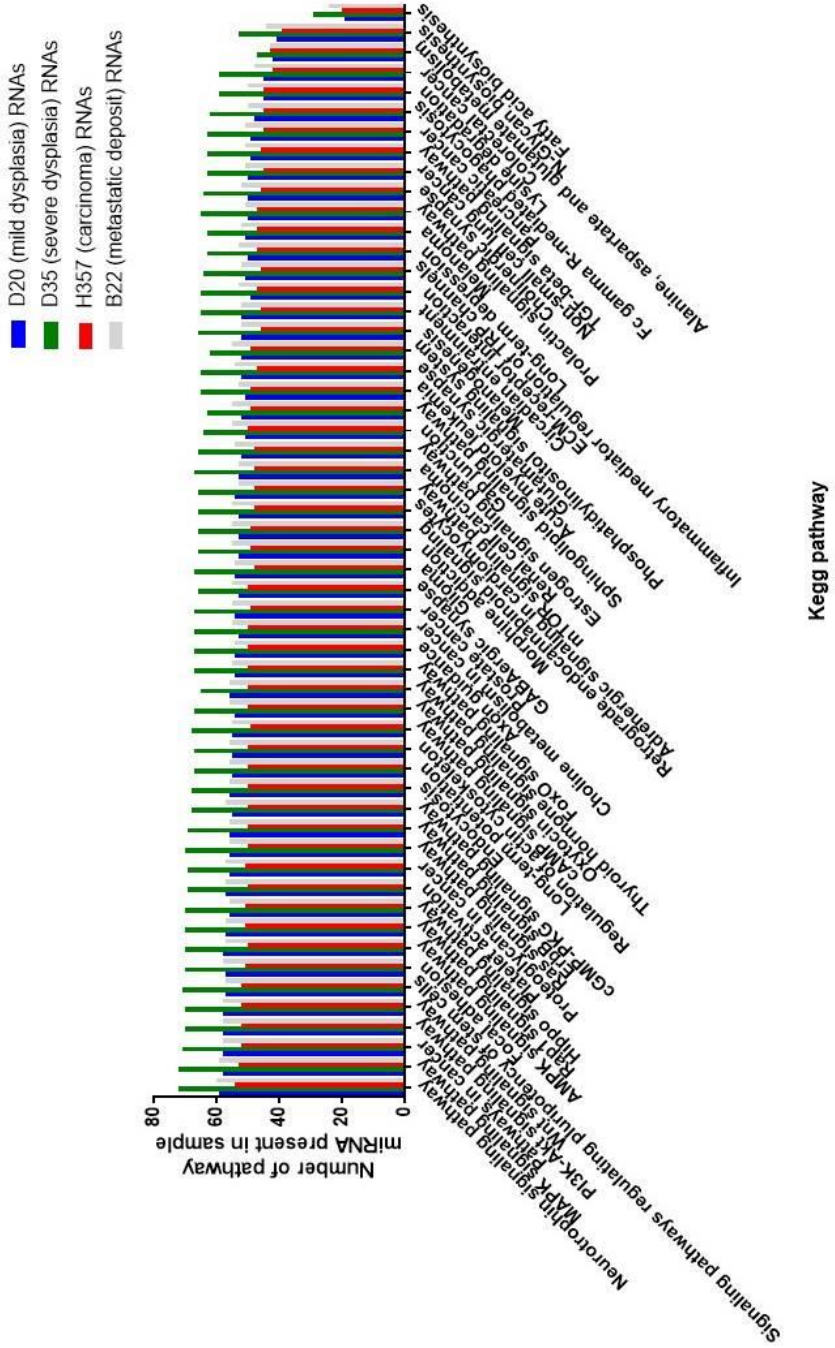

Figure 5.11 KEGG pathways represented by the 44 shared miRNA. Shared miRNA with over 1000 RPM were entered into the DIANA miRNA database to identify the KEGG pathways represented. The database search reveals that the majority of miRNA target several pathways with most of the pathways being represented by over 50% of the miRNA over 1000 RPM.

5.9. Validation of IonTorrent sequencing data

5.9.1. Selection of targets

In order to validate the IonTorrent data, qPCR was employed to examine the abundance of target miRNA sequences in whole cell RNA preparations and EV samples. Candidates were selected for one of two characteristics. Firstly, sequences were selected which had high and consistent abundance in all samples and would therefore have a high likelihood of being detected by qPCR in both EVs and cells. Secondly, some sequences were selected which were not consistently abundant in all the samples, detection of similar patterns of abundance by qPCR would indicate that the patterns seen by sequencing were valid. Detection of these candidates in both EV and cell samples would indicate that the IonTorrent experiments had identified sequences successfully in all of our EV samples. Both let-7a and miR-29 have high abundance in each of the samples however miR-29 has higher abundance in the severe dysplastic cell derived EVs (figure 5.12) detection of this sequence via qPCR in both EVs and WCL would indicate the IonTorrent had both detected the correct miRNA and had detected any patterns of variation of miRNA between EV samples successfully. miR-199 was only present in the severe dysplastic cell derived EVs and would also act to confirm any indications of variance seen in the IonTorrent data.

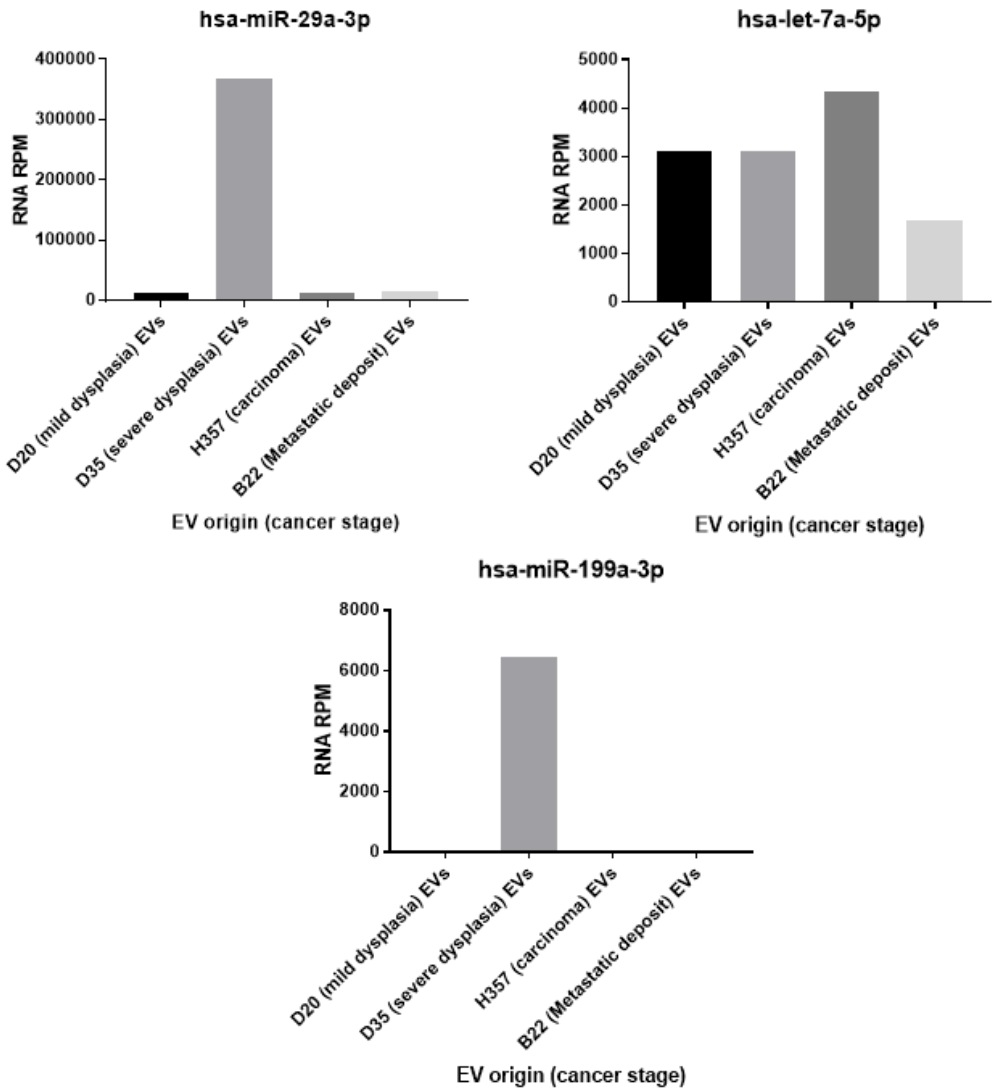

Figure 5.12 To select suitable targets to validate the ion torrent sequencing reads per million mapped reads for different miRNA sequences was compared for each of the EV samples. This figure details the RPM for three putative validation candidates. Let-7a-5p and miR-29a-3p were selected because they were seen to be abundant in all the samples, in the case of miR-29a-3p there was also a difference in abundance seen by ion torrent with the severe dysplastic vesicles containing several fold more reads of this species. miR-199a-3p was selected as it was only abundant in the severe dysplastic samples. Detection of these 3 miRNA in similar proportions with qPCR would confirm both the patterns seen with ion torrent and the miRNA identified. n =1

5.9.2. Validation by qPCR

Following the qPCR, the raw cycle numbers (figure 5.13) show that the EVs of all the cancer cell lines contain the miRNA let-7a-5p (figure 5.13 A) and miR-29a-3p (figure 5.13 C) as was shown in the Ion Torrent data, however the same enrichment of miR-29a-3p in the severe dysplastic EVs which was observed in the sequencing experiment was not seen in the qPCR. This could suggest that this variation is a technical variation and might not have been present in subsequent sequencing experiments. Both of the miR-29a and let-7a were present in the producing cells of these vesicle types. In the case of let-7a it was detected 6/7 cycles earlier in the cell samples than in the vesicle samples (figure 5.13 A) when ΔCT values were calculated for the samples (figure 5.13 D) the miRNA was significantly more abundant in the cells as opposed to the EVs in each of the cancer cell lines. Although there was substantial variation between the replicates the general trend demonstrates a significant reduction in the amounts of this miRNA in EVs relative to the producing cells.

In the case of miR29a (figure 5.13 F) the miRNA varied considerably in terms of relative abundance. In the mild dysplastic cells miR-29a was marginally more abundant (but with no statistical significance) in the EVs, this abundance increases in the severe dysplastic EVs to around 1-fold more abundant. In the carcinoma cells however, this trend is reversed, and the miRNA is significantly more abundant in the cells than in the EVs compared to the other samples. The trend reverses a second time in the metastatic deposit cells where the miRNA is some 900-fold more abundant in the EVs than compared to the cells. miR-199a was selected as is it was only present in the EVs of the severe dysplastic cells. Using qPCR (figure 5.13 B) it was seen to be significantly more abundant in both the severe dysplastic cells and the EVs when compared to the cells and

EVs of the mild dysplasia, the carcinoma and the cells of the metastatic deposit, however it was also present in the EVs of the metastatic deposit although at a much higher cycle number. When the relative abundance was calculated (figure 5.13 E) this miRNA was 4-fold more abundant in the EVs of the severe dysplastic cells and 8-fold more abundant in the EVs of the metastatic deposit cells when compared to their respective cells.

Presence of all three validation candidates is confirmed by qPCR

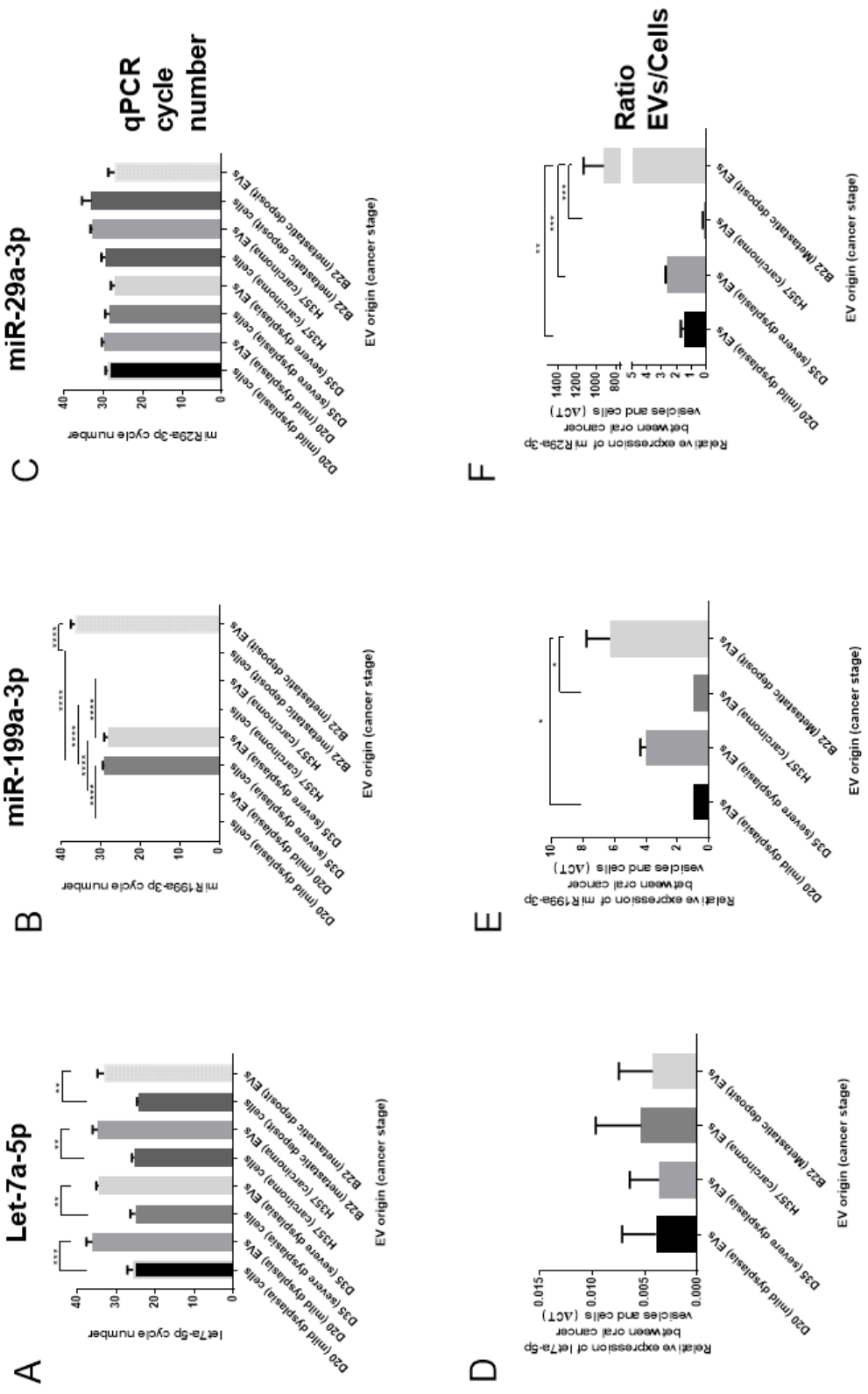

Figure 5.13 RNA extracted from the oral cancer cell lines and their respective EVs using the miRCURY kit was normalized to 10ng in 5µl and converted into cDNA before being used for qPCR with TaqMan Probes for let-7a-5p miR-199a-3p and miR-29a-3p. A, B and C show the qPCR cycle numbers at which the signal intensities crossed a threshold of 0.05 for let-7a miR-199a and miR-29a. Both let-7a and miR-29a are detected in the cells and EVs of all samples. miR-199 is in the EVs and cells of the severe dysplastic cells and was present in the EVs of the metastatic deposit but not in the cells. D, E and F show the corresponding ΔCT values indicating the relative abundance of the miRNA sequences in the EVs compared to their respective cells. let-7a is significantly more abundant in the cells of all the oral cancer lines, miR-199a is less abundant in the mild dysplastic and carcinoma EVs. For miR-29a the miRNA is marginally more abundant in the EVs of the mild and severe dysplasia. In the carcinoma cells the miRNA is more abundant than in the EVs whereas in the EVs of the metastatic deposit the miRNA is 900 times more abundant than in the originating cells. n=3 biological replicates error bars representing SEM. One-way Anova with Tukeys multiple corrections were used to compare between variables * = $p>0.05$ ***= $p>0.001$ ****= >0.0001.

5.10. Discussion

It was the discovery that EVs could transfer RNA species between other cells which caused the fields rapid expansion. The majority of these papers focus either on the coding mRNA or the non-coding miRNA, many of these have benefitted from the increasing availability of next generation sequencing technology (Jenjaroenpun et al., 2013; Lunavat et al., 2015). Several groups have made use of the different technologies to compare the RNA contents of EVs and producing cells. A group working on breast cancer cell lines showed the EVs purified at 100,000 x *g* contained large peaks for Y-RNA and tRNA and lower levels of other small RNA. This was very different to the distribution of small RNA observed in the parent cell (Tosar et al., 2015). Breast cancer cells small RNA is predominantly miRNA whereas the vesicle small RNA is only 0.26% miRNA with the majority being tRNA or 5' tRNA halves, something observed in EVs from a non-malignant cell line too (Tosar et al., 2015).

This strongly suggests that either the large rRNA peaks observed in EVs purified at lower speeds are cellular in origin introduced by the difference in formation pathways or they are cellular fragments co-precipitated with the EVs at this speed. The proportion of miRNA they observed in the vesicle small RNA samples is consistent with that observed in our experiments where less than 0.5% of the small RNA was miRNA species in each of the cell lines. Given the number of papers that focus on the miRNA contents of EVs the low proportion of the total small RNA peak represented by miRNA sequences was unexpected. However, our data did not see a similarly large proportion of tRNA fragmented or otherwise, the largest proportion of our small RNA was categorized as "other", although this may be due to software differences. This segment

covers a large number of poorly studied RNA types including vault RNA and Y-RNA which are not coding sequences. All samples were treated to rRNA depletion as part of the work flow, despite this step the severe dysplastic EVs show a large amount of rRNA suggesting either a problem with this step or an abnormally large amount of rRNA in this cell line as has recently been reported in HEK293T cells (Memet et al., 2017 and Eckenfelder et al., 2017). It is also worth noting that RNA purified from urine EVs contain 12% rRNA after an Illumina sequencing experiment with a similar rRNA depletion step (Koppers-Lalic et al., 2016).

One of the reasons for performing this kind of experiment is to enable changes in the miRNA contents of the EVs with tumour stage to be explored in detail. Although hierarchical clustering did show that the miRNA contents are varying with the vesicle source the clustering observed was independent of cancer stage. The EVs from the severe dysplastic cells have the most varied miRNA contents when compared to the other EVs types with the mild dysplastic and metastatic deposit cell vesicle being most similar. Where this data is only produced from a single biological replicate, any issues caused by the differences in the number of reads and the difference in the number of miRNA with over 1000 reads per million in the difference vesicle sources are unable to be corrected for. It is possible that the differences observed in the clustering are impacted by the severe dysplastic EVs having the highest number of miRNA reads and the lowest percentage of mapped reads. The lack of biological replicates is also responsible for the low number of miRNA above the significance threshold in the volcano plots. It is worth noting that the largest number of significantly enriched miRNA were seen in the volcano plot which compared the contents of two dysplastic cell derived EVs, which created the effect of replicates, with those of the carcinoma

cells. Despite this however there were some miRNA identified as being significantly enriched in the EVs of the mild dysplastic cells miR-1285-1-5p and miR-1307-1-3p. miR-1285 has not previously been detected in EVs but database searches reveal it functions as a tumour suppressor (Hidaka et al., 2012; Huang et al., 2017). miR-1307 has been detected in EVs of colorectal cancer cell lines (Ji et al., 2014) and patient plasma (Huang et al., 2013) two papers from this year show this miRNA to be involved in chemo resistance (Chen et al., 2017) and promoting proliferation in tumour cells (Qiu and Dou, 2017). The enrichment of these miRNA in the EVs of the mild dysplastic cells would suggest that they are removing a tumour suppressor from the dysplastic cells and encouraging their proliferation in a bid to drive tumourigenesis.

A larger number of miRNA were significantly enriched in the EVs of the severe dysplastic cells these included members of the miR-199 and miR-34 families both of which have been seen in EVs from plasma (Huang et al., 2013), miR-199 has been seen to be anti-tumourigenic, inhibiting invasion and migration in head and neck cancer in a recent publication (Koshizuka et al., 2017). The miR-34 family is a well-studied group of miRNA that are also seen to be tumour suppressing via SIRT1(Yamakuchi et al., 2008). The enrichment of tumour suppressive miRNA in the EVs of this cell line is interesting when placed in context of the patient data, shortly after the establishment of this cell line the patients dysplasia progressed to a carcinoma. Indeed, comparing the contents of the dysplastic EVs with those of the carcinoma cells reveals that these tumour suppressing miRNAs are absent in the carcinoma cells EVs and if a similar pattern of enrichment was observed in EVs from other oral dysplasia and carcinoma cell it could be said that the release of EVs constitutes an important part of tumourigenesis. However, it would be instructive to determine if blocking the release of EVs prevents

tumourigenesis in an animal model. When comparing the miRNA contents of the EVs from the two different dysplastic vesicle types and those of the carcinoma EVs the miR-34 family RNAs were enriched in the severe dysplastic cell EVs this family but were not present in the other vesicle types from later stages of cancer possibly suggesting that its removal from the cell is something that is necessary for continued progression through tumourigenesis.

Although there appears to be an enrichment of tumour suppressing miRNA in the severe dysplastic EVs there is a group of miRNA which are common to both vesicle types which comprises several of the let-7 superfamily of miRNA this well characterised group of miRNA has been seen in various vesicle types and is considered to be tumour suppressing. Another common miRNA is miR-27b-3p which has been detected in colorectal cancer EVs (Ji et al., 2014) but is a pro-tumourigenic miRNA in contrast to some of the others (Lánczky et al., 2016). The most abundant miRNA in all the vesicle types is miR-23a which is a tumour suppressor in osteosarcoma (He et al., 2014) and has been detected in in EVs from colorectal cancer cells and patient plasma. Because there exist within the shared miRNA both tumour suppressing and oncogenic miRNA it is difficult to assign a particular role to the EVs from either of these tumour stages. Some of these miRNAs are present in all vesicle types both in the sequencing experiments and by qPCR, the let-7 family is known to be differentially regulated in many cancers (Shell et al., 2007) and its abundance has been linked to the differentiation state of the producing cell. In our study the levels of this miRNA family were reasonably consistent across the different vesicle types suggesting that any variation in abundance with differentiation doesn't extend to the contents of the EVs. The fact similar miRNA are seen to be in all the vesicle types is something that should

be explored further, it would be valuable to see if the same miRNA are also common to EVs of healthy cells of the oral cavity such as fibroblasts and keratinocytes or if their presence is as a result of an enrichment that occurs as part of tumourigenesis.

Only four miRNA were significantly enriched when comparing between the non-metastatic cell and metastatic cell derived EVs and all of them were in the non-metastatic cell derived EVs. Three of these four miRNA belong to the miR-200 superfamily, which in addition to having been detected in the EVs of colorectal cancer cells and patient plasma is also found in melanoma cells (Lunavat et al., 2015). When comparing between the vesicle contents of the dysplastic and carcinoma cell derived this family of miRNA are three of the seven miRNA enriched in the carcinoma cell EVs. This family is heavily implicated in cancer and there are papers showing that miR200a miR-200b and miR-200c function as tumour suppressors which inhibits invasion and metastasis (Damiano et al., 2017; Xu et al., 2016). The fact it is significantly enriched in the non-metastatic carcinoma EVs, but not present above the 1000 RPM threshold in any other vesicle types, potentially suggests that again their removal from the cell is something that must occur for metastasis to happen. It is worth noting however that a paper from 2009 (Dykxhoorn et al., 2009) shows that the miR-200 family promotes rather than inhibiting metastasis albeit its positive effect is exerted on a later stage of the process. The hypothesis linking removal of the miR-200 from the cells in EVs to metastasis may not stand up to testing. This duality of function observed in the literature for one miRNA family does highlight some of the challenges when attempting bioinformatic analysis of miRNA sequencing data.

The data presented here identifies several miRNA whose abundance varies between the EVs produced by the cells of different cancer stages. One of these miRNA is miR-181a-5p which appears to decrease in the severe dysplastic cell derived EVs relative to those of the mild dysplasia, but in the EVs produced by the carcinoma and metastatic deposit cells the levels of this miRNA increase dramatically. A search of Exocarta reveals that this miRNA has previously been detected in colorectal cancer cell EVs (Ji et al., 2014) and patient plasma (Huang et al., 2013). In several papers it has been shown to function as a tumour suppressor (Shi et al., 2017) which is under the control of TGFβ (Neel and Lebrun, 2013). Perhaps more significantly however a paper from 2011 reveals that this miRNA is upregulated in OSCC cells which developed from leukoplakia and its over expression is correlated with lymph node metastasis vascular invasion and poor survival (Yang et al., 2011) which given its previously reported function as a tumour suppressor is unexpected. The group also reported that ectopically over expressing this miRNA caused an increase in the invasion and migration of OSCC cells. In this respect miR-181a is similar to the miR-200 family in that there is evidence indicating it can act as both a tumour suppressor and as a tumour promoter, in the case of the miR-200 family it appears that the miRNA acts on different stages of the metastatic process with different effects, it is possible that the miR-181 family behaves in a similar way. The findings of this paper are reflected in the data presented in this chapter, with the EVs from the carcinoma cells having greater levels of this miRNA that those which originate from the leukoplakia, the levels of the miRNA in the producing cells should be determined in order to see if the cell line data is consistent with that from clinical samples and if there are any differences with in the enrichment between the EVs and their producing cells.

Some miRNA have different levels in the EVs from the dysplastic cells as opposed to the carcinoma and metastatic deposit cells. In the dysplastic cell EVs miR-31-5p, which has been seen in EVs from colorectal cancer cells and patient plasma is twice as abundant compared to those of the carcinoma and metastatic deposit cells, this miRNA has been well studied in oral cancer, it has been shown to be upregulated in oral cancer tissue samples (Yan et al., 2017) a mouse model of tongue carcinogenesis showed that miR-31 was one of the first miRNA to appear in the saliva of the mice suggesting that it could be in salivary EVs (Kao et al., 2015) another paper which focused on the formation of leukoplakia identified the 3p form of this miRNA as one of the miRNA upregulated during the formation of leukoplakia (Xiao et al., 2012), miR-31 has also been proposed as a biomarker of cancers of the tongue (Liu et al., 2012). Again, the findings presented in this chapter seem to be consistent with the published data in that the miRNA levels in the EVs match what has been reported in tissue or cells however the levels of miR-31-5p should be checked in the producing cells to determine if the levels are consistent with those reported in the literature and with those in the cell lines.

A second miRNA is miR-126 which has been detected in the same colorectal cancer cell and patient plasma studies as the other miRNA. This miRNA is twice as abundant in the EVs of the mild dysplastic cells and in oral cancer this miRNA is tumour suppressive (Han et al., 2016; Yang et al., 2014), so as with other miRNA its enrichment in the EVs of the dysplastic cells could be contributing to the progression of oral cancer. Conversely miR-27a-3p is significantly more abundant in the EVs of the severe dysplastic cells compared to the other vesicle types, this miRNA is oncogenic in breast cancer (Guttilla and White, 2009; Li et al., 2010) with links to proliferation.

Four miRNA species were mentioned in the introduction as being currently under study as biomarkers for oral cancer. The first of these miR-21 and miR-1245 have been detected in EVs from the serum of oesophageal cancer patients, neither of these were detected above the 1000 RPM cut of in our study, which is likely to be because of the different cellular origin, the epithelium found on the tongue is different from that found in the oesophagus. The second two miR-31 and miR-139 have not previously been detected in EVs either in saliva or from oral cancer cells, but were detected in our study, miR-139 was in the EVs of the mild dysplastic cells and miR-31 was present in all vesicle types but enriched in the EVs from both dysplastic cell lines. Our findings would suggest that at least some of the miRNA for these two-species detected in saliva is enclosed within EVs, the proportion of the salivary miR-139 and miR-31 which is in EVs could be easily determined using qPCR experiments on RNA extracted from whole saliva and on salivary EVs from patients.

Alongside these one on one comparisons, KEGG pathways analysis of the miRNA was performed using the DIANA tool and miRBase. The outputs from this tool reveal just how multifunctional the miRNA contents of these EVs are. Unfortunately, this makes it difficult to draw any conclusions as to the EVs functions let alone changes in function with tumour stage. With the exception of fatty acid metabolism, each of the pathways is represented by around 80% of the miRNA in the EVs. It is possible that the EVs purified by this protocol are from different populations each with a distinct miRNA population, if this were the case it could offer some explanation for this difficult to interpret pathway data. If there were multiple populations with distinct miRNA contents and therefore affected pathways this could be masked by viewing the miRNA data for all the EVs. There are several interesting pathways targeted by the miRNA in these EVs,

including those that regulate adhesion and the regulation of the cytoskeleton, both of which are influential in metastasis. A missing piece of this jigsaw is the copy number of miRNA per vesicle in the literature this value has been speculated to be significantly lower than 1 copy number per vesicle (Chevillet et al., 2014), should similar numbers be observed in our EVs it would indicate one of two things, either random packaging or miRNA into the EVs or that multiple populations are purified. In either case it would limit any conclusions that could be drawn from further exploration of the pathway data.

The validation experiments performed using TaqMan qPCR primers showed that as in the RNA sequencing experiments the miRNAs, miR-29a-3p and let-7a-5p were present in all of the vesicle samples, these miRNAs were also present in the cells that produced these EVs, it also confirmed the pattern observed in the RNA sequencing where miR-199a-3p was only present in the EVs of the severe dysplastic cells which would suggest that other patterns in the data are reliable observations. There were a few differences seen by qPCR however. Firstly, miR-199a was also detected in the EVs of the metastatic deposit cells although the high cycle represents the fact it was below the 1000 rpm cut of in the sequencing data. Secondly miR-29a was seen by RNA sequencing to have a much higher abundance in the EVs of the severe dysplasia however by qPCR there was little variation in the cycle number at which the miRNA was detected in any of the samples with the carcinoma EVs and metastatic deposit cells having the highest cycle numbers indicating the lowest levels, but this difference was only marginal. It is possible that these variations were only observed via RNA sequencing because of technical variation and would not have been detected in subsequent experiments whereas the qPCR was performed from three different biological samples. Whilst the RNA was normalised prior to running the Ion Torrent, the

number of different reads per sample indicates that there was considerable variability in the quality of the samples which could also account for this variation. The consistent similarity between the results from the two different techniques gives some confidence to the conclusions drawn from the Ion Torrent data.

Let-7a-5p was one of the core miRNA species common to all the EVs types, calculating the ΔCT values reveals that this miRNA is actually more abundant in the originating cell. The Let-7 family of miRNA is commonly enriched in cancer and its presence in significantly lower levels in the EVs suggests it is not being actively packaged into these EVs. The substantial variation observed between biological replicates does not mask the overall difference pattern which is a reduction of between 100 and 1000-fold of the miRNA in the EVs. Let-7a-5p is an evolutionarily conserved miRNA and if it were being actively packaged into the EVs the ΔCT values would be expected to be closer together. Research has shown that the levels of Let-7 family miRNA could be of prognostic value in cancer, (Shell et al., 2007) with this in mind the amounts of Let-7a-5p should be compared in healthy oral squamous cells to the cancerous cells as our qPCR experiments give no indication as to differences in the abundance of this miRNA in the different cancer stages. The information gained from this experiment could give some biological context to the significant difference in the abundance of this miRNA in the EVs and cancer cells. It is possible that the miRNA is deliberately maintained in the cells as opposed to being packaged into the EVs, however this wouldn't fit with documented evidence detailing the Let-7 family as being tumour suppressive (Lee and Dutta, 2007).

miR-199a-3p was selected as a validation candidate as it was only present in EVs from the severe dysplastic EVs, calculating ΔCT values shows that there is a fourfold increase in the levels of the miRNA in the EVs relative to the severe dysplastic cells. This miRNA was also enriched in the EVs of the metastatic deposit cells, although this ΔCT value was calculated from replicates with extremely high cycle numbers and should be viewed with caution. Evidence in the literature shows that this miRNA is heavily implicated in the acquisition of the invasive and migratory behaviours necessary for migration (Deng et al., 2017; Koshizuka et al., 2017) and it is possible that its release in the EVs of this cell line enabled it to obtain those phenotypes. However, this miRNA was not detected in the other cell lines, this suggests two possibilities, firstly that this mechanism is not occurring in every case of oral cancer or secondly that this miRNA is not alone in driving the acquisition of these behaviours.

As with Let-7a-5p, miR-29a-3p was one of the core RNA shared by all the vesicle types in the sequencing data. qPCR showed that it was consistently present in all the cancer cells and the EVs they produced, it was also detected at a similar cycle number for all the cells and EVs, between 28-32, however these small variations in cycle number did indicate that the abundance of the miRNA in the EVs and the cells is not consistent. Whilst the abundance of the miRNA in the EVs relative to the cells steadily increases with the severity of the dysplasia, for the carcinoma this miRNA is more abundant in the cells than the EVs. The inverse of which is seen in the metastatic deposit cells where an 800-fold increase relative to the producing cells is observed. This is an extreme change in relative abundance when compared to the other cell and vesicle pairs, unfortunately without a suitable internal control this cannot be correlated to an increase in this miRNA in the cells or in the EVs. Unfortunately, we were unable to

establish a similar control for the vesicle samples which prevents robust comparisons between the miRNA levels of the different vesicle types in the same way.

As is common with many miRNA there are conflicting reports in the literature as to its role in cancers, some articles report that it is anti-tumour in gastric cancer cells (L. Chen et al., 2014) and pancreatic cancer cells (Tréhoux et al., 2015) whereas in colorectal cancer it promoted metastasis (Tang et al., 2014) and in breast cancer it promoted proliferation of tumour cells (Pei et al., 2016). It is possible that the function of the miRNA switches at some stage during tumour progression which would explain the change in distribution of miR29a between cells and EVs at the different stages. The additional information and questions raised by the comparison of the miRNA of the cells and the producing EVs demonstrates the importance of doing this with the other candidates identified during the analysis of the Ion Torrent data.

5.10.1. Future work

This chapter hints that the field (ourselves included) should shift some of the focus on the miRNA contents of the EVs to the more abundant types of other small RNA present in these EVs. The Ion Torrent data was validated by confirming the expression of three miRNA candidates in the EVs and the corresponding cell lines the consistency of the results with two different techniques gives a reasonable confidence to the Ion Torrent data. Although limited in scope the Ion Torrent sequencing has provided some interesting options for further experimentation. The miRNA that appear to be differentially abundant in the EVs from the different tumour stages all merit further exploration, although there is one notable caveat that should be addressed. The amounts of RNA used for sequencing and for the qPCR were not normalised against the number

of EVs in part due to the technical difficulties of doing so. Because of this it would be valuable to perform experiments using PCR-based approaches on the RNA isolated from a known number of EVs to determine the copy number of the RNA species per vesicle. This would ensure that any changes observed in miRNA abundance were not caused by a different number of EVs being used to produce the miRNA, these experiments would be reliant on the identifying suitable controls however.

If possible additional biological replicates of the IonTorrent sequencing should be performed, although an alternative approach would be to use a TILDA microarray or qPCR for a wider array of targets. Once this has been resolved the of these miRNA should be confirmed in the cell lines that produced the EVs used in these experiments along with other cells from the same stages as well as healthy keratinocytes to enable a wider and more reliable comparison to be drawn. If ethical permission could be obtained, then these targets could also be validated in EVs produced from cells extracted from patient biopsies or EV from patient saliva. Ectopic over expression and knockdown of the miRNA should be used to determine what phenotypic effects delivery of these species could have on surrounding cells of the TME. Given the number of miRNA that are linked to invasion and metastasis found in our EVs it would be interesting to establish a model using transwell or scratch assays to determine the effects on both cancerous cells, which would implicate these miRNA in metastasis, and immune cells or fibroblasts which would implicate these miRNA in the establishment of the TME.

Considering the findings in this chapter that miRNA represent a very small proportion of the total RNA in the EVs, it would perhaps be most valuable to perform a

similar range of experiments on other less well studied RNA species in the EVs. Y-RNA and tRNA have both been identified in similar studies, although normally non-coding their apparent enrichment in EVs suggests a biological role which is yet to be uncovered.

6. Proteomic analysis of the contents of oral cancer cell EVs

6.1. Introduction

Vesicles are formed by the cell as a method of membrane protein recycling or as part of a mechanism receptor internalisation. EVs were first identified by tracking transferrin receptor recycling (Johnstone et al., 1987). The membrane contents of EVs are particularly significant for vesicles that form via inwards invagination of the intraluminal membrane in MVBs. Because the membrane undergoes two inversions during their biogenesis any membrane proteins are presented in their active configuration when released from the cell. This is important for trastuzumab resistance (Ciravolo et al., 2012) as EVs are released bearing active forms of the decoy receptor which bind drug molecules preventing them from binding the tumour cells. Non-membrane proteins have also been detected in EVs, including proteins such as survivin (Khan et al., 2011), which is released during times of stress from the cell, or misfolded proteins in the case of Alzheimer's disease (Saman et al., 2012). In cancer, these proteins have been shown to have multiple functions: they can be oncogenic forms of proteins (Al-Nedawi et al., 2008), transporter proteins that aid in drug resistance (Chen et al., 2014), or they can be ligands that can kill immune cells (Lundholm et al., 2014).

Proteins contained within or on EVs form one of two of the major bioactive groups of molecules within EVs. With the increasing body of evidence for the selective packaging of proteins into EVs, the comparison of vesicle protein contents between those produced by diseased and healthy cells or patients has become an increasingly important step in studying diseases like cancer (Moon et al., 2016). As EVs yield a

small amount of protein the sensitivity of mass spectrometry techniques makes them valuable, enabling the identification of large numbers of proteins from a minimal amount of protein. This is particularly useful when applied to patient samples like saliva, a study by a group from Brazil has used label free analysis of salivary vesicle protein from healthy and unhealthy patients (Winck et al., 2015). From only 2 μg of vesicle protein 247 different proteins were identified post processing using a HPLC-MS system. Label free mass spectrometry assumes that the ion signal detected by the instrument correlates in a linear fashion with the proteins concentration, the machine relies on spectral counting or spectral peak intensities to determine this. Spectral counting works on the principle that peptides that are more abundant will be selected for fragmentation more often and will therefore produce spectra of a greater intensity. This contrasts to iTRAQ which is an isobaric labelling technique where all proteins in a sample are labelled with small molecular tags which produce fragments of a characteristic mass enabling the different samples to be compared. Two recent papers have made use of iTRAQ tagging to analyse vesicle proteins in both prostate cancer using urine samples from healthy and unhealthy patients (Fujita et al., 2017), and malignant mesothelioma using cancerous and primary mesothelial cells (Creaney et al., 2017).

6.2. Aims and Objectives

The aims of this chapter were to use mass spectrometry to profile the protein contents of EVs from cell lines representing the different stages of oral cancer. Detected proteins were analysed using a variety of bioinformatics tools enabling us to identify any changes in vesicle contents with tumour progression. GO analysis tools were used to provide details on the subcellular origin and pathways identified proteins belong to. This information provided details on the potential biological effect of EVs on receptor cells enabling future experiments to be designed. The mass spectrometry data was validated by western blotting for suitable candidates identified by the mass spectrometry. These validation experiments were carried out with whole cell lysates as well as vesicle lysates to enable comparison of relative abundance between the EVs and their parent cells.

6.3. iTRAQ mass spectrometry of EV contents

EVs were purified from the media of multiple confluent T175 flasks conditioned for 72 hours per cell line using size exclusion chromatography. The vesicle containing fractions were pooled and pelleted at 100,000 x g. This pellet was lysed using 0.1 M TEAB buffer containing 0.1% SDS and samples analysed by iTRAQ 8 plex. Protein yields were too low from the mild dysplastic cell (D20) EVs and so this sample was excluded from the iTRAQ experiment. As the samples for this experiment were allocated four of the eight iTRAQ tags available (with the other four being used for another user's experiments), the severe dysplastic vesicle sample was loaded in duplicate. Following the iTRAQ run the differential abundance of the proteins was

determined for the EVs from the dysplastic and carcinoma cells and between the non-metastatic and the metastatic cell derived EVs. Immediately evident is that despite the effort to separate these EVs from the protein and create pure samples there is contamination with serum proteins in these samples. Once the bovine proteins are removed there are 6 proteins decreased in the severe dysplastic EVs and 5 that are increased when compared to the carcinoma cell derived EVs (table 6.1). No proteins have significant differences in abundance when the most stringent statistical filters were used. If the multiple test corrections are removed however, then several proteins are decreased in the dysplastic EVs (table 6.2); histone 2 b (H2B), elongation factor 2 (EF2) histone 3.2 (H3.2) and nidogen-1 a basement membrane protein. Only 1 protein is significantly increased ($p=<0.01$) in the dysplastic EVs; splicing factor, proline- and glutamine-rich (100 kDa DNA-pairing protein).

Protein name	Fold change in severe dysplastic vesicles relative to carcinoma vesicles	Number of quantifications	Number of unique peptides	Species
Alpha-1B-glycoprotein	*0.75*	*14*	*1*	*Bos taurus*
Histone H2B	*0.7*	*13*	*2*	*Homo sapiens*
V-type proton ATPase catalytic subunit A (Fragment)	0.7	4	1	Homo sapiens
Alpha-2-HS-glycoprotein (Asialofetuin) (Fetuin-A)	*0.75*	*53*	*3*	*Bos taurus*
Beta-2-glycoprotein 1 (Apolipoprotein H) (Apo-H)	*0.65*	*5*	*1*	*Bos taurus*
IGK protein	0.7	6	2	Bos taurus
Bifunctional glutamate/proline--tRNA ligase (Fragment)	0.55	2	1	Homo sapiens
Elongation factor 2 (EF-2)	*0.6*	*13*	*3*	*Homo sapiens*
Serotransferrin	0.65	3	1	Bos taurus
Histone H3.2 (Histone H3/m) (Histone H3/o)	*0.4*	*22*	*2*	*Homo sapiens*
Nidogen-1 (NID-1) (Entactin)	*0.4*	*5*	*1*	*Homo sapiens*

Table 6.1 Proteins downregulated in the EVs of the severe dysplastic cells by iTRAQ (two replicates) compared to the carcinoma cell derived EVs (single replicate). p values were determined using a student's t-test with several correction options to give varying levels of stringency. Proteins in italics have a p value of 0.01. Those in normal script have a p value of 0.05. The large number of bovine proteins present indicates the samples are still contaminated with serum proteins. Number of quantifications and unique peptides are included as a measure of quality control, proteins with a high number of quantifications are unique peptides are likely to be present as a complete protein and are abundant within the sample.

Protein name	Fold change in severe dysplastic vesicles relative to carcinoma vesicles	Number of quantifications	Number of unique peptides	Species
Collagen alpha-2(I) chain	6.35	2	1	Homo sapiens
Uncharacterized protein KIAA0408 (Fragment)	1.9	2	1	Homo sapiens
Splicing factor, proline- and glutamine-rich (100 kDa DNA-pairing protein)	*1.3*	*3*	*1*	*Homo sapiens*
60S ribosomal protein L8	1.2	3	1	Homo sapiens
Fibrinogen alpha chain	1.2	8	3	Bos taurus
Inter-alpha-trypsin inhibitor HC2 component homolog (Fragment)	1.15	9	4	Bos taurus
Calmodulin	1.25	4	1	Homo sapiens

Table 6.2 Proteins upregulated in the EVs of the severe dysplastic cells by iTRAQ (two replicates) compared to the carcinoma cell derived EVs (single replicate). p values were determined using a student's t-test with several correction options to give varying levels of stringency. Proteins in italics have a p value of 0.01. Those in normal script have a p value of 0.05. The large number of bovine proteins present indicates the samples are still contaminated with serum proteins. Number of quantifications and unique peptides are included as a measure of quality control, proteins with a high number of quantifications are unique peptides are likely to be present as a complete protein and are abundant within the sample.

Protein name	Fold change in metastatic deposit vesicles relative to carcinoma vesicles	Number of quantifications	Number of unique peptides	Species
Transforming growth factor-beta-induced protein ig-h3 (Fragment)	*9.4*	*2*	*1*	*Homo Sapiens*
Fibronectin (FN)	*7.5*	*4*	*1*	*Homo sapiens*
Immunoglobulin superfamily member 8 (Fragment)	*5.3*	*3*	*1*	*Homo sapiens*
Major vault protein (MVP) (Lung resistance-related protein)	*2.3*	*9*	*1*	*Homo sapiens*
Elongation factor 2 (EF-2)	**2.0**	**13**	**3**	**Homo sapiens**
Inter-alpha-trypsin inhibitor heavy chain H3	*1.8*	*17*	*5*	*Bos taurus*
Nidogen-1 (NID-1) (Entactin)	*1.8*	*5*	*1*	*Bos taurus*
Apolipoprotein E (Fragment)	1.8	4	1	Homo sapiens
Alpha-1,4 glucan phosphorylase (EC 2.4.1.1)	1.8	4	1	Homo sapiens
Collagen alpha-2 (I) chain	*1.7*	*2*	*1*	*Homo sapiens*
?	1.6	2	1	?
Inter-alpha-trypsin inhibitor	1.6	9	4	Bos taurus
Fibrinogen alpha chain	*1.6*	*3*	*1*	*Homo sapiens*
Protein AMBP	*1.6*	*4*	*1*	*Bos taurus*
Charged multivesicular body protein 1b	1.6	2	1	Homo sapiens
Thrombospondin-4	1.5	5	1	Homo sapiens
Fibrinogen alpha chain	*1.4*	*8*	*3*	*Bos taurus*

Coatomer subunit gamma-2	1.3	2	1	Homo sapiens
Galectin-3-binding protein (Fragment)	**1.3**	**22**	**2**	**Homo sapiens**
Heat shock protein HSP 90-beta	1.3	2	1	Homo sapiens
Galectin-7	*1.2*	*8*	*1*	*Homo sapiens*
Complement component C7	1.2	4	1	Bos taurus
Chromobox protein homolog 3 (HECH)	*1.2*	*3*	*1*	*Homo sapiens*
Pre-mRNA-processing factor 19 (Fragment)	1.2	2	1	Homo sapiens

Table 6.3 Proteins upregulated in the EVs of the metastatic deposit compared to the EVs of the carcinoma cells by iTRAQ. p values were determined using a student's t-test with several correction options to give varying levels of stringency. Proteins in bold have a p value of 0.05 with multiple corrections applied. Proteins in italics have a p value of 0.01 and those in normal script have a p value of 0.05 but no multiple corrections are applied. The large number of bovine proteins present indicates the samples are still contaminated with serum proteins. Number of quantifications and unique peptides are included as a measure of quality control, proteins with a high number of quantifications are unique peptides are likely to be present as a complete protein and are abundant within the sample.

Protein name	Fold change in metastatic deposit vesicles relative to carcinoma vesicles	Number of quantifications	Number of unique peptides	Species
Aminoacyl tRNA synthase complex-interacting multifunctional protein 2	0.9	2	1	Homo sapiens
Apolipoprotein A-II (Apo-AII)	0.9	2	1	Bos taurus
Integrin beta-4 (GP150) (CD antigen CD104)	0.9	4	2	Homo sapiens
Histone H2B	0.9	34	1	Homo sapiens
Regulator of nonsense transcripts 2	0.9	2	1	Homo sapiens
Deoxyuridine 5'-triphosphate nucleotidohydrolase	0.9	4	1	Homo sapiens
Protein RCC2 (RCC1-like protein TD-60)	*0.9*	*5*	*1*	*Homo sapiens*
Histone H1.3 (Histone H1c) (Histone H1s-2)	0.8	3	2	Homo sapiens
Cofilin-1 (Fragment)	*0.8*	*5*	*1*	*Homo sapiens*
Beta-2-glycoprotein 1 (Apolipoprotein H)	*0.8*	*5*	*1*	*Bos taurus*
Alpha-fetoprotein	0.7	3	2	Bos taurus
Fructose-bisphosphate aldolase A (Fragment)	0.7	4	1	Homo sapiens
Serotransferrin	*0.7*	*3*	*1*	*Bos taurus*
Laminin subunit gamma-2 a)	0.7	2	2	Homo sapiens
Alpha-2-HS-glycoprotein (Asialofetuin) (Fetuin-A)	*0.7*	*53*	*3*	*Bos taurus*
Alpha-1B-glycoprotein (Alpha-1-B glycoprotein)	*0.6*	*14*	*1*	*Bos taurus*
Integrin alpha-6	*0.6*	*15*	*3*	*Homo sapiens*
Mutant myocilin (Myocilin)	0.6	3	1	Homo sapiens

Table 6.4 Proteins downregulated in the EVs of the metastatic deposit compared to the EVs of the carcinoma cells by iTRAQ. p values were determined using a student's t-test with several correction options to give varying levels of stringency. Proteins in bold have a p value of 0.05 with multiple corrections applied. Proteins in italics have a p value of 0.01 and those in normal script have a p value of 0.05 but no multiple corrections are applied. but no multiple corrections are applied. The large number of bovine proteins present indicates the samples are still contaminated with serum proteins. Number of quantifications and unique peptides are included as a measure of quality control, proteins with a high number of quantifications are unique peptides are likely to be present as a complete protein and are abundant within the sample.

Much like the comparison between the dysplastic cell EVs and those of the carcinoma cells the comparison between the non-metastatic and metastatic cell EVs (table 6.3 and 6.4) is heavily contaminated with bovine serum components like fibrinogen α chain. This is unexpected as any serum contamination would be expected to be consistent across all EV samples. There are two proteins which show a statistically significant difference in abundance even with the most robust stringency settings: EF2 and galectin-3-binding protein are both increased in metastatic cell-derived EVs, although the latter was only identified as a fragment of the main protein (table 6.3). If the multiple test correction is removed more proteins have significantly different abundances. The structural proteins fibrinogen α chain (the human version), nidogen-1, fibronectin and collagen α 2 (I) chain are all enriched in the metastatic EVs along with major vault protein and thrombospondin 4. Integrins α 6 and β 4 and H2B are decreased in the metastatic cell EVs compared to the non-metastatic cell EVs (table 6.4). EF2, major vault protein, the galectin-3-binding protein and integrin α 6 were all selected for validation with western blotting as they were enriched in one or two vesicle sources and in the case of EF2 were seen in multiple samples. However, given the contamination

with bovine proteins and having inadequate amounts of protein to run all of our samples, the decision was taken to repeat these experiments using label free mass spectrometry. This had two advantages over iTRAQ, firstly it could be run with a lower amount of protein, and secondly it would enable us to generate a list of all proteins detected as opposed to just the differential intensities of the tagged proteins.

6.4. Label free mass spectrometry of oral cancer EV contents

6.4.1. Mass spectrometry data processing

EVs were purified from the conditioned media of three confluent T175 flasks per cell line using SEC. Multiple preparations were pooled to give sufficient protein for analyses by reverse phase HPLC-MS. Samples were reduced, alkylated and then digested using trypsin. A 105 min data dependent acquisition on an Orbitrap Velos instrument yielded 1054 identified proteins following processing of the raw data with MaxQuant. The data was then subjected to post processing in Perseus (figure 6.1A). Removal of the contaminants identified by MaxQuant reduced the number of proteins to 910. These contaminants included keratin and glucose-6-phosphate isomerase, which are often detected in very high quantities in samples masking other signals.

The data was subsequently screened for quality by removing proteins with a low number of unique peptides; proteins with a razor and unique peptide score of less than 2 were removed leaving 376 proteins. With so few unique peptides detected these matches could not be viewed with the same reliability as those with a greater number of unique peptides. Razor peptides are those peptides assigned by the software to a protein on the principle of Occam's razor. Therefore, if the razor peptide is unique it can only match

with a single protein group. If it is not unique it will only be a razor peptide for the protein group with the largest number of peptides. Finally, statistics were used to identify those proteins with significant differences in abundance between different samples using a multiway Anova test with appropriate corrections, which gave 194 proteins common to the EVs from all cell lines with a p value of <0.05. The distribution of these proteins however wasn't even across the different cell lines (figure 6.1B), ranging from between 18 and 177 proteins detected within the EVs from the cell lines. Twice the number of proteins were detected in the EV sample isolated from the carcinoma cell line than in any other sample.

6.4.2. Comparison of protein contents of oral cancer EVs

As part of the data processing in Perseus a heatmap was created using Euclidean clustering (figure 6.2). This clustering produced an unexpected result where the EVs from the carcinoma cells (H357) clustered independently from the other three vesicle types, which were clustered from left to right in order of increasing cancer stage. The heat map also places the EVs from the severe dysplastic cells and the metastatic deposit in a separate branch from those of the mild dysplastic EVs. A core of proteins is common to all vesicle types with smaller sections that are unique to one or two of the types. The heat map also shows that a number of proteins were only detected in one of the two technical replicates, which were subsequently removed from the data processing by the statistical tests.

Work flow for post processing of label free mass spectrometry data and range in protein number with EV type

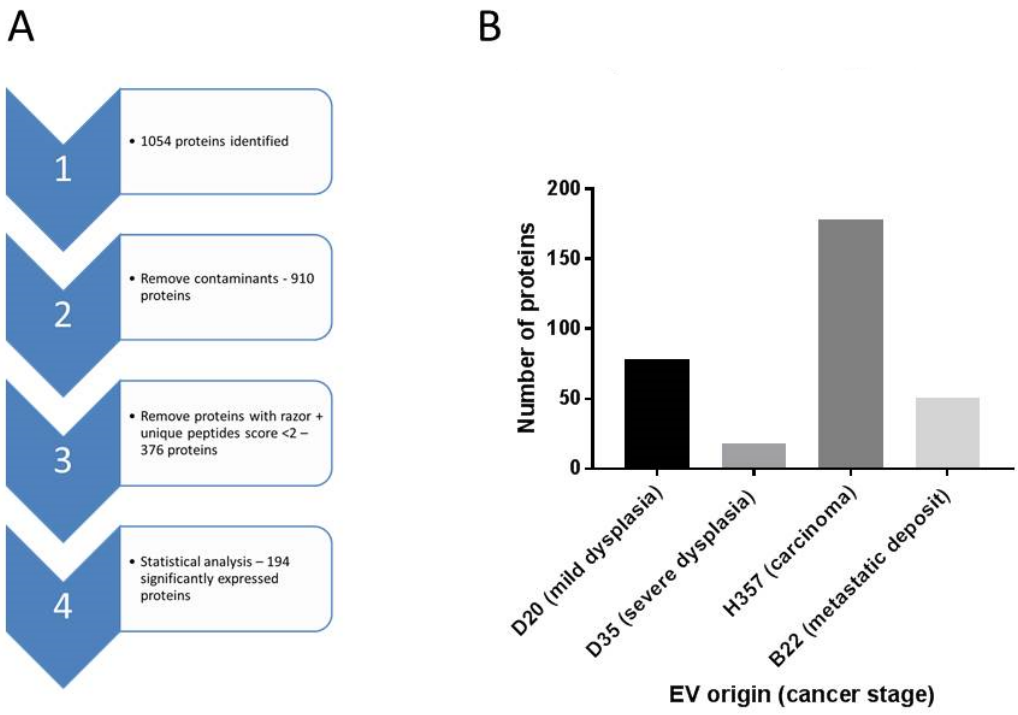

Figure 6.1 A) Workflow detailing data processing carried out in Perseus and the corresponding reduction in protein number achieved by the steps taken. B) Shows the variability in number of significantly detected proteins between the different cell lines. Data produced from n=2 technical replicates which were merged to allow statistical tests to be used.

Protein contents of OSCC EVs do not cluster by tumour stage

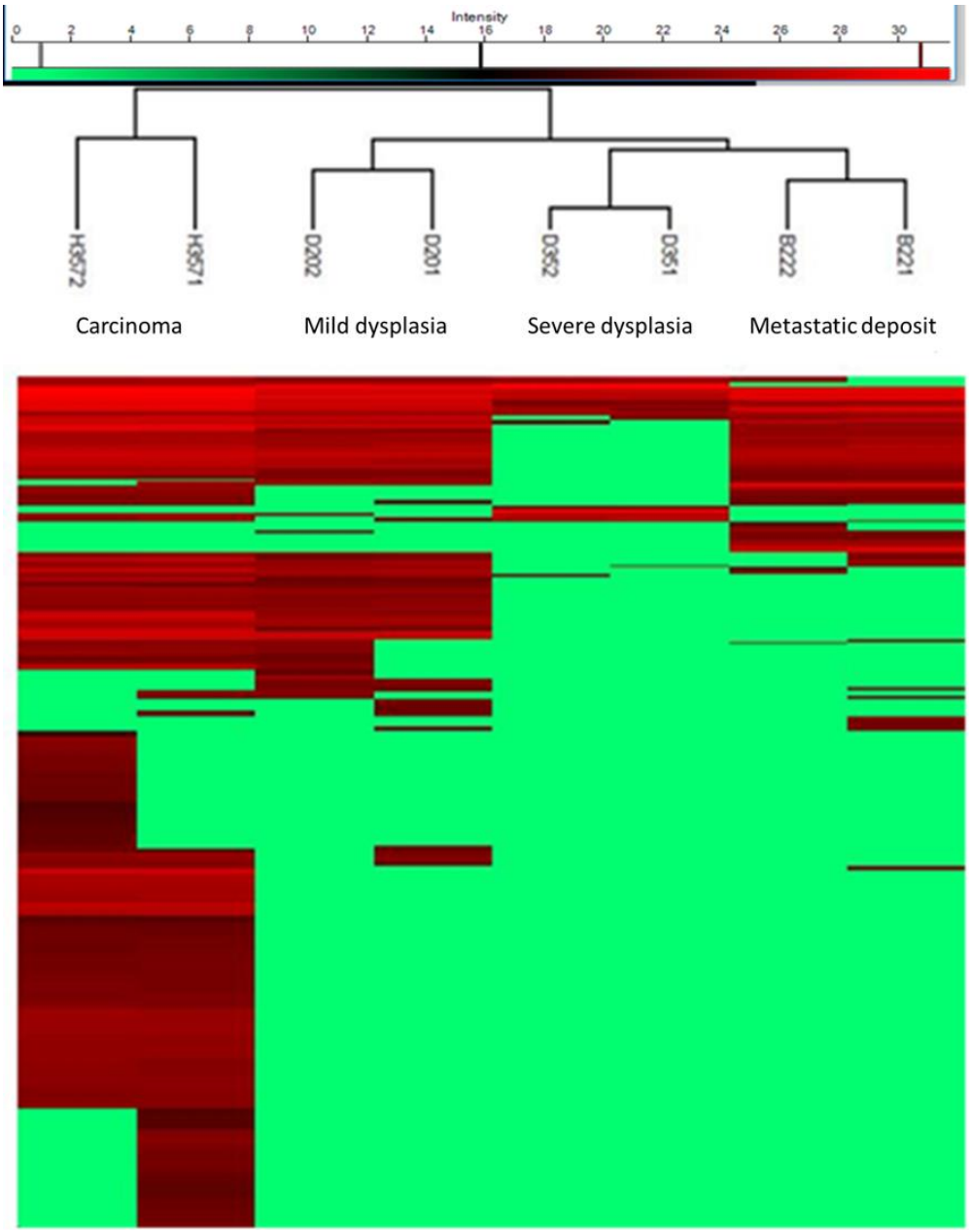

Figure 6.2 Following label free MS protein hits were mapped using MaxQuant and the resulting data imported into Perseus where identified contamination and poorly identified peptides were removed. A Euclidean heat map of 376 oral cancer cell vesicle proteins with a razor + unique peptide score =>2 was produced. This shows the technical replicates of the mass spectrometry runs clustering together but also indicates the vesicles from the carcinoma cells cluster distinctly from those of the other cell lines which cluster from left to right in order of increasing cancer stage. Red coloured proteins are those with the highest abundance. n=2 technical replicates.

Following data processing in Perseus, gene ontology analysis was performed using the Panther database. The first characteristic compared was the molecular function of the proteins (figure 6.3). The most common protein type observed were binding proteins, which accounted for between 40-65% of the identified proteins. Catalytic proteins were more abundant in the EVs produced by the carcinoma cells (H357) and metastatic cells (B22). The EVs from the severe dysplastic cells lacked proteins with translation regulator or signal transduction activity, possibly caused by the lower number of proteins detected in these EVs in comparison to the other stages. These protein classes are highest in the mild dysplastic cell EVs.

The distribution of cellular origins was reasonably consistent across the vesicle types (figure 6.4). A large proportion of the proteins originate from the extracellular region in all vesicle types, although this is seen to decrease to around 10% in carcinoma cells. However, there is also a significant proportion of proteins that are classified as cell parts, perhaps suggesting the presence of contaminants from cell debris. Again, a difference is observed in the severe dysplastic cell EVs with a decrease in the proportion of proteins derived from organelles to under 10% which are around 15-20% of the proteins in the other samples. All vesicle types have between 8-25% of proteins derived from organelles, upon further analysis (figure 6.5) the majority of these proteins were from the nucleus in all sources except for the severe dysplastic EVs where the only proteins present were cytoskeletal in origin. Further exploration of the cell part category (figure 6.6) indicates the majority of proteins for all the vesicle types are intracellular or plasma membrane in origin with few belonging to the nuclear outer membrane ER membrane network in the mild dysplastic and carcinoma derived EVs.

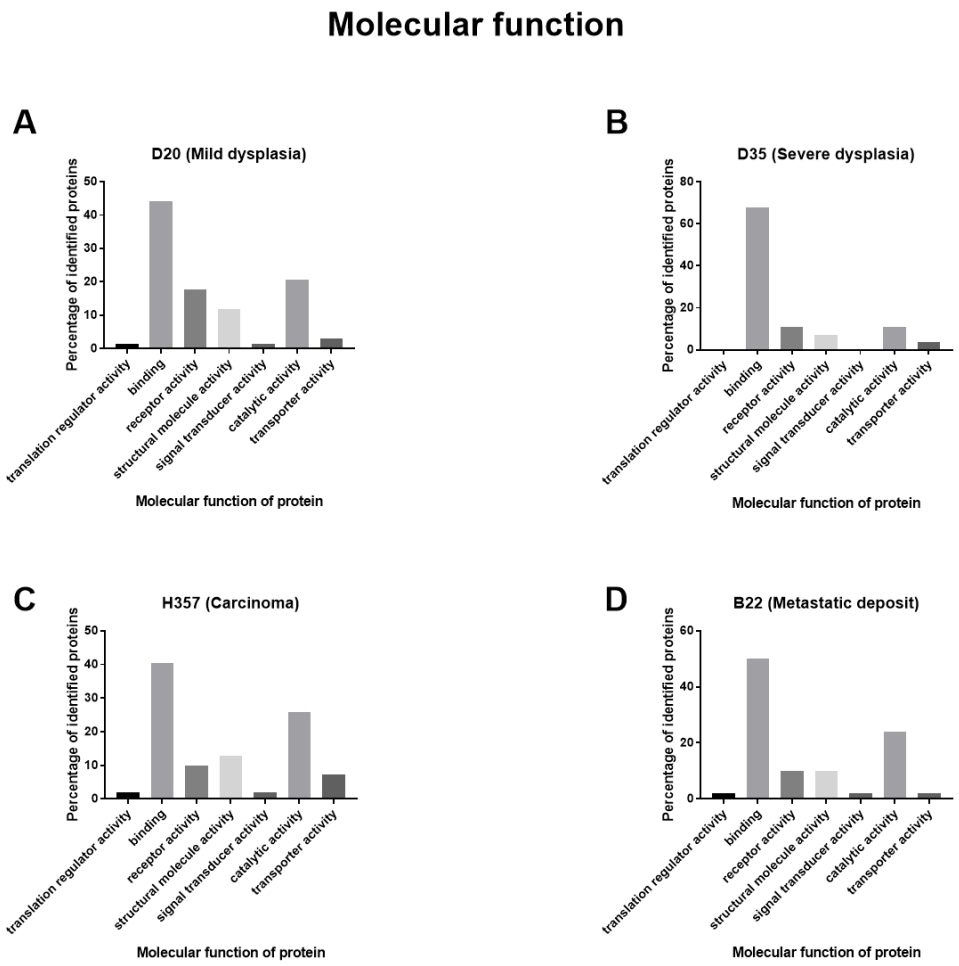

Figure 6.3 GO molecular function results for 194 statistically significant proteins purified from the conditioned media of confluent flasks of cell lines from different stages of oral cancer. A) mild dysplasia, B) severe dysplasia, C) a non-metastatic carcinoma and D) a metastatic deposit. Proteins were analysed by reverse phase HPLC coupled to label free mass spectroscopy, detected peptides were quantified and identified using MaxQuant before clean up and post processing with Perseus. Statistically significant proteins were run through the Panther Gene Ontology databases, with the above graphs detailing the distribution of molecular roles for the proteins detected. The majority of the proteins for all vesicle types were binding proteins with large numbers also involved in catalysis. n=2 technical replicates.

EV proteins are predominately cell part of extracellular region in origin

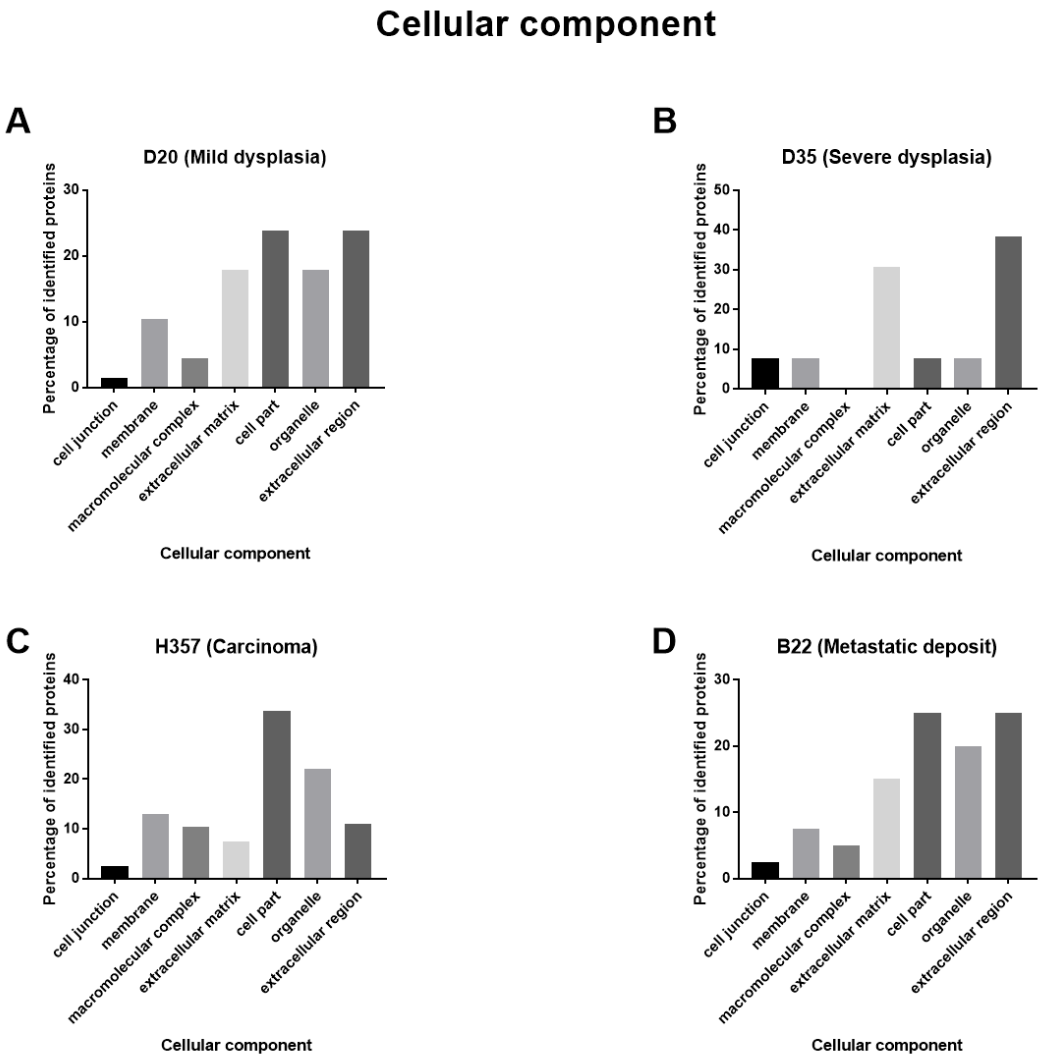

Figure 6.4 GO cellular component results for 194 statistically significant proteins purified from the conditioned media of confluent flasks of cell lines from different stages of oral cancer. A) mild dysplasia, B) severe dysplasia, C) a non-metastatic carcinoma and D) a metastatic deposit. Proteins were analysed by reverse phase HPLC coupled to label free mass spectroscopy, detected peptides were quantified and identified using MaxQuant before clean up and post processing with Perseus. Statistically significant proteins were run through the Panther Gene Ontology databases, with the above graphs detailing the distribution of cellular origins for the proteins detected. For all cell types large numbers of proteins were from the extracellular region which is expected. There were also large numbers of proteins with origins in organelles, extracellular matrix or cellular parts. n=2 technical replicates.

EV proteins from organelles are predominantly from nucleus or cytoskeleton in origin

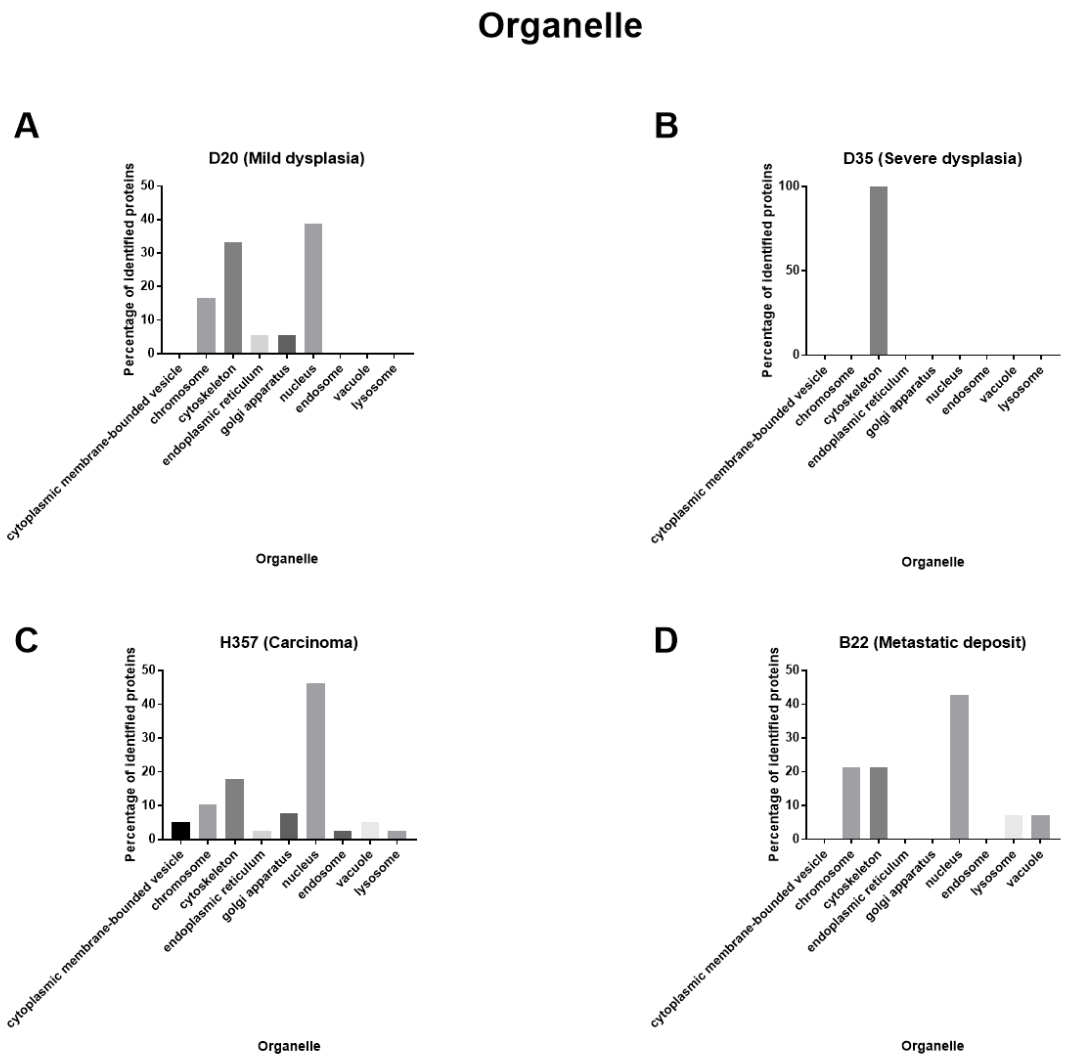

Figure 6.5 GO organelle results for 194 statistically significant proteins purified from the conditioned media of confluent flasks of cell lines from different stages of oral cancer. A) mild dysplasia, B) severe dysplasia, C) a non-metastatic carcinoma and D) a metastatic deposit. Proteins were analysed by reverse phase HPLC coupled to label free mass spectroscopy, detected peptides were quantified and identified using MaxQuant before clean up and post processing with Perseus. Statistically significant proteins were run through the Panther Gene Ontology databases, with the above graphs detailing the distribution of organelle origins for the proteins detected. The largest group of proteins is from the nucleus for all sources except the severe dysplastic cell derived EVs (B). n=2 technical replicates.

EV proteins from cell parts are predominantly intracellular or plasma membrane in origin

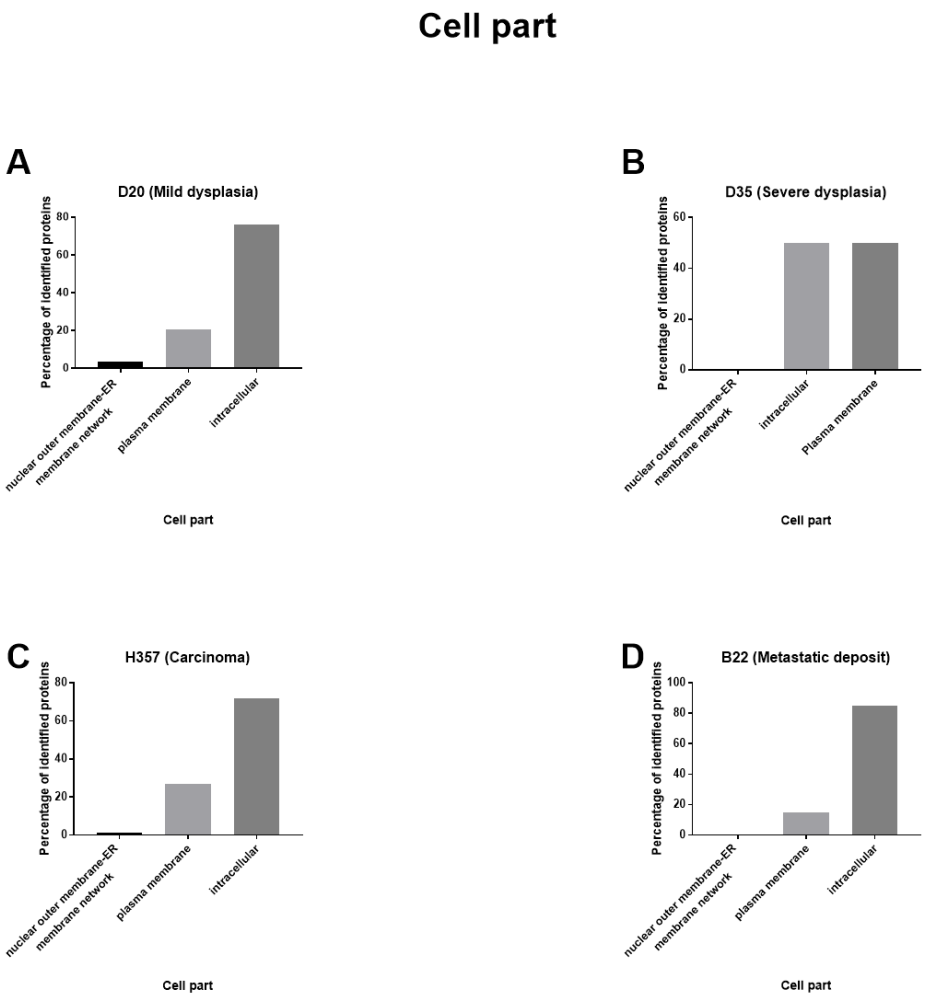

Figure 6.6 GO Cell part results for 194 statistically significant proteins purified from the conditioned media of confluent flasks of cell lines from different stages of oral cancer. A) mild dysplasia, B) severe dysplasia, C) a non-metastatic carcinoma and D) a metastatic deposit. Proteins were analysed by reverse phase HPLC coupled to label free mass spectroscopy, detected peptides were quantified and identified using MaxQuant before clean up and post processing with Perseus. Statistically significant proteins were run through the Panther Gene Ontology databases, with the above graphs detailing the distribution of cell part origins for the proteins detected. Proteins are predominantly intracellular or plasma membrane in origin for all samples with a few belonging to the nuclear outer membrane ER membrane network in the mild dysplastic (A) and carcinoma derived EVs (C). n=2 technical replicates.

Nucleic acid binding is the most common function of OSCC EV proteins

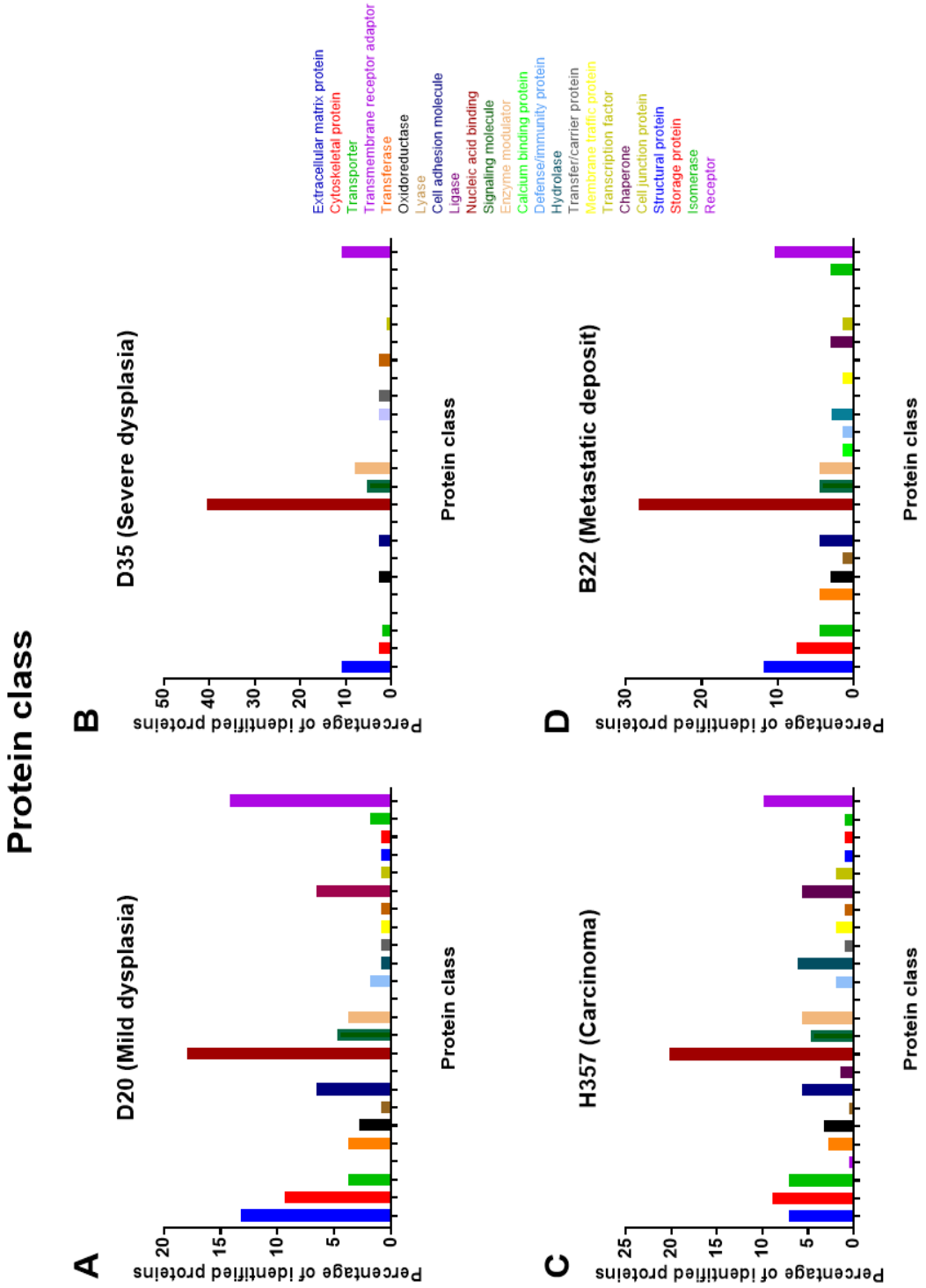

Figure 6.7 GO Protein class results for 194 statistically significant proteins purified from the conditioned media of confluent flasks of cell lines from different stages of oral cancer. A) mild dysplasia, B) severe dysplasia, C) a non-metastatic carcinoma and D) a metastatic deposit. Proteins were analysed by reverse phase HPLC coupled to label free mass spectroscopy, detected peptides were quantified and identified using MaxQuant before clean up and post processing with Perseus. Statistically significant proteins were run through the Panther Gene Ontology databases, with the above graphs detailing protein classes for the proteins detected. Large numbers of nucleic acid binding proteins are all samples, along with cytoskeletal and matrix proteins. EVs from the carcinoma cells have a wider range of protein classes within them in comparison to other vesicle types. n=2 technical replicates.

Analysis of the protein class reveals more variation than for the protein origin and molecular function (figure 6.7). Consistent with the large number of proteins identified as being from the nucleus, there are large numbers of nucleic acid binding proteins in all samples. However, these are not transcription factors which are listed as a separate category and are far less abundant in all samples. There are also large numbers of cytoskeletal and matrix proteins in all samples. As is expected, cell adhesion proteins are present in all samples and account for ~4-5% of the proteins in each sample. Given the expected origin of some of these EVs is the intraluminal vesicles of MVBs, the presence of membrane traffic proteins in all bar the severe dysplastic vesicle type is expected. There is variation in the number of protein classes across the samples, which is likely to be due to the variation in number of proteins detected across the samples. There are several enzyme classes in the different samples, including isomerases, transferases, hydrolases and lyases. Ligases only appear in the carcinoma cell EVs (figure 6.7 C), as do transmembrane receptor regulator and adaptor proteins. With the exception of the severe dysplastic cell EVs (figure 6.7 B) immune system proteins are seen in all the EVs, as are chaperone proteins. Calcium binding proteins appear to be unique to the metastatic deposit EVs (figure 6.7 D) which in turn lack any transfer or carrier proteins.

6.4.3. Comparing the protein contents of EVs from mild and severe dysplastic cells

The advantage of using discovery proteomics approaches is it allows the entire protein contents of EVs from the different cell lines to be compared at once using bioinformatics tools. The two dysplastic cell lines used in this project represent differing severity of pre-malignant oral lesions, which may be reflected in the vesicle contents of these cells. Comparison of the fold changes in abundance and the p values of the proteins detected in mild and severe dysplastic cell derived EVs (figure 6.8 and 6.9) reveals three distinct populations of proteins that were significant. A group of four proteins that are unique to the severe dysplastic EVs are phosphate & actin regulator 3, tumour necrosis factor inducible gene 6 protein and collagens α 1 and 2 (V) chain. A large group of proteins are significantly detected and common to both vesicle types including fibronectin, several histone proteins and collagen α 3 (VI) chain. By far the largest group is unique to the mild dysplastic cell derived EVs. Two of those with the highest significance values are another collagen in this case α-1 XII chain and guanine nucleotide binding protein G(i) subunit α-2.

A core group of proteins is seen to be common to both EV types, including several histone proteins, thrombospondin 1 which was detected by western blots in previous experiments, and proteins like fibronectin. The laminin subunit proteins are all unique to the EVs from the mild dysplastic cells (>20 fold more abundant), as are several chaperone proteins including HSP90. Interestingly, glyceraldehyde-3-phosphate dehydrogenase (GAPDH), which is commonly used as a loading control for western blots, was only detected in the mild dysplastic EVs illustrating the difficulty in finding loading controls for vesicle western blots. The 10 proteins with the largest changes in

the mild dysplastic EVs all have fold changes in excess of 20, whereas only 7 of the top 10 changes in the severe dysplastic EVs are above 3-fold. This is because the majority of the proteins are more abundant in the mild dysplastic EVs (figure 6.9). In the severe dysplastic EVs phosphate actin regulator 3 saw the largest difference in abundance being 25-fold more abundant in the severe dysplastic EVs. Also listed are the five chains of collagen α-1 and 2 both of which are over 20-fold more abundant in the severe dysplastic EVs.

Largest population of EVs is enriched in mild dysplastic cell derived EVs compared to severe dysplastic cell derived EVs

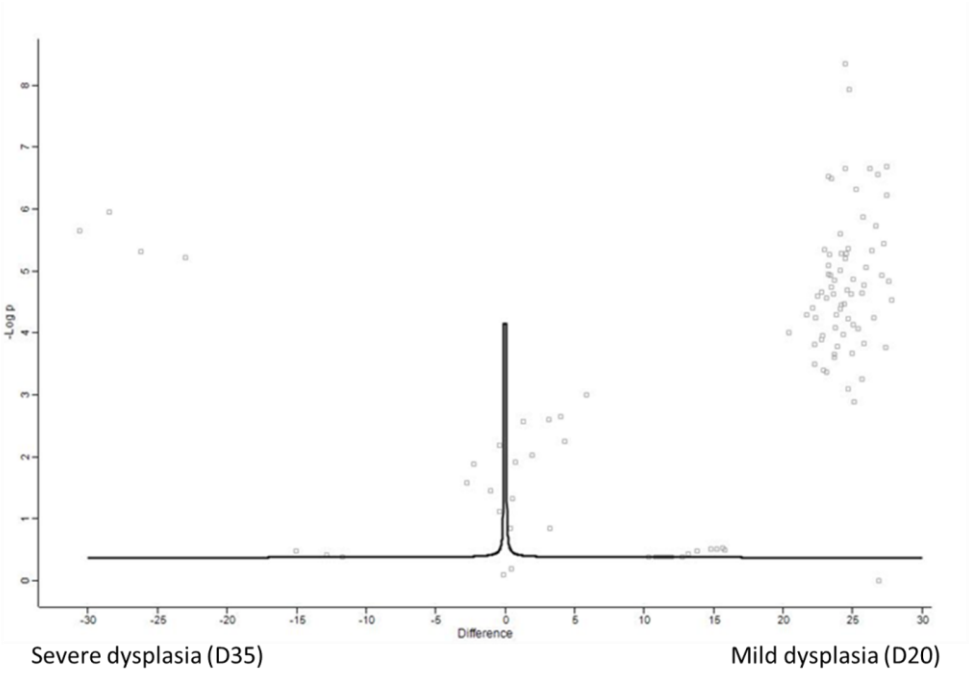

Figure 6.8 Volcano plot comparing the filtered proteins from the EVs of mild and severe dysplastic cells. Significance was set at p=>0.05 in Perseus, very few of the filtered proteins were below this line. Three distinct populations of proteins can be seen on the graph. A small group of proteins are significantly detected and are unique to the severe dysplastic EVs seen on the far left of the graph. A second population is common to both vesicle types, the largest population is unique to the mild dysplastic EVs. n=2 technical replicates.

Top 10 differentially abundant proteins in mild and severe dysplastic cell derived EVs

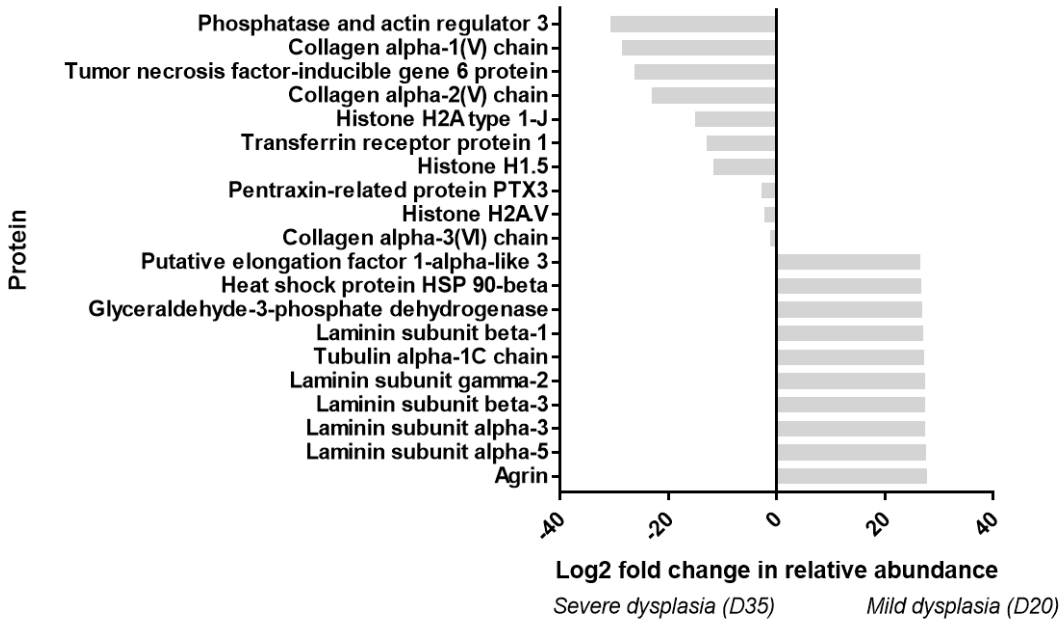

Figure 6.9 Fold change in abundance of the 10 most differentially abundant proteins in mild and severe dysplastic cell derived EVs purified from the conditioned media of confluent T175 flasks. More proteins were identified in the mild dysplastic EVs than those of the severe dysplastic cells. A group of proteins including several histone proteins were common to both vesicle types. Several laminin subunits were present in the mild dysplastic EVs but not present in those from the severe dysplasia derived EVs. n=2 technical replicates.

6.4.4. Comparison of the protein contents of EVs from non-metastatic carcinoma and metastatic deposit cells

Another valuable comparison to make is between the contents of the carcinoma cell derived EVs and those of the metastatic deposit cells. The cells of the metastatic deposit despite originating from the same anatomical site will likely exhibit many changes from those of the primary carcinoma. As with the comparison between the EVs of the two dysplastic cell types, comparison of the fold changes in abundance and the p values of the proteins detected in carcinoma and metastatic deposit cell derived EVs (figure 6.10 and 6.11) show three distinct populations of proteins. Ten proteins were significantly increased in the EVs from the metastatic deposit cells including the (I) chains of both collagen α 1 and α 2 along with extracellular matrix proteins fibulin 2 and emilin 2 (figure 6.10 and 6.11). Nespirin 1, a nuclear membrane cytoskeletal protein with key roles in cellular movement, was 23-fold more abundant in EVs from metastatic deposit cells. A group of proteins are significantly detected and similarly present in each of the groups including histone H3, collagen α 3 (VI) chain, fibronectin, actin and thrombospondin 4.

158 proteins with increased abundance were detected in the non-metastatic carcinoma cell derived EVs, which includes syndecan 4 (SDC4), the HLA class compatibility antigen A and the lipolysis stimulated lipoprotein receptor being among the most significantly detected of this group (appendix 3). Agrin is abundant in both EVs from the carcinoma cells and mild dysplastic cells this is a proteoglycan with three potential attachment points for heperan sulphate in its structure.

A group of proteins were common to both of the vesicle types, many of these were also present in the carcinoma cell derived EVs. Including subunits of histones H2, 3 and 4 along with collagen α 3 (VI) chain and thrombospondin 4. Many of these proteins are cytoskeletal in nature with fibronectin, tubulin β chain and clatherin heavy chain units. Thrombospondin 1 and major vault protein are marginally more abundant in the EVs from the non-metastatic cells whereas the versican core protein is slightly enriched in the metastatic deposit cell derived EVs. Among the interesting proteins enriched in the non-metastatic carcinoma cells is integrin β4 which is 26-fold more abundant in these EVs, which is consistent with the iTRAQ dataset. Another interesting protein enriched in the EVs from the non-metastatic carcinoma cells, is the transferrin receptor protein 1, which is the protein through which EVs were first identified (Appendix 3).

Largest population of EVs is enriched in non-metastatic carcinoma cell derived EVs compared to metastatic deposit cell derived EVs

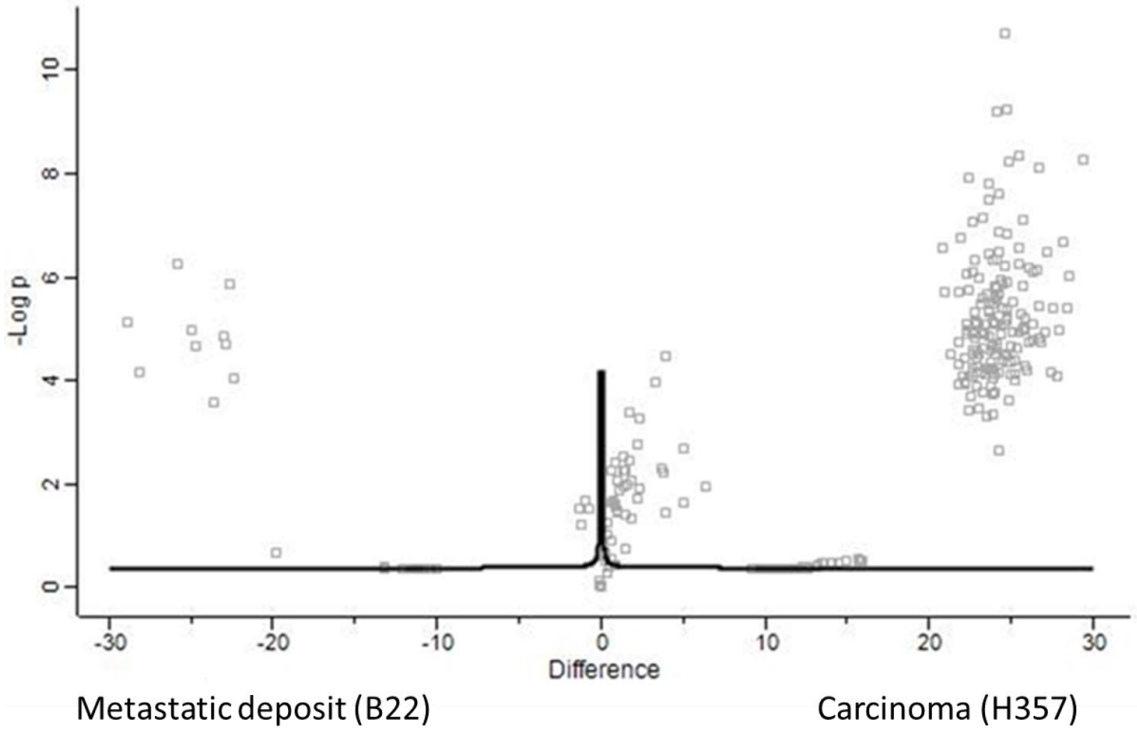

Figure 6.10 Volcano plot comparing the filtered proteins from the EVs of non-metastatic cells with those of the metastatic deposit cells. Significance was set at p=>0.05 in Perseus. Very few proteins were seen to be below this threshold. Three distinct populations of proteins can be seen on the graph. A small group of 10 proteins are significantly detected and are unique to the metastatic deposit cell EVs seen on the far left of the graph. A second population is common to both types or marginally more abundant in the EVs from the non-metastatic carcinoma cells. The largest group of proteins is most abundant in the non-metastatic carcinoma cell derived EVs. n=2 technical replicates.

Top 10 differentially abundant proteins in non-metastatic carcinoma and metastatic deposit cell derived EVs

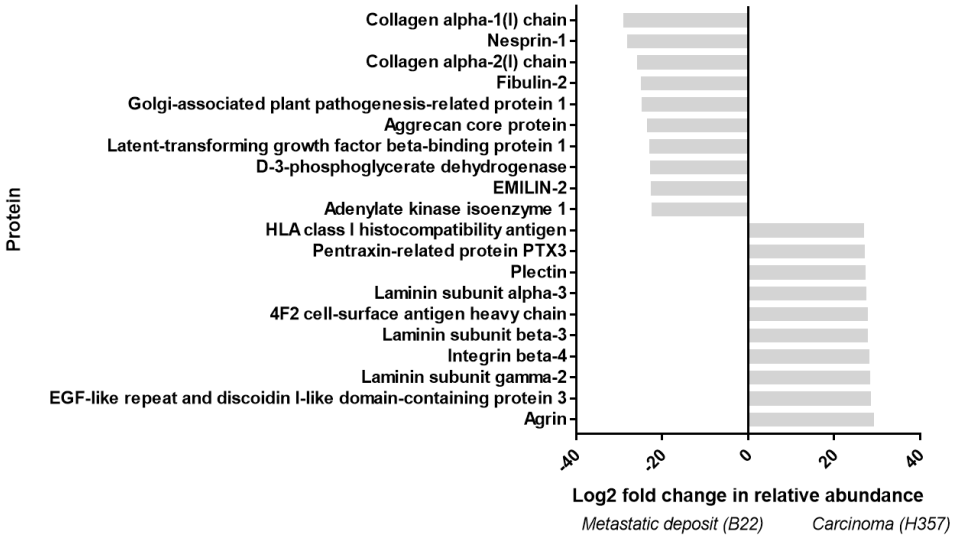

Figure 6.11 Fold change in abundance of the 10 most differentially abundant proteins in non-metastatic carcinoma and metastatic cell derived EVs purified from the conditioned media of confluent t175 flasks. More proteins are present in the non-metastatic carcinoma cell derived EVs than those of the metastatic deposit cells these include several laminin subunits, agrin and an EGF-like repeat and discoidin I-like domain-containing protein 3. A group of proteins including several histone proteins and extracellular matrix proteins are common to both vesicle types. A smaller group of proteins including some collagen α chain units are enriched in the metastatic deposit cell derived EVs. n=2 technical replicates.

6.4.5. Comparison of the protein contents of EVs from two oral dysplastic cell lines with those of oral carcinoma

Because the cell lines used in this study originate from the same primary site it is appropriate to combine the protein content of the EVs from the two-dysplastic cell derived EVs into one dataset to compare with those detected in the carcinoma cell derived EVs. This allows for the identification of any changes in vesicle protein content as a result of a dysplasia progressing into carcinoma. Strikingly most of the proteins detected (69) were more abundant in the carcinoma cell EVs. Among the most differentially abundant and significantly detected proteins were SDC4, the HLA class compatibility antigen A and the lipolysis stimulated lipoprotein receptor (figure 6.12). There is a shared group of 20 proteins present in EVs from dysplastic and carcinoma cells including fibronectin and histones 2A and 2B. The third population visible is 4 proteins that are more abundant in the carcinoma cell derived EVs but were not detected in significant amounts, including R-Ras 2 and the 40s ribosomal protein s16. The most abundant protein in the carcinoma EVs is the EGF like and discoidin 1 like domain containing protein 3 which is 30-fold more abundant in these EVs. Laminin subunit proteins are also highly abundant as is integrin α 6, a protein with implications in oral cancer (Garzino-Demo et al., 1998). Thrombospondin 4 is also more abundant in carcinoma EVs whereas thrombospondin 1 is present in similar levels in each of the vesicle types.

A common set of proteins was observed including both histone H2 and H3 subunits as well as the proteins laminin and fibronectin. The latter was marginally more abundant in the dysplastic cell derived EVs. Histone H2E was one of the most abundant proteins in the carcinoma EVs as is a laminin subunit β2, which is one of the subunits

not present in the mild dysplastic EVs. Plotting the log fold change of the 10 most differentially abundant proteins in each sample (figure 6.13) shows how the majority of proteins are enriched in the carcinoma EVs with only 3 being enriched in the dysplastic cell derived EVs. These are fibronectin lactadherin and collagen α 3 (VI) chain all of which are between 1 and 3-fold more abundant in these EVs. There are 7 proteins that are less than 5-fold enriched in the carcinoma cell derived EVs including four histone proteins as well as a heat shock protein. The 10 proteins most differentially abundant in the carcinoma cell EVs are over 25-fold more abundant in these EVs and include a receptor tyrosine kinase, fatty acid synthetase and the HLA class 1 histocompatibility antigen.

Majority of proteins enriched in carcinoma cell derived EVs compared to dysplastic cell derived EVs

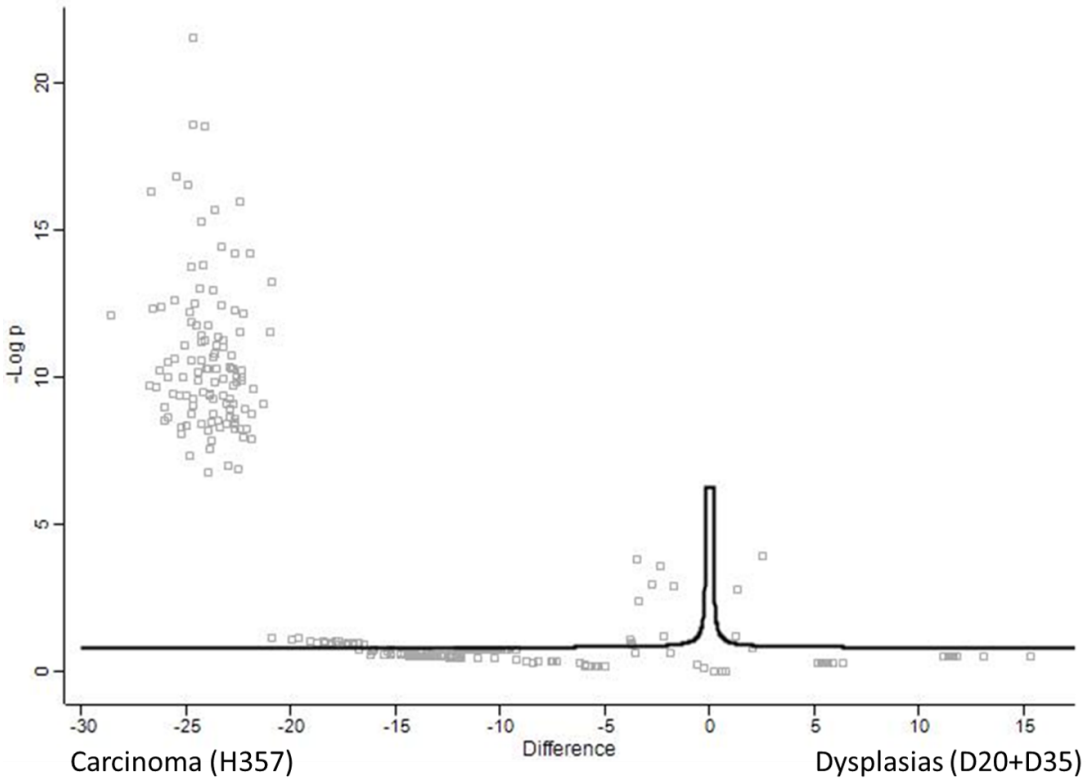

Figure 6.12 Volcano plot comparing the filtered proteins from the EVs of dysplastic cells with those of carcinoma cells. Significance was set at p=>0.05 in Perseus, there were many proteins seen to be on or below this line predominantly with greater abundance in the carcinoma samples. Three distinct populations of proteins can be seen on the graph. A very large group of proteins are significantly detected and are unique to the carcinoma cell EVs seen on the far left of the graph. A second population is more abundant in the carcinoma EVs but not detected at significant levels, a small group of proteins is common to the two vesicle classes and significantly detected. n=2 technical replicates.

Top 10 differentially abundant proteins carcinoma and dysplastic cell derived EVs

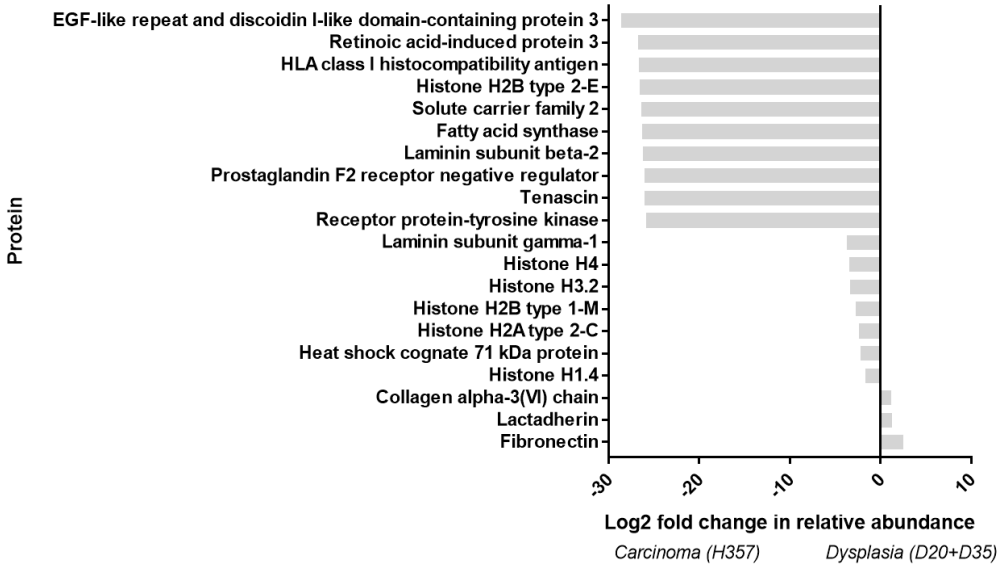

Figure 6.13 Fold change in abundance of the 10 most differentially abundant proteins in dysplastic and carcinoma cell derived EVs purified from the conditioned media of confluent T175 flasks. More proteins are present in the carcinoma cell derived EVs than those of the dysplastic cells. A group of proteins including several histone proteins are common to both vesicle types. An EGF like and discoidin 1 like domain containing protein 3 is highly abundant in the carcinoma cell EVs but is absent in the dysplastic cell EVs. n=2 technical replicates.

6.5. Validation of mass spectrometry data

In order to validate these data proteins were selected as candidates for western blotting in both cell and vesicle protein lysates. Candidates were selected that were detected in all samples as well as those which were enriched in individual samples. As previously mentioned, antibodies had initially been selected to validate the iTRAQ dataset. In order to determine if they would also be suitable for validation of the label free data, the label free intensities scores and the sequence coverage of these proteins were examined (table 6.5). Thrombospondin 1 had high scores in all samples and had been shown to be present in vesicle samples during previous experiments (figure 4.6). Major vault protein similarly had high scores in all samples bar one of the replicates for D35, which may be due to instrumentation error. EF2 was present in all bar the D35 replicates and along with L-galectin 3 binding protein (LGAL3BP), which is present in both D20 and H357 replicates, would enable the trends observed by the mass spectrometer to be confirmed.

Also considered was the percentage coverage, which is the percentage of the total protein sequence covered by the peptides detected by the instrument. The higher the percentage coverage score the more likely that antibody binding epitopes for these proteins would be present in the EVs meaning they were more likely to be successfully validated by western blot. The majority of these were above 25%, the exception being integrin α 6 which is 18.7%. As thrombospondin-1 had both high label free intensities in all samples and a comparable sequence coverage to EF2 it was added to the validation panel to further increase the reliability of the screen. Western blots were carried out on whole cell lysates as well as their respective vesicle samples to compare the abundance of the target proteins in the EVs against that of their parent cell. Thrombospondin 1 was

detected in all of the EV samples as well as the cells from which they originate (figure 6.14). EF2 was detectable in all samples except for H357 EVs and B22 cell lysate. This is inconsistent with mass spectrometry data by which it was detected in both of these EV types but not in the EVs of the D35 cells, which along with its producing cells were seen to contain the protein by western blot. Major vault protein, which was detected in all of the vesicle samples by mass spectrometry, was only detectable in the D20 cell lysates and EVs, and the B22 cell lysate by western blotting (figure 6.14). Strangely LGAL3BP which was seen by mass spectrometry to be abundant in the D20 and H357 EVs was detected in the D20 EVs but not in the H357 EVs by western blot. It was however in the B22 EVs, albeit with significantly lower abundance than in the D20 EVs. Integrin α 6 however was not detected in any of the samples by western blot, possibly because of its low sequence coverage not including any antibody epitopes.

	D20.1	D20.2	D35.1	D35.2	H357.1	H357.2	B22.1	B22.2
Elongation factor 2 (27.6%)	24.5	24.4	0	0	26.5	26.2	0	21.3
Integrin alpha 6 (18.7%)	0	0	0	0	25.5	25.5	0	0
Major vault protein (45.5%)	26.2	26.8	0	22.6	26.4	26.5	21.8	23.3
Thrombospondin 1 (26.6%)	28	28.3	24.1	24	29.6	29.7	26.1	25.5
L-galectin 3 binding protein (38.1%)	25.6	25.7	0	0	26.3	26.3	0	0

Table 6.5 Log 2x of the label free intensity scores for the selected validation candidates. Thrombospondin 1 and major vault protein were selected because they are present in all samples, L-galectin 3 binding protein integrin α 6 and elongation factor 2 were selected as they were present in 1 2 and 3 of the samples respectively. Percentage value in brackets is the percentage of the total peptide sequence covered by the peptides detected. n=2 technical replicates.

Validation of label free mass spectrometry by western blot confirms presence of some candidates

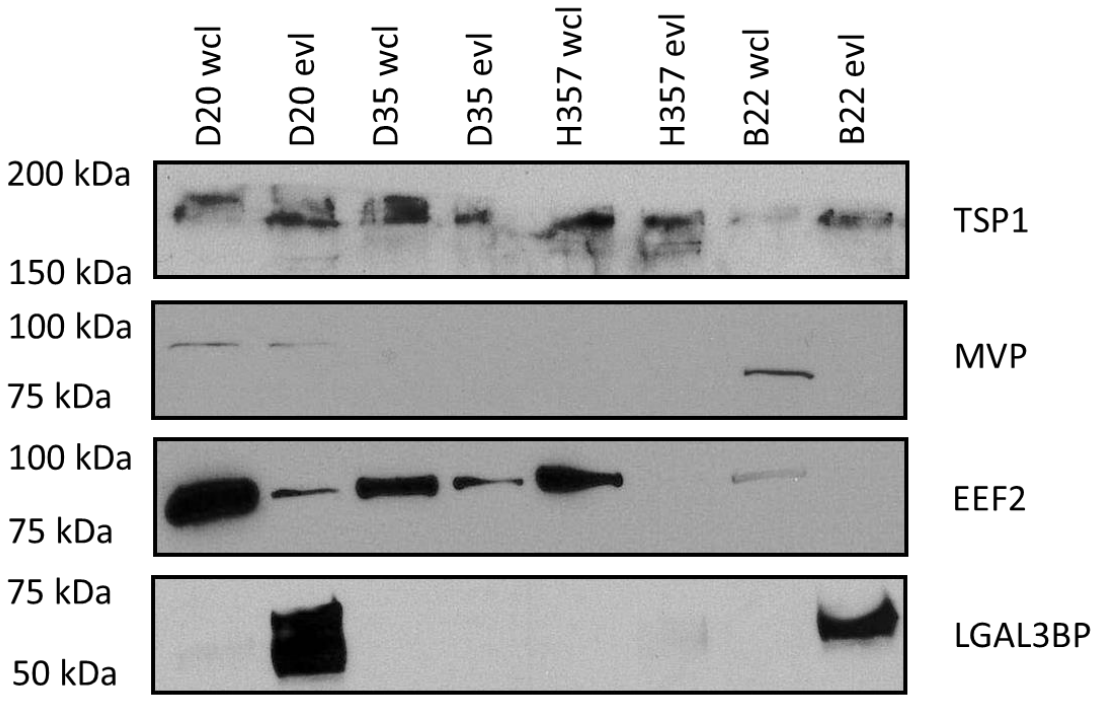

Figure 6.14 Validation of mass spectrometry data by western blotting. EVs were purified from the culture media of confluent oral cancer cell lines using size exclusion chromatography. Fractions 6-9 were pooled and pelleted at 100,000 x g for 90 min before lysing in 1xRIPA buffer with protease inhibitors. Protein lysate was produced from 250000 cells of each line. Protein from all samples was normalised and 10µg loaded per sample in a 12% acrylamide gel. Following transfer to a nitrocellulose membrane samples were blocked and incubated with primary antibodies overnight. Blots were imaged by incubation with a secondary antibody conjugated with HRP before treating with a chemiluminescent substrate and exposing to X ray film and developing with a Xograph X4 compact. Thrombospondin 1 is present in all cell lysate and EV samples. Major vault protein was detectable only in the cell and EV lysates of the D20 cells and the whole cell lysate of B22 cells. Elongation factor 2 was present in all bar H357 and B22 EVs with LGAL3BP detected in both D20 and B22 EVs. Western blots representative from a minimum of 2 experiments

6.6. Oral cancer EVs are enriched in proteins from oral cancer associated pathways

Along with identifying any changes in protein contents across the EVs of the different cancer stages another reason for performing proteomic experiments was to identify possible functional roles the EVs could have. Using the Panther GO database tool the significantly detected proteins were matched to pathways (figure 6.15). Several of these are of importance in cancer. Most abundant is the integrin pathway with inflammatory and cytoskeletal regulation proteins also present in large amounts. There are small numbers of proteins involved in the angiogenic, apoptotic and DNA replication pathways along with a few protein signalling pathways including P35 P38 MAPK fibroblast growth factor and EGF factor pathway. Because of the number of pathways present in this data set it is very difficult to observe any fluctuations in the distribution of pathways across the tumour stages.

Focusing on those pathways with the most implication in cancer (figure 6.16), shows that two of the pathways, the angiogenic and DNA replication are only present in one of the vesicle types. The angiogenic pathway is only present in carcinoma EVs and the DNA replication pathway in the metastatic deposit cell derived EVs. Only the pathways for apoptosis, cytoskeletal, regulation, inflammation, integrin and P53 are represented in all vesicle types. The EGF and FGF pathways have no proteins in the EVs from the severe dysplastic cells and neither the severe dysplastic cells nor the metastatic cells produce EVs containing P38 and MAPK pathway proteins. Because of the variation in the number of proteins detected in the different samples it is difficult to determine however if any of these pathways are increasing or decreasing in representation across the different stages.

Integrin signalling, and other pathways are most abundantly represented in OSCC EV proteins

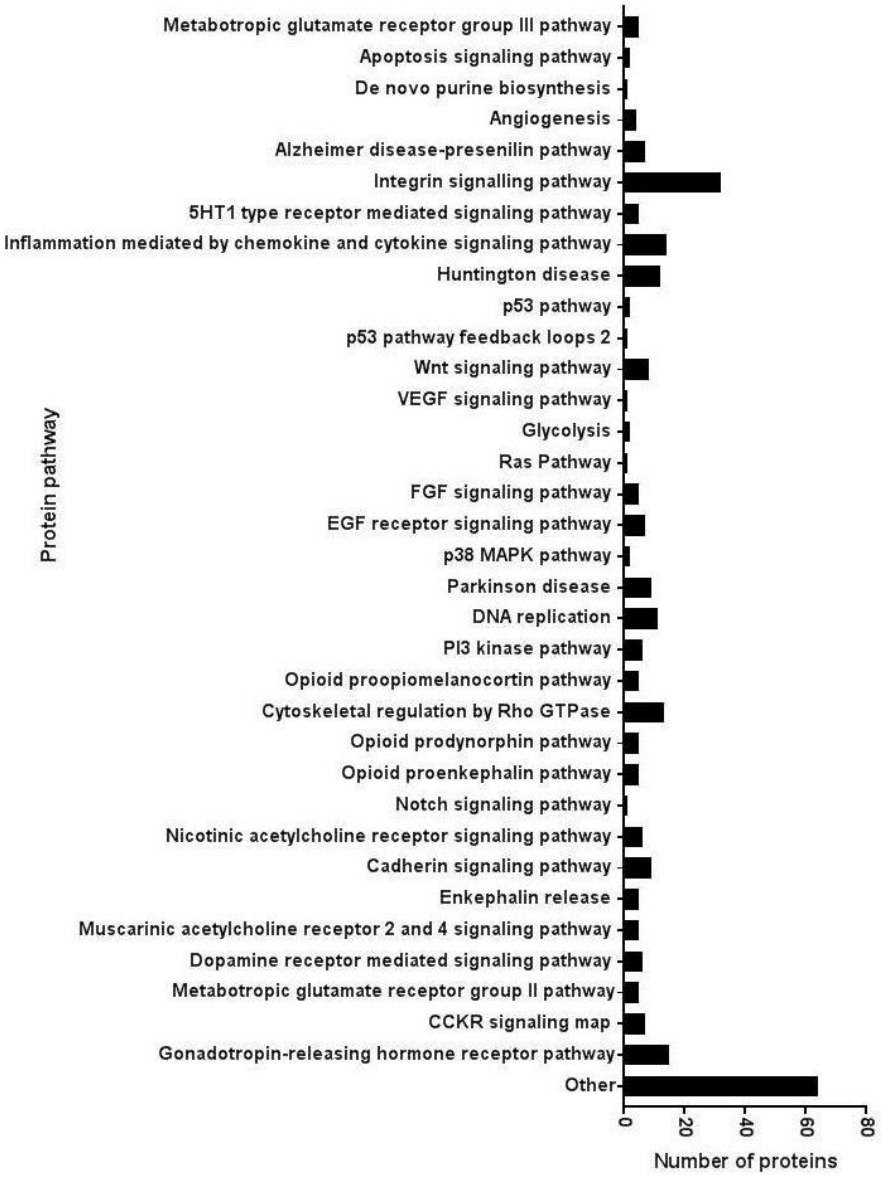

Figure 6. 15 Protein pathways represented in the protein content of oral cancer cell derived EVs. Following label free mass spectrometry of EV proteins from four oral cancer cell lines the data was pooled and EV proteins with statistically significant label free intensities and a razor and unique peptide score of =>2 were entered into the Panther database and the GO pathways returned. While the majority of pathways were labelled as "other", integrin signalling and cytoskeletal regulation pathways are seen to be the most abundant. n=2 technical replicates.

Integrin signalling, inflammation, apoptosis and cytoskeletal regulation pathways all represented in OSCC EVs

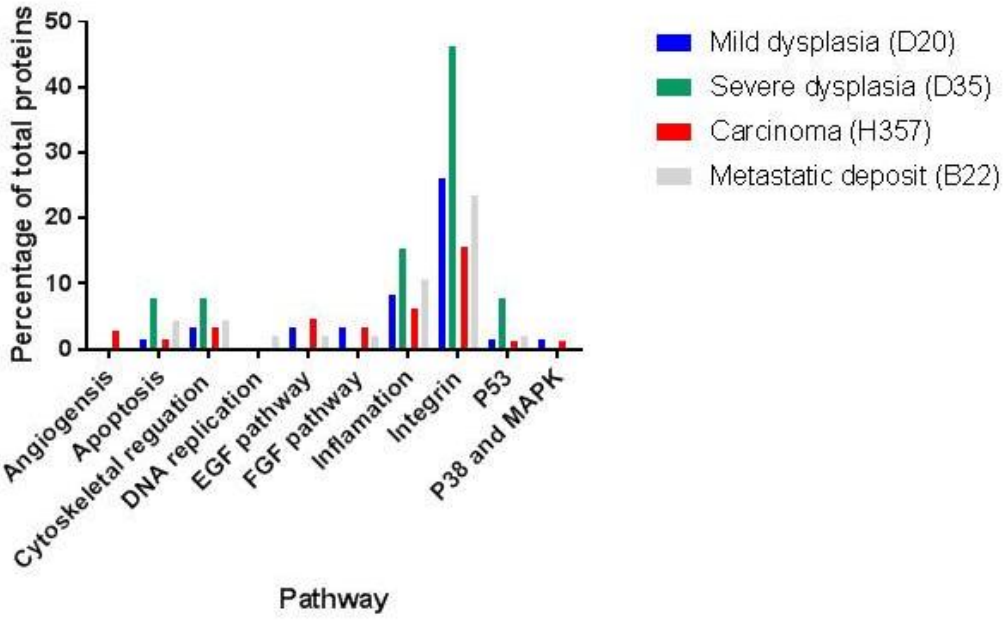

Figure 6.16 Oral cancer EV proteins with statistically significant label free intensities and a razor and unique peptide score of =>2 were entered into the Panther database and the GO pathways returned. The percentage of total proteins for each of the pathways was calculated. n=2 technical replicates.

6.7. Discussion

An unexpected outcome of this chapter was the comparison of iTRAQ and label free mass spectrometry techniques for the analysis of EV protein contents. Unfortunately, the biggest finding from the iTRAQ data was that the samples were contaminated with bovine serum proteins despite the multiple processing steps and the great care taken to remove all protein contaminations. In hindsight, these experiments were performed in the wrong order. Label free mass spectrometry should have been performed first to identify targets that appeared to be differentially packaged into the EV types, this could then have been confirmed using iTRAQ. Even allowing for the limitations of the data output the iTRAQ data did identify several proteins which were subsequently identified by the label free experiments, including all the validation candidates and several histone proteins.

However, differences in abundance seen via iTRAQ were not seen in the label free results and vice versa. Label free mass spectrometry is not without its drawbacks as each sample must be run individually causing a large increase in the required instrument time for experiments and necessitating careful cleaning of the system between each sample. iTRAQ however enables a degree of multiplexing reducing the instrument time required, which is desirable, but this is what presents limitations when working with EVs. EV contents are known to exhibit a degree of heterogeneity, something which will be particularly true when working with patient samples. Because iTRAQ outputs the comparative amounts of the protein between the samples, the heterogeneity of EVs means that some proteins that are not present in all samples could be missed. Although there are studies which have successfully used iTRAQ to study EVs these are only comparing protein contents of EVs between two states, healthy and cancerous cells or

individuals which are more suitable for iTRAQ than our more ambitious study with its four different cell lines from different stages of oral cancer.

Label free mass spectrometry was able to identify 376 proteins within EVs from the different oral cancer cell lines of which 194 were present in statistically significant quantities. The number of detected proteins varied considerably between the producing cell lines from 18-155, this is however unlikely to be entirely caused by any biological variation but will almost certainly be caused in part by technical variation. Ideally the mass spectrometry itself would have been carried out in replicate but this was not possible, however because samples were pooled to generate enough material to run the analysis this will have introduced a degree of biological variation into the dataset. The heat map produced during the processing indicates one of the problems introduced by the range in protein number observed in the samples. The carcinoma cell EVs have over double the number of proteins of the next highest EV type, which could explain why it is clustered distinctly from the other EV types, it is also interesting how many of the proteins are only detected in one of the technical replicates for the mass spectrometry run. It was expected that the EVs would cluster by cancer stage, which is seen for three of the four EV types and it is possible that had the H357 EVs had a smaller number of proteins associated with them they would have conformed to this pattern.

Gene ontology (GO) tools were used to give a further insight into the proteins present within the EVs, firstly the molecular function was compared, this indicated that the distribution of functions across the EVs was largely similar with the majority of them in all cases being binding proteins. This would suggest that they are largely membrane-bound proteins which was shown not to be the case when the cellular origin

of these proteins was explored with the majority in all samples being classified as originating from cell parts. The GO tools suggest that there is an increase in the proportion of catalytic proteins in the carcinoma cell derived EVs and a lack of translation regulator and signal transduction proteins in the severe dysplastic EVs. This should however be viewed with some caution given these two samples are at the extreme ranges of the number of proteins seen in our samples and the proportions maybe affected by this. With the exception of the EVs from the severe dysplastic cells a similar distribution with respect to cellular origin is seen in all samples, although the carcinoma cell derived EVs saw fewer proteins from the extracellular spaces, with both cell parts and organelles being the largest groups. On closer examination of the cellular origin the of the proteins they were predominantly nuclear and intracellular which is unexpected. Given the origin of at least some of these EVs will be from the outer membrane and others would be from MVBs it was expected that the more proteins would be extracellular and of lysosomal origin.

A study from a group in Brazil performed mass spectrometry on salivary EVs from oral cancer patients (Winck et al., 2015), their data indicates similarly high levels of binding proteins, with a large amount of the proteins originating from cell parts, and much like our data this was predominantly intracellular, however the majority of their proteins were classified as extracellular region in origin. This is the only paper published in English that has used mass spectrometry to analyse the protein content of oral cancer EVs. The similarities between their data and ours end with the protein class however, none of the proteins they detected in the salivary EVs were characterised as nucleic acid binding which was the most abundant class of proteins present in our EVs. Whilst these comparisons are interesting it is important to consider that the EVs isolated

from a patient's saliva will have been produced by more than one cell type whereas ours are produced by a single cell type. Taken together this data shows a stronger than expected similarity between the contents of our EVs with very similar distributions of protein origin and function. The prevalence of proteins originating in the nucleus and with nucleic acid binding abilities suggests that these EVs are enriched in proteins like transcription factors, which has been seen in large oncosomes with AKT1 (Minciacchi et al., 2017) in prostate cancer and also in HEK293 cell derived EVs which carry 14-3-3 and β-catenin (Dovrat et al., 2014). Our data shows many of the 14-3-3 family proteins are actually in our carcinoma EVs with a few of the proteins detected in the mild dysplastic and metastatic cell derived vesicle. There are however none of them in the severe dysplastic cell derived EVs. Such variation in protein content is one of the major reasons for performing proteomic analysis of the vesicle contents.

Comparisons between the vesicle proteins of the cell lines indicates that there is a group of proteins common to all the vesicle types, it would be valuable to determine if these proteins are also common to EVs produced by non-cancerous cells. Included in these proteins are histone proteins, whilst the presence of histones does not necessarily indicate the presence of genomic DNA this is something that should be tested. During the RNA extraction protocols the columns are treated with DNase, but this was done more as a precaution than because of any suspicion of DNA being present. There are currently very few papers that explore the DNA contents of EV, genomic DNA has been detected in in EVs produced by various cancer cell lines (Lázaro-Ibáñez et al., 2014) and (Montermini et al., 2015) but also in those found in patient plasma (Cai et al., 2013). These papers do suggest that this DNA can have functional effects and is capable of being actively transcribed. It would be simple to determine if the histones are

associated with DNA by use of immune affinity techniques.

Comparing the proteins compositions also raises the possibility that the different collagen α chain subunits are differentially distributed between the vesicle types, with α 1 (V) and (XVII) chain being enriched in the mild dysplasia and α 1 and 2 (V) chain enriched in the severe dysplasia EVs, α 3 (VI) chain common to all types α 2 (IV) chain enriched in the carcinoma and α 1 and 2 (X) chain enriched in the metastatic EVs. Because the collagen chains will share some sequence commonality there is a degree of uncertainty in the ability of the mass spectrometer to accurately determine between the different chains if they are present in small quantities, so these findings would need to be confirmed using western blotting before being pursued further. The experiments should also be performed in a larger panel of cells from the different stages to see if this observation is consistent. Another interesting finding is SDC4 a protein that is significantly enriched in the carcinoma cell EVs but not detected in the other vesicle types, SDC4 is one of a family of plasma membrane proteoglycans and associates with integrins and thrombospondin receptors. Although it hasn't yet been studied in oral cancer, it is a protein which has been linked to more aggressive forms of breast cancer (Baba et al., 2006) glioblastoma (Huang et al., 2001) and testicular cancer (Labropoulou et al., 2013). It is commonly associated with the acquisition of metastatic potential in these tumours and it would be useful to determine if this enrichment was just seen in the EVs or whether it is present in the producing cells as well. Searching for SDC4 in the Vesiclepeida and Exocarta databases, shows that it has been detected in salivary EVs, (Gonzalez-Begne et al., 2009) as well as in those from undifferentiated keratinocytes (Chavez-Muñoz et al., 2009) and various cancer cells (Demory Beckler et al., 2013; Hurwitz et al., 2016).

Searching for a protein with SDC4 like extremes of expression in the dysplastic cell vesicle types was not as successful. Although some laminin subunits appear to be enriched in the mild dysplastic EVs, they are absent from the severe dysplastic EVs but are found in both the metastatic and carcinoma cell EVs. Likewise, agrin which is present in the mild dysplastic cell EVs and absent from those of the severe dysplastic cells, but it is also present in the carcinoma cell derived EVs. The differential distribution of agrin is interesting when placed in the context of two separate pieces of work on the role of heparan sulphate proteoglycans (HSPGs) in EVs. Firstly, a paper from 2013 which demonstrated that heparin treatment reversibly blocked the transfer of EVs between cells (Atai et al., 2013). The second paper demonstrated that TGFβ tethered to the surface of EVs by HSPGs was functionally active in receptor cells (Webber et al., 2010). HSPG supporting proteins potentially then have an influence on both the functions and destinations of EVs, the different distribution of agrin suggests that while the HSPGs are required for EV function the proteins that bear them can vary from EV to EV. It could also indicate that the vesicles enriched in agrin bear different HSPGs and therefore have different functions or destinations to the others.

Nesprin 1 was shown to be unique to the metastatic cell derived EVs, this is a nuclear membrane protein which interacts with actin and has implications in the invasion and migration of cells. Searching for nesprin 1 in the Vesiclepeida and Exocarta databases reveals that this protein has not previously been detected in EVs. There are several proteins for which the relative label free intensities vary across the different vesicle samples, which is possibly an indication of changing abundance and therefore selective incorporation. However, the label free intensities are insufficient to

determine any enrichment and to confirm this densitometry experiments would need to be done with antibodies for these proteins. As with other interesting candidates identified in this chapter it is also necessary to determine their abundance in EVs from other cell lines from the different stages.

Alongside comparing the different proteins found within these EVs types this chapter has begun to place these protein contents in the context of cancer and tumourigenesis. These initial findings show that two significant pathways, angiogenesis and DNA replication only have proteins in EVs from one of the cancer stages. Angiogenesis is now recognized as one of the hallmarks of cancer and proteins from this pathway are only present in the carcinoma cell derived EVs. It is not known what the vascular status of this patient's tumour was but as an established tumour it is likely to have had its own blood supply. The presence of these proteins in the EVs could then be interpreted as them being removed from the cells as no longer needed or alternatively being shipped to other cells to change the angiogenic pathways activity in them.

The presence of DNA replication pathway proteins in the metastatic deposit cell derived EVs is interesting and closer analysis shows these to be Histone H3 and proliferating cell nuclear antigen. Whilst cancer cells are replicating the DNA replication pathway will obviously be highly dysregulated and whether these two proteins could affect such dysregulation alone is doubtful. Given this pathways absence in all other vesicle types it suggests that the metastatic cells DNA replication pathway is in different status to those of the other cells. Both angiogenesis and DNA replication are more significant in the early stages of a tumour another such pathway is the inflammatory pathway proteins; these proteins could be capable of establishing

inflammatory conditions that are favourable to the progression of the tumour. The largest proportion of the proteins belong to the integrin pathway, a pathway that is heavily implicated in oral cancer (Moilanen et al., 2017; Ramos et al., 2009) particularly in the invasion and migration phenotype required for metastasis. A paper from 2016 details a mechanism in prostate cancer where the vesicle mediated transfer of αVβ3 integrins to non-tumourigenic cells from the tumourigenic cells promotes migration (Singh et al., 2016). Integrin αV isn't seen in our data but β3 is, which alongside α6 another protein implicated in oral cancer. It is possible that the integrin proteins in these oral cancer EVs will play a similar role to that seen in prostate cancer in a co culture experiment. Integrins normally function as adhesion molecules, given they are the most abundantly represented proteins in these EVs and cytoskeletal regulatory proteins are one of the other abundant pathways it is very likely these EVs could exhibit a pro migratory effect on receptor cells. This role could be tested by dosing the non-metastatic cells with EVs from the metastatic cells and performing migration assays to determine if the phenotype can be transferred. Metastasis isn't the only requirement a tumour has for invasion and migration, early in a tumours development the recruitment of immune cells and fibroblasts into the developing tumour are both beneficial. This drive could explain the presence of these proteins in the EVs from all the stages of tumourigenesis and could equally be tested in the same assays used to test the migration of tumour cells.

The validation experiments performed using western blotting produced mixed results. While TSP1 was present in all the vesicle samples in both the mass spectrometry and the western blotting,EF2 was a protein detected in all bar the severe dysplastic EVs on the mass spectrometry but was missing from both the carcinoma and metastatic deposit EVs in western blotting. Likewise, major vault protein was detected in all

vesicle samples via mass spectrometry but was only present in the lysate of the mild dysplastic cells. One likely reason for these discrepancies is the relative sensitivity of western blotting vs mass spectrometry. The bands for major vault protein in particular are extremely weak and it is possible that if higher amounts of protein were loaded then a greater similarity between the two techniques would have been observed. The lack of signal for integrin α6 in the carcinoma EVs is possibly because of the low sequence coverage, possibly indicating that the protein is only present as a fragment in the EVs and that this fragment doesn't include the antibody epitope for this particular antibody. Throughout this project performing western blotting on vesicle samples was fraught with difficulty, a recurring issue was generating sufficient protein to ensure the detection of the protein with the antibodies. Although 10 µg of protein was loaded as a minimum for each of the samples because these samples contain a mixture of proteins it is still evidently not sufficient to detect some low abundance proteins. Although the EVs protein concentration was compared to that of the whole cell lysate a lack of loading controls all cases prevented densitometry being performed and the bands being quantified. However, this comparison has revealed that thrombospondin 1 is present in the whole cell lysate of all the cell lines as is EF2.

Despite the issues with the validation experiments, the mass spectrometry experiments have opened several promising avenues for further research. It is evident that the protein contents of the EV vary with tumour stage with several proteins that appear to be unique or differentially in some of our vesicle samples, these require further validation with western blots in the cell lysates and vesicle lysates of both the cells in this panel and additional cells covering the stages. Proteomics tools indicate several phenotypic changes these EVs could possibly drive, of these the most likely is

invasion and migration. But it also possible that the EVs from the carcinoma cells could affect angiogenesis and those from the metastatic deposit could impact on DNA replication. The cancer associated pathways which are well represented in the vesicle contents are all promising candidates to explore further with functional assays like transwell assays for migration or tubule forming assays for angiogenesis. Should the EVs impact on these pathways then a next step would be to deplete these proteins in the producing cells and observe any changes in this effect. Whilst this data needs further validation and additional experiments it does suggest that the EVs produced by oral cancer cell lines could have quite profound biological effects.

6.7.1. Future work

Although the western blots have confirmed some of the findings of the mass spectrometry such as the enrichment of LGAL3BP in the EVs of the mild dysplasia and the presence of TSP1 in all vesicle samples, improving the confidence in this validation is essential and could be achieved in a variety of ways. Firstly, additional antibodies with different epitopes should be used to determine if the non-detection of the proteins is due to the epitopes not being covered or a weak binding affinity. A second approach would be to identify other candidates for use with western blotting experiments, these targets should have a higher sequence coverage and similar patterns of expression to the existing targets. Another approach would be to use a higher sensitivity technique such as targeted mass spectrometry, this could be done using iTRAQ and whole cell lysates run alongside vesicle samples in an 8 plex experiment.

Once these issues are addressed the findings of this chapter can be expanded upon. Levels of proteins like SDC4, nespirin 1 and agrin should be investigated in other examples of cells from the different stages of oral cancer, healthy normal cells of the oral cavity and potentially patient samples. This would give more confidence in the trends spotted in these experiments are representative of changes occurring in the development of oral cancer. Should the enrichment of these proteins in oral cancer vesicles be seen to be conserved across a wider range of oral cancer samples the testing the impact of these proteins on the phenotype of receptor cells should be explored. This could be done by depleting vesicles of these proteins and performing functional assays that tested effects on angiogenesis, EV uptake, cell proliferation and invasion and migration.

7. Effect of oral cancer EVs on cells of the tumour microenvironment

7.1. Introduction

In recent years the role of fibroblasts within the TME has come under increasing scrutiny, with the fibroblasts within the microenvironment displaying a markedly different phenotype to their normal relatives. These CAFs have been shown to drive cell growth (Castells et al., 2012; Olumi et al., 1999), metastasis, angiogenesis and immune escape (Leef and Thomas, 2013; Togo et al., 2013). They have even been seen to facilitate therapy resistance (Sun and Nelson, 2012) and inflammation (Erez et al., 2010, Sharon et al., 2010). The activation of normal fibroblasts to CAFs is now considered to be one of the major steps in tumourigenesis (Hanahan and Weinberg, 2011).

During tumourigenesis activation is driven by a range of biological mediators, primarily TGFβ1 but other proteins and RNA species have also been linked to the process. It has also been noted that cigarette smoke, a major risk factor in oral cancer, can also contribute to this activation (Pal et al., 2013). More recent work by Clayton and Webber has identified a role for prostate cancer EVs in the process. They initially showed that TGFβ1 associated with exosomes on a sucrose density gradient and that these exosomes were capable of activating fibroblasts in a similar way to soluble TGFβ1(Webber et al., 2010). Further experiments showed that the TGFβ1 was tethered to the surface of the EVs via betaglycans. Interestingly, although they showed that this activation produced morphological and some biological changes which were similar to those that occurred when fibroblast were treated with soluble TGFβ1, changes to mRNA expression were subtly different.

This was the first time that EVs had been linked to the activation of fibroblasts in cancer. Since then similar phenomena have been observed in malignant ascites (Wei et al., 2017), breast cancer (Baroni et al., 2016) and leukaemia (Paggetti et al., 2015). These are not the only signals to be passed between tumour cells and normal fibroblasts, Gutkin et al (2016) showed that hTERT mRNA could be passed to fibroblasts from immortalized tumour cells. Another paper from the same year showed that EVs from rhabdomyosarcoma cells carry miRNA cargos that promote the invasion of fibroblasts (Ghayad et al., 2016). Taken together the data shows extensive EV mediated cross talk between tumour cells and fibroblasts within the TME with a range of outcomes, not just activation of the fibroblasts, which are beneficial to the progression of the tumour.

7.2. Aims and objectives

The aims of this chapter were to study EV signalling in the TME and to test the hypothesis that oral cancer EVs could activate normal oral fibroblasts (NOFs) into CAFs. First the ability of tumour cell derived EVs to be taken up by cells of the microenvironment was visualised using a fluorescence-based assay. The impacts of this uptake on NOF growth was assessed using a range of assays. In order to assess if oral cancer EVs could activate NOFs, immunofluorescence, immunoblotting and qPCR for αSMA expression were used in combination to monitor any changes following EV and TGFβ1 treatment.

7.3. EVs produced by oral cancer cells can be taken up by a range of cell types

A fluorescence-based assay was used to visualise the uptake of EVs by receptor

cells. EVs purified from conditioned media of oral cancer cells were stained with two different fluorescent labels. The first of these, CellMask red, binds to the lipid membrane, the second is a lipid-permeable RNA dye which fluoresces green when in contact with RNA. Stained EVs were incubated with cells for 1 h at 37^{o}C, alongside mock controls (the same volume of PBS exposed to the dyes). After 1 h the cells were fixed and mounted on slides and imaged on a Zeiss Axioplan microscope. The presence of red fluorescence in the treated samples but not in the controls indicated that the EVs were taken up by the carcinoma cells (figure 7.1) an immortalised oral keratinocyte cell line (figure 7.2) a dermal microvascular endothelial cell line (figure 7.3) and normal oral fibroblasts (figure 7.4). Additionally, the presence of the green fluorescence in the treated samples suggests that this uptake causes the release of the EV contents into the receptor cells.

EVs can be taken up by other OSCC cells

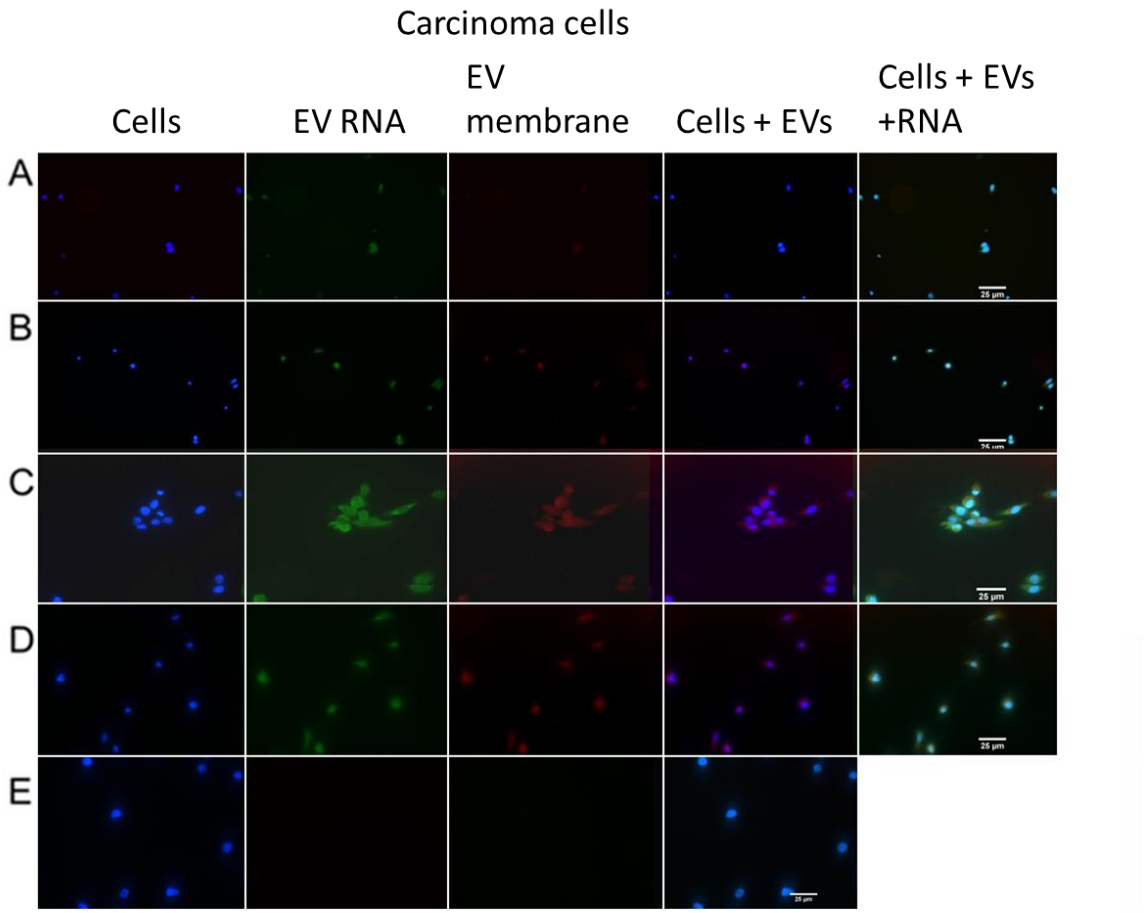

Figure 7.1 EV uptake by OSCC. EVs were harvested from the medium of confluent cancer cells using the serial centrifugation protocol. The final EV pellet was stained with 0.01 µM Cyto RNA Select (Life Technologies) and CellMask Red (Life Technologies) for 1 h at 37ºC. A standard dose of stained EVs was added to 10000 OSCC cells seeded onto coverslips in EV free medium. After 1h at 37ºC the cells were fixed in 4% paraformaldehyde and mounted on slides to image. The images show that EVs (RED) produced by mild dysplastic cells (A) severe dysplastic cells (B) carcinoma cells (C) and cells from a metastatic deposit (D) are all capable of transferring encapsulated RNA dye (GREEN) to OSCC. E is a EV free control where the same number of cells were treated with the same volume of EV free PBS. Images are representative from three experiments. Scale bars are 25 µm.

EVs can be taken up by oral keratinocytes

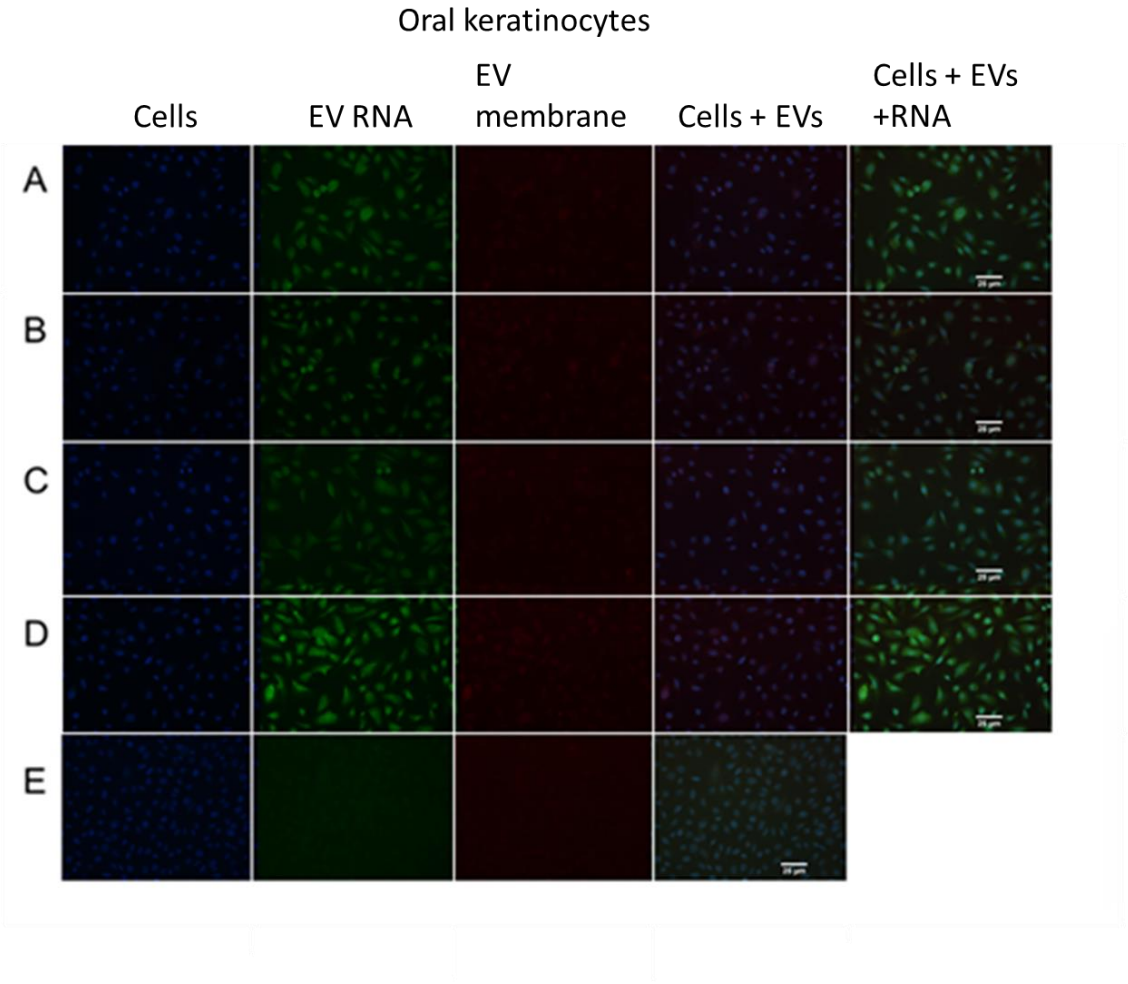

Figure 7.2 EV uptake by oral keratinocytes. EVs were harvested from the medium of confluent cancer cells using the serial centrifugation protocol. The final EV pellet was stained with 0.01 µM Cyto RNA Select (Life Technologies) and CellMask Red (Life Technologies) for 1 hour at 37ºC. A standard dose of stained EVs was added to 10000 OKF6 cells an hTERT immortalised oral keratinocyte cell line seeded onto coverslips in EV free medium. After 1 h at 37ºC the cells were fixed in 4% paraformaldehyde and mounted on slides to image. The images show that EVs (RED) produced by mild dysplastic cells (A) severe dysplastic cells (B) carcinoma cells (C) and cells from a metastatic deposit (D) are all capable of transferring encapsulated RNA dye (GREEN) to OKF6 cells. E is an EV free control where the same number of cells were treated with the same volume of EV free PBS. Images are representative from three experiments. Scale bars are 25 µm.

OSCC EVs can be taken up by endothelial cells

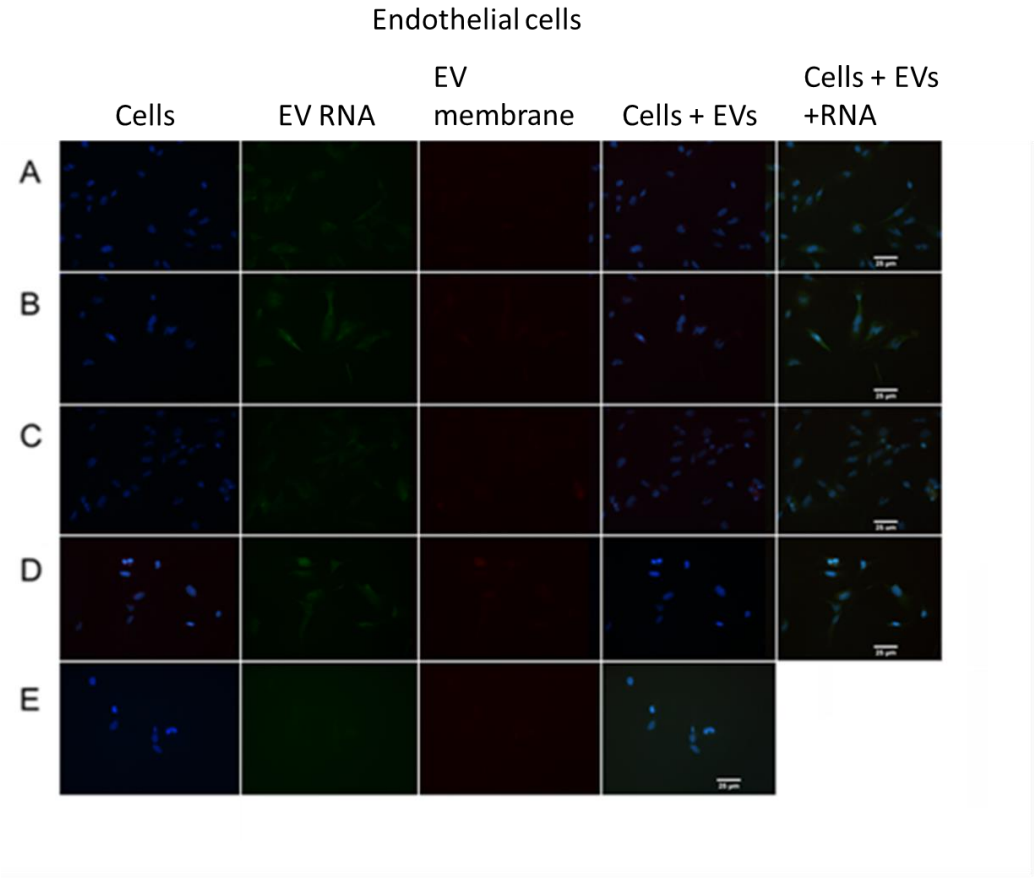

Figure 7.3 EV uptake by endothelial cells. EVs were harvested from the medium of confluent flasks of cancer cells using the serial centrifugation protocol. The final EV pellet was stained with 0.01 µM Cyto RNA Select (Life Technologies) and CellMask Red (Life Technologies) for 1 h at 37ºC. A standard dose of stained EVs was added to 10000 HMEC-1 cells, a dermal microvascular endothelial cell line, seeded onto coverslips in EV free medium. After 1 h at 37ºC the cells were fixed in 4% paraformaldehyde and mounted on slides to image. The images show that EVs (RED) produced by mild dysplastic cells (A) severe dysplastic cells (B) carcinoma cells (C) and cells from a metastatic deposit (D) are all capable of transferring encapsulated RNA dye (GREEN) to HMEC-1 cells. E is a vesicle free control where the same number of cells were treated with the same volume of EV free PBS. Images are representative from three experiments. Scale bars are 25 µm.

OSCC EVs can be taken up by NOFs

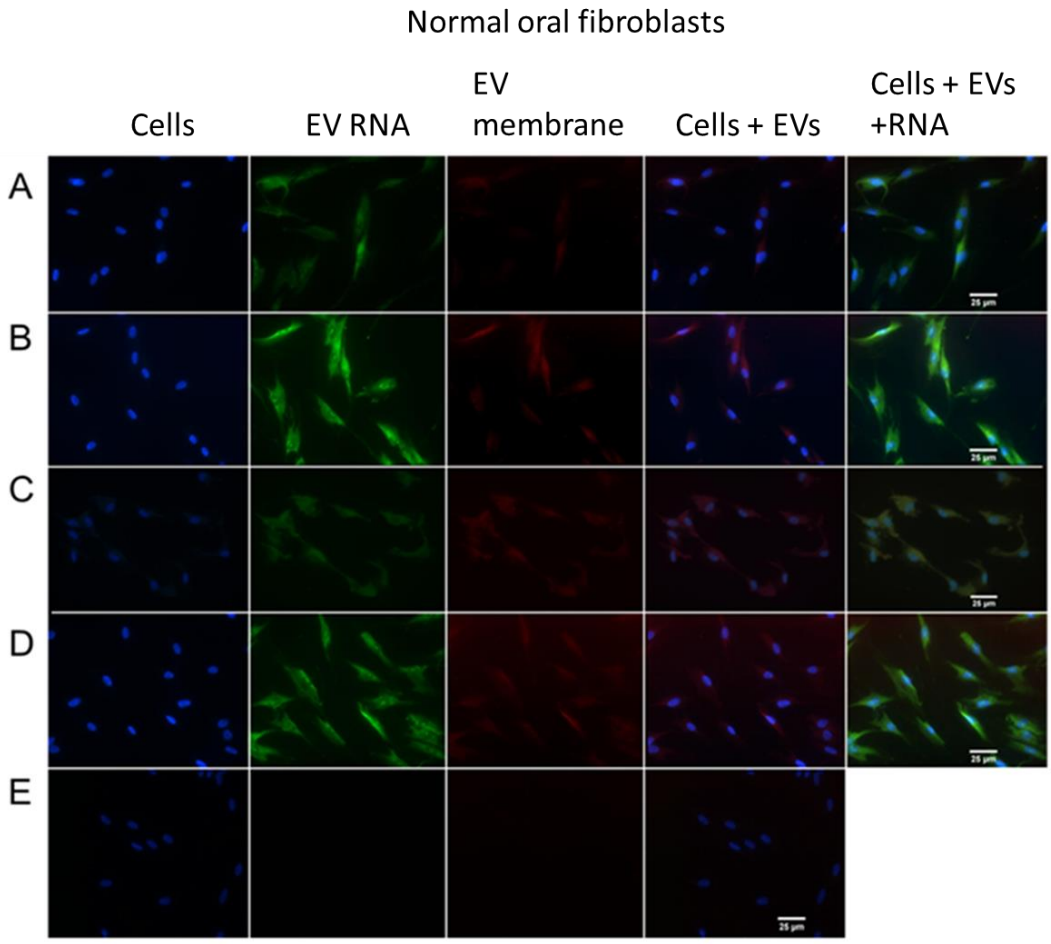

Figure 7.4 EV uptake by normal oral fibroblasts. EVs were harvested from the medium of confluent flasks of cancer cells using the serial centrifugation protocol. The final EV pellet was stained with 0.01 µM Cyto RNA Select (Life Technologies) and CellMask Red (Life Technologies) for 1 h at 37ºC. A standard dose of stained EVs was added to 8000 normal oral fibroblasts seeded onto coverslips in EV free medium. After 1 h at 37ºC the cells were fixed in 4% paraformaldehyde and mounted on slides to image. The images show that EVs (RED) produced by mild dysplastic cells (A) severe dysplastic cells (B) carcinoma cells (C) and cells from a metastatic deposit (D) are all capable of transferring encapsulated RNA dye (GREEN) to oral fibroblasts. E is a vesicle free control where the same number of fibroblasts were treated with the same volume of EV free PBS. Images are representative from three experiments. Scale bars are 25 µm.

7.4. Optimisation of fibroblast seeding densities in full serum and serum free conditions

In order to assess any EV-mediated impact on NOF growth, the characteristics of the fibroblasts in normal conditions needed to be determined before experiments could be designed. Fibroblasts were seeded at various densities in a 96 well plate in full serum and serum free media presto blue staining was performed at 0, 24, 48 and 72 hours. Figure 7.5 shows the growth curves for the NOFs in normal medium (A) and serum free medium (B). In normal medium the cells show proliferation across the full 72 h incubation with an increase in fluorescence at each time point. The rate of growth slows between 5000 and 10000 cells per well at 72 h suggesting the wells have reached contact inhibition. In serum free medium the reverse is observed with almost no growth observed at 72 h for all cell densities. At densities up to 3000 cells there is an increase in fluorescence over 48 h, at higher densities a decrease in fluorescence is observed at 24 h. For subsequent proliferation experiments densities of 2000 cells per well and medium containing 2% serum was used to allow some growth to occur over a 48 h period.

NOF growth curves in presence and absence of serum

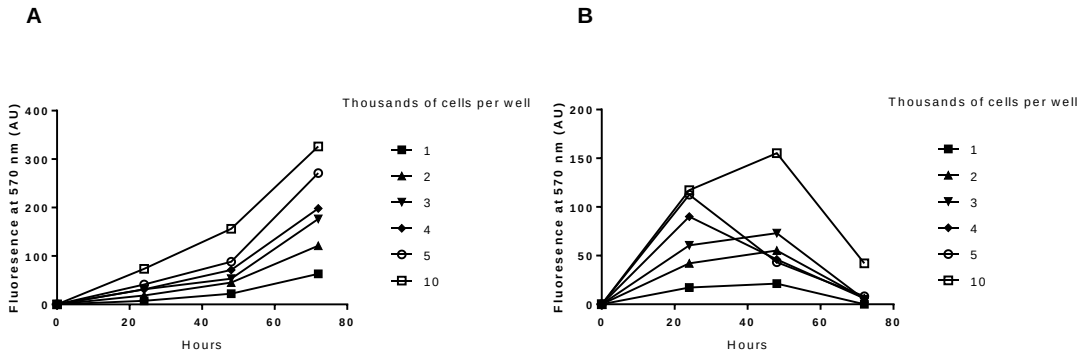

Figure 7.5 Growth curves for NOFs in normal medium (A) and serum free medium (B). Varying densities of cells were seeded in a 96 well plate and stained with presto blue at 0, 24, 48 and 72 hours with fluorescence at 570 nm being proportional to cell number. In normal medium the cells continue to replicate over the 72 h incubation, in serum free medium however the reverse is seen with no growth at 72 hours. At densities above 3000 cells per well in serum free medium the growth arrest begins at 24 hours. n=3 technical replicates.

7.5. EVs from cancer cells have a minimal impact on fibroblast turnover

Firstly, the impact of EV treatment on NOFs viability was determined using a live/dead assay. NOFs isolated from three different patients (NOF804, NOF805 and NOF806) were seeded at 2000 cells per well in low serum medium and treated with various doses of EVs for 24 and 48 h. Cells were then incubated with an ethidium dimer and a spectrophotometer used to measure uptake. The percentage of dead cells was calculated by comparing with wells containing 100% dead cells. This assay (figure 7.6) shows that the uptake of EVs from all of the cancer cell lines causes a small but not significant increase (~10%) in cell death after 24 hours with the severe dysplastic cell (figure 7.6 B) derived EVs being marginally less cytotoxic than those of the mild dysplastic (figure 7.6 A), carcinoma cells (figure 7.6 C) and metastatic deposit cells (figure 7.6 D). By 48 hours however this increase in cell death relative to the negative control is no longer detectable. This effect does not show any dose dependency at either time point with all EV doses causing a similar effect at 24 hours and no effect at 48 hours.

Treatment with increasing doses of OSCC EVs has no effect on NOF viability after 48 hours

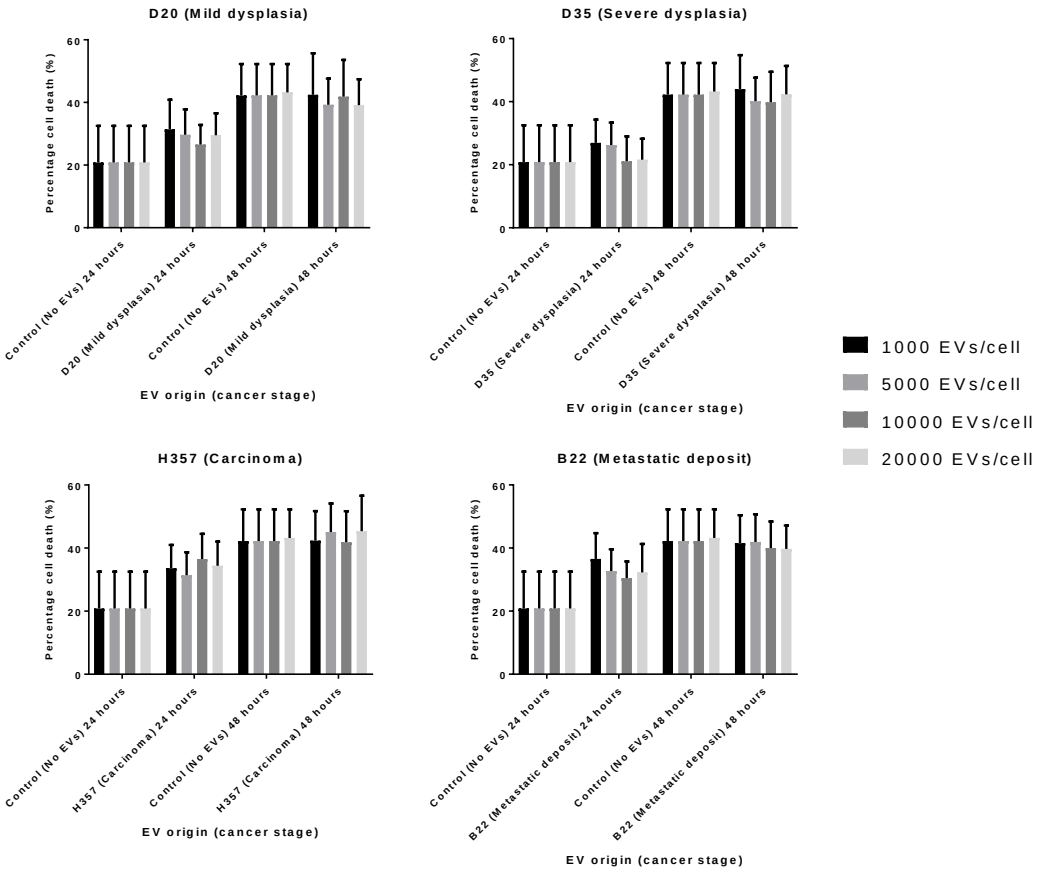

Figure 7.6 Effect of EV uptake on NOF viability. NOFs (NOF 804, 805 and 806) were seeded at 2000 cells per well in a 96 well plate and treated for 24 and 48 h with varying doses of cancer derived EVs in medium supplemented with 2% EV free serum. Cells were treated with 4 µM EthD-1, which stains dead cells, the fluorescence was read on a Tecan plate reader at 645 nm. The resulting values were compared to wells treated with the same volume of medium with 2% EV free serum. A positive control was used to measure 100% dead cells by treating with 100% methanol for 20 min. The fold changes in the 100% dead controls indicate an increase in the number of dead cells in the non EV treated samples after 48 hours in the minimal medium. n=3 biological replicates error bars representing SEM. Data was non-significant with both a student's t-test and one-way Anova with Tukeys multiple test correction.

Cell death is not the only aspect contributing to NOF turn over. Changes in the proliferation of the NOFs following EV uptake was assessed using a BRDU ELISA kit. NOFs from four different patients (NOF 806, NOF316, NOF319 and NOF335) were treated with the maximum dose of EVs used in the cell viability experiments and treated for 48 h. After 48 h the cells were treated with BRDU for 4 h and then incubated with an antibody conjugated to a peroxidase enzyme. Changes in proliferation were detected by treatment with tetramethyl benzidine which when cleaved by the peroxidase produces a blue coloured product that can be detected by a spectrophotometer. EVs produced by the severe dysplastic, carcinoma and metastatic deposit cells have no significant impact on proliferation (figure 7.7) with even a slight negative impact on the proliferation of fibroblasts. There was a trend of increased proliferation in NOFs treated with EVs from the mild dysplastic cells. However, neither of these changes were statistically significant.

Treatment with OSCC EVs produces no significant change in NOF proliferation after 48 hours

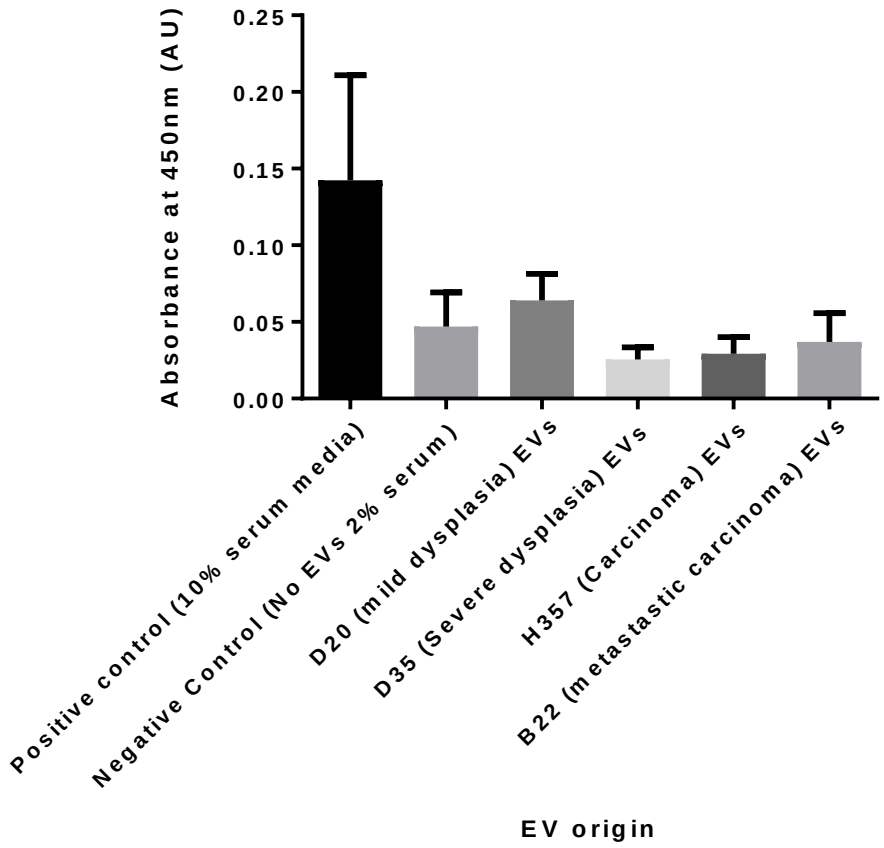

Figure 7.7 Effect of EV uptake on NOF proliferation. NOFs (NOF 806, 316, 319 and NOF335) were seeded at 2000 cells per well and serum starved overnight. They were then treated with 20,000 cancer cells derived EVs per cell in medium containing 2% EV free serum and incubated for 48 h. cells were incubated with 10 μM BrdU labelling solution for 4 h. Cells were fixed and incubated with antibody solution. Following this, cells were treated with substrate and allowed to develop for 15 min to produce a detectable colorimetric response. Reactions were then stopped using 1 M H_2SO_4 and read at 450 nm on a Fluorstar plate reader. n=4 biological replicates error bars representing SEM. Results were non-significant with a student's T test.

7.6. Uptake of oral cancer derived EVs causes normal oral fibroblasts to display cancer associated fibroblast characteristics.

NOFs can be activated in vitro to adopt CAF like phenotype by treatment with 5 ng/µl TGFβ1 (Webber et al., 2010). This activation can be characterised by an increased expression of alpha smooth muscle actin (αSMA), this is one of the major components of the stress fibres responsible for the activated fibroblast morphology. Webber et al (2010) have shown that treatment of lung fibroblasts with prostate, bladder and breast cancer cell derived EVs causes them to adopt a similar morphology (Webber et al., 2010). NOFs from four patients were treated with a standard dose of EVs, alongside TGFβ1 treated controls. αSMA expression at the gene and protein level were assayed by qPCR and western blot, respectively. In addition, the formation of stress fibres was visualised by immunofluorescence.

Following EV uptake by NOF803 cells the qPCR data (figure 7.8 A) indicates an increase in the mRNA for αSMA upon uptake of the EVs from the carcinoma and metastatic deposit derived EVs but not the dysplastic cell derived EVs. This increase is 2-fold less than in the TGFβ1 treated controls. Western blotting (figure 7.8 B) shows an increase in αSMA protein when the fibroblasts are treated with EVs from all the cancer cell lines and this increase is similar to the 2-fold increase in the positive control samples. Fluorescent staining for αSMA (figure 7.8 C) show similar green fibres as the TGFβ1 treated controls that are absent in the untreated fibroblasts.

Gene expression data (figure 7.9 A) showed a decrease in αSMA mRNA transcript when NOF316 were treated with TGFβ1 and dysplastic cell derived EVs; there is,

however, between a 2 and 3-fold increase in the mRNA in these cells when treated with the EVs from the carcinoma and metastatic deposit cell derived EVs. The western blot (figure 7.9 B) shows that the TGFβ1 treatment causes an increase in the amount of αSMA protein, in contrast to the qPCR which shows the mRNA expression has decreased, however EV treatment has no effect on the amount of αSMA protein in this fibroblast culture. NOF316 cells exhibited similar αSMA fibre formation upon EV treatment as the positive controls (figure 7.9 C).

NOF 319 cells show a different trend at the mRNA level when treated with EV's (figure 7.10 A). This cell line was again unresponsive to TGFβ1 with respect to the mRNA for αSMA, however there was an increase in the mRNA when they were treated with EVs from the mild dysplastic, carcinoma and metastatic deposit cells but not the severe dysplastic cells which actually caused a decrease in the amount of mRNA for αSMA. The western blot and associated densitometry (figure 7.10 B) shows that this patient fibroblasts are not responsive to TGFβ1 with respect to αSMA protein either. Nor does the level of αSMA protein change when they are treated with EVs from the cancer cell lines, with the exception of those from the metastatic deposit cell line which causes a very slight increase in the protein abundance. NOF319 cells (figure 7.10 C) show the presence of the αSMA fibres following treatment with cancer cell derived EVs and TGFβ1 using immunofluorescence, in keeping with the other fibroblast cultures.

The qPCR data for NOF335 cells show that (figure 7.11 A), whilst the treatment with TGFβ1 causes no change in the mRNA for αSMA, there is also no change in mRNA when they are treated with EVs from the mild dysplasia, carcinoma and metastatic deposit cells. There is however a 20-fold increase in the αSMA mRNA when

treated with EVs from the severe dysplastic cells. The western blot data shows similar changes in the αSMA protein as the NOF319 cells (figure 7.11 B), these fibroblasts are not responsive to TGFβ1 with respect to αSMA protein either, and the concentration of αSMA protein doesn't change when they are treated with EVs from the cancer cell lines, with the exception of those from the metastatic deposit cell line which causes a very slight increase in the protein abundance. NOF335 again shows the same stress fibre formations under immunofluorescence (figure 7.11 C) as the other patients fibroblasts following EV and TGFβ1 treatment. Taken together this data indicates that the EVs from oral cancer cells can cause the formation of αSMA stress fibres in oral fibroblasts allowing them to adopt a phenotype similar to the CAFs. However, this is always not accompanied by a corresponding detectable increase in αSMA mRNA and protein in all patients NOFs after 24 hours.

EV treatment of NOF803 cells produces increase in αSMA mRNA and protein and the formation of stress fibres

A

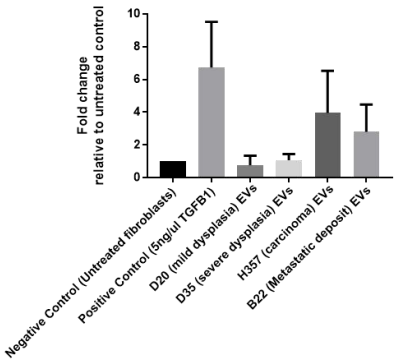

B

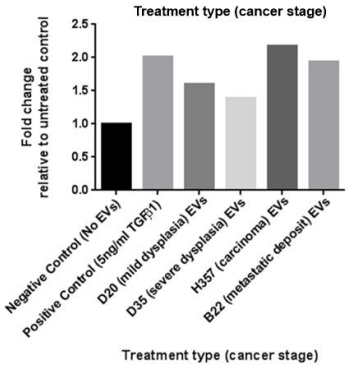

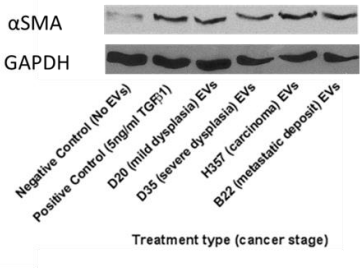

C

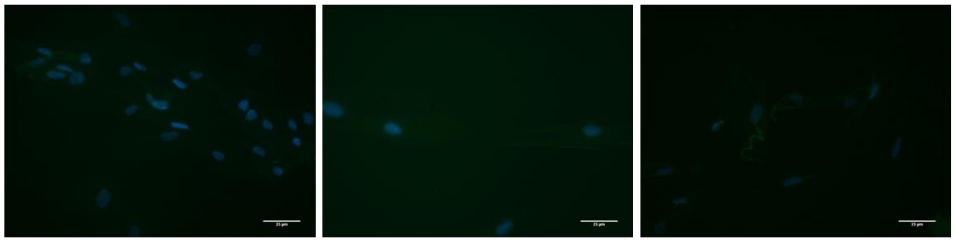

Positive control TGFβ treated fibroblasts

EVs from mild dysplastic cells

EVs from severe dysplastic cells

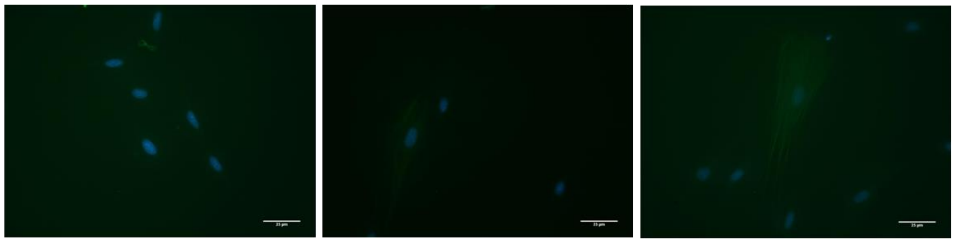

Negative control no EVs

EVs from carcinoma cells

EVs from metastatic deposit cells

Figure 7.8 EV mediated activation of NOF 803 cells. NOFs were serum starved for 24 h before treatment with 20000 EVs per cell in serum free medium and allowed to incubate for 24 h. Negative controls were treated with the same volume of serum free medium, positive controls were treated with 5 ng/µl of TGFβ1. RNA was harvested and used to run qPCR with probes for αSMA, U6 was used as a housekeeping gene to allow the calculation of ΔΔCT values relative to the control samples (A). αSMA mRNA did not increase in samples treated with dysplastic EVs but did increase when samples were treated with carcinoma and metastatic EVs. Following TGFβ1 treatment these cells showed no increase in αSMA mRNA. n=2 technical replicates error bars representing SEM. Data was non-significant with a student's test Protein lysates were also harvested from the treated NOFS and were run on a 12% acrylamide gel before transferring to a nitrocellulose membrane. The membrane was probed with a mouse monoclonal antibody for αSMA diluted 1:500 (v/v) and a HRP conjugated rabbit monoclonal antibody for GAPDH as a loading control diluted 1:20000 (v/v). Densitometry of the bands was performed using ImageJ (B), unlike the mRNA αSMA protein increased in samples treated with all the EV samples n=1. Finally, cells were incubated with a FITC conjugated αSMA antibody diluted 1:1000 (v/v) with blocking buffer for 1 h before mounting on slides. After imaging on a Zeiss Axioplan comparable αSMA stress fibres were visible in EV treated samples and in TGFβ1 treated control samples with no fibres visible in the negative controls (C).

EV treatment of NOF316 cells produces no change in αSMA mRNA. except with the EVs from carcinoma and metastatic deposit cells, no change at the protein level but does produce stress fibres

A

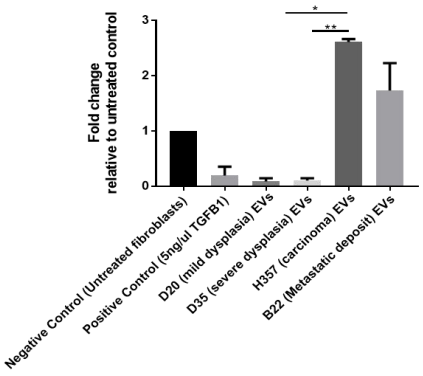

B

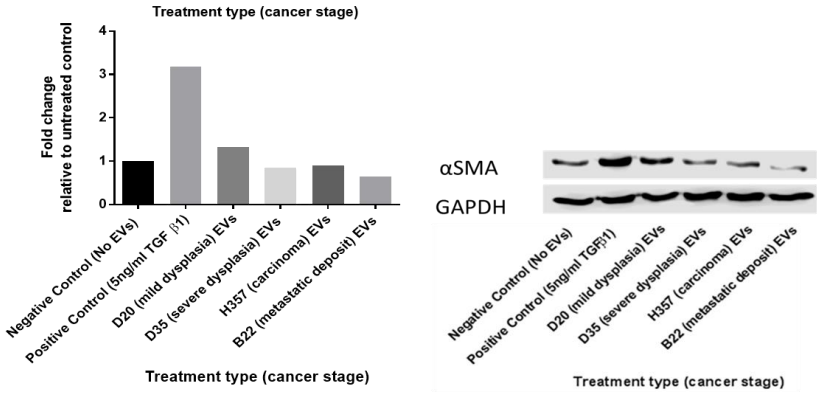

C

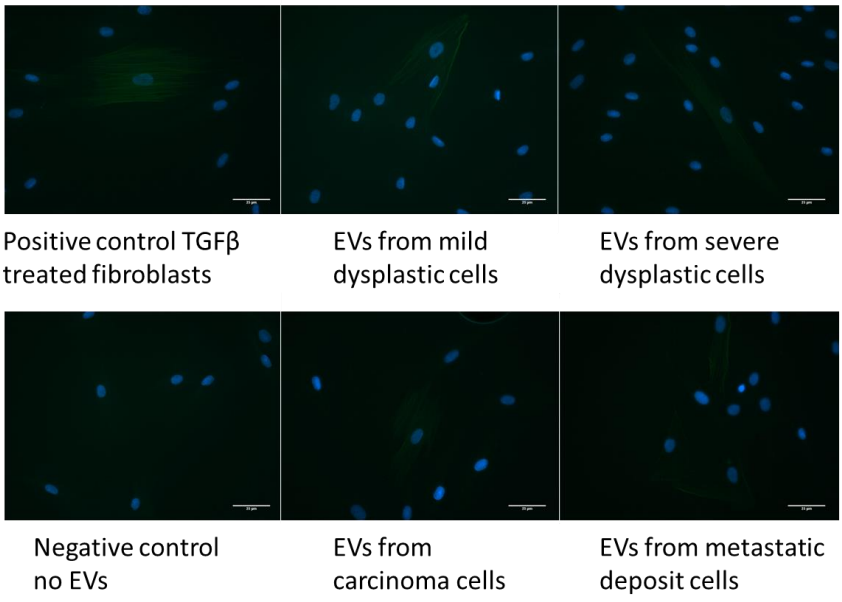

Figure 7.9 EV mediated activation of NOF 316 cells. NOFs were serum starved for 24 h before treatment with 20000 EVs per cell in serum free medium and allowed to incubate for 24 h. Negative controls were treated with the same volume of serum free medium, positive controls were treated with 5 ng/µl of TGFβ1. RNA was harvested and used to run qPCR with probes for αSMA, U6 was used as a housekeeping gene to allow the calculation of ΔΔCT values relative to the control samples (A). αSMA mRNA didn't increase in samples treated with dysplastic EVs but did increase when samples were treated with carcinoma and metastatic EVs. Following TGFβ1 treatment these cells showed no increase in αSMA mRNA. n=2 technical replicates error bars representing SEM. Significance was tested using a student's t-test ***** = p>0.05 ***= p>0.001 ****= >0.0001. Protein lysates were also harvested from the treated NOFS and were run on a 12% acrylamide gel before transferring to a nitrocellulose membrane. The membrane was probed with a mouse monoclonal antibody for αSMA diluted 1:500 (v/v) and an HRP conjugated rabbit monoclonal antibody for GAPDH as a loading control diluted 1:20000 (v/v). Densitometry of the bands was performed using ImageJ (B), unlike the mRNA αSMA protein increased samples treated by TGFβ1 but not with those treated by EVs, there was no increase in αSMA protein with any of the EV treatments n=1. Finally, cells were incubated with a FITC conjugated αSMA antibody diluted 1:1000 (v/v) with blocking buffer for 1 h before mounting on slides. After imaging on a Zeiss Axioplan comparable αSMA stress fibres were visible in EV treated samples and in TGFβ1 treated control samples with no fibres visible in the negative controls (C).

EV treatment of NOF319 cells produces no change in αSMA mRNA. except with the EVs from carcinoma and metastatic deposit cells, no change at the protein level but does produce stress fibres

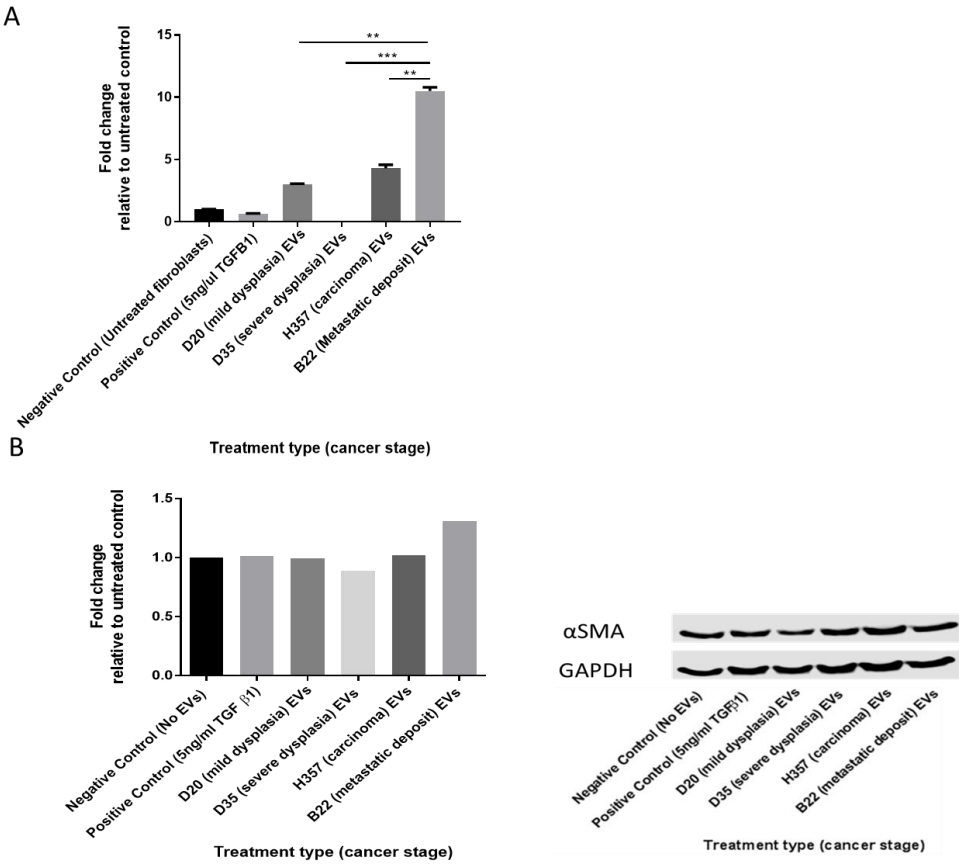

C

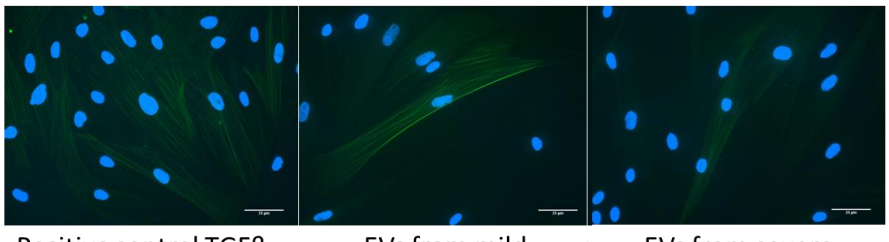

Positive control TGFβ treated fibroblasts

EVs from mild dysplastic cells

EVs from severe dysplastic cells

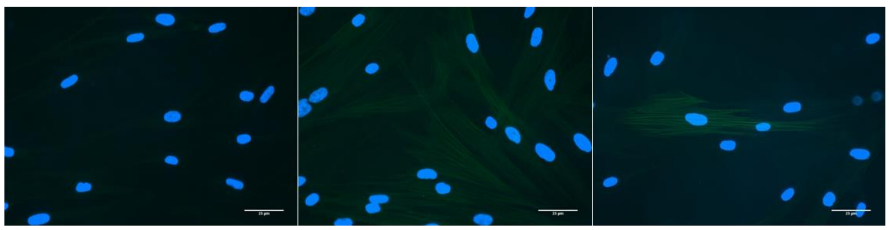

Negative control no EVs

EVs from carcinoma cells

EVs from metastatic deposit cells

Figure 7.10 EV mediated activation of NOF 319 cells. NOFs were serum starved for 24 h before treatment with 20000 EVs per cell in serum free medium and allowed to incubate for 24 h. Negative controls were treated with the same volume of serum free medium, positive controls were treated with 5 ng/µl of TGFβ1. RNA was harvested and used to run qPCR with probes for αSMA, U6 was used as a housekeeping gene to allow the calculation of ΔΔCT values relative to the control samples (A). No increase in αSMA mRNA occurred in samples treated with TGFβ1. αSMA mRNA increased in the samples treated with mild dysplastic, carcinoma and metastatic EVs but a decreased in the samples treated with severe dysplastic derived EVs. Following TGFβ1 treatment these cells showed no increase in αSMA mRNA. n=2 technical replicates error bars representing SEM. Significance was tested using a student's t-test ***** = p>0.05 ***= p>0.001 ****= >0.0001. Protein lysates were also harvested from the treated NOFS and were run on a 12% acrylamide gel before transferring to a nitrocellulose membrane. The membrane was probed with a mouse monoclonal antibody for αSMA diluted 1:500 (v/v) and an HRP conjugated rabbit monoclonal antibody for GAPDH as a loading control diluted 1:20000 (v/v). Densitometry of the bands was performed using ImageJ (B), unlike the mRNA an αSMA protein levels increased samples treated by TGFβ1 but not with those treated by EVs, there was no increase in αSMA protein with any of the treatments except the EVs from the metastatic deposit which showed a very small increase in protein concentration n=1. Cells were seeded at 8000 per well on coverslips in a 24 well plate and allowed to adhere overnight. Finally, cells were incubated with a FITC conjugated αSMA antibody diluted 1:1000 (v/v) with blocking buffer for 1 h before mounting on slides. After imaging on a Zeiss Axioplan comparable αSMA stress fibres were visible in EV treated samples and in TGFβ1 treated control samples with no fibres visible in the negative controls (C).

EV treatment of NOF335 cells only produces a change in mRNA levels when treated with EVs from severe dysplastic cells and produces no change in protein levels but does produce stress fibres

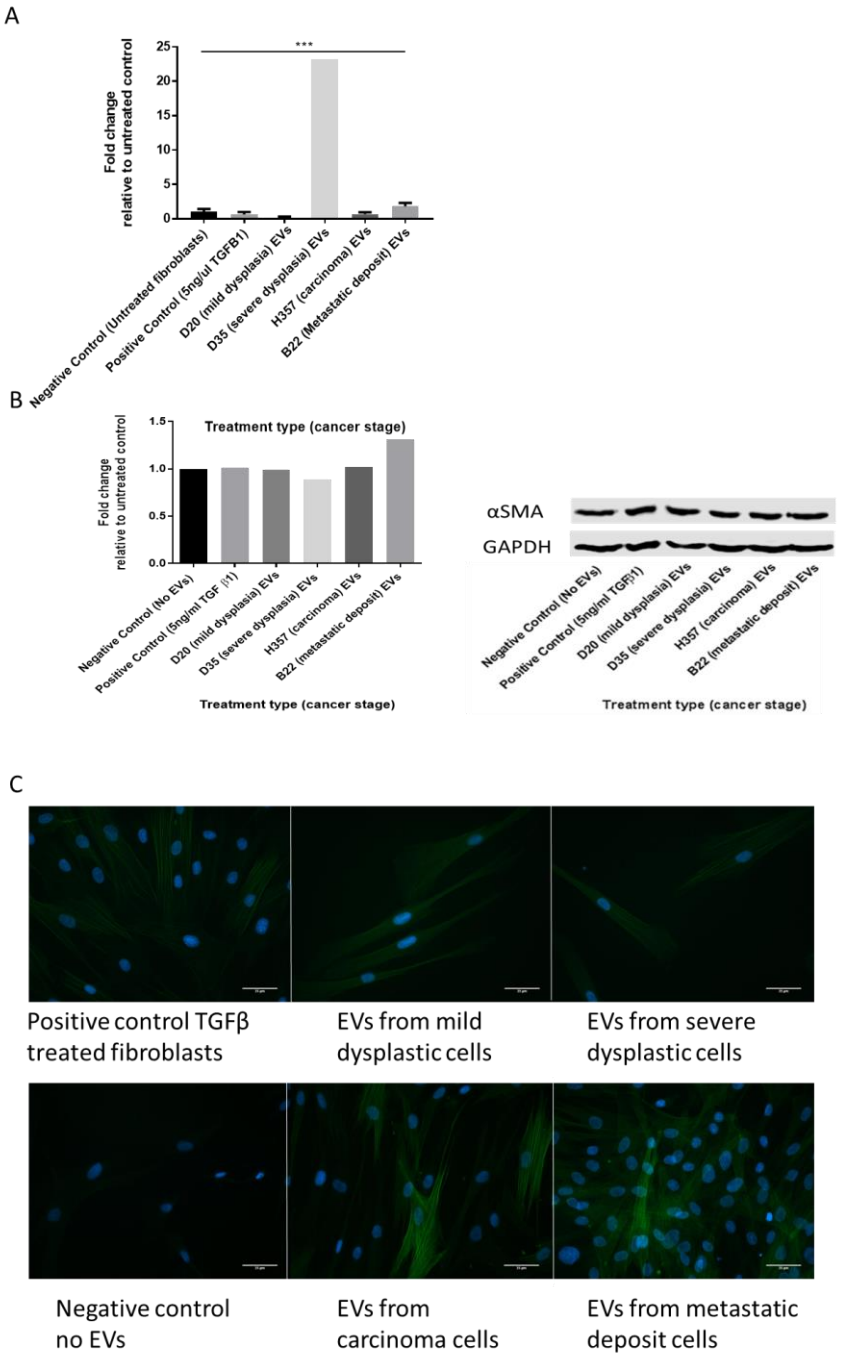

Figure 7.11 EV mediated activation of NOF 335 cells. NOFs were serum starved for 24 h before treatment with 20000 EVs per cell in serum free medium and allowed to incubate for 24 h. Negative controls were treated with the same volume of serum free medium, positive controls were treated with 5 ng/µl of TGFβ1. RNA was harvested and used to run qPCR with probes for αSMA, U6 was used as a housekeeping gene to allow the calculation of ΔΔCT values relative to the control samples (A). No change in αSMA mRNA expression occurred in any samples except those treated with severe dysplastic cell derived EVs. n=2 technical replicates error bars representing SEM Significance was tested using a student's t-test ***** = p>0.05 ***= p>0.001 ****= >0. 0001.. Protein lysates were also harvested from the treated NOFS and were run on a 12% acrylamide gel before transferring to a nitrocellulose membrane. The membrane was probed with a mouse monoclonal antibody for αSMA diluted 1:500 (v/v) and an HRP conjugated rabbit monoclonal antibody for GAPDH as a loading control diluted 1:20000 (v/v). Densitometry of the bands was performed using ImageJ (B), similarly to the mRNA there was no change in the protein levels of αSMA in this cell line in any of the samples n-=1. There was a marginal increase in samples treated with EVs from a metastatic deposit cell. Finally, cells were incubated with a FITC conjugated αSMA antibody diluted 1:1000 (v/v) with blocking buffer for 1 h before mounting on slides. After imaging on a Zeiss Axioplan comparable αSMA stress fibres were visible in EV treated samples and in TGFβ1 treated control samples with no fibres visible in the negative controls (C).

7.7. Discussion

Here we have demonstrated that EVs produced by cells at different stages of oral cancer tumourigenesis are capable of being taken up by a range of cell types that could be present in the TME. The fluorescence technique used indicates that the RNA contents of the EVs at least are released into the cells. As no green fluorescence is visible in the controls, which are vesicle free PBS treated with the same dyes as the vesicle samples and run through dye removal columns, it is likely that this fluorescent signal is caused by RNA internalised within EVs rather than co-precipitated free RNA. However, this does need to be confirmed with further experiments ideally vesicles or liposomes depleted of RNA and labelled with the dye alongside vesicle free RNA in PBS labelled with the dye and run through the spin columns should be used. The combination of such controls would give a better insight into the behaviour of the dye in this experiment. The assay does not allow the protein contents of the EVs to be monitored as neither fluorescent label associated specifically with proteins, but it is likely that protein contents are also released into the receptor cells. The fate of EV-associated proteins once taken up by cells, however, remains unclear. The cell types used as receptor cells in this assay represent cells that would be present in a developing oral tumour and each of them could potentially respond to the signals borne by the tumour cell derived EVs.

This assay is a very crude representation of conditions within the microenvironment and it should be noted that both the endothelial cell line and the keratinocyte cell line have been artificially immortalised which may have changed their phenotype with respect to vesicle uptake over their normal form. It is also not clear if this uptake is occurring because the conditions have been rendered favourable by saturation kinetics. A physiologically relevant number of EVs in a system is currently

not possible to determine, and it is possible that the dose used in this assay exceeds the physiological level. It is likely that some of these EVs would not be taken up by local cells once released as they would be removed from the area by blood flow or that some EVs are prioritised for uptake by certain cell types within the area. Because this assay only has a single donor and receptor cell if the doses used were far above a physiological level it is possible that the EVs are being taken up because they have nowhere else to go. In its current form the assay is also unable to give an insight into any variation in uptake efficiencies between the different combinations tested. The assay could be adapted to use flow cytometry as the endpoint as opposed to fluorescence microscopy. This would allow comparisons of the rate of uptake of EVs from the different OSCC cells by the various recipient cells to be made.

Limitations aside however this assay does reveal the potential for a complex network of EV mediated communication throughout oral cancer tumourigenesis with EVs being used to convey signals to normal and cancerous cells. It would be useful to develop this assay further to allow the kinetics of the uptakes to be quantified and compared, either through live cell imaging or through a FACs based microplate assay. Such an assay would identify any possible preferences for uptake with cell lines, something which hasn't been demonstrated in the literature to date. The fate of these EVs within the cell is beyond the scope of this assay to reveal, the fact the RNA bound dye remains visible and is spread throughout the cell suggests that the contents are trafficked quickly throughout the cell and remain intact post uptake. The dye only fluoresces detectably when bound to RNA, if the RNA contents of the EVs were being broken down it would be expected that the fluorescent signal would be reduced. This assay has its limitations compared to more recent advances used by other groups with

Cre-Lox or similar reporter systems to visualise the uptake of EVs which have the advantage of demonstrating that some of the EV contents remain biologically active.

EVs are not normally considered to be cytotoxic, but there are a few exceptions to this, notably in lymphocytes the death of can benefit a developing tumour (Andreola et al., 2002). Although there have been studies that show macrophages can be more beneficial to the developing tumour alive (Huber et al., 2005). There are a number of studies which have transferred EVs between different cell types without reporting cell death upon uptake. Our data are consistent with this, increasing doses of EVs up to 20000 per cell were shown to have no impact on fibroblast death at 48 hours. The small increase in cell death at 24 h in our system is unlikely to have a significant biological effect. The notable caveat with this data is of course the physiological relevance of this EV dose is unknown. The maximum dose was established from previous fluorescence experiments performed before our lab had the ability to count the EVs in our samples. The dose used was at the lower threshold of the average EV dose used in these experiments, as determined by triplicate measurements using the qNano of similar sized preparations. It is possible that significantly higher doses of EVs could prove to be cytotoxic, but again the physiological relevance of such doses is unknown.

Whilst tumour cell derived EVs are not often shown to be cytotoxic, they have been shown to have growth promoting effects (Gutkin et al., 2016; Hong et al., 2009; Wei et al., 2017) on a variety of cell types. This was not seen in our model system; no change in fibroblast proliferation was observed in any of the patient samples following EV treatment. However, neither of these studies focused on fibroblasts but mesothelial and endothelial cells respectively. Despite the variability in gender, age and smoking

status of the patients from which the fibroblasts used in these experiments were derived, the data from these experiments was more consistent than that obtained from similar sets of fibroblasts used in fibroblast activation experiments.

This data demonstrates neatly the heterogeneity of healthy fibroblasts. The different fibroblasts are each taken from a different healthy volunteer and exhibit a range of responses in terms of αSMA mRNA and both abundance and localisation of the protein following EV and TGFβ1 treatment. Healthy fibroblasts normally exhibit an increase in αSMA protein expression when treated with TGFβ1 but both NOF319 and 335 exhibit no change in protein level following the treatment. Only the NOF803 cells showed an increase in αSMA mRNA following treatment with the other three fibroblast lines showing no change in mRNA levels and NOF316 even showing a reduction in αSMA mRNA. Despite this apparent lack of response to TGFβ1 based on mRNA and protein levels the immunofluorescence shows that there are changes in αSMA organisation occurring in all the fibroblast cells lines following the treatment. A similar change is observed in all samples when they are treated with tumour cell-derived EVs, however predictably a different response is observed at the mRNA and protein level.

Much of this variability will be down to inter patient variation, between NOFs 316 and 319 there is a 51-year age range. A seventy-year-old patients fibroblasts would not be expected to respond as robustly as a twenty-year old as is seen in responses to UV in skin fibroblasts (Pernodet et al., 2016). NOF335 and 803 were both established from patients in their 40's but showed a different response to TGFβ1 and EV treatments indicating that age is not the only contributing factor. Of the patient samples used only NOF316 was established from a female making it difficult to determine the impact of

gender on these results. Smoking status of the patient should also be taken into effect as exposure to the mutagenic compounds in tobacco smoke will have altered the patients cells. NOF335 was established from a patient who smoked, all other patients were non-smokers, and NOF335 showed a distinctive mRNA profile for αSMA with only the severe dysplastic vesicles producing an increase in the mRNA levels for αSMA.

Although a consistent response with respect to mRNA and protein levels of αSMA is not seen following EVs uptake the increased formation of αSMA stress fibres does indicate that the normal oral fibroblasts are activated into the cancer associated form following EV uptake. The more differentiated carcinoma and metastatic deposit cell derived EVs produce a more dramatic increase on the αSMA mRNA than that of the dysplastic cell derived EVs suggesting this effect is more potent in the later stages of tumour development. This would fit with the idea of niche construction, an increasing number of CAFs will create a more favourable environment for metastatic deposits to form, remodelling the matrix and creating an inflammation rich environment.

7.7.1. Future work

This data does however have its limitations and further work would be needed to confirm some of the findings. To confirm the observed changes in NOF morphology as activation into CAFs, Changes to different markers such as vimentin or fibronectin should be studied in the same way as αSMA following the uptake of EVs, it would also be interesting to study the changes in markers over different time scales than those used in this study. Lastly these EV activated fibroblasts should be compared to TGFβ1 activated fibroblasts and cancer associated fibroblasts from patient samples in functional

assays like contractility and invasion assays to compare any differences in the types of activated cells.

There is much opportunity for further work with the fluorescence uptake imaging assay. As mentioned earlier in the chapter additional controls should be incorporated to confirm the green fluorescence observed in the images is produced by EV mediated transfer of RNA. Adapting the assay to include labels specific for lipid or protein components of the EVs could allow for those to be tracked in the same fashion. Use of super resolution microscopy and pH sensitive dyes could be used to image and monitor endosomal escape of the EVs contents. The assay also has the potential to be adapted to explore the kinetics of this uptake through use of FAC sorting.

8. Discussion

In the last ten years increasing attention has focused on the role of EVs in cancer progression with a variety of elegant studies revealing a complex signalling network. Oral cancer research lags behind research into other tumour types such as breast cancer. There are very few studies focusing on vesicle-mediated signalling in head and neck cancer. The few published studies focus on biomarker discovery or on tumours of the nasopharynx, which given that 90% of oral cancers arise from squamous cells in the oral cavity is perhaps a missed opportunity. Four studies explicitly use carcinomas of the tongue and of these, two focus on which cells of the TME the EVs can interact with (Al-Samadi et al., 2017; Dayan et al., 2012) others are focused on the contents of these EVs (Han et al., 2014; Kawakubo-Yasukochi et al., 2017). This project attempted to explore both questions.

8.1. Method optimisation and characterization

One of the strengths of this project is the assembly of a panel of cell lines isolated from the same primary anatomical site and that are representative of the distinct histological stages of tumourigenesis. This offered the opportunity to compare how EV cargo and mode of action are altered with progressing tumour stage. Whilst such a study has not yet been published in oral cancer, similar approaches have been used in other tumour models, which utilise patient samples or animal models to study EVs from the different stages of tumourigenesis (Liu et al., 2015; Melo et al., 2015). Those that do use cell lines do not have such an extensive panel of site matched cells (Lázaro-Ibáñez et al., 2017). Whilst patient and animal models have their advantages over 2D tissue culture models they are more expensive and more complicated to establish, which still

leaves a place for using cell lines as models particularly in such early stage studies. The panel of site matched cell lines allow our study to be compared favourably with the others that explore EV signalling in different cancer stages. Crucially our cell lines are accompanied by a large amount of patient information including the smoking status, which is particularly relevant to oral cancer. One of the differences between the two dysplastic cell lines is the smoking status of the patients, the mild dysplasia having arisen from a non-smoker, the severe dysplasia from a smoker. This difference adds an extra dimension to any comparisons drawn between the EVs produced by these cell lines as they could be caused either by the difference in tumour stage or the difference in smoking status. This is particularly relevant to the study of EV miRNA cargo as cellular miRNA expression has previously been shown to be altered on exposure to cigarette smoke (Pal et al., 2013). The difference in disease aetiology between these cell lines may mask any changes that occur purely as a result of tumour progression but given the correlation between smoking and oral cancer it would be difficult to find patients with severe oral dysplasia that are non-smokers. An ideal panel of cell lines would be site and patient matched so that the lesions could be compared throughout their development. However, whilst patients with mild dysplasias are often observed for malignant transformation, those with severe dysplasia normally undergo medical intervention and it would be unethical to allow a severe dysplastic lesion to progress to carcinoma for the purpose of research. This is where animal models have an advantage over cell lines and human samples.

The first years of this project were spent establishing protocols for the purification and characterisation of EVs from the conditioned media of oral cancer cell lines. Established protocols for serial centrifugation performed on conditioned media of oral

cancer cells yielded EVs which were positive for protein EV markers including TSP1 and CD63. Measurements using a qNano instrument, which was purchased part way through the study, showed that the serial centrifugation protocols were purifying particles of a size range (50-200 nm) consistent with the published literature (Johnstone et al., 1987 and Valadi et al., 2007). We also sought to determine if storage of EVs at -20^{o}C and freeze-thawing was causing a reduction in EV concentration or integrity. Whilst this work hasn't explicitly analysed the effect of multiple freeze thaw cycles (Sokolova et al., 2011) or performed assays to check the function of the EVs is not lost by freeze thawing (Kalra et al., 2013) the EVs used in several of the functional assays and imaging experiments were subject to multiple freeze thaw cycles with no discernible loss of function during between the replicates.

In order to generate sufficient yields of RNA and protein for the sequencing and proteomic experiments, respectively, this project took advantage of size exclusion chromatography (SEC) to purify the EVs (Böing et al., 2014). EVs purified using SEC were a similar size by TEM and TRPS and contained the same protein markers as those purified by serial centrifugation (Appendix 1). The issue of differences in functionality between EVs purified by different techniques is one that is currently being debated by the field. A recent paper showed that in a cardiac model, EVs purified by SEC produced a higher pERK/ERK ratio in endothelial cells post uptake than those purified by ultracentrifugation (Mol et al., 2017). Because this problem is one that can affect EVs purified from any source the most suitable functional assay would be one that tests a function common to all EVs allowing for a single answer to this question. However, such a universal function has not been identified, meaning that the question should be addressed in each individual model system. During this project one such function was

identified in oral cancer EVs, the ability to activate normal oral fibroblasts into a cancer associated phenotype. Whilst this function appeared to be common to all EV types the variability in responses from normal patient fibroblasts makes quantifying this effect too difficult to use in this role. It is possible that different purification techniques isolate subtly different populations of EVs which could result in different functional effects and this should be tested in every model system once a suitable function has been identified. Such a function would ideally be a positive or negative effect on proliferation or another similarly easily measurable trait. Whilst the size distribution profiles from the two different techniques used here are similar, size is known to be insufficient to determine between EV populations. The detection of the same proteins by western blots in EVs purified by both techniques is encouraging and does suggest that a similar EV population was isolated by both. Mol et al (2017) demonstrated that electron microscopy is unable to distinguish between the EVs purified by the different techniques. They showed a large amount of variability in EV structure even within grids containing EVs from the same source. This variability would make any differences observed by TEM inconclusive.

8.2. Oral cancer cell derived vesicles deliver cargos to the surrounding cells of the tumour microenvironment

Through the use of fluorescent dyes, the uptake of oral cancer cell-derived EVs by a range of normal cell types was examined. The cells used for these experiments included some of the major components of the OSCC TME: normal oral fibroblasts, endothelial cells, carcinoma cells and oral keratinocytes. Although this assay has many limitations it does show that EVs from oral cancer cells can be taken up by surrounding

normal cells *in vitro*. The assay used two different stains, one of which was encapsulated in the EV lumen and fluoresced when bound to RNA. This allowed visualisation of the release of luminal contents of EV after uptake. After only 60 min incubation with the stained EVs green fluorescence, from the RNA dye, was observed to be widespread across the cell. This observation indicates that the EV contents can be released from the EV into the recipient cell however it is still unclear whether the dye is remaining bound to the EV RNA or is merely being delivered unbound by the EVs. Experiments using EVs loaded with prestained RNA would be needed to resolve this uncertainty

In this study we have focused on the effect of uptake of cancer-derived EVs by the cells of the TME. However, given reports in other tumour models that normal cells produce EVs capable of being taken up by the cancer cells (Hu et al., 2015) it is likely that this signalling is bi-directional in oral cancer, with EVs flowing between normal and cancerous cells as well as between cancer cells and normal cells. Isolation of EVs from primary stromal cells is challenging and whether sufficient EVs could be purified from endothelial cells or fibroblasts to produce detectable fluorescence using this assay remains to be elucidated. Given the range of reported functions for EVs in cancer it is highly likely that different populations of EVs will exhibit preferential targeting to a particular cell type in order to produce a desired effect. It is also possible that some EVs, such as those which contain cisplatin when it is shuttled out of resistant ovarian cancer cells (Safaei et al., 2005), are never intended to be delivered to a cell, but because of the limitations of an *in vitro* set up like this one are being taken up. Each of the normal cell types used in these imaging experiments has potential for further experiments. It would be valuable to study any changes in cell turnover following EV

uptake in each case as well as any changes in phenotypic behaviour such as motility or tubule formation.

8.3. Next generation sequencing and label free mass spectrometry techniques reveal differences in vesicle contents which are linked to tumour stage

IonTorrent sequencing and mass spectrometry techniques were used to elucidate the contents of the EVs produced by oral cancer cells. Proteomic and transcriptomic analysis of the EV contents have identified some patterns relative to the tumour stage of the producing cell (figure 8.1). A core group of miRNA and proteins were detected, these include the let-7 miRNA superfamily, miR-29a-3p, miR-27b-3p a, collagen α 3 (IV) chain, histone proteins, EEF2 and major vault protein. These cargoes are commonly associated with tumourigenesis and their presence in EVs could be due to their abundance in the cells from which they originate. The release of EVs containing several members of anti-tumourigenic miRNA families like miR-199 miR-34 and miR-200 from severe dysplastic cells or carcinoma cells suggests that this could be necessary for tumour progression. Particularly interesting is the EV-mediated export of miR-200 from the carcinoma cells. Blocking EV-mediated export of anti-tumourigenic miRNAs could be a novel therapeutic strategy. Each of these proteins and miRNA represent good candidates for follow up, but validation in human *ex vivo* samples would be preferable before subsequent functional studies.

miRNA and protein enrichment in OSCC EVs changes with tumour stage

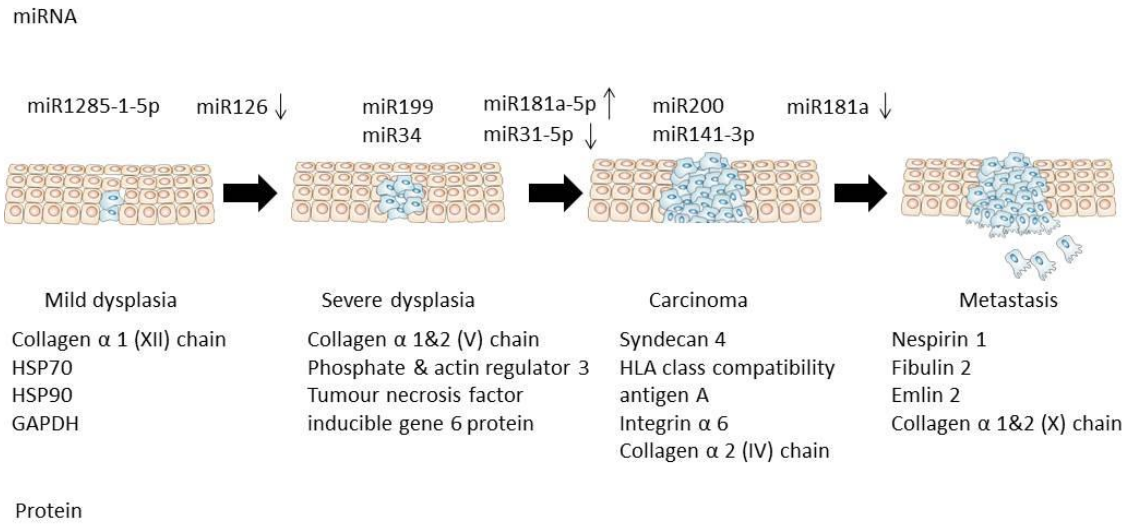

Figure 8.1 miRNA and protein identified by proteomic analysis as being enriched in EVs produced by different tumour stages. Several miRNA were changed in enrichment between tumour stage, miR-126-3p and 5p were reduced in all EVs compared to those of the mild dysplastic cells. miR-181a-5p increases in EVs produced by cells of later stages. Whole families of miRNA were enriched in EVs of severe dysplastic cells and carcinoma cells including miR-199 and miR-200.

8.4. Oral cancer vesicles can promote pro-tumourigenic changes in normal oral fibroblasts

The uptake of EVs produced by the oral cancer cell lines was sufficient to cause a rearrangement of αSMA molecules in normal oral fibroblasts which is indicative of them acquiring a CAF phenotype. In the laboratory this is often mimicked using treatment with TGFβ1. Prostate cancer-derived EVs can have a similar effect on fibroblasts (Webber et al., 2010). It was subsequently demonstrated that TGFβ1 tethered to the outside of the EVs by heparan sulphate proteoglycans was responsible for mediating this effect (Chowdhury et al., 2015; Webber et al., 2010). In our experiments TGFβ1 could not be detected in the EV either by western blotting or by mass spectrometry. However previous studies revealed that TGFβ1 was present in picogram amounts on the surface of EVs, making it unlikely that it would be present in sufficient quantities to detect by western blot. Mass spectrometry should have been sensitive enough to detect such small amounts of protein. However, it is uncertain if the sample processing technique would have conserved any protein tethered to surface of EVs.

It is probable that a similar mechanism is responsible for this phenomenon in oral cancer EVs and more suitable experiments such as ELISAs with intact EV samples should be performed to determine if TGFβ1 is present on the EV surface. It is also possible that miRNA cargo could be responsible for driving the observed fibroblast activation. In silico analysis showed that more than 70 miRNA in each sample are predicted to interact with transcripts of proteins involved in the TGFβ1 pathway (figure 8.2). However, the miRNA are predicted to target transcripts of proteins that both inhibit and activate the pathway. This indicates that rather than having a distinct activating or inhibitory impact on this pathway the EVs are more likely to have a more nuanced

modulatory role. It is difficult to reconcile the packaging of miRNA like miR-200, which has an inhibitory effect on fibroblast activation (Tang et al., 2016), into OSCC-derived EV. It is also possible that the observed NOF activation occurs by presentation of EV-tethered TGFβ1 at the cell surface and is independent of the EV miRNA cargo. Further in silico work and more sensitive methods to detect TGFβ1 would be required to answer the question.

OSCC EV miRNA interact with regulatory members of TGFβ-1 pathway

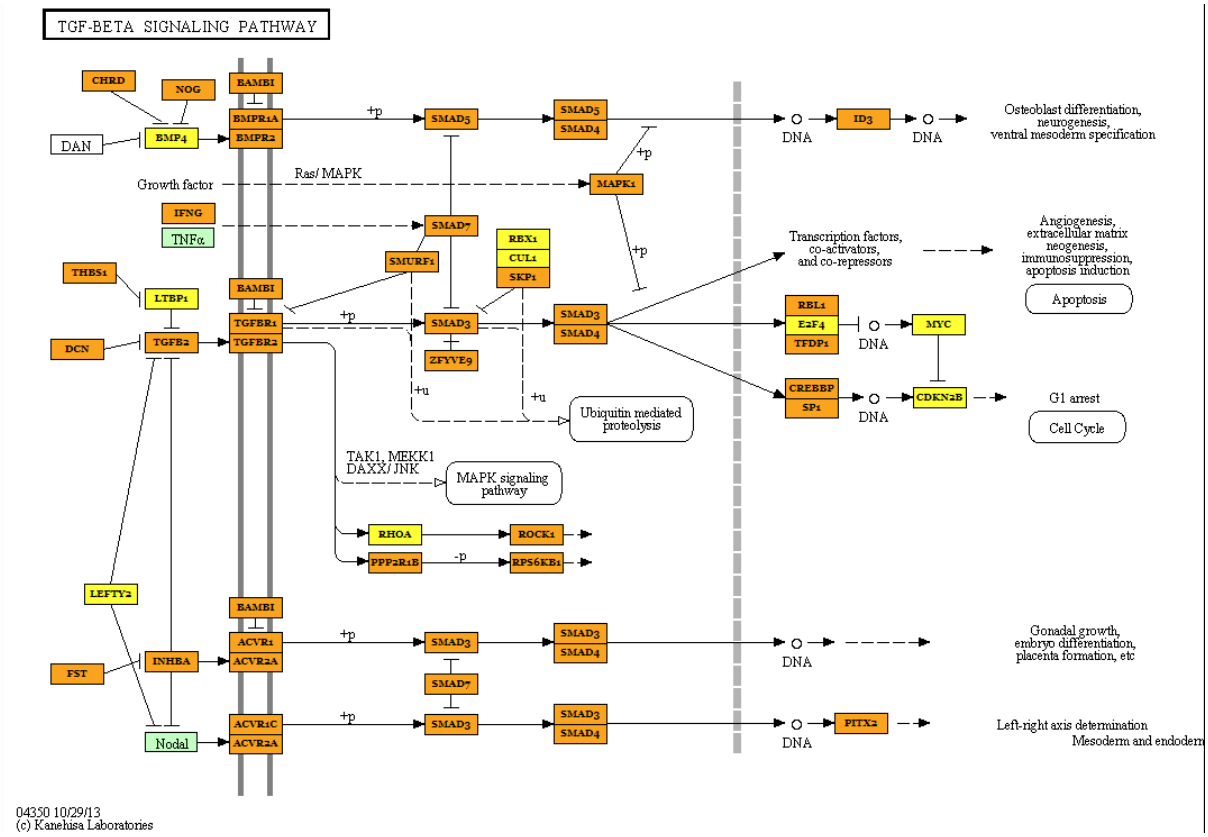

Figure 8.2 TGFβ1 signalling pathway and interactions with miRNA found in the EVs from oral cancer cells as determined by miRPath V.3 database. Proteins coloured green interact with no miRNAs in the EVs, those coloured in yellow interact with 1 miRNA and those in orange interact with multiple miRNA. miRNA interact with transcripts from proteins that both inhibit and activate the pathway.

8.5. Limitations of the study

There are several limitations to this study, some of which are unique to this project and others which are experienced by the entire field. The qNano arriving a year into this work meant that many methods were developed and optimised without a knowledge of the EV concentration. This included the fluorescence imaging experiments. Had the EV concentrations been known at the time these experiments could have been done with a standardised dose of EVs possibly allowing for some quantification to be done and any preferential uptake to be detected. Although in later experiments the EV doses were reverse engineered and dose curves for EV treatment were performed, ideally these should have been established earlier in the project. The question of EV doses is one with which the field is struggling. There is still no understanding of what a physiologically relevant dose of EVs is.

Determining this in an animal model or in a patients tumour remains a challenge. The fields approach to this problem is slowly changing, with many early studies using µg of EV protein as a measure of EV dose. It is now more common to use particle number as a dose which is determined by qNano or Nanosight instruments. Although our EV doses did not cause cell death and were observed to produce a physiological response in normal oral fibroblasts, suggesting that they are physiologically relevant, it is also possible that the doses of EVs used are significantly higher or lower than those experienced by cells in vivo, which is why a phenotypic effect is observed. Solving the question of physiologically relevant doses of EVs remains a priority for the field particularly if EVs are to become established therapy options.

Whilst the cell lines used in this study were site matched and were associated with a large amount of patient data, they do not represent a perfect model of tumourigenesis. Ideally, they would originate from the same patient, allowing actual changes in the composition of the EVs to be directly linked to stage changes in a patients tumour. The current panel only includes one cell line for each pathological stage; this makes it difficult to be certain if any changes in behaviour or contents are typical of all cells of that stage or just the ones in our panel. Any changes or behaviours detected in the EVs of these cells should be validated in other cells from the same site and stage but from different patients. A second problem with the cells is an issue common to many studies, a lack of available non-immortalised normal cells. There are two different immortalised normal cell lines used routinely in our lab, the first of these, OKF6, are hTERT immortalized oral keratinocytes and were found to be suitable for some experiments but could not be grown in sufficient numbers to harvest enough EVs for transcriptomic and proteomic analysis. The second is FNB6 which are also hTERT immortalized, and while these can be grown in higher volumes they cannot be grown without a feeder layer. These are normally irradiated mouse fibroblasts, which will be producing EVs of their own making them unsuitable for use in our experiments. The same issue arises when using primary keratinocytes.

In order to generate sufficient RNA and protein yields for the next generation sequencing and mass spectrometry experiments EVs were prepared by SEC. This was done to combat a combination of the low yields of RNA and protein produced from the EVs and the limited capacity of our ultracentrifuge rotor. While limited work was done to compare the EVs purified by the two different techniques, no extensive comparison of the functions or contents of these EVs were performed. The EVs were similar in size

and bear the same markers suggesting consistency between the EVs purified by the two techniques. The lack of a suitable functional assay to test any differences in function between the two methods is a limitation of this project. Other limitations are presented by the single biological replicates for the next generation sequencing and mass spectrometry experiments, although protein and RNA samples were collected from a pool of several different EV preparations thereby introducing some biological variation. The addition of at least one biological replicate would help to offset some of the issues in the quality of this data notably the much higher number of detected RNA but the lower mapped reads percentage in the D35 RNA and the huge variation in proteins detected in each of the EV types. Both of these issues have had some impact on the data analysis for these samples.

The research field of EVs is a relatively young one and it is important to appreciate how rapidly the field is progressing. Many studies have use lipophilic dyes, such as PKH26, for labelling EVs used in uptake experiments. It has only recently been noted that these dyes form micelles of similar proportions to EVs, resulting in artefacts in fluorescence experiments (Morales-Kastresana et al., 2017). Fortunately, no such structures were observed in our experiments. The weaknesses of the commonly used dyes and the advent of new technologies have led to a range of approaches being used. A recently published paper used a thiol-based dye (Roberts-Dalton et al., 2017) that is well characterised and is known not to impair EV formation or function by the introduction of bulky fluorophores. Fusion tagging of proteins found in EVs with fluorescent labels (Lai et al., 2015) and advanced microscopy techniques have produced high resolution images and videos of EV uptake. Another advance is the application of Cre-lox reporter systems (Zomer et al., 2016). These systems are complicated and

expensive but have significant potential for imaging the movement of EVs between cells of a model system. Whilst these advances offer something beyond that offered by the techniques used in this project, simple fluorescence assays performed with the correct controls still have a place in the field for confirming that EVs can be exchanged between cells.

One of the major issues that continues to present problems for the EV research community is EV heterogeneity. It has increasingly become accepted that because current technology does not allow EV classes to be fully separated then extensive characterization of the EVs being studied should be carried out by all groups. A paper from 2016 demonstrates the extent to which the current proteins used as markers are probably inadequate (Kowal et al., 2016). The use of western blotting or targeted proteomics for the candidates identified by the Théry group should become standard for EV experiments where the role of a distinct population of EVs is being tested. This would ensure that the vesicles populations being used are characterized and defined as stringently as current methods allow and would serve to increase the reproducibility of experiments. Although this wasn't a stated goal of this project the addition of this information would allow for far more detail to be given on the EVs produced by oral cancer cells.

Another change in focus concerns the RNA content of the EVs. Much of the RNA cargo research focuses on miRNA but work done in breast cancer (Tosar et al., 2015) and our own data suggest that miRNA represent one of the least abundant RNA types in the EVs. In breast cancer cell EVs the majority of the RNA were tRNA fragments, but despite this no studies have been published that focus on tRNA cargo of EVs. The

majority of EV RNA in our study was classified “other” RNA, which includes a mix of poorly understood non-coding RNA species including vault RNA and Y-RNA. Given that they make up the majority of the RNA in our samples the analysis of these species is arguably more important than the study of the miRNA. This is an area of EV research that is yet to be explored in great depth but as our understanding of those RNA types improves additional functions of these EVs may be revealed.

8.6. Further work

The immediate priority for further work should be to improve the validation of the proteomics data. This should be done using a combination of approaches to ensure the detection of the validation candidates in the EV samples. Successful validation of this data set would identify a number of candidates for verification in patient samples. A range of interesting candidates have been identified in both the RNA and protein contents of the EVs, these include miRNA such as miR-181a-5p and the miR-200 family proteins like SDC4 and nesprin 1 which were shown to be differentially packaged into the EVs from the different tumour stages. If the patterns seen in the RNA sequencing and mass spectrometry were replicated by qPCR and western blotting, respectively, then further experiments could be performed to determine if these proteins or RNA molecules have any functional effects. In order to determine if any of these molecules could function as biomarkers the abundance of these molecules in the EVs in patient biofluid samples should be determined.

It was intended to explore the impact of EV uptake on other cell types of the oral cancer micro environment. Transfer experiments have shown that EVs from the tumour

cells can be taken up by endothelial cells, other carcinoma cells and oral keratinocytes. Given the contents of these EVs include a number of proteins and RNA implicated in angiogenesis it is possible that there will be an effect of the EVs on the ability of endothelial cells to form tubules, which could be quantified in tubule formation assays. Many of the RNA have been linked to invasion and metastasis and it is likely that the EVs can change the ability of cells to migrate. This should be tested using transwell assays on carcinoma cells, fibroblasts and immune cells, which are all beneficial to various stages of a tumours development. Before any such transfers are performed similar experiments to those performed in the fibroblasts should be performed in order to test if EV uptake has a detrimental effect on the receptor cells. As has been alluded to previously, it is unlikely that the EV signalling in the TME is entirely one directional. If appropriate normal cells could be sourced, or if sufficient quantities of vesicles could be purified from the NOFs used in this study, it would be instructive to perform similar experiments to see if there are any similarities in EV contents and if these EVs can have any effect on tumour cells. As with all of the experiments these should ideally be performed in multiple cell lines representative of the different stages of a tumour, which would enable a more reliable picture of the changes in EV signalling with cancer stage to be determined.

A more ambitious direction to take this work would be to continue exploring the EV uptake visualised by the fluorescence imaging experiments. The fluorescence approach used in this study to image EV uptake could potentially be adapted to study the kinetics of EV uptake. This could be done using a technique such as flow cytometry to track the kinetics of different combinations of EV doses and receptor cells. Whilst these assays have begun to identify some possible branches of a more complicated EV

signalling network the experiments performed are simple in nature and are in an in vitro model. Establishing a 3D culture model would create a more realistic tumour model in which to study EV signalling. Such a model has recently been published by a group in Finland (Al-Samadi et al., 2017) which utilised myoma discs and zebrafish as models for studying EV signalling. A combination of these models with Cre lox techniques for visualising EV uptake in vivo could allow for a more comprehensive picture of EV signalling in a tumour to be created. The oral cavity is not a static environment and several groups have started to use fluid flow chambers to represent this (Nithianantha n et al., 2017). An extremely ambitious model combining a flow chamber style set up with cells producing fluorescently labelled EVs could even allow for real time imaging of the EV signalling network in the oral cancer microenvironment.

8.7. Conclusion

The data generated during this project has begun to answer some of the major questions regarding the role of EVs in oral cancer progression. EVs have been shown to be produced throughout oral cancer tumourigenesis. Fluorescence assays have shown that these EVs can be delivered to various cells of the oral cancer microenvironment and that upon uptake the contents of these EVs are released into the receptor cells. The RNA and protein contents of EVs are predicted to have a range of potential pro-tumourigenic effects as well exhibiting some differential packaging which could distinguish between the tumour stage of the producing cells. Lastly the EVs produced by the oral cancer cells activate fibroblasts into a CAF like phenotype which would benefit a developing tumour by creating favourable conditions for its continuing progression. Whilst these experiments complete part of the jigsaw there are other parts still to complete. EVs have the potential to play an important role in the progression of oral cancer and could represent a vital source of diagnostic biomarkers.

9. References

Aalberts, M., Dissel-Emiliani, F., Adrichem, N., Wijnen, M., Wauben, M., Stout, T., Stoorvogel, W., 2012. Identification of distinct populations of prostasomes that differentially express prostate stem cell antigen, annexin A1, and GLIPR2 in humans. Biology of reproduction 86, 82.

Abrami, L., Brandi, L., Moayeri, M., Brown, M.J., Krantz, B.A., Leppla, S.H., van der Goot, F.G., 2013. Hijacking multivesicular bodies enables long-term and exosome-mediated long-distance action of anthrax toxin. Cell Rep 5, 986–96.

Ades, E.W., Candal, F.J., Swerlick, R.A., George, V.G., Summers, S., Bosse, D.C., Lawley, T.J., 1992. HMEC-1: establishment of an immortalized human microvascular endothelial cell line. J. Invest. Dermatol. 99, 683–90.

Admyre, C., Grunewald, J., Thyberg, J., Gripenbäck, S., Tornling, G., Eklund, A., Scheynius, A., Gabrielsson, S., 2003. Exosomes with major histocompatibility complex class II and co-stimulatory molecules are present in human BAL fluid. Eur. Respir. J. 22, 578–83.

Admyre, C., Johansson, S.M., Qazi, K.R., Filén, J.-J.J., Lahesmaa, R., Norman, M., Neve, E.P., Scheynius, A., Gabrielsson, S., 2007. Exosomes with immune modulatory features are present in human breast milk. J. Immunol. 179, 1969–78.

Aga, M., Bentz, G.L., Raffa, S., Torrisi, M.R., Kondo, S., Wakisaka, N., Yoshizaki, T., Pagano, J.S., Shackelford, J., 2014. Exosomal HIF1α supports invasive potential of nasopharyngeal carcinoma-associated LMP1-positive exosomes. Oncogene 33, 4613–22.

Ahmed, W., Philip, P.S., Tariq, S., Khan, G., 2014. Epstein-Barr virus-encoded small RNAs (EBERs) are present in fractions related to exosomes released by EBV-transformed cells. PLoS ONE 9, e99163.

Akers, J.C., Gonda, D., Kim, R., Carter, B.S., Chen, C.C., 2013. Biogenesis of extracellular vesicles (EV): exosomes, microvesicles, retrovirus-like vesicles, and apoptotic bodies. J. Neurooncol. 113, 1–11.

Akiyama, K., Ohga, N., Hida, Y., Kawamoto, T., Sadamoto, Y., Ishikawa, S., Maishi, N., Akino, T., Kondoh, M., Matsuda, A., Inoue, N., Shindoh, M., Hida, K., 2012. Tumor endothelial cells acquire drug resistance by MDR1 up-regulation via VEGF signaling in tumor microenvironment. Am. J. Pathol. 180, 1283–93.

Al-Dossary, A.A., Strehler, E.E., Martin-Deleon, P.A., 2013. Expression and secretion of plasma membrane Ca2+-ATPase 4a (PMCA4a) during murine estrus: association with oviductal exosomes and uptake in sperm. PLoS ONE 8, e80181.

Al-Nedawi, K., Meehan, B., Micallef, J., Lhotak, V., May, L., Guha, A., Rak, J., 2008. Intercellular transfer of the oncogenic receptor EGFRvIII by microvesicles derived from tumour cells. Nat. Cell Biol. 10, 619–24.

Al-Samadi, A., Awad, S.A., Tuomainen, K., Zhao, Y., Salem, A., Parikka, M., Salo, T., 2017. Crosstalk between tongue carcinoma cells, extracellular vesicles, and immune cells in in vitro and in vivo models. Oncotarget 8, 60123–60134.

Aliotta, J.M., Sanchez-Guijo, F.M., Dooner, G.J., Johnson, K.W., Dooner, M.S., Greer, K.A., Greer, D., Pimentel, J., Kolankiewicz, L.M., Puente, N., Faradyan, S., Ferland, P., Bearer, E.L., Passero, M.A., Adedi, M., Colvin, G.A., Quesenberry, P.J., 2007. Alteration of marrow cell gene expression, protein production, and engraftment into lung by lung-derived microvesicles: a novel mechanism for phenotype modulation. Stem Cells 25, 2245–56.

Alvarez-Erviti, L., Seow, Y., Yin, H., Betts, C., Lakhal, S., Wood, M.J., 2011. Delivery of siRNA to the mouse brain by systemic injection of targeted exosomes. Nat. Biotechnol. 29, 341–5.

Amin, D., Hida, K., Bielenberg, D., Klagsbrun, M., 2006. Tumor endothelial cells express epidermal growth factor receptor (EGFR) but not ErbB3 and are responsive to EGF and to EGFR kinase inhibitors. Cancer Res 66, 2173–80.

Andreola, G., Rivoltini, L., Castelli, C., Huber, V., Perego, P., Deho, P., Squarcina, P., Accornero, P., Lozupone, F., Lugini, L., Stringaro, A., Molinari, A., Arancia, G., Gentile, M., Parmiani, G., Fais, S., 2002. Induction of lymphocyte apoptosis by tumor cell secretion of FasL-bearing microvesicles. J. Exp. Med. 195, 1303–16.

Arck, P.C., Hecher, K., 2013. Fetomaternal immune cross-talk and its consequences for maternal and offspring's health. Nat. Med. 19, 548–56.

Arellano-Anaya, Z.E., Huor, A., Leblanc, P., Lehmann, S., Provansal, M., Raposo, G., Andréoletti, O., Vilette, D., 2015. Prion strains are differentially released through the exosomal pathway. Cell. Mol. Life Sci. 72, 1185–96.

Atai, N.A., Balaj, L., van Veen, H., Breakefield., X.O., Jarzyna, P.A, Van Noorden, C.J, Skogg, J., Maguire, C.A., 2013. Heparin blocks transfer of extracellular vesicles between donor and recipient cells. Journal of neurooncology. 115, 343-51.

Au Yeung, C.L., Co, N.-N.N., Tsuruga, T., Yeung, T.-L.L., Kwan, S.-Y.Y., Leung, C.S., Li, Y., Lu, E.S., Kwan, K., Wong, K.-K.K., Schmandt, R., Lu, K.H., Mok, S.C., 2016. Exosomal transfer of stroma-derived miR21 confers paclitaxel resistance in ovarian cancer cells through targeting APAF1. Nat Commun 7, 11150.

Baba, F., Swartz, K., van Buren, R., Eickhoff, J., Zhang, Y., Wolberg, W., Friedl, A., 2006. Syndecan-1 and syndecan-4 are overexpressed in an estrogen receptor-negative, highly proliferative breast carcinoma subtype. Breast Cancer Res. Treat. 98, 91–8.

Baietti, M.F., Zhang, Z., Mortier, E., Melchior, A., Degeest, G., Geeraerts, A., Ivarsson, Y., Depoortere, F., Coomans, C., Vermeiren, E., Zimmermann, P., David, G., 2012. Syndecan-syntenin-ALIX regulates the biogenesis of exosomes. Nat. Cell Biol. 14, 677–85.

Barile, L., Lionetti, V., Cervio, E., Matteucci, M., Gherghiceanu, M., Popescu, L.M., Torre, T., Siclari, F., Moccetti, T., Vassalli, G., 2014. Extracellular vesicles from human cardiac progenitor cells inhibit cardiomyocyte apoptosis and improve cardiac function after myocardial infarction. Cardiovasc. Res. 103, 530–41.

Baroni, S., Romero-Cordoba, S., Plantamura, I., Dugo, M., D'Ippolito, E., Cataldo, A., Cosentino, G., Angeloni, V., Rossini, A., Daidone, M.G., Iorio, M.V., 2016. Exosome-mediated delivery of miR-9 induces cancer-associated fibroblast-like properties in human breast fibroblasts. Cell Death Dis 7, e2312.

Bavik, C., Coleman, I., Dean, J., Knudsen, B., Plymate, S., Nelson, P., 2006. The gene expression program of prostate fibroblast senescence modulates neoplastic epithelial cell proliferation through paracrine mechanisms. Cancer Res 66, 794–802.

Beatty, G., Chiorean, E., Fishman, M., Saboury, B., Teitelbaum, U., Sun, W., Huhn, R., Song, W., Li, D., Sharp, L., Torigian, D., O'Dwyer, P., Vonderheide, R., 2011. CD40 Agonists Alter Tumor Stroma and Show Efficacy Against Pancreatic Carcinoma in Mice and Humans. Science 331, 1612–1616.

Berckmans, R.J.J., Sturk, A., van Tienen, L.M., Schaap, M.C., Nieuwland, R., 2011. Cell-derived vesicles exposing coagulant tissue factor in saliva. Blood 117, 3172–80.

Bissig, C., Gruenberg, J., 2014. ALIX and the multivesicular endosome: ALIX in Wonderland. Trends Cell Biol. 24, 19–25.

Bobrie, A., Colombo, M., Krumeich, S., Raposo, G., Théry, C., 2012. Diverse subpopulations of vesicles secreted by different intracellular mechanisms are present in exosome preparations obtained by differential ultracentrifugation. J Extracell Vesicles 1.

Boelens, M.C., Wu, T.J., Nabet, B.Y., Xu, B., Qiu, Y., Yoon, T., Azzam, D.J., Twyman-Saint Victor, C., Wiemann, B.Z., Ishwaran, H., Ter Brugge, P.J., Jonkers, J., Slingerland, J., Minn, A.J., 2014. Exosome transfer from stromal to breast cancer cells regulates therapy resistance pathways. Cell 159, 499–513.

Bouhlel, M.A., Derudas, B., Rigamonti, E., Dievart, R., Brozek, J., Haulon, S., Zawadaki, C., Jude, B., Torpier, G., Marx, N., Staels, B., Chinetti-Gbaguidi, G., 2007. PPARg Activation Primes Human Monocytes into Alternative M2 Macrophages with Anti-in□ammatory Properties. Cell Metabolism August, 137–143.

Brouwers, J.F., Aalberts, M., Jansen, J.W., van Niel, G., Wauben, M.H., Stout, T.A., Helms, J.B., Stoorvogel, W., 2013. Distinct lipid compositions of two types of human prostasomes. Proteomics 13, 1660–6.

Buschow, S.I., Nolte-'t Hoen, E.N., van Niel, G., Pols, M.S., ten Broeke, T., Lauwen, M., Ossendorp, F., Melief, C.J., Raposo, G., Wubbolts, R., Wauben, M.H., Stoorvogel, W., 2009. MHC II in dendritic cells is targeted to lysosomes or T cell-induced exosomes via distinct multivesicular body pathways. Traffic 10, 1528–42.

Bussolati, B., Deambrosis, I., Russo, S., Deregibus, M.C., Camussi, G., 2003. Altered angiogenesis and survival in human tumor-derived endothelial cells. FASEB J. 17, 1159–61.

Böing, A.N., van der Pol, E., Grootemaat, A.E., Coumans, F.A., Sturk, A., Nieuwland, R., 2014. Single-step isolation of extracellular vesicles by size-exclusion chromatography. J Extracell Vesicles 3.

Cai, J., Han, Y., Ren, H., Chen, C., He, D., Zhou, L., Eisner, G.M., Asico, L.D., Jose, P.A., Zeng, C., 2013. Extracellular vesicle-mediated transfer of donor genomic DNA to recipient cells is a novel mechanism for genetic influence between cells. J Mol Cell Biol 5, 227–38.

Cancer Research UK., 2014 http://www.cancerresearchuk.org/health-professional/cancer-statistics/statistics-by-cancer-type/oral-cancer?script=true#heading-Six. Accessed January 2018

Carayon, K., Chaoui, K., Ronzier, E., Lazar, I., Bertrand-Michel, J., Roques, V., Balor, S., Terce, F., Lopez, A., Salomé, L., Joly, E., 2011. Proteolipidic composition of exosomes changes during reticulocyte maturation. J. Biol. Chem. 286, 34426–39.

Caruso, R.A., Bellocco, R., Pagano, M., Bertoli, G., Rigoli, L., Inferrera, C,. 2002. Prognostic value of intratumoral neutrophils in advanced gastric carcinoma in a high‐risk area in northern Italy. Mod Pathol 15: 831–837.

Castells, M., Thibault, B., Delord, J.-P.P., Couderc, B., 2012. Implication of tumor microenvironment in chemoresistance: tumor-associated stromal cells protect tumor cells from cell death. Int J Mol Sci 13, 9545–71.

Chan, Y.-K.K., Zhang, H., Liu, P., Tsao, S.-W.W., Lung, M.L., Mak, N.-K.K., Ngok-Shun Wong, R., Ying-Kit Yue, P., 2015. Proteomic analysis of exosomes from nasopharyngeal carcinoma cell identifies intercellular transfer of angiogenic proteins. Int. J. Cancer 137, 1830–41.

Chaput, N., Flament, C., Viaud, S., Taieb, J., Roux, S., Spatz, A., André, F., LePecq, J.-B.B., Boussac, M., Garin, J., Amigorena, S., Théry, C., Zitvogel, L., 2006. Dendritic cell derived-exosomes: biology and clinical implementations. J. Leukoc. Biol. 80, 471–8.

Chargaff, E., West, R., 1946. The biological significance of the thromboplastic protein of blood. J. Biol. Chem. 166, 189–97.

Chavez-Muñoz, C., Kilani, R.T., Ghahary, A., 2009. Profile of exosomes related proteins released by differentiated and undifferentiated human keratinocytes. J. Cell. Physiol. 221, 221–31.

Chen, G., Zhang, Y., Wu, X., 2014. 786-0 Renal cancer cell line-derived exosomes promote 786-0 cell migration and invasion in vitro. Oncol Lett 7, 1576–1580.

Chen, L., Xiao, H., Wang, Z.-H.H., Huang, Y., Liu, Z.-P.P., Ren, H., Song, H., 2014. miR-29a suppresses growth and invasion of gastric cancer cells in vitro by targeting VEGF-A. BMB Rep 47, 39–44.

Chen, W.-T.T., Yang, Y.-J.J., Zhang, Z.-D.D., An, Q., Li, N., Liu, W., Yang, B., 2017. MiR-1307 promotes ovarian cancer cell chemoresistance by targeting the ING5 expression. J Ovarian Res 10, 1.

Chen, W.-X.X., Cai, Y.-Q.Q., Lv, M.-M.M., Chen, L., Zhong, S.-L.L., Ma, T.-F.F., Zhao, J.-H.H., Tang, J.-H.H., 2014. Exosomes from docetaxel-resistant breast cancer cells alter chemosensitivity by delivering microRNAs. Tumour Biol. 35, 9649–59.

Chen, W.X., Liu, X.M., Lv, M.M., Chen, L., Zhao, J.H., Zhong, S.L., Ji, M.H., Hu, Q., Luo, Z., Wu, J.Z., Tang, J.H., 2014. Exosomes from drug-resistant breast cancer cells transmit chemoresistance by a horizontal transfer of microRNAs. PLoS ONE 9, e95240.

Chen, X., Bode, A.M., Dong, Z., Cao, Y., 2016. The epithelial-mesenchymal transition (EMT) is regulated by oncoviruses in cancer. FASEB J. 30, 3001–10.

Chen, Y.-W.W., Chen, Y.-C.C., Wang, J.-S.S., 2013. Absolute hypoxic exercise training enhances in vitro thrombin generation by increasing procoagulant platelet-derived microparticles under high shear stress in sedentary men. Clin. Sci. 124, 639–49.

Chevillet, J.R., Kang, Q., Ruf, I.K., Briggs, H.A., Vojtech, L.N., Hughes, S.M., Cheng, H.H., Arroyo, J.D., Meredith, E.K., Gallichotte, E.N., Pogosova-Agadjanyan, E.L., Morrissey, C., Stirewalt, D.L., Hladik, F., Yu, E.Y., Higano, C.S., Tewari, M., 2014. Quantitative and stoichiometric analysis of the microRNA content of exosomes. Proc. Natl. Acad. Sci. U.S.A. 111, 14888–93.

Chiche, J., Brahimi-Horn, MC., Pouysségur, J., 2010 Tumour hypoxia induces a metabolic shift causing acidosis: a common feature in cancer. J Cell Mol Med. 14, 771-94.

Chowdhury, R., Webber, J.P., Gurney, M., Mason, M.D., Tabi, Z., Clayton, A., 2015. Cancer exosomes trigger mesenchymal stem cell differentiation into pro-angiogenic and pro-invasive myofibroblasts. Oncotarget 6, 715–31.

Christianson, H.C., Svensson, K.J., van Kuppevelt, T.H., Li, J.-P.P., Belting, M., 2013. Cancer cell exosomes depend on cell-surface heparan sulfate proteoglycans for their internalization and functional activity. Proc. Natl. Acad. Sci. U.S.A. 110, 17380–5.

Chua, S., Wilkins, T., Sargent, I., Redman, C., 1991. Trophoblast deportation in pre-eclamptic pregnancy. Br J Obstet Gynaecol 98, 973–9.

Ciardiello, C., Cavallini, L., Spinelli, C., Yang, J., Reis-Sobreiro, M., de Candia, P., Minciacchi, V.R., Di Vizio, D., 2016. Focus on Extracellular Vesicles: New Frontiers of Cell-to-Cell Communication in Cancer. Int J Mol Sci 17, 175.

Ciravolo, V., Huber, V., Ghedini, G.C., Venturelli, E., Bianchi, F., Campiglio, M., Morelli, D., Villa, A., Della Mina, P., Menard, S., Filipazzi, P., Rivoltini, L., Tagliabue, E., Pupa, S.M., 2012. Potential role of HER2-overexpressing exosomes in countering trastuzumab-based therapy. J. Cell. Physiol. 227, 658–67.

Coleman, B.M., Hanssen, E., Lawson, V.A., Hill, A.F., 2012. Prion-infected cells regulate the release of exosomes with distinct ultrastructural features. FASEB J. 26, 4160–73.

Collins, L., Dawes, C., 1987. The Surface Area of the Adult Human Mouth and Thickness of the Salivary Film Covering the Teeth and Oral Mucosa. Journal of Dental Research August, 1300–1302.

Colombo, M., Moita, C., van Niel, G., Kowal, J., Vigneron, J., Benaroch, P., Manel, N., Moita, L.F., Théry, C., Raposo, G., 2013. Analysis of ESCRT functions in exosome biogenesis, composition and secretion highlights the heterogeneity of extracellular vesicles. J. Cell. Sci. 126, 5553–65.

Conde-Vancells, J., Gonzalez, E., Lu, S.C., Mato, J.M., Falcon-Perez, J.M., 2010. Overview of extracellular microvesicles in drug metabolism. Expert Opin Drug Metab Toxicol 6, 543–54.

Conde-Vancells, J., Rodriguez-Suarez, E., Embade, N., Gil, D., Matthiesen, R., Valle, M., Elortza, F., Lu, S.C., Mato, J.M., Falcon-Perez, J.M., 2008. Characterization and comprehensive proteome profiling of exosomes secreted by hepatocytes. J. Proteome Res. 7, 5157–66.

Cooper, J.M., Wiklander, P.B., Nordin, J.Z., Al-Shawi, R., Wood, M.J., Vithlani, M., Schapira, A.H., Simons, J.P., El-Andaloussi, S., Alvarez-Erviti, L., 2014. Systemic exosomal siRNA delivery reduced alpha-synuclein aggregates in brains of transgenic mice. Mov. Disord. 29, 1476–85.

Coppé, J.-P.P., Patil, C.K., Rodier, F., Sun, Y., Muñoz, D.P., Goldstein, J., Nelson, P.S., Desprez, P.-Y.Y., Campisi, J., 2008. Senescence-associated secretory phenotypes reveal cell-nonautonomous functions of oncogenic RAS and the p53 tumor suppressor. PLoS Biol. 6, 2853–68.

Corcoran, C., Rani, S., O'Brien, K., O'Neill, A., Prencipe, M., Sheikh, R., Webb, G., McDermott, R., Watson, W., Crown, J., O'Driscoll, L., 2012. Docetaxel-resistance in prostate cancer: evaluating associated phenotypic changes and potential for resistance transfer via exosomes. PLoS ONE 7, e50999.

Coussens, L.M., Werb, Z., 2002. Inflammation and cancer. Nature 420, 860–7.

Creaney, J., Dick, I.M., Leon, J.S., Robinson, B.W., 2017. A Proteomic Analysis of the Malignant Mesothelioma Secretome Using iTRAQ. Cancer Genomics Proteomics 14, 103–117.

Crescitelli, R., Lässer, C., Szabó, T.G., Kittel, A., Eldh, M., Dianzani, I., Buzás, E.I., Lötvall, J., 2013. Distinct RNA profiles in subpopulations of extracellular vesicles: apoptotic bodies, microvesicles and exosomes. J Extracell Vesicles 2.

Crespin, M., Vidal, C., Picard, F., Lacombe, C., Fontenay, M., 2009. Activation of PAK1/2 during the shedding of platelet microvesicles. Blood Coagul. Fibrinolysis 20, 63–70.

Cussac, D., Leblanc, P., L'Heritier, A., Bertoglio, J., Lang, P., Kordon, C., Enjalbert, A., Saltarelli, D., 1996. Rho proteins are localized with different membrane compartments involved in vesicular trafficking in anterior pituitary cells. Mol. Cell. Endocrinol. 119, 195–206.

Damiano, V., Brisotto, G., Borgna, S., di Gennaro, A., Armellin, M., Perin, T., Guardascione, M., Maestro, R., Santarosa, M., 2017. Epigenetic silencing of miR-200c in breast cancer is associated with aggressiveness and is modulated by ZEB1. Genes Chromosomes Cancer 56, 147–158.

Dayan, D., Salo, T., Salo, S., Nyberg, P., Nurmenniemi, S., Costea, D.E., Vered, M., 2012. Molecular crosstalk between cancer cells and tumor microenvironment components suggests potential targets for new therapeutic approaches in mobile tongue cancer. Cancer Med 1, 128–40.

De Gassart, A., Geminard, C., Fevrier, B., Raposo, G., Vidal, M., 2003. Lipid raft-associated protein sorting in exosomes. Blood 102, 4336–44.

De Lourdes Mora-García, M., García-Rocha, R., Morales-Ramírez, O., Montesinos, J.J., Weiss-Steider, B., Hernández-Montes, J., Ávila-Ibarra, L.R., Don-López, C.A., Velasco-Velázquez, M.A., Gutiérrez-Serrano, V., Monroy-García, A., 2016. Mesenchymal stromal cells derived from cervical cancer produce high amounts of adenosine to suppress cytotoxic T lymphocyte functions. J Transl Med 14, 302.

Del Conde, I., Shrimpton, C.N., Thiagarajan, P., López, J.A.A., 2005. Tissue-factor-bearing microvesicles arise from lipid rafts and fuse with activated platelets to initiate coagulation. Blood 106, 1604–11.

Demory Beckler, M., Higginbotham, J.N., Franklin, J.L., Ham, A.-J.J., Halvey, P.J., Imasuen, I.E., Whitwell, C., Li, M., Liebler, D.C., Coffey, R.J., 2013. Proteomic analysis of exosomes from mutant KRAS colon cancer cells identifies intercellular transfer of mutant KRAS. Mol. Cell Proteomics 12, 343–55.

Di Vizio, D., Kim, J., Hager, M.H., Morello, M., Yang, W., Lafargue, C.J., True, L.D., Rubin, M.A., Adam, R.M., Beroukhim, R., Demichelis, F., Freeman, M.R.,

2009. Oncosome formation in prostate cancer: association with a region of frequent chromosomal deletion in metastatic disease. Cancer Res. 69, 5601–9.

Di Vizio, D., Morello, M., Dudley, A.C., Schow, P.W., Adam, R.M., Morley, S., Mulholland, D., Rotinen, M., Hager, M.H., Insabato, L., Moses, M.A., Demichelis, F., Lisanti, M.P., Wu, H., Klagsbrun, M., Bhowmick, N.A., Rubin, M.A., D'Souza-Schorey, C., Freeman, M.R., 2012. Large oncosomes in human prostate cancer tissues and in the circulation of mice with metastatic disease. Am. J. Pathol. 181, 1573–84.

Dickson, M.A., Hahn, W.C., Ino, Y., Ronfard, V., Wu, J.Y., Weinberg, R.A., Louis, D.N., Li, F.P., Rheinwald, J.G., 2000. Human keratinocytes that express hTERT and also bypass a p16(INK4a)-enforced mechanism that limits life span become immortal yet retain normal growth and differentiation characteristics. Mol. Cell. Biol. 20, 1436–47.

Doherty, G.J., McMahon, H.T., 2009. Mechanisms of endocytosis. Annu. Rev. Biochem. 78, 857–902.

Dovrat, S., Caspi, M., Zilberberg, A., Lahav, L., Firsow, A., Gur, H., Rosin-Arbesfeld, R., 2014. 14-3-3 and β-catenin are secreted on extracellular vesicles to activate the oncogenic Wnt pathway. Mol Oncol 8, 894–911.

Duz, M.B., Karatas, O.F., Guzel, E., Turgut, N.F., Yilmaz, M., Creighton, C.J., Ozen, M., 2016. Identification of miR-139-5p as a saliva biomarker for tongue squamous cell carcinoma: a pilot study. Cell Oncol (Dordr) 39, 187–93.

Dvorak HF. Tumor microenvironment and progression. J .Surg. Oncol. 2011;103:468–474.

Dykxhoorn, D.M., Wu, Y., Xie, H., Yu, F., Lal, A., Petrocca, F., Martinvalet, D., Song, E., Lim, B., Lieberman, J., 2009. miR-200 enhances mouse breast cancer cell colonization to form distant metastases. PLoS ONE 4, e7181.

Eckenfelder, A., Segeral, E., Pinzon, N., Ulveling, D., Amadori, C., Charpentier, M., Nidelet, S., Concordet, J.P., Zagury, J.F., Palliart, J.C., Berlioz-Torrent, C., Seitz, H., Emilani, S., Gallois-Montbrun, S,. 2017. Argonaute proteins regulate HIV-1 multiply spliced RNA and viral production in a Dicer independent manner. Nucleic Acids Res. 45, 4158-4173.

El-Saghir, J., Nassar, F., Tawil, N., El-Sabban, M., 2016. ATL-derived exosomes modulate mesenchymal stem cells: potential role in leukemia progression. Retrovirology 13, 73.

Erez, N., Truitt, M., Olson, P., Arron, S, T., Hanahan, D., 2010. Cancer-associated fibroblasts are activated in incipient neoplasia to orchestrate tumour promoting inflammation in an NF-kappaB-dependent manner. Cancer Cell 17, 135-147.

Escola, J.M., Kleijmeer, M.J., Stoorvogel, W., Griffith, J.M., Yoshie, O., Geuze, H.J., 1998. Selective enrichment of tetraspan proteins on the internal vesicles of

multivesicular endosomes and on exosomes secreted by human B-lymphocytes. J. Biol. Chem. 273, 20121–7.

Escrevente, C., Keller, S., Altevogt, P., Costa, J., 2011. Interaction and uptake of exosomes by ovarian cancer cells. BMC Cancer 11, 108.

Escudier, B., Dorval, T., Chaput, N., André, F., Caby, M.-P.P., Novault, S., Flament, C., Leboulaire, C., Borg, C., Amigorena, S., Boccaccio, C., Bonnerot, C., Dhellin, O., Movassagh, M., Piperno, S., Robert, C., Serra, V., Valente, N., Le Pecq, J.-B.B., Spatz, A., Lantz, O., Tursz, T., Angevin, E., Zitvogel, L., 2005. Vaccination of metastatic melanoma patients with autologous dendritic cell (DC) derived-exosomes: results of thefirst phase I clinical trial. J Transl Med 3, 10.

Feng, D., Zhao, W.-L.L., Ye, Y.-Y.Y., Bai, X.-C.C., Liu, R.-Q.Q., Chang, L.-F.F., Zhou, Q., Sui, S.-F.F., 2010. Cellular internalization of exosomes occurs through phagocytosis. Traffic 11, 675–87.

Fitzner, D., Schnaars, M., van Rossum, D., Krishnamoorthy, G., Dibaj, P., Bakhti, M., Regen, T., Hanisch, U.-K.K., Simons, M., 2011. Selective transfer of exosomes from oligodendrocytes to microglia by macropinocytosis. J. Cell. Sci. 124, 447–58.

Fridlender, Z., Sun, J., Kim, S., Kapoor, V., Cheng, G., Ling, L., Worthen, G., Albelda, S., 2009. Polarization of tumor-associated neutrophil phenotype by TGF-beta: “N1” versus “N2” TAN. Cancer Cell 16, 183–94.

Fujita, K., Kume, H., Matsuzaki, K., Kawashima, A., Ujike, T., Nagahara, A., Uemura, M., Miyagawa, Y., Tomonaga, T., Nonomura, N., 2017. Proteomic analysis of urinary extracellular vesicles from high Gleason score prostate cancer. Sci Rep 7, 42961.

Février, B., Raposo, G., 2004. Exosomes: endosomal-derived vesicles shipping extracellular messages. Curr. Opin. Cell Biol. 16, 415–21.

Gao, F., Abdulrahman, A., Sandeep, A., Arti, V., Payaningal R.S., 2018. Endothelial Akt1 loss promotes prostate cancer metastasis via β-catenin-regulated tight-junction protein turnover. British Journal of Cancer. Epub ahead of print

Garzino-Demo, P., Carrozzo, M., Trusolino, L., Savoia, P., Gandolfo, S., Marchisio, P.C., 1998. Altered expression of alpha 6 integrin subunit in oral squamous cell carcinoma and oral potentially malignant lesions. Oral Oncol. 34, 204–10.

Gauvreau, M.-E.E., Côté, M.-H.H., Bourgeois-Daigneault, M.-C.C., Rivard, L.-D.D., Xiu, F., Brunet, A., Shaw, A., Steimle, V., Thibodeau, J., 2009. Sorting of MHC class II molecules into exosomes through a ubiquitin-independent pathway. Traffic 10, 1518–27.

Geissmann, F., Manz, M., Jung, S., Sieweke, M., Merad, M., Ley, K., 2010. Development of Monocytes, Macrophages, and Dendritic Cells. Science 327, 656–661.

Ghayad, S.E., Rammal, G., Ghamloush, F., Basma, H., Nasr, R., Diab-Assaf, M., Chelala, C., Saab, R., 2016. Exosomes derived from embryonal and alveolar rhabdomyosarcoma carry differential miRNA cargo and promote invasion of recipient fibroblasts. Sci Rep 6, 37088.

Golub, E.E., 2009. Role of matrix vesicles in biomineralization. Biochim. Biophys. Acta 1790, 1592–8.

Gomes, C., Keller, S., Altevogt, P., Costa, J., 2007. Evidence for secretion of Cu, Zn superoxide dismutase via exosomes from a cell model of amyotrophic lateral sclerosis. Neurosci. Lett. 428, 43–6.

Gonzalez-Begne, M., Lu, B., Han, X., Hagen, F.K., Hand, A.R., Melvin, J.E., Yates, J.R., 2009. Proteomic analysis of human parotid gland exosomes by multidimensional protein identification technology (MudPIT). J. Proteome Res. 8, 1304–14.

Gould, S., Raposo, G., 2013. As we wait: coping with an imperfect nomenclature for extracellular vesicles. J Extracell Vesicles 2.
Gregory, C.D., Pound, J.D., 2011. Cell death in the neighbourhood: direct microenvironmental effects of apoptosis in normal and neoplastic tissues. J.Pathol. 223, 177-94.

Greening, D.W., Xu, R., Ji, H., Tauro, B.J., Simpson, R.J., 2015. A protocol for exosome isolation and characterization: evaluation of ultracentrifugation, density-gradient separation, and immunoaffinity capture methods. Methods Mol Biol. 1295, 179-209.

Griffiths, G.S., Galileo, D.S., Reese, K., Martin-Deleon, P.A., 2008. Investigating the role of murine epididymosomes and uterosomes in GPI-linked protein transfer to sperm using SPAM1 as a model. Mol. Reprod. Dev. 75, 1627–36.

Gross, J.C., Chaudhary, V., Bartscherer, K., Boutros, M., 2012. Active Wnt proteins are secreted on exosomes. Nat. Cell Biol. 14, 1036–45.

Gupta, S.C., Patchva, S., Aggarwal, B.B., 2013. Therapeutic roles of curcumin: lessons learned from clinical trials. AAPS J 15, 195–218.

Gutkin, A., Uziel, O., Beery, E., Nordenberg, J., Pinchasi, M., Goldvaser, H., Henick, S., Goldberg, M., Lahav, M., 2016. Tumor cells derived exosomes contain hTERT mRNA and transform non-malignant fibroblasts into telomerase positive cells. Oncotarget 7, 59173–59188.

Guttilla, I.K., White, B.A., 2009. Coordinate regulation of FOXO1 by miR-27a, miR-96, and miR-182 in breast cancer cells. J. Biol. Chem. 284, 23204–16.

György, B., Szabó, T.G.G., Turiák, L., Wright, M., Herczeg, P., Lédeczi, Z., Kittel, A., Polgár, A., Tóth, K., Dérfalvi, B., Zelenák, G., Böröcz, I., Carr, B., Nagy, G., Vékey, K., Gay, S., Falus, A., Buzás, E.I., 2012. Improved flow cytometric assessment

reveals distinct microvesicle (cell-derived microparticle) signatures in joint diseases. PLoS ONE 7, e49726.

Géminard, C., De Gassart, A., Blanc, L., Vidal, M., 2004. Degradation of AP2 during reticulocyte maturation enhances binding of hsc70 and Alix to a common site on TFR for sorting into exosomes. Traffic 5, 181–93.

Hager, M.H., Morley, S., Bielenberg, D.R., Gao, S., Morello, M., Holcomb, I.N., Liu, W., Mouneimne, G., Demichelis, F., Kim, J., Solomon, K.R., Adam, R.M., Isaacs, W.B., Higgs, H.N., Vessella, R.L., Di Vizio, D., Freeman, M.R., 2012. DIAPH3 governs the cellular transition to the amoeboid tumour phenotype. EMBO Mol Med 4, 743–60.

Hakulinen, J., Sankkila, L., Sugiyama, N., Lehti, K., Keski-Oja, J., 2008. Secretion of active membrane type 1 matrix metalloproteinase (MMP-14) into extracellular space in microvesicular exosomes. J. Cell. Biochem. 105, 1211–8.

Han, J., Wang, L., Wang, X., Li, K., 2016. Downregulation of Microrna-126 Contributes to Tumorigenesis of Squamous Tongue Cell Carcinoma via Targeting KRAS. Med. Sci. Monit. 22, 522–9.

Han, X., Zhang, Z., Huang, Y., Xia, Y., Li, L., 2014. [Differential proteomics research on exosomes derived from tongue squamous cell carcinoma cells and normal mucosa cells]. Hua Xi Kou Qiang Yi Xue Za Zhi 32, 283–7.

Hanahan, D., Weinberg, R., 2000. The hallmarks of cancer. Cell 100, 57–70.

Hanahan, D., Weinberg, R.A., 2011. Hallmarks of cancer: the next generation. Cell 144, 646–74.

Hawkins, L.A., Devitt, A., 2013. Current understanding of the mechanisms for clearance of apoptotic cells-a fine balance. J Cell Death 6, 57–68.

He, Y., Meng, C., Shao, Z., Wang, H., Yang, S., 2014. MiR-23a functions as a tumor suppressor in osteosarcoma. Cell. Physiol. Biochem. 34, 1485–96.

Henne, W.M., Buchkovich, N.J., Emr, S.D., 2011. The ESCRT pathway. Dev. Cell 21, 77–91.

Hicke, L., Protein regulation by monoubiquitin. 2001. Nat Rev Mol Cell Biol 2, 195-201.

Hidaka, H., Seki, N., Yoshino, H., Yamasaki, T., Yamada, Y., Nohata, N., Fuse, M., Nakagawa, M., Enokida, H., 2012. Tumor suppressive microRNA-1285 regulates novel molecular targets: aberrant expression and functional significance in renal cell carcinoma. Oncotarget 3, 44–57.

Hill, A.F., Pegtel, D.M., Lambertz, U., Leonardi, T., O'Driscoll, L., Pluchino, S., Ter-Ovanesyan, D., Nolte-'t Hoen, E.N., 2013. ISEV position paper: extracellular vesicle RNA analysis and bioinformatics. J Extracell Vesicles 2.

Hoen, E., Buermans, H., Waasdorp, M., Stoorvogel, W., Wauben, M., Hoen, P., 2012. Deep sequencing of RNA from immune cell-derived vesicles uncovers the selective incorporation of small non-coding RNA biotypes with potential regulatory functions. Nucleic Acids Res 40, 9272–9285.

Hong, B.S., Cho, J.-H.H., Kim, H., Choi, E.-J.J., Rho, S., Kim, J., Kim, J.H., Choi, D.-S.S., Kim, Y.-K.K., Hwang, D., Gho, Y.S., 2009. Colorectal cancer cell-derived microvesicles are enriched in cell cycle-related mRNAs that promote proliferation of endothelial cells. BMC Genomics 10, 556.

Hood, J.L., San, R.S., Wickline, S.A., 2011. Exosomes released by melanoma cells prepare sentinel lymph nodes for tumor metastasis. Cancer Res. 71, 3792–801.

Horejsí, V., Vlcek, C., 1991. Novel structurally distinct family of leucocyte surface glycoproteins including CD9, CD37, CD53 and CD63. FEBS Lett. 288, 1–4.

Hoshino, D., Kirkbride, K.C., Costello, K., Clark, E.S., Sinha, S., Grega-Larson, N., Tyska, M.J., Weaver, A.M., 2013. Exosome secretion is enhanced by invadopodia and drives invasive behavior. Cell Rep 5, 1159–68.

Houghton, A.M., Rzymkiewicz, D.M., Ji, H., Gregory, A.D., Egea, E.E., Metz HE, Stolz DB, Land SR, Marconcini LA, Kliment CR, Jenkins KM, Beaulieu KA, Mouded, M., Frank, S.J., Wong, K.K., Shapiro, S.D,. 2010. Neutrophil elastase‐mediated degradation of IRS‐1 accelerates lung tumor growth. Nat Med 16: 219–223.

Hu, Y., Yan, C., Mu, L., Huang, K., Li, X., Tao, D., Wu, Y., Qin, J., 2015. Fibroblast-Derived Exosomes Contribute to Chemoresistance through Priming Cancer Stem Cells in Colorectal Cancer. PLoS ONE 10, e0125625.

Huang, H., Xiong, G., Shen, P., Cao, Z., Zheng, L., Zhang, T., Zhao, Y., 2017. MicroRNA-1285 inhibits malignant biological behaviors of human pancreatic cancer cells by negative regulation of YAP1. Neoplasma 64, 358–366.

Huang, W., Chiquet-Ehrismann, R., Moyano, J.V., Garcia-Pardo, A., Orend, G., 2001. Interference of tenascin-C with syndecan-4 binding to fibronectin blocks cell adhesion and stimulates tumor cell proliferation. Cancer Res. 61, 8586–94.

Huang, X., Yuan, T., Tschannen, M., Sun, Z., Jacob, H., Du, M., Liang, M., Dittmar, R.L., Liu, Y., Liang, M., Kohli, M., Thibodeau, S.N., Boardman, L., Wang, L., 2013. Characterization of human plasma-derived exosomal RNAs by deep sequencing. BMC Genomics 14, 319.

Huber, V., Fais, S., Iero, M., Lugini, L., Canese, P., Squarcina, P., Zaccheddu, A., Colone, M., Arancia, G., Gentile, M., Seregni, E., Valenti, R., Ballabio, G., Belli, F.,

Leo, E., Parmiani, G., Rivoltini, L., 2005. Human colorectal cancer cells induce T-cell death through release of proapoptotic microvesicles: role in immune escape. Gastroenterology 128, 1796–804.

Hurley, J.H., Odorizzi, G., 2012. Get on the exosome bus with ALIX. Nat. Cell Biol. 14, 654–5.

Hurwitz, S.N., Rider, M.A., Bundy, J.L., Liu, X., Singh, R.K., Meckes, D.G., 2016. Proteomic profiling of NCI-60 extracellular vesicles uncovers common protein cargo and cancer type-specific biomarkers. Oncotarget 7, 86999–87015.

Ikeda, M., Longnecker, R., 2007. Cholesterol is critical for Epstein-Barr virus latent membrane protein 2A trafficking and protein stability. Virology 360, 461–8.

Iwai, K., Minamisawa, T., Suga, K., Yajima, Y., Shiba, K., 2016. Isolation of human salivary extracellular vesicles by iodixanol density gradient ultracentrifugation and their characterizations. J Extracell Vesicles 5, 30829.

Jenjaroenpun, P., Kremenska, Y., Nair, V.M., Kremenskoy, M., Joseph, B., Kurochkin, I.V., 2013. Characterization of RNA in exosomes secreted by human breast cancer cell lines using next-generation sequencing. PeerJ 1, e201.

Ji, H., Chen, M., Greening, D.W., He, W., Rai, A., Zhang, W., Simpson, R.J., 2014. Deep sequencing of RNA from three different extracellular vesicle (EV) subtypes released from the human LIM1863 colon cancer cell line uncovers distinct miRNA-enrichment signatures. PLoS ONE 9, e110314.

Johnstone, R., Adam, M., Hammond, J., Orr, L., Turbide, C., 1987. Vesicle formation during reticulocyte maturation. Association of plasma membrane activities with released vesicles (exosomes). The Journal of biological chemistry 262, 9412–20.

Johnstone, R.M., Bianchini, A., Teng, K., 1989. Reticulocyte maturation and exosome release: transferrin receptor containing exosomes shows multiple plasma membrane functions. Blood 74, 1844–51.

Judd, N.P., Allen, C.T., Winkler, A.E., Uppaluri, R. 2012. Comparative analysis of tumour-infiltrating lymphocytes in a syngeneic mouse model of oral cancer. Otolaryngoly head and neck surgery. 147, 485-500.

Jung, K.-H.H., Chu, K., Lee, S.-T.T., Park, H.-K.K., Bahn, J.-J.J., Kim, D.-H.H., Kim, J.-H.H., Kim, M., Kun Lee, S., Roh, J.-K.K., 2009. Circulating endothelial microparticles as a marker of cerebrovascular disease. Ann. Neurol. 66, 191–9.

Jy, W., Minagar, A., Jimenez, J.J., Sheremata, W.A., Mauro, L.M., Horstman, L.L., Bidot, C., Ahn, Y.S., 2004. Endothelial microparticles (EMP) bind and activate monocytes: elevated EMP-monocyte conjugates in multiple sclerosis. Front. Biosci. 9, 3137–44.

Kalra, H., Adda, C.G., Liem, M., Ang, C.-S.S., Mechler, A., Simpson, R.J., Hulett, M.D., Mathivanan, S., 2013. Comparative proteomics evaluation of plasma exosome isolation techniques and assessment of the stability of exosomes in normal human blood plasma. Proteomics 13, 3354–64.

Kao, Y.-Y.Y., Tu, H.-F.F., Kao, S.-Y.Y., Chang, K.-W.W., Lin, S.-C.C., 2015. The increase of oncogenic miRNA expression in tongue carcinogenesis of a mouse model. Oral Oncol. 51, 1103–12.

Kawahara, R., Bollinger, J.G., Rivera, C., Ribeiro, A.C., Brandão, T.B.B., Paes Leme, A.F., MacCoss, M.J., 2016. A targeted proteomic strategy for the measurement of oral cancer candidate biomarkers in human saliva. Proteomics 16, 159–73.

Kawakubo-Yasukochi, T., Morioka, M., Hazekawa, M., Yasukochi, A., Nishinakagawa, T., Ono, K., Kawano, S., Nakamura, S., Nakashima, M., 2017. miR-200c-3p spreads invasive capacity in human oral squamous cell carcinoma microenvironment. Mol. Carcinog.

Keller, S., Rupp, C., Stoeck, A., Runz, S., Fogel, M., Lugert, S., Hager, H.-D.D., Abdel-Bakky, M.S., Gutwein, P., Altevogt, P., 2007. CD24 is a marker of exosomes secreted into urine and amniotic fluid. Kidney Int. 72, 1095–102.

Kerr, J.F.R., Wyllie, A.H., Currie, A.R., 1972. Apoptosis: A basic biological phenomenon with wide ranging implications in tissue kinetics. Br. J. Cancer. 26, 239.

Keryer-Bibens, C., Pioche-Durieu, C., Villemant, C., Souquère, S., Nishi, N., Hirashima, M., Middeldorp, J., Busson, P., 2006. Exosomes released by EBV-infected nasopharyngeal carcinoma cells convey the viral latent membrane protein 1 and the immunomodulatory protein galectin 9. BMC Cancer 6, 283.

Khan, S., Aspe, J.R., Asumen, M.G., Almaguel, F., Odumosu, O., Acevedo-Martinez, S., De Leon, M., Langridge, W.H., Wall, N.R., 2009. Extracellular, cell-permeable survivin inhibits apoptosis while promoting proliferative and metastatic potential. Br. J. Cancer 100, 1073–86.

Khan, S., Jutzy, J., Aspe, J., McGregor, D., Neidigh, J., Wall, N., 2011. Survivin is released from cancer cells via exosomes. Apoptosis: an international journal on programmed cell death 16, 1–12.

Kim, C.W., Lee, H.M., Lee, T.H., Kang, C., Kleinman, H.K., Gho, Y.S., 2002. Extracellular membrane vesicles from tumor cells promote angiogenesis via sphingomyelin. Cancer Res. 62, 6312–7.

Kim, H.S., Chen, Y.C., Nör, F., Warner, KA., Andrews, A., Wagner, VP, Zhang, Z., Zhang, Z., Martins, M.D., Pearson, AT., Yoon, E., Nör, JE. 2017. Endothelial-derived interleukin-6 induces cancer stem cell motility by generating a chemotactic gradient towards blood vessels. Oncotarget. 8, 100339-100352.

Kinoshita, T., Yip, K.W., Spence, T., Liu, F.-F.F., 2016. MicroRNAs in extracellular vesicles: potential cancer biomarkers. J. Hum. Genet.

Kirchhausen, T., 2000. Clathrin. Annu. Rev. Biochem. 69, 699–727.

Klibi, J., Niki, T., Riedel, A., Pioche-Durieu, C., Souquere, S., Rubinstein, E., Le Moulec, S., Moulec, S.L., Guigay, J., Hirashima, M., Guemira, F., Adhikary, D., Mautner, J., Busson, P., 2009. Blood diffusion and Th1-suppressive effects of galectin-9-containing exosomes released by Epstein-Barr virus-infected nasopharyngeal carcinoma cells. Blood 113, 1957–66.

Klinker, M.W., Lizzio, V., Reed, T.J., Fox, D.A., Lundy, S.K., 2014. Human B Cell-Derived Lymphoblastoid Cell Lines Constitutively Produce Fas Ligand and Secrete MHCII(+)FasL(+) Killer Exosomes. Front Immunol 5, 144.

Knepper, M.A., Pisitkun, T., 2007. Exosomes in urine: who would have thought...? Kidney Int. 72, 1043–5.

Knudson, A., 2001. Two genetic hits (more or less) to cancer. Nat Rev Cancer 1, 157–62.

Koppers-Lalic, D., Hackenberg, M., de Menezes, R., Misovic, B., Wachalska, M., Geldof, A., Zini, N., de Reijke, T., Wurdinger, T., Vis, A, van Moorselaar, J., Pegtel, M., Bijnsdorp, I., 2016. Non-invasive prostate cancer detection by measuring miRNA variants (isomiRs) in urine extracellular vesicles. Oncotarget. 7, 22566-22578.

Koshizuka, K., Hanazawa, T., Kikkawa, N., Arai, T., Okato, A., Kurozumi, A., Kato, M., Katada, K., Okamoto, Y., Seki, N., 2017. Regulation of ITGA3 by the anti-tumor miR-199 family inhibits cancer cell migration and invasion in head and neck cancer. Cancer Sci. 108, 1681–1692.

Kostelansky, M.S., Sun, J., Lee, S., Kim, J., Ghirlando, R., Hierro, A., Emr, S.D., Hurley, J.H., 2006. Structural and functional organization of the ESCRT-I trafficking complex. Cell 125, 113–26.

Kotzerke, K., Mempel, M., Aung, T., Wulf, G.G., Urlaub, H., Wenzel, D., Schön, M.P., Braun, A., 2013. Immunostimulatory activity of murine keratinocyte-derived exosomes. Exp. Dermatol. 22, 650–5.

Kowal, J., Arras, G., Colombo, M., Jouve, M., Morath, J.P., Primdal-Bengtson, B., Dingli, F., Loew, D., Tkach, M., Théry, C., 2016. Proteomic comparison defines novel markers to characterize heterogeneous populations of extracellular vesicle subtypes. Proc. Natl. Acad. Sci. U.S.A. 113, E968–77.

Kowal, J., Tkach, M., Théry, C., 2014. Biogenesis and secretion of exosomes. Curr. Opin. Cell Biol. 29, 116–25.

Kreger, B.T., Dougherty, A.L., Greene, K.S., Cerione, R.A., Antonyak, M.A., 2016. Microvesicle Cargo and Function Changes upon Induction of Cellular Transformation. J. Biol. Chem. 291, 19774–85.

Labropoulou, V.T., Skandalis, S.S., Ravazoula, P., Perimenis, P., Karamanos, N.K., Kalofonos, H.P., Theocharis, A.D., 2013. Expression of syndecan-4 and correlation with metastatic potential in testicular germ cell tumours. Biomed Res Int 2013, 214864.

Lai, C.P., Kim, E.Y., Badr, C.E., Weissleder, R., Mempel, T.R., Tannous, B.A., Breakefield, X.O., 2015. Visualization and tracking of tumour extracellular vesicle delivery and RNA translation using multiplexed reporters. Nat Commun 6, 7029.

Lakkaraju, A., Rodriguez-Boulan, E., 2008. Itinerant exosomes: emerging roles in cell and tissue polarity. Trends Cell Biol. 18, 199–209.

Langenkamp, E., Molema, G., 2009. Microvascular endothelial cell heterogeneity: general concepts and pharmacological consequences for anti-angiogenic therapy of cancer. Cell Tissue Res. 335, 205–22.

Laulagnier, K., Grand, D., Dujardin, A., Hamdi, S., Vincent-Schneider, H., Lankar, D., Salles, J.-P.P., Bonnerot, C., Perret, B., Record, M., 2004a. PLD2 is enriched on exosomes and its activity is correlated to the release of exosomes. FEBS Lett. 572, 11–4.

Laulagnier, K., Motta, C., Hamdi, S., Roy, S., Fauvelle, F., Pageaux, J.-F.F., Kobayashi, T., Salles, J.-P.P., Perret, B., Bonnerot, C., Record, M., 2004b. Mast cell- and dendritic cell-derived exosomes display a specific lipid composition and an unusual membrane organization. Biochem. J. 380, 161–71.

Le, M.T., Hamar, P., Guo, C., Basar, E., Perdigão-Henriques, R., Balaj, L., Lieberman, J., 2014. miR-200-containing extracellular vesicles promote breast cancer cell metastasis. J. Clin. Invest. 124, 5109–28.

Leca, J., Martinez, S., Lac, S., Nigri, J., Secq, V., Rubis, M., Bressy, C., Sergé, A., Lavaut, M.-N.N., Dusetti, N., Loncle, C., Roques, J., Pietrasz, D., Bousquet, C., Garcia, S., Granjeaud, S., Ouaissi, M., Bachet, J.B., Brun, C., Iovanna, J.L., Zimmermann, P., Vasseur, S., Tomasini, R., 2016. Cancer-associated fibroblast-derived annexin A6+ extracellular vesicles support pancreatic cancer aggressiveness. J. Clin. Invest. 126, 4140–4156.

Lee, C., Mitsialis, S.A., Aslam, M., Vitali, S.H., Vergadi, E., Konstantinou, G., Sdrimas, K., Fernandez-Gonzalez, A., Kourembanas, S., 2012. Exosomes mediate the cytoprotective action of mesenchymal stromal cells on hypoxia-induced pulmonary hypertension. Circulation 126, 2601–11.

Lee, J.-E.E., Moon, P.-G.G., Cho, Y.-E.E., Kim, Y.-B.B., Kim, I.-S.S., Park, H., Baek, M.-C.C., 2016. Identification of EDIL3 on extracellular vesicles involved in breast cancer cell invasion. J Proteomics 131, 17–28.

Lee, S.-O.O., Masyuk, T., Splinter, P., Banales, J.M.M., Masyuk, A., Stroope, A., Larusso, N., 2008. MicroRNA15a modulates expression of the cell-cycle regulator Cdc25A and affects hepatic cystogenesis in a rat model of polycystic kidney disease. J. Clin. Invest. 118, 3714–24.

Lee, S.-T.T., Chu, K., Jung, K.-H.H., Kim, J.-M.M., Moon, H.-J.J., Bahn, J.-J.J., Im, W.-S.S., Sunwoo, J., Moon, J., Kim, M., Lee, S.K., Roh, J.-K.K., 2012. Circulating CD62E+ microparticles and cardiovascular outcomes. PLoS ONE 7, e35713.
Leef, G., Thomas, S.M., 2013. Molecular communication between tumor-associated fibroblasts and head and neck squamous cell carcinoma. Oral Oncol. 49, 381–6.

Lener, T., Gimona, M., Aigner, L., Börger, V., Buzas, E., Camussi, G., Chaput, N., Chatterjee, D., Court, F.A., Del Portillo, H.A., O'Driscoll, L., Fais, S., Falcon-Perez, J.M., Felderhoff-Mueser, U., Fraile, L., Gho, Y.S., Görgens, A., Gupta, R.C., Hendrix, A., Hermann, D.M., Hill, A.F., Hochberg, F., Horn, P.A., de Kleijn, D., Kordelas, L., Kramer, B.W., Krämer-Albers, E.-M.M., Laner-Plamberger, S., Laitinen, S., Leonardi, T., Lorenowicz, M.J., Lim, S.K., Lötvall, J., Maguire, C.A., Marcilla, A., Nazarenko, I., Ochiya, T., Patel, T., Pedersen, S., Pocsfalvi, G., Pluchino, S., Quesenberry, P., Reischl, I.G., Rivera, F.J., Sanzenbacher, R., Schallmoser, K., Slaper-Cortenbach, I., Strunk, D., Tonn, T., Vader, P., van Balkom, B.W., Wauben, M., Andaloussi, S.E., Théry, C., Rohde, E., Giebel, B., 2015. Applying extracellular vesicles based therapeutics in clinical trials - an ISEV position paper. J Extracell Vesicles 4, 30087.

Li, B., Antonyak, M.A., Zhang, J., Cerione, R.A., 2012. RhoA triggers a specific signaling pathway that generates transforming microvesicles in cancer cells. Oncogene 31, 4740–9.

Li, X., Mertens-Talcott, S.U., Zhang, S., Kim, K., Ball, J., Safe, S., 2010. MicroRNA-27a Indirectly Regulates Estrogen Receptor {alpha} Expression and Hormone Responsiveness in MCF-7 Breast Cancer Cells. Endocrinology 151, 2462–73.

Liang, Y., Eng, W.S., Colquhoun, D.R., Dinglasan, R.R., Graham, D.R., Mahal, L.K., 2014. Complex N-linked glycans serve as a determinant for exosome/microvesicle cargo recruitment. J. Biol. Chem. 289, 32526–37.

Lima, L.G., Chammas, R., Monteiro, R.Q., Moreira, M.E., Barcinski, M.A., 2009. Tumor-derived microvesicles modulate the establishment of metastatic melanoma in a phosphatidylserine-dependent manner. Cancer Lett. 283, 168–75.

Lin, E., Nguyen, A., Russell, R., Pollard, J., 2001. Colony-Stimulating Factor 1 Promotes Progression of Mammary Tumors to Malignancy. J Exp Medicine 193, 727–740.

Lin, Z., Swan, K., Zhang, X., Cao, S., Brett, Z., Drury, S., Strong, M.J., Fewell, C., Puetter, A., Wang, X., Ferris, M., Sullivan, D.E., Li, L., Flemington, E.K., 2016. Secreted Oral Epithelial Cell Membrane Vesicles Induce Epstein-Barr Virus Reactivation in Latently Infected B Cells. J. Virol. 90, 3469–79.

Liu, C.-J.J., Lin, S.-C.C., Yang, C.-C.C., Cheng, H.-W.W., Chang, K.-W.W., 2012. Exploiting salivary miR-31 as a clinical biomarker of oral squamous cell carcinoma. Head Neck 34, 219–24.

Liu, S.-Y., Chang, L.-C., Pan, L.-F., Hung, Y.-J., Lee, C.-H., Shieh, Y.-S., 2008. Clinicopathologic significance of tumor cell-lined vessel and microenvironment in oral squamous cell carcinoma. Oral Oncol 44, 277–285.

Liu, W.H., Ren, L.N., Wang, X., Wang, T., Zhang, N., Gao, Y., Luo, H., Navarro-Alvarez, N., Tang, L.J., 2015. Combination of exosomes and circulating microRNAs may serve as a promising tumor marker complementary to alpha-fetoprotein for early-stage hepatocellular carcinoma diagnosis in rats. J. Cancer Res. Clin. Oncol. 141, 1767–78.

Llorente, A., Skotland, T., Sylvänne, T., Kauhanen, D., Róg, T., Orłowski, A., Vattulainen, I., Ekroos, K., Sandvig, K., 2013. Molecular lipidomics of exosomes released by PC-3 prostate cancer cells. Biochim. Biophys. Acta 1831, 1302–9.
Lodi, G., Sardella, A., Bez, C., Demarosi, F., Carrassi, A., 2006. Interventions for treating oral leukoplakia. Cochrane Libr CD001829.

Logozzi, M., Milito, A., Lugini, L., Borghi, M., Calabrò, L., Spada, M., Perdicchio, M., Marino, M., Federici, C., Iessi, E., Brambilla, D., Venturi, G., Lozupone, F., Santinami, M., Huber, V., Maio, M., Rivoltini, L., Fais, S., 2009. High levels of exosomes expressing CD63 and caveolin-1 in plasma of melanoma patients. PloS one 4, e5219.

Lu, C., Bonome, T., Li, Y., Kamat, A., Han, L., Schmandt, R., Coleman, R., Gershenson, D., Jaffe, R., Birrer, M., Sood, A., 2007. Gene alterations identified by expression profiling in tumor-associated endothelial cells from invasive ovarian carcinoma. Cancer Res 67, 1757–68.

Lucchetti, D., Calapà, F., Palmieri, V., Fanali, C., Carbone, F., Papa, A., De Maria, R., De Spirito, M., Sgambato, A., 2017. Differentiation affects the release of exosomes from colon cancer cells and their ability to modulate the behaviour of recipient cells. American Journal of Pathology. 187, 1633-1647.

Luga, V., Zhang, L., Viloria-Petit, A.M., Ogunjimi, A.A., Inanlou, M.R., Chiu, E., Buchanan, M., Hosein, A.N., Basik, M., Wrana, J.L., 2012. Exosomes mediate stromal mobilization of autocrine Wnt-PCP signaling in breast cancer cell migration. Cell 151, 1542–56.

Lunavat, T.R., Cheng, L., Kim, D.-K.K., Bhadury, J., Jang, S.C., Lässer, C., Sharples, R.A., López, M.D., Nilsson, J., Gho, Y.S., Hill, A.F., Lötvall, J., 2015. Small RNA deep sequencing discriminates subsets of extracellular vesicles released by melanoma cells--Evidence of unique microRNA cargos. RNA Biol 12, 810–23.

Lundholm, M., Schröder, M., Nagaeva, O., Baranov, V., Widmark, A., Mincheva-Nilsson, L., Wikström, P., 2014. Prostate tumor-derived exosomes down-

regulate NKG2D expression on natural killer cells and CD8+ T cells: mechanism of immune evasion. PLoS ONE 9, e108925.

Lv, M.M., Zhu, X.Y., Chen, W.X., Zhong, S.L., Hu, Q., Ma, T.F., Zhang, J., Chen, L., Tang, J.H., Zhao, J.H., 2014. Exosomes mediate drug resistance transfer in MCF-7 breast cancer cells and a probable mechanism is delivery of P-glycoprotein. Tumour Biol. 35, 10773–9.

Lánczky, A., Nagy, Á., Bottai, G., Munkácsy, G., Szabó, A., Santarpia, L., Győrffy, B., 2016. miRpower: a web-tool to validate survival-associated miRNAs utilizing expression data from 2178 breast cancer patients. Breast Cancer Res. Treat. 160, 439–446.

Lázaro-Ibáñez, E., Neuvonen, M., Takatalo, M., Thanigai Arasu, U., Capasso, C., Cerullo, V., Rhim, J.S., Rilla, K., Yliperttula, M., Siljander, P.R., 2017. Metastatic state of parent cells influences the uptake and functionality of prostate cancer cell-derived extracellular vesicles. J Extracell Vesicles 6, 1354645.

Lázaro-Ibáñez, E., Sanz-Garcia, A., Visakorpi, T., Escobedo-Lucea, C., Siljander, P., Ayuso-Sacido, A., Yliperttula, M., 2014. Different gDNA content in the subpopulations of prostate cancer extracellular vesicles: apoptotic bodies, microvesicles, and exosomes. Prostate 74, 1379–90.

Lässer, C., Alikhani, V.S., Ekström, K., Eldh, M., Paredes, P.T., Bossios, A., Sjöstrand, M., Gabrielsson, S., Lötvall, J., Valadi, H., 2011a. Human saliva, plasma and breast milk exosomes contain RNA: uptake by macrophages. J Transl Med 9, 9.

Lässer, C., O'Neil, S.E., Ekerljung, L., Ekström, K., Sjöstrand, M., Lötvall, J., 2011b. RNA-containing exosomes in human nasal secretions. Am J Rhinol Allergy 25, 89–93.

Lässer, C., Eldh, M., Lötval, J., 2012. Isolation and characterization of RNA-containing exosomes. J Vis Exp. 59, e3037

Lőrincz, Á.M.M., Timár, C.I., Marosvári, K.A., Veres, D.S.S., Otrokocsi, L., Kittel, Á., Ligeti, E., 2014. Effect of storage on physical and functional properties of extracellular vesicles derived from neutrophilic granulocytes. J Extracell Vesicles 3, 25465.

Macklin, R., Wang, H., Loo, D., Martin, S., Cumming, A., Cai, N., Lane, R., Ponce, N.S., Topkas, E., Inder, K., Saunders, N.A., Endo-Munoz, L., 2016. Extracellular vesicles secreted by highly metastatic clonal variants of osteosarcoma preferentially localize to the lungs and induce metastatic behaviour in poorly metastatic clones. Oncotarget 7, 43570–43587.

Majno, G., Gabbiani, G., Hirschel, B.J., Ryan, G.B., Statkov, P.R., 1971. Contraction of granulation tissue in vitro: similarity to smooth muscle. Science 173, 548–50.

Marzesco, A.-M.M., Janich, P., Wilsch-Bräuninger, M., Dubreuil, V., Langenfeld, K., Corbeil, D., Huttner, W.B., 2005. Release of extracellular membrane particles carrying the stem cell marker prominin-1 (CD133) from neural progenitors and other epithelial cells. J. Cell. Sci. 118, 2849–58.

Mathews, J.A., Gibb, D.R., Chen, B.-H.H., Scherle, P., Conrad, D.H., 2010. CD23 Sheddase A disintegrin and metalloproteinase 10 (ADAM10) is also required for CD23 sorting into B cell-derived exosomes. J. Biol. Chem. 285, 37531–41.

Matsuda, K., Ohga, N., Hida, Y., Muraki, C., Tsuchiya, K., Kurosu, T., Akino, T., Shih, S.-C., Totsuka, Y., Klagsbrun, M., Shindoh, M., Hida, K., 2010. Isolated tumor endothelial cells maintain specific character during long-term culture. Biochem Bioph Res Co 394, 947–54.

Matsuo, H., Chevallier, J., Mayran, N., Le Blanc, I., Ferguson, C., Fauré, J., Blanc, N.S., Matile, S., Dubochet, J., Sadoul, R., Parton, R.G., Vilbois, F., Gruenberg, J., 2004. Role of LBPA and Alix in multivesicular liposome formation and endosome organization. Science 303, 531–4.

McKenzie, A.J., Hoshino, D., Hong, N.H., Cha, D.J., Franklin, J.L., Coffey, R.J., Patton, J.G., Weaver, A.M., 2016. KRAS-MEK Signaling Controls Ago2 Sorting into Exosomes. Cell Rep 15, 978–87.

Medina, A., Ghahary, A., 2010. Transdifferentiated circulating monocytes release exosomes containing 14-3-3 proteins with matrix metalloproteinase-1 stimulating effect for dermal fibroblasts. Wound Repair Regen. 18, 245-53.

Medzhitov, R., 2008. Origin and physiological roles of inflammation. Nature 454, 428–35.

Meehan, B., Rak, J., Di Vizio, D., 2016. Oncosomes - large and small: what are they, where they came from? J Extracell Vesicles 5, 33109.

Melo, S.A., Luecke, L.B., Kahlert, C., Fernandez, A.F., Gammon, S.T., Kaye, J., LeBleu, V.S., Mittendorf, E.A., Weitz, J., Rahbari, N., Reissfelder, C., Pilarsky, C., Fraga, M.F., Piwnica-Worms, D., Kalluri, R., 2015. Glypican-1 identifies cancer exosomes and detects early pancreatic cancer. Nature 523, 177–82.

Memet, I., Doebele, C., Sloan, K.E., Bohnsack, M.T., 2017. The G-patch protein NF-κB repressing factor mediates the recruitment of the exonuclease XRN2 and activation of RNA helicase DHX15 in human ribosome biogenesis. Nucleic Acids Res. 45, 5259-5374.

Metzelaar, M.J., Wijngaard, P.L., Peters, P.J., Sixma, J.J., Nieuwenhuis, H.K., Clevers, H.C., 1991. CD63 antigen. A novel lysosomal membrane glycoprotein, cloned by a screening procedure for intracellular antigens in eukaryotic cells. J. Biol. Chem. 266, 3239–45.

Minciacchi, V.R., Spinelli, C., Reis-Sobreiro, M., Cavallini, L., You, S., Zandian, M., Li, X., Mishra, R., Chiarugi, P., Adam, R.M., Posadas, E.M., Viglietto, G., Freeman, M.R., Cocucci, E., Bhowmick, N.A., Di Vizio, D., 2017. MYC Mediates Large Oncosome-Induced Fibroblast Reprogramming in Prostate Cancer. Cancer Res. 77, 2306–2317.

Minciacchi, V.R., You, S., Spinelli, C., Morley, S., Zandian, M., Aspuria, P.-J.J., Cavallini, L., Ciardiello, C., Reis Sobreiro, M., Morello, M., Kharmate, G., Jang, S.C., Kim, D.-K.K., Hosseini-Beheshti, E., Tomlinson Guns, E., Gleave, M., Gho, Y.S., Mathivanan, S., Yang, W., Freeman, M.R., Di Vizio, D., 2015. Large oncosomes contain distinct protein cargo and represent a separate functional class of tumor-derived extracellular vesicles. Oncotarget 6, 11327–41.

Mineo, M., Garfield, S.H., Taverna, S., Flugy, A., De Leo, G., Alessandro, R., Kohn, E.C., 2012. Exosomes released by K562 chronic myeloid leukemia cells promote angiogenesis in a Src-dependent fashion. Angiogenesis 15, 33–45.

Miyahara, M., Tanuma, J.-I., Sugihara, K., Semba, I., 2007. Tumor lymphangiogenesis correlates with lymph node metastasis and clinicopathologic parameters in oral squamous cell carcinoma. Cancer 110, 1287–94.

Moilanen, J.M., Löffek, S., Kokkonen, N., Salo, S., Väyrynen, J.P., Hurskainen, T., Manninen, A., Riihilä, P., Heljasvaara, R., Franzke, C.-W.W., Kähäri, V.-M.M., Salo, T., Mäkinen, M.J., Tasanen, K., 2017. Significant Role of Collagen XVII And Integrin β4 in Migration and Invasion of The Less Aggressive Squamous Cell Carcinoma Cells. Sci Rep 7, 45057.

Mol, E.A., Goumans, M.-J.J., Doevendans, P.A., Sluijter, J.P.G.P., Vader, P., 2017. Higher functionality of extracellular vesicles isolated using size-exclusion chromatography compared to ultracentrifugation. Nanomedicine 13, 2061–2065.

Montecalvo, A., Larregina, A.T., Shufesky, W.J., Stolz, D.B., Sullivan, M.L., Karlsson, J.M., Baty, C.J., Gibson, G.A., Erdos, G., Wang, Z., Milosevic, J., Tkacheva, O.A., Divito, S.J., Jordan, R., Lyons-Weiler, J., Watkins, S.C., Morelli, A.E., 2012. Mechanism of transfer of functional microRNAs between mouse dendritic cells via exosomes. Blood 119, 756–66.

Montermini, L., Meehan, B., Garnier, D., Lee, W.J., Lee, T.H., Guha, A., Al-Nedawi, K., Rak, J., 2015. Inhibition of oncogenic epidermal growth factor receptor kinase triggers release of exosome-like extracellular vesicles and impacts their phosphoprotein and DNA content. J. Biol. Chem. 290, 24534–46.

Morales-Kastresana, A., Telford, B., Musich, T., McKinnon, K., Clayborne, C., Braig, Z., Rosner, A., Demberg, T., Watson, D., Karpova, T., Freeman, G., DeKruyff, R., Pavlakis, G., Terabe, M., Robert-Guroff, M., Berzofsky, J., Jones, J., 2017. Labelling extracellular vesicles for nanoscale flow cytometry. Science reports 7, 1878.

Morello, M., Minciacchi, V.R., de Candia, P., Yang, J., Posadas, E., Kim, H., Griffiths, D., Bhowmick, N., Chung, L.W., Gandellini, P., Freeman, M.R., Demichelis,

F., Di Vizio, D., 2013. Large oncosomes mediate intercellular transfer of functional microRNA. Cell Cycle 12, 3526–36.

Morita, E., Sandrin, V., Chung, H.-Y.Y., Morham, S.G., Gygi, S.P., Rodesch, C.K., Sundquist, W.I., 2007. Human ESCRT and ALIX proteins interact with proteins of the midbody and function in cytokinesis. EMBO J. 26, 4215–27.

Morse, M.A., Garst, J., Osada, T., Khan, S., Hobeika, A., Clay, T.M., Valente, N., Shreeniwas, R., Sutton, M.A., Delcayre, A., Hsu, D.-H.H., Le Pecq, J.-B.B., Lyerly, H.K., 2005. A phase I study of dexosome immunotherapy in patients with advanced non-small cell lung cancer. J Transl Med 3, 9.

Mu, J., Zhuang, X., Wang, Q., Jiang, H., Deng, Z.-B.B., Wang, B., Zhang, L., Kakar, S., Jun, Y., Miller, D., Zhang, H.-G.G., 2014. Interspecies communication between plant and mouse gut host cells through edible plant derived exosome-like nanoparticles. Mol Nutr Food Res 58, 1561–73.

Munoz, J.L., Bliss, S.A., Greco, S.J., Ramkissoon, S.H., Ligon, K.L., Rameshwar, P., 2013. Delivery of Functional Anti-miR-9 by Mesenchymal Stem Cell-derived Exosomes to Glioblastoma Multiforme Cells Conferred Chemosensitivity. Mol Ther Nucleic Acids 2, e126.

Muppalla, J.N., Muddana, K., Dorankula, S.P., Thokala, M.R., Pasupula, A.P., 2013. Microenvironment-a role in tumour progression and prognosis. J Clin Diagn Res 7, 2096–9.

Muralidharan-Chari, V., Clancy, J., Plou, C., Romao, M., Chavrier, P., Raposo, G., D'Souza-Schorey, C., 2009. ARF6-regulated shedding of tumor cell-derived plasma membrane microvesicles. Curr. Biol. 19, 1875–85.

Na, Y.-R., Yoon, Y.-N., Son, D.-I., Seok, S.-H., 2013. Cyclooxygenase-2 Inhibition Blocks M2 Macrophage Differentiation and Suppresses Metastasis in Murine Breast Cancer Model. Plos One 8, e63451.

Nahar, N.N., Missana, L.R., Garimella, R., Tague, S.E., Anderson, H.C., 2008. Matrix vesicles are carriers of bone morphogenetic proteins (BMPs), vascular endothelial growth factor (VEGF), and noncollagenous matrix proteins. J. Bone Miner. Metab. 26, 514–9.

Nanbo, A., Kawanishi, E., Yoshida, R., Yoshiyama, H., 2013. Exosomes derived from Epstein-Barr virus-infected cells are internalized via caveola-dependent endocytosis and promote phenotypic modulation in target cells. J. Virol. 87, 10334–47.

Neel, J.-C.C., Lebrun, J.-J.J., 2013. Activin and TGFβ regulate expression of the microRNA-181 family to promote cell migration and invasion in breast cancer cells. Cell. Signal. 25, 1556–66.

Nithiananthan, S., Crawford, A., Knock, J.C., Lambert, D.W., Whawell, S.A., 2017. Physiological Fluid Flow Moderates Fibroblast Responses to TGF-β1. J. Cell. Biochem. 118, 878–890.

Öhman, J., Mowjood, R., Larsson, L., Kovacs, A., Magnusson, B., Kjeller, G., Jontell, M., Hasseus, B., 2015. Presence of CD3-positive T-cells in oral premalignant leukoplakia indicates prevention of cancer transformation. Anticancer research 35, 311-7.

Okoye, I.S., Coomes, S.M., Pelly, V.S., Czieso, S., Papayannopoulos, V., Tolmachova, T., Seabra, M.C., Wilson, M.S., 2014. MicroRNA-containing T-regulatory-cell-derived exosomes suppress pathogenic T helper 1 cells. Immunity 41, 89–103.

Olumi, A., Grossfeld, G., Hayward, S., Carroll, P., Tlsty, T., Cunha, G., 1999. Carcinoma-associated fibroblasts direct tumor progression of initiated human prostatic epithelium. Cancer Res 59, 5002–11.

Oppel, F., Müller, N., Schackert, G., Hendruschk, S., Martin, D., Geiger, K.D., Temme, A., 2011. SOX2-RNAi attenuates S-phase entry and induces RhoA-dependent switch to protease-independent amoeboid migration in human glioma cells. Mol. Cancer 10, 137.

Ostenfeld, M.S., Jeppesen, D.K., Laurberg, J.R., Boysen, A.T., Bramsen, J.B., Primdal-Bengtson, B., Hendrix, A., Lamy, P., Dagnaes-Hansen, F., Rasmussen, M.H., Bui, K.H., Fristrup, N., Christensen, E.I., Nordentoft, I., Morth, J.P., Jensen, J.B.B., Pedersen, J.S., Beck, M., Theodorescu, D., Borre, M., Howard, K.A., Dyrskjøt, L., Ørntoft, T.F., 2014. Cellular disposal of miR23b by RAB27-dependent exosome release is linked to acquisition of metastatic properties. Cancer Res. 74, 5758–71.

Ostrand-Rosenberg, S., Sinha, P., 2009. Myeloid-derived suppressor cells: linking inflammation and cancer. J. Immunol. 182, 4499–506.

Ow SY, Salim M, Noirel J, Evans C, Rehman I, Wright PC., 2009. iTRAQ underestimation in simple and complex mixtures: “the good, the bad and the ugly” J Proteome Res. 8, 5347–5355.

Paggetti, J., Haderk, F., Seiffert, M., Janji, B., Distler, U., Ammerlaan, W., Kim, Y.J., Adam, J., Lichter, P., Solary, E., Berchem, G., Moussay, E., 2015. Exosomes released by chronic lymphocytic leukemia cells induce the transition of stromal cells into cancer-associated fibroblasts. Blood 126, 1106–17.

Pal, A., Melling, G., Hinsley, E.E., Kabir, T.D., Colley, H.E., Murdoch, C., Lambert, D.W., 2013. Cigarette smoke condensate promotes pro-tumourigenic stromal-epithelial interactions by suppressing miR-145. J. Oral Pathol. Med. 42, 309–14.

Palanichamy, J.K., Rao, D.S., 2014. miRNA dysregulation in cancer: towards a mechanistic understanding. Front Genet 5, 54.

Palanisamy, V., Sharma, S., Deshpande, A., Zhou, H., Gimzewski, J., Wong, D.T., 2010. Nanostructural and transcriptomic analyses of human saliva derived exosomes. PLoS ONE 5, e8577.

Pang, W., Su, J., Wang, Y., Feng, H., Dai, X., Yuan, Y., Chen, X., Yao, W., 2015. Pancreatic cancer-secreted miR-155 implicates in the conversion from normal fibroblasts to cancer-associated fibroblasts. Cancer Sci. 106, 1362–9.

Parolini, I., Federici, C., Raggi, C., Lugini, L., Palleschi, S., Milito, A., Coscia, C., Iessi, E., Logozzi, M., Molinari, A., Colone, M., Tatti, M., Sargiacomo, M., Fais, S., 2009. Microenvironmental pH Is a Key Factor for Exosome Traffic in Tumor Cells. J Biol Chem 284, 34211–34222.

Pazolli, E., Luo, X., Brehm, S., Carbery, K., Chung, J.-J.J., Prior, J.L., Doherty, J., Demehri, S., Salavaggione, L., Piwnica-Worms, D., Stewart, S.A., 2009. Senescent stromal-derived osteopontin promotes preneoplastic cell growth. Cancer Res. 69, 1230–9.

Pei, Y.-F.F., Lei, Y., Liu, X.-Q.Q., 2016. MiR-29a promotes cell proliferation and EMT in breast cancer by targeting ten eleven translocation 1. Biochim. Biophys. Acta 1862, 2177–2185.

Pernodet, N., Dong, K., Pelle, E., 2016. Autophagy in human skin fibroblasts: Comparison between young and aged cells and evaluation of its cellular rhythm and response to Ultraviolet A radition. J Cosmet Sci. 67, 13-20.

Piccin, A., Murphy, W.G., Smith, O.P., 2007. Circulating microparticles: pathophysiology and clinical implications. Blood Rev. 21, 157–71.

Pires, R., Hartlieb, B., Signor, L., Schoehn, G., Lata, S., Roessle, M., Moriscot, C., Popov, S., Hinz, A., Jamin, M., Boyer, V., Sadoul, R., Forest, E., Svergun, D.I., Göttlinger, H.G., Weissenhorn, W., 2009. A crescent-shaped ALIX dimer targets ESCRT-III CHMP4 filaments. Structure 17, 843–56.

Pitiyage, G.N., Slijepcevic, P., Gabrani, A., Chianea, Y.G., Lim, K.P., Prime, S.S., Tilakaratne, W.M., Fortune, F., Parkinson, E.K., 2011. Senescent mesenchymal cells accumulate in human fibrosis by a telomere-independent mechanism and ameliorate fibrosis through matrix metalloproteinases. J. Pathol. 223, 604–17.

Prime, S., Cirillo, N., Hassona, Y., Lambert, D., Paterson, I., Mellone, M., Thomas, G., James, E., Parkinson, E., 2016. Fibroblast activation and senescence in oral cancer. J Oral Pathol Med.

Puri, N., Roche, P.A., 2008. Mast cells possess distinct secretory granule subsets whose exocytosis is regulated by different SNARE isoforms. Proc. Natl. Acad. Sci. U.S.A. 105, 2580–5.

Putz, U., Howitt, J., Lackovic, J., Foot, N., Kumar, S., Silke, J., Tan, S.-S.S., 2008. Nedd4 family-interacting protein 1 (Ndfip1) is required for the exosomal secretion of Nedd4 family proteins. J. Biol. Chem. 283, 32621–7.

Qiu, X., Dou, Y., 2017. miR-1307 promotes the proliferation of prostate cancer by targeting FOXO3A. Biomed. Pharmacother. 88, 430–435.

Ramos, D.M., Dang, D., Sadler, S., 2009. The role of the integrin alpha v beta6 in regulating the epithelial to mesenchymal transition in oral cancer. Anticancer Res. 29, 125–30.

Rao, S.K., Huynh, C., Proux-Gillardeaux, V., Galli, T., Andrews, N.W., 2004. Identification of SNAREs involved in synaptotagmin VII-regulated lysosomal exocytosis. J. Biol. Chem. 279, 20471–9.

Ratajczak, J., Miekus, K., Kucia, M., Zhang, J., Reca, R., Dvorak, P., Ratajczak, M.Z., 2006. Embryonic stem cell-derived microvesicles reprogram hematopoietic progenitors: evidence for horizontal transfer of mRNA and protein delivery. Leukemia 20, 847–56.

Ren, J.G., Zhang, W., Liu, B., Man, Q.W., Xiong, X.P., Li, C., Zhu, J.Y., Wang, W.M., Jia, J., Sun, Z.J., Zhang, W.F., Chen, G., Zhao, Y.F., 2016. Clinical Significance and Roles in Angiogenesis of Circulating Microparticles in Oral Cancer. J. Dent. Res. 95, 860–7.

Richards, K.E., Zeleniak, A.E., Fishel, M.L., Wu, J., Littlepage, L.E., Hill, R., 2016. Cancer-associated fibroblast exosomes regulate survival and proliferation of pancreatic cancer cells. Oncogene.

Ristorcelli, E., Beraud, E., Mathieu, S., Lombardo, D., Verine, A., 2009. Essential role of Notch signaling in apoptosis of human pancreatic tumoral cells mediated by exosomal nanoparticles. Int. J. Cancer 125, 1016–26.

Roberts-Dalton, H.D., Cocks, A., Falcon-Perez, J.M., Sayers, E.J., Webber, J.P., Watson, P., Clayton, A., Jones, A.T., 2017. Fluorescence labelling of extracellular vesicles using a novel thiol-based strategy for quantitative analysis of cellular delivery and intracellular traffic. Nanoscale 9, 13693–13706.

Rouwkema J. Rivron N.C. van Blitterswijk C.A. Vascularization in tissue engineering. Trends Biotechnol. 2008;26:434.

Royo, F., Schlangen, K., Palomo, L., Gonzalez, E., Conde-Vancells, J., Berisa, A., Aransay, A.M., Falcon-Perez, J.M., 2013. Transcriptome of extracellular vesicles released by hepatocytes. PLoS ONE 8, e68693.

Saez, F., Frenette, G., Sullivan, R., 2003. Epididymosomes and prostasomes: their roles in posttesticular maturation of the sperm cells. J. Androl. 24, 149–54.

Safaei, R., Larson, B.J., Cheng, T.C., Gibson, M.A., Otani, S., Naerdemann, W., Howell, S.B., 2005. Abnormal lysosomal trafficking and enhanced exosomal export of cisplatin in drug-resistant human ovarian carcinoma cells. Mol. Cancer Ther. 4, 1595–604.

Saman, S., Kim, W., Raya, M., Visnick, Y., Miro, S., Saman, S., Jackson, B., McKee, A.C., Alvarez, V.E., Lee, N.C., Hall, G.F., 2012. Exosome-associated tau is secreted in tauopathy models and is selectively phosphorylated in cerebrospinal fluid in early Alzheimer disease. J. Biol. Chem. 287, 3842–9.

Sandhu, J.K., Privora, H.F., Wenckebach, G., Birnboim, H.C,. 2000. Neutrophils, nitric oxide synthase, and mutations in the mutatect murine tumor model. Am J Pathol 156: 509–518.

Sato, S., Zhu, X.L., Sly, W.S., 1990. Carbonic anhydrase isozymes IV and II in urinary membranes from carbonic anhydrase II-deficient patients. Proc. Natl. Acad. Sci. U.S.A. 87, 6073–6.

Schiera, G., Di Liegro, C.M., Saladino, P., Pitti, R., Savettieri, G., Proia, P., Di Liegro, I., 2013. Oligodendroglioma cells synthesize the differentiation-specific linker histone H1˚ and release it into the extracellular environment through shed vesicles. Int. J. Oncol. 43, 1771–6.

Schipmann, S., Wermker, K., Schulze, HJ., Kleinheinz, J., Brunner, G., 2014. Cutaneous and oral squamous cell carcinoma-dual immunosuppression via recruitment of FOXP3+ regulatory T cells and endogenous tumour FOXP3 expression? J Crainomaxillofac surg. 43, 1827-33.

Segura, E., Amigorena, S., Théry, C., 2005. Mature dendritic cells secrete exosomes with strong ability to induce antigen-specific effector immune responses. Blood Cells Mol. Dis. 35, 89–93.

Sento, S., Sasabe, E., Yamamoto, T., 2016. Application of a Persistent Heparin Treatment Inhibits the Malignant Potential of Oral Squamous Carcinoma Cells Induced by Tumor Cell-Derived Exosomes. PLoS ONE 11, e0148454.

Serini, G., Bochaton-Piallat, M.L., Ropraz, P., Geinoz, A., Borsi, L., Zardi, L., Gabbiani, G., 1998. The fibronectin domain ED-A is crucial for myofibroblastic phenotype induction by transforming growth factor-beta1. J. Cell Biol. 142, 873–81.

Sharon, Y., Raz, Y., Cohen, N., Ben-Shmuel, A., Schwartz, H., Geiger, T., Erez, N. Tumour derived osteopontin reprograms normal mammary fibroblasts to promote inflammation and tumour growth in breast cancer. Cancer Research. 75, 963-73.

Shelke, G.V., Lässer, C., Gho, Y.S., Lötvall, J., 2014. Importance of exosome depletion protocols to eliminate functional and RNA-containing extracellular vesicles from fetal bovine serum. J Extracell Vesicles 3.

Shell, S., Park, S.-M.M., Radjabi, A.R., Schickel, R., Kistner, E.O., Jewell, D.A., Feig, C., Lengyel, E., Peter, M.E., 2007. Let-7 expression defines two differentiation stages of cancer. Proc. Natl. Acad. Sci. U.S.A. 104, 11400–5.

Sheremata, W.A., Jy, W., Delgado, S., Minagar, A., McLarty, J., Ahn, Y., 2006. Interferon-beta1a reduces plasma CD31+ endothelial microparticles (CD31+EMP) in multiple sclerosis. J Neuroinflammation 3, 23.

Shi, J., Ren, Y., Zhen, L., Qu, X., 2015. Exosomes from breast cancer cells stimulate proliferation and inhibit apoptosis of CD133+ cancer cells in vitro. Molecular Medicine Reports 11, 405–409.

Shi, Q., Zhou, Z., Ye, N., Chen, Q., Zheng, X., Fang, M., 2017. MiR-181a inhibits non-small cell lung cancer cell proliferation by targeting CDK1. Cancer Biomark.

Shimoda, M., Khokha, R., 2013. Proteolytic factors in exosomes. Proteomics 13, 1624–36.

Singer, S.J., Nicolson, G.L., 1972. The fluid mosaic model of the structure of cell membranes. Science 175, 720–31.

Singh, A., Fedele, C., Lu, H., Nevalainen, M.T., Keen, J.H., Languino, L.R., 2016. Exosome-mediated Transfer of αvβ3 Integrin from Tumorigenic to Nontumorigenic Cells Promotes a Migratory Phenotype. Mol. Cancer Res. 14, 1136–1146.

Skriner, K., Adolph, K., Jungblut, P.R., Burmester, G.R., 2006. Association of citrullinated proteins with synovial exosomes. Arthritis Rheum. 54, 3809–14.

Sokolova, V., Ludwig, A.-K.K., Hornung, S., Rotan, O., Horn, P.A., Epple, M., Giebel, B., 2011. Characterisation of exosomes derived from human cells by nanoparticle tracking analysis and scanning electron microscopy. Colloids Surf B Biointerfaces 87, 146–50.

Song, X., Ding, Y., Liu, G., Yang, X., Zhao, R., Zhang, Y., Zhao, X., Anderson, G.J., Nie, G., 2016. Cancer Cell-derived Exosomes Induce Mitogen-activated Protein Kinase-dependent Monocyte Survival by Transport of Functional Receptor Tyrosine Kinases. J. Biol. Chem. 291, 8453–64.

Squadrito, M.L., Baer, C., Burdet, F., Maderna, C., Gilfillan, G.D., Lyle, R., Ibberson, M., De Palma, M., 2014. Endogenous RNAs modulate microRNA sorting to exosomes and transfer to acceptor cells. Cell Rep 8, 1432–46.

Squier, CA, Kremer, MJ, 2001. Biology of oral mucosa and esophagus. J Natl Cancer Inst Monogr 7–15.

St Croix, B., Rago, C., Velculescu, V., Traverso, G., Romans, K.E., Montgomery, E., Lal, A., Riggins, G.J., Lengauer, C., Vogelstein, B., Kinzler, K.W., 2000. Genes expressed in human tumor endothelium. Science 289, 1197–202.

Strauss, K., Goebel, C., Runz, H., Möbius, W., Weiss, S., Feussner, I., Simons, M., Schneider, A., 2010. Exosome secretion ameliorates lysosomal storage of cholesterol in Niemann-Pick type C disease. J. Biol. Chem. 285, 26279–88.

Street, J.M., Barran, P.E., Mackay, C.L., Weidt, S., Balmforth, C., Walsh, T.S., Chalmers, R.T., Webb, D.J., Dear, J.W., 2012. Identification and proteomic profiling of exosomes in human cerebrospinal fluid. J Transl Med 10, 5.

Stuffers, S., Sem Wegner, C., Stenmark, H., Brech, A., 2009. Multivesicular endosome biogenesis in the absence of ESCRTs. Traffic 10, 925–37.

Suades, R., Padró, T., Vilahur, G., Badimon, L., 2012. Circulating and platelet-derived microparticles in human blood enhance thrombosis on atherosclerotic plaques. Thromb. Haemost. 108, 1208–19.

Sullivan, R., Saez, F., Girouard, J., Frenette, G., 2005. Role of exosomes in sperm maturation during the transit along the male reproductive tract. Blood Cells Mol. Dis. 35, 1–10.

Sun, D., Zhuang, X., Xiang, X., Liu, Y., Zhang, S., Liu, C., Barnes, S., Grizzle, W., Miller, D., Zhang, H.-G.G., 2010. A novel nanoparticle drug delivery system: the anti-inflammatory activity of curcumin is enhanced when encapsulated in exosomes. Mol. Ther. 18, 1606–14.

Sun, Y., Nelson, P.S., 2012. Molecular pathways: involving microenvironment damage responses in cancer therapy resistance. Clin. Cancer Res. 18, 4019–25.

Svensson, K.J., Christianson, H.C., Wittrup, A., Bourseau-Guilmain, E., Lindqvist, E., Svensson, L.M., Mörgelin, M., Belting, M., 2013. Exosome uptake depends on ERK1/2-heat shock protein 27 signaling and lipid Raft-mediated endocytosis negatively regulated by caveolin-1. J. Biol. Chem. 288, 17713–24.

Sverdlov, E., 2012. Amedeo Avogadro's cry: What is 1 μg of exosomes? BioEssays 34, 873–875.

Swanson, J.A., 2008. Shaping cups into phagosomes and macropinosomes. Nat. Rev. Mol. Cell Biol. 9, 639–49.

Takeshita, N., Hoshino, I., Mori, M., Akutsu, Y., Hanari, N., Yoneyama, Y., Ikeda, N., Isozaki, Y., Maruyama, T., Akanuma, N., Komatsu, A., Jitsukawa, M., Matsubara, H., 2013. Serum microRNA expression profile: miR-1246 as a novel diagnostic and prognostic biomarker for oesophageal squamous cell carcinoma. Br. J. Cancer 108, 644–52.

Tamai, K., Tanaka, N., Nakano, T., Kakazu, E., Kondo, Y., Inoue, J., Shiina, M., Fukushima, K., Hoshino, T., Sano, K., Ueno, Y., Shimosegawa, T., Sugamura, K., 2010. Exosome secretion of dendritic cells is regulated by Hrs, an ESCRT-0 protein. Biochem. Biophys. Res. Commun. 399, 384–90.

Tanaka, K., Miyata, H., Sugimura, K., Fukuda, S., Kanemura, T., Yamashita, K., Miyazaki, Y., Takahashi, T., Kurokawa, Y., Yamasaki, M., Wada, H., Nakajima, K., Takiguchi, S., Mori, M., Doki, Y., 2015. miR-27 is associated with chemoresistance in esophageal cancer through transformation of normal fibroblasts to cancer-associated fibroblasts. Carcinogenesis 36, 894–903.

Tanaka, Y., Kamohara, H., Kinoshita, K., Kurashige, J., Ishimoto, T., Iwatsuki, M., Watanabe, M., Baba, H., 2013. Clinical impact of serum exosomal microRNA-21 as a clinical biomarker in human esophageal squamous cell carcinoma. Cancer 119, 1159–67.

Tang, W., Zhu, Y., Gao, J., Fu, J., Liu, C., Liu, Y., Song, C., Zhu, S., Leng, Y., Wang, G., Chen, W., Du, P., Huang, S., Zhou, X., Kang, J., Cui, L., 2014. MicroRNA-29a promotes colorectal cancer metastasis by regulating matrix metalloproteinase 2 and E-cadherin via KLF4. Br. J. Cancer 110, 450–8.

Tang, X., Hou, Y., Yang, G., Wang, X., Tang, S., Du, Y.-E.E., Yang, L., Yu, T., Zhang, H., Zhou, M., Wen, S., Xu, L., Liu, M., 2016. Stromal miR-200s contribute to breast cancer cell invasion through CAF activation and ECM remodeling. Cell Death Differ. 23, 132–45.

Tauro, B.J., Greening, D.W., Mathias, R.A., Mathivanan, S., Ji, H., Simpson, R.J., 2013. Two distinct populations of exosomes are released from LIM1863 colon carcinoma cell-derived organoids. Mol. Cell Proteomics 12, 587–98.

Taylor, D., Gercel-Taylor, C., 2008. MicroRNA signatures of tumor-derived exosomes as diagnostic biomarkers of ovarian cancer. Gynecologic Oncology 110.

Taylor, D.D., Gerçel-Taylor, C., Lyons, K.S., Stanson, J., Whiteside, T.L., 2003. T-cell apoptosis and suppression of T-cell receptor/CD3-zeta by Fas ligand-containing membrane vesicles shed from ovarian tumors. Clin. Cancer Res. 9, 5113–9.

Teo, H., Gill, D.J., Sun, J., Perisic, O., Veprintsev, D.B., Vallis, Y., Emr, S.D., Williams, R.L., 2006. ESCRT-I core and ESCRT-II GLUE domain structures reveal role for GLUE in linking to ESCRT-I and membranes. Cell 125, 99–111.

Thomson, P., Potten, C., Appleton, D., 1999. Characterization of epithelial cell activity in patients with oral cancer. Br J Oral Maxillofac Surg 37, 384–90.

Théry, C., Amigorena, S., Raposo, G., Clayton, A., 2006. Isolation and characterization of exosomes from cell culture supernatants and biological fluids., Current protocols in cell biology / editorial board, Juan S. Bonifacino ... [et al.].

Tiwari, N., Wang, C.-C.C., Brochetta, C., Ke, G., Vita, F., Qi, Z., Rivera, J., Soranzo, M.R., Zabucchi, G., Hong, W., Blank, U., 2008. VAMP-8 segregates mast cell-preformed mediator exocytosis from cytokine trafficking pathways. Blood 111, 3665–74.

Todd, R., Donoff, R., Wong, D., 1997. The molecular biology of oral carcinogenesis: toward a tumor progression model. J Oral Maxillofac Surg Official J Am Assoc Oral Maxillofac Surg 55, 613–23; discussion 623–5.

Togo, S., Polanska, U., Horimoto, Y., Orimo, A., 2013. Carcinoma-Associated Fibroblasts Are a Promising Therapeutic Target. Cancers 5, 149–169.

Tomasek, J.J., Gabbiani, G., Hinz, B., Chaponnier, C., Brown, R.A., 2002. Myofibroblasts and mechano- regulation of connective tissue remodelling. Nature Reviews Molecular Biology 3, 349–363.

Tominaga, N., Yoshioka, Y., Ochiya, T., 2015. A novel platform for cancer therapy using extracellular vesicles. Adv. Drug Deliv. Rev. 95, 50–5.

Tosar, J.P., Cayota, A., Eitan, E., Halushka, M.K., Witwer, K.W., 2017. Ribonucleic artefacts: are some extracellular RNA discoveries driven by cell culture medium components? J Extracell Vesicles 6, 1272832.

Torano, V., Royo, F., Peinado, H., Loizaga-Iriarte, A., Unda, M., Falcón-Perez, J.M,. Carracedo, A., 2016. Vesicle-MaNia: extracellular vesicles in liquid biopsy and cancer. Curr Opin Pharmacol. 29, 47-53.

Tosar, J.P., Gámbaro, F., Sanguinetti, J., Bonilla, B., Witwer, K.W., Cayota, A., 2015. Assessment of small RNA sorting into different extracellular fractions revealed by high-throughput sequencing of breast cell lines. Nucleic Acids Res. 43, 5601–16.

Trajkovic, K., Hsu, C., Chiantia, S., Rajendran, L., Wenzel, D., Wieland, F., Schwille, P., Brügger, B., Simons, M., 2008. Ceramide triggers budding of exosome vesicles into multivesicular endosomes. Science 319, 1244–7.

Trams, E., Lauter, C., Salem, N., Heine, U., 1981. Exfoliation of membrane ecto-enzymes in the form of micro-vesicles. Biochim Biophys Acta 645, 63–70.

Tréhoux, S., Lahdaoui, F., Delpu, Y., Renaud, F., Leteurtre, E., Torrisani, J., Jonckheere, N., Van Seuningen, I., 2015. Micro-RNAs miR-29a and miR-330-5p function as tumor suppressors by targeting the MUC1 mucin in pancreatic cancer cells. Biochim. Biophys. Acta 1853, 2392–403.

Trellakis, S., Bruderek, K., Dumitru, C.A., Gholaman, H., Gu, X., Bankfalvi, A., Scherag, A., Hutte, J., Dominas, N., Lehnerdt, G.F., Hoffmann, T.K., Lang, S., Brandau, S,. 2011a. Polymorphonuclear granulocytes in human head and neck cancer: Enhanced inflammatory activity, modulation by cancer cells and expansion in advanced disease. Int J Cancer 129: 2183–2193.

Umezu, T., Tadokoro, H., Azuma, K., Yoshizawa, S., Ohyashiki, K., Ohyashiki, J.H., 2014. Exosomal miR-135b shed from hypoxic multiple myeloma cells enhances angiogenesis by targeting factor-inhibiting HIF-1. Blood 124, 3748–57.

Valadi, H., Ekström, K., Bossios, A., Sjöstrand, M., Lee, J.J., Lötvall, J.O., 2007. Exosome-mediated transfer of mRNAs and microRNAs is a novel mechanism of genetic exchange between cells. Nat. Cell Biol. 9, 654–9.

Valapala, M., Vishwanatha, J.K., 2011. Lipid raft endocytosis and exosomal transport facilitate extracellular trafficking of annexin A2. J. Biol. Chem. 286, 30911–25.

Vallabhaneni, K.C., Hassler, M.-Y.Y., Abraham, A., Whitt, J., Mo, Y.-Y.Y., Atfi, A., Pochampally, R., 2016. Mesenchymal Stem/Stromal Cells under Stress Increase Osteosarcoma Migration and Apoptosis Resistance via Extracellular Vesicle Mediated Communication. PLoS ONE 11, e0166027.

Vallee, R.B., Herskovits, J.S., Aghajanian, J.G., Burgess, C.C., Shpetner, H.S., 1993. Dynamin, a GTPase involved in the initial stages of endocytosis. Ciba Found. Symp. 176, 185–93; discussion 193–7.

Van Balkom, B.W., Pisitkun, T., Verhaar, M.C., Knepper, M.A., 2011. Exosomes and the kidney: prospects for diagnosis and therapy of renal diseases. Kidney Int. 80, 1138–45.

van Engeland, M., Nieland, L.J., Ramaekers, F.C., Schutte, B., Reutelingsperger, C.P., 1998. Annexin-V affinity assay: a review on an apoptosis detection system based on phosphatidylserine exposure. Cytometry. 31, 1-9.

Van Niel, G., Charrin, S., Simoes, S., Romao, M., Rochin, L., Saftig, P., Marks, M.S., Rubinstein, E., Raposo, G., 2011. The tetraspanin CD63 regulates ESCRT-independent and -dependent endosomal sorting during melanogenesis. Dev. Cell 21, 708–21.

Vidal, M., Sainte-Marie, J., Philippot, J.R., Bienvenue, A., 1989. Asymmetric distribution of phospholipids in the membrane of vesicles released during in vitro maturation of guinea pig reticulocytes: evidence precluding a role for "aminophospholipid translocase". J. Cell. Physiol. 140, 455–62.

Villarroya-Beltri, C., Gutiérrez-Vázquez, C., Sánchez-Cabo, F., Pérez-Hernández, D., Vázquez, J., Martin-Cofreces, N., Martinez-Herrera, D.J., Pascual-Montano, A., Mittelbrunn, M., Sánchez-Madrid, F., 2013. Sumoylated hnRNPA2B1 controls the sorting of miRNAs into exosomes through binding to specific motifs. Nat Commun 4, 2980.

Waller, J., 2008. HPV vaccination in the UK. BMJ. 336, 1028.

Wang, G., Dinkins, M., He, Q., Zhu, G., Poirier, C., Campbell, A., Mayer-Proschel, M., Bieberich, E., 2012. Astrocytes secrete exosomes enriched with proapoptotic ceramide and prostate apoptosis response 4 (PAR-4): potential mechanism of apoptosis induction in Alzheimer disease (AD). J. Biol. Chem. 287, 21384–95.

Wang, J., Hendrix, A., Hernot, S., Lemaire, M., De Bruyne, E., Van Valckenborgh, E., Lahoutte, T., De Wever, O., Vanderkerken, K., Menu, E., 2014.

Bone marrow stromal cell-derived exosomes as communicators in drug resistance in multiple myeloma cells. Blood 124, 555–66.

Wang, T., Gilkes, D.M., Takano, N., Xiang, L., Luo, W., Bishop, C.J., Chaturvedi, P., Green, J.J., Semenza, G.L., 2014. Hypoxia-inducible factors and RAB22A mediate formation of microvesicles that stimulate breast cancer invasion and metastasis. Proc. Natl. Acad. Sci. U.S.A. 111, E3234–42.

Webber, J., Clayton, A., 2013. How pure are your vesicles? J Extracell Vesicles 2.

Webber, J., Steadman, R., Mason, M.D., Tabi, Z., Clayton, A., 2010. Cancer exosomes trigger fibroblast to myofibroblast differentiation. Cancer Res. 70, 9621–30.

Webber, J.P., Spary, L.K., Sanders, A.J., Chowdhury, R., Jiang, W.G., Steadman, R., Wymant, J., Jones, A.T., Kynaston, H., Mason, M.D., Tabi, Z., Clayton, A., 2015. Differentiation of tumour-promoting stromal myofibroblasts by cancer exosomes. Oncogene 34, 290–302.

Wei, M., Yang, T., Chen, X., Wu, Y., Deng, X., He, W., Yang, J., Wang, Z., 2017. Malignant ascites-derived exosomes promote proliferation and induce carcinoma-associated fibroblasts transition in peritoneal mesothelial cells. Oncotarget 8, 42262–42271.

Wei, Z., Batagov, A.O., Carter, D.R., Krichevsky, A.M., 2016. Fetal Bovine Serum RNA Interferes with the Cell Culture derived Extracellular RNA. Sci Rep 6, 31175.

Weigelt, B., Ghajar, C.M., Bissell, M.J., 2014. The need for complex 3D culture models to unravel novel pathways and identify accurate biomarkers in breast cancer. Adv. Drug Deliv. Rev. 69-70, 42–51.

Winck, F.V., Prado Ribeiro, A.C., Ramos Domingues, R., Ling, L.Y., Riaño-Pachón, D.M., Rivera, C., Brandão, T.B.B., Gouvea, A.F., Santos-Silva, A.R., Coletta, R.D., Paes Leme, A.F., 2015. Insights into immune responses in oral cancer through proteomic analysis of saliva and salivary extracellular vesicles. Sci Rep 5, 16305.

Witwer, K., Buzás, E., Bemis, L., Bora, A., Lässer, C., Lötvall, J., Hoen, E., Piper, M., Sivaraman, S., Skog, J., Théry, C., Wauben, M., Hochberg, F., 2013. Standardization of sample collection, isolation and analysis methods in extracellular vesicle research. Journal of extracellular vesicles 2.

Wolf, K., Mazo, I., Leung, H., Engelke, K., von Andrian, U.H., Deryugina, E.I., Strongin, A.Y., Bröcker, E.-B.B., Friedl, P., 2003. Compensation mechanism in tumor cell migration: mesenchymal-amoeboid transition after blocking of pericellular proteolysis. J. Cell Biol. 160, 267–77.

Wolf, P., 1967. The nature and significance of platelet products in human plasma. Br. J. Haematol. 13, 269–88.

Wolfers, J., Lozier, A., Raposo, G., Regnault, A., Théry, C., Masurier, C., Flament, C., Pouzieux, S., Faure, F., Tursz, T., Angevin, E., Amigorena, S., Zitvogel, L., 2001. Tumor-derived exosomes are a source of shared tumor rejection antigens for CTL cross-priming. Nat. Med. 7, 297–303.

Wubbolts, R., Leckie, R.S., Veenhuizen, P.T., Schwarzmann, G., Möbius, W., Hoernschemeyer, J., Slot, J.-W.W., Geuze, H.J., Stoorvogel, W., 2003. Proteomic and biochemical analyses of human B cell-derived exosomes. Potential implications for their function and multivesicular body formation. J. Biol. Chem. 278, 10963–72.

Xiao, W., Bao, Z.-X.X., Zhang, C.-Y.Y., Zhang, X.-Y.Y., Shi, L.-J.J., Zhou, Z.-T.T., Jiang, W.-W.W., 2012. Upregulation of miR-31* is negatively associated with recurrent/newly formed oral leukoplakia. PLoS ONE 7, e38648.

Xiong, Y.-Q.Q., Sun, H.-C.C., Zhang, W., Zhu, X.-D.D., Zhuang, P.-Y.Y., Zhang, J.-B.B., Wang, L., Wu, W.-Z.Z., Qin, L.-X.X., Tang, Z.-Y.Y., 2009. Human hepatocellular carcinoma tumor-derived endothelial cells manifest increased angiogenesis capability and drug resistance compared with normal endothelial cells. Clin. Cancer Res. 15, 4838–46.

Xu, F., He, H., Huang, W., Lin, Y., Luo, S., Du, Q., Duan, R., 2016. Decreased expression of MicroRNA-200 family in human breast cancer is associated with lymph node metastasis. Clin Transl Oncol 18, 283–8.

Yamakuchi, M., Ferlito, M., Lowenstein, C.J., 2008. miR-34a repression of SIRT1 regulates apoptosis. Proc. Natl. Acad. Sci. U.S.A. 105, 13421–6.

Yan, Z.-Y.Y., Luo, Z.-Q.Q., Zhang, L.-J.J., Li, J., Liu, J.-Q.Q., 2017. Integrated Analysis and MicroRNA Expression Profiling Identified Seven miRNAs Associated With Progression of Oral Squamous Cell Carcinoma. J. Cell. Physiol. 232, 2178–2185.

Yang, C., Ruffner, M.A., Kim, S.-H.H., Robbins, P.D., 2012. Plasma-derived MHC class II+ exosomes from tumor-bearing mice suppress tumor antigen-specific immune responses. Eur. J. Immunol. 42, 1778–84.

Yang, C.-C.C., Hung, P.-S.S., Wang, P.-W.W., Liu, C.-J.J., Chu, T.-H.H., Cheng, H.-W.W., Lin, S.-C.C., 2011. miR-181 as a putative biomarker for lymph-node metastasis of oral squamous cell carcinoma. J. Oral Pathol. Med. 40, 397–404.

Yang, L., Huang, J., Ren, X., Gorska, A., Chytil, A., Aakre, M., Carbone, D., Matrisian, L., Richmond, A., Lin, P.C., Moses, H., 2008. Abrogation of TGFβ signaling in mammary carcinomas recruits Gr-1+CD11b+ myeloid cells that promote metastasis. Cancer cell 13, 23–35.

Yang, L., Wu, X.-H.H., Wang, D., Luo, C.-L.L., Chen, L.-X.X., 2013. Bladder cancer cell-derived exosomes inhibit tumor cell apoptosis and induce cell proliferation in vitro. Mol Med Rep 8, 1272–8.

Yang, M., Liu, J., Piao, C., Shao, J., Du, J., 2015. ICAM-1 suppresses tumor metastasis by inhibiting macrophage M2 polarization through blockade of efferocytosis. Cell Death Dis 6, e1780.

Yang, X., Wu, H., Ling, T., 2014. Suppressive effect of microRNA-126 on oral squamous cell carcinoma in vitro. Mol Med Rep 10, 125–30.

Yao, Q., Cao, S., Li, C., Mengesha, A., Kong, B., Wei, M., 2011. Micro-RNA-21 regulates TGF-β-induced myofibroblast differentiation by targeting PDCD4 in tumor-stroma interaction. Int J Cancer 128, 1783–1792.

Yap, T., Vella, L., Seers, C., Nastri, A., Reynolds, E., Cirillo, N., McCullough, M., 2016. Oral Swirl (OS) samples - A robust source of microRNA protected by extracellular vesicles. Oral Dis.

Yoshizaki, T., Kondo, S., Wakisaka, N., Murono, S., Endo, K., Sugimoto, H., Nakanishi, S., Tsuji, A., Ito, M., 2013. Pathogenic role of Epstein-Barr virus latent membrane protein-1 in the development of nasopharyngeal carcinoma. Cancer Lett. 337, 1–7.

Yu, X., Deng, L., Wang, D., Li, N., Chen, X., Cheng, X., Yuan, J., Gao, X., Liao, M., Wang, M., Liao, Y., 2012. Mechanism of TNF-α autocrine effects in hypoxic cardiomyocytes: initiated by hypoxia inducible factor 1α, presented by exosomes. J. Mol. Cell. Cardiol. 53, 848–57.

Yuan, D., Xia, H., Zhang, Y., Chen, L., Leng, W., Chen, T., Chen, Q., Tang, Q., Mo, X., Liu, M., Bi, F., 2014. P-Akt/miR-200 signaling regulates epithelial-mesenchymal transition, migration and invasion in circulating gastric tumor cells. Int. J. Oncol. 45, 2430–8.

Yuan, J.H., Yang, F., Wang, F., Ma, J.Z., Guo, Y.J., Tao, Q.F., Liu, F., Pan, W., Wang, T.T., Zhou, C.C., Wang, S.B., Wang, Y.Z., Yang, Y., Yang, N., Zhou, W.P., Yang, G.S., Sun, S.H., 2014. A long noncoding RNA activated by TGF-β promotes the invasion-metastasis cascade in hepatocellular carcinoma. Cancer Cell 25, 666–81.

Yuyama, K., Sun, H., Mitsutake, S., Igarashi, Y., 2012. Sphingolipid-modulated exosome secretion promotes clearance of amyloid-β by microglia. J. Biol. Chem. 287, 10977–89.

Zhang, H., Bai, M., Deng, T., Liu, R., Wang, X., Qu, Y., Duan, J., Zhang, L., Ning, T., Ge, S., Li, H., Zhou, L., Liu, Y., Huang, D., Ying, G., Ba, Y., 2016. Cell-derived microvesicles mediate the delivery of miR-29a/c to suppress angiogenesis in gastric carcinoma. Cancer Lett. 375, 331–9.

Zhang, L., Wu, X., Luo, C., Chen, X., Yang, L., Tao, J., Shi, J., 2013. The 786-0 renal cancer cell-derived exosomes promote angiogenesis by downregulating the expression of hepatocyte cell adhesion molecule. Mol Med Rep 8, 272–6.

Zhang, Z., Dong, Z., Lauxen, I.S., Filho, M.S., Nör, J.E., 2014. Endothelial cell-secreted EGF induces epithelial to mesenchymal transition and endows head and neck cancer cells with a stem like phenotype. Cancer Research. 74, 2869-81.

Zheng, H., Li, L.L., Hu, D.S., Deng, X.Y., Cao, Y., 2007. Role of Epstein-Barr virus encoded latent membrane protein 1 in the carcinogenesis of nasopharyngeal carcinoma. Cell. Mol. Immunol. 4, 185–96.

Zheng, X., Carstens, J., Kim, J., Scheible, M., Kaye, J., Sugimoto, H., Wu, C.-C., LeBleu, V., Kalluri, R., 2015. Epithelial-to-mesenchymal transition is dispensable for metastasis but induces chemoresistance in pancreatic cancer. Nature 527, 525–530.

Zitvogel, L., Regnault, A., Lozier, A., Wolfers, J., Flament, C., Tenza, D., Ricciardi-Castagnoli, P., Raposo, G., Amigorena, S., 1998. Eradication of established murine tumors using a novel cell-free vaccine: dendritic cell-derived exosomes. Nat. Med. 4, 594–600.

Zlotogorski-Hurvitz, A., Dayan, D., Chaushu, G., Salo, T., Vered, M., 2016. Morphological and molecular features of oral fluid-derived exosomes: oral cancer patients versus healthy individuals. J. Cancer Res. Clin. Oncol. 142, 101–10.

Zomer, A., Steenbeek, S.C., Maynard, C., van Rheenen, J., 2016. Studying extracellular vesicle transfer by a Cre-loxP method. Nat Protoc 11, 87–101.

10. Appendix

10.1. Comparison of EVs purified by serial centrifugation and SEC

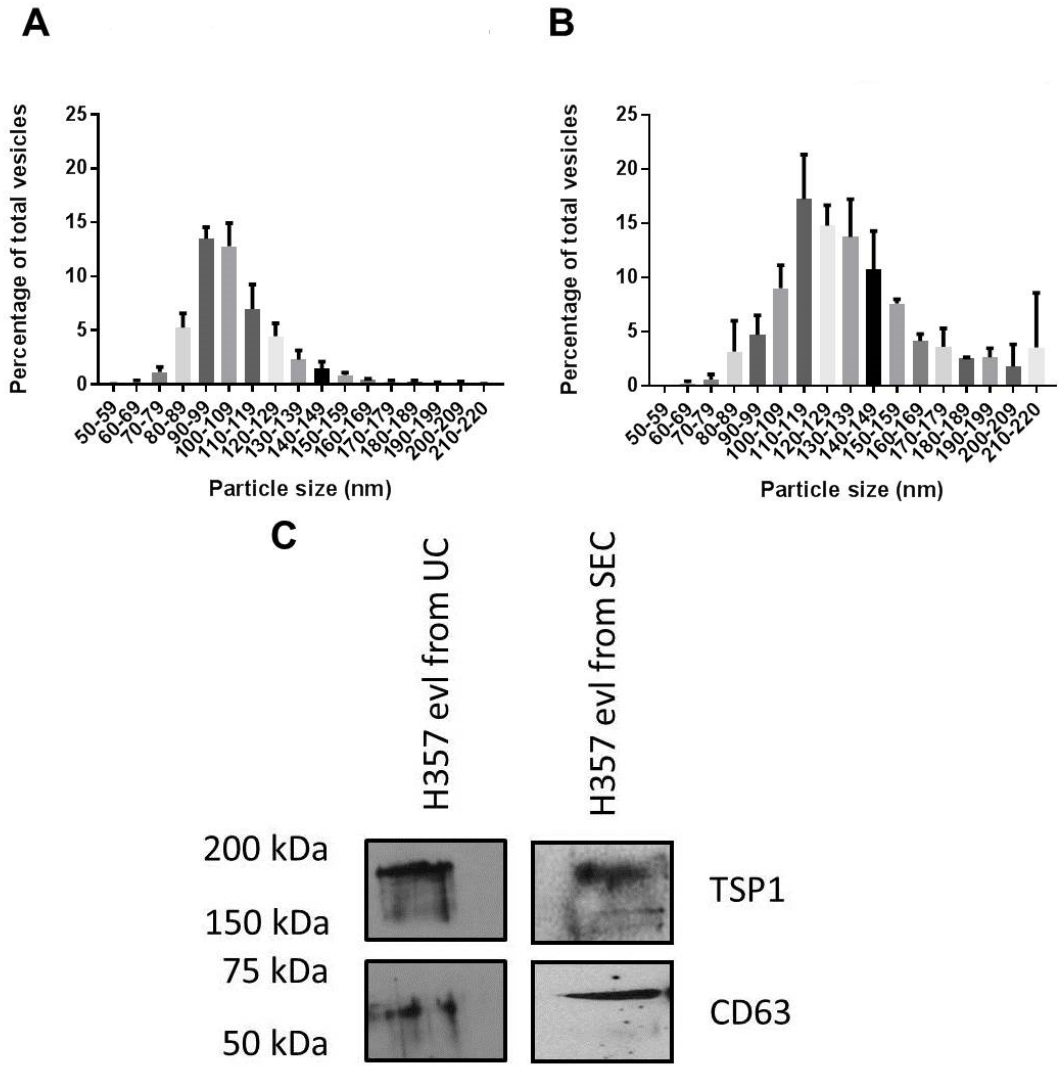

Figure 10.1 Characterisation of EVs purified by serial centrifugation and size exclusion chromatography. EVs purified by SEC (B) cover the same size ranges as those purified by serial centrifugation (A) although there is a greater proportion of larger EVs purified by the size exclusion columns. EVs purified by both techniques were positive for CD63 and TSP1 by western blot (C). Error bars SEM for n=4 biological replicates and western blots representative of at least 3 experiments.

10.2. miRNA sequencing data table

Gene	D20	D35	H357	B22
hsa-let-7a-1_hsa-let-7a-5p	55	539	144	25
hsa-let-7a-2_hsa-let-7a-5p	32	527	124	29
hsa-let-7a-3_hsa-let-7a-5p	51	480	153	31
hsa-let-7b_hsa-let-7b-5p	80	873	188	42
hsa-let-7d_hsa-let-7d-3p	0	303	0	0
hsa-let-7d_hsa-let-7d-5p	0	931	118	0
hsa-let-7e_hsa-let-7e-5p	0	416	0	0
hsa-let-7f-1_hsa-let-7f-5p	32	682	104	34
hsa-let-7f-2_hsa-let-7f-5p	25	713	116	22
hsa-let-7g_hsa-let-7g-5p	46	855	79	23
hsa-mir-100_hsa-miR-100-5p	198	468	184	173
hsa-mir-101-1_hsa-miR-101-3p	0	428	0	16
hsa-mir-103a-2_hsa-miR-103a-3p	19	511	133	24
hsa-mir-106b_hsa-miR-106b-5p	70	1187	151	45
hsa-mir-10a_hsa-miR-10a-5p	0	298	0	0
hsa-mir-10b_hsa-miR-10b-5p	47	655	0	0
hsa-mir-125a_hsa-miR-125a-5p	52	848	0	31
hsa-mir-125b-1_hsa-miR-125b-5p	47	1936	0	37
hsa-mir-125b-2_hsa-miR-125b-5p	47	1892	0	50
hsa-mir-126_hsa-miR-126-3p	427	705	103	108
hsa-mir-126_hsa-miR-126-5p	400	1277	148	105
hsa-mir-1285-1_hsa-miR-1285-3p	0	0	0	21
hsa-mir-1285-1_hsa-miR-1285-5p	74	0	99	93
hsa-mir-1307_hsa-miR-1307-3p	0	0	64	0
hsa-mir-139_hsa-miR-139-5p	47	0	0	0
hsa-mir-140_hsa-miR-140-3p	22	841	0	0
hsa-mir-140_hsa-miR-140-5p	0	0	0	0
hsa-mir-141_hsa-miR-141-3p	0	0	123	0
hsa-mir-143_hsa-miR-143-3p	0	206	0	0
hsa-mir-144_hsa-miR-144-3p	0	0	0	25
hsa-mir-146a_hsa-miR-146a-5p	0	0	0	19
hsa-mir-149_hsa-miR-149-5p	0	236	56	0
hsa-mir-151a_hsa-miR-151a-5p	62	442	85	37
hsa-mir-152_hsa-miR-152-3p	0	231	0	0
hsa-mir-15a_hsa-miR-15a-5p	0	328	43	29
hsa-mir-16-1_hsa-miR-16-5p	38	680	50	18
hsa-mir-16-2_hsa-miR-16-5p	42	589	54	0
hsa-mir-17_hsa-miR-17-5p	49	645	92	30

hsa-mir-181a-1_hsa-miR-181a-5p	180	1050	1650	397
hsa-mir-181b-2_hsa-miR-181b-5p	19	0	614	39
hsa-mir-182_hsa-miR-182-5p	0	467	0	0
hsa-mir-183_hsa-miR-183-5p	0	446	0	0
hsa-mir-185_hsa-miR-185-5p	26	615	142	26
hsa-mir-186_hsa-miR-186-5p	0	531	55	30
hsa-mir-18a_hsa-miR-18a-5p	83	3120	157	60
hsa-mir-191_hsa-miR-191-5p	109	1967	163	75
hsa-mir-193a_hsa-miR-193a-5p	0	0	0	20
hsa-mir-193b_hsa-miR-193b-3p	44	227	58	50
hsa-mir-197_hsa-miR-197-3p	0	0	34	0
hsa-mir-199a-1_hsa-miR-199a-3p	0	1117	0	0
hsa-mir-199a-2_hsa-miR-199a-3p	0	1121	0	0
hsa-mir-199b_hsa-miR-199b-3p	0	1094	0	0
hsa-mir-19a_hsa-miR-19a-3p	45	481	106	55
hsa-mir-19b-1_hsa-miR-19b-3p	69	931	108	58
hsa-mir-19b-2_hsa-miR-19b-3p	86	992	133	64
hsa-mir-200a_hsa-miR-200a-3p	0	0	610	0
hsa-mir-200b_hsa-miR-200b-3p	0	0	103	0
hsa-mir-200c_hsa-miR-200c-3p	0	0	291	0
hsa-mir-20a_hsa-miR-20a-5p	154	1908	309	100
hsa-mir-22_hsa-miR-22-3p	43	2496	90	98
hsa-mir-221_hsa-miR-221-3p	42	2493	179	99
hsa-mir-222_hsa-miR-222-3p	32	778	74	24
hsa-mir-223_hsa-miR-223-3p	130	578	63	104
hsa-mir-23a_hsa-miR-23a-3p	598	8799	1332	544
hsa-mir-25_hsa-miR-25-3p	0	193	0	0
hsa-mir-26a-1_hsa-miR-26a-5p	126	494	82	70
hsa-mir-26a-2_hsa-miR-26a-5p	114	439	84	50
hsa-mir-27a_hsa-miR-27a-3p	93	3183	259	116
hsa-mir-27b_hsa-miR-27b-3p	41	515	84	73
hsa-mir-29a_hsa-miR-29a-3p	196	6412	434	234
hsa-mir-29b-1_hsa-miR-29b-3p	24	739	36	0
hsa-mir-301a_hsa-miR-301a-3p	0	339	0	0
hsa-mir-3074_hsa-miR-3074-5p	108	2307	183	69
hsa-mir-30a_hsa-miR-30a-5p	51	876	492	84
hsa-mir-30b_hsa-miR-30b-5p	36	326	0	18
hsa-mir-30d_hsa-miR-30d-5p	85	2972	203	94
hsa-mir-30e_hsa-miR-30e-5p	51	625	49	20
hsa-mir-31_hsa-miR-31-3p	30	316	0	17
hsa-mir-31_hsa-miR-31-5p	318	4514	247	140
hsa-mir-342_hsa-miR-342-3p	45	212	0	21
hsa-mir-34a_hsa-miR-34a-5p	0	1717	0	0

hsa-mir-34b_hsa-miR-34b-3p	0	325	0	0
hsa-mir-34b_hsa-miR-34b-5p	0	413	0	0
hsa-mir-34c_hsa-miR-34c-5p	0	729	0	0
hsa-mir-361_hsa-miR-361-5p	36	0	0	20
hsa-mir-365a_hsa-miR-365a-3p	30	0	0	16
hsa-mir-365b_hsa-miR-365b-3p	21	0	0	0
hsa-mir-374b_hsa-miR-374b-5p	0	247	0	29
hsa-mir-376c_hsa-miR-376c-3p	63	180	0	33
hsa-mir-378a_hsa-miR-378a-3p	46	1589	40	164
hsa-mir-423_hsa-miR-423-3p	32	630	70	33
hsa-mir-423_hsa-miR-423-5p	27	524	0	19
hsa-mir-424_hsa-miR-424-5p	0	364	66	19
hsa-mir-425_hsa-miR-425-5p	24	235	0	0
hsa-mir-494_hsa-miR-494-3p	20	0	0	0
hsa-mir-503_hsa-miR-503-5p	0	229	0	0
hsa-mir-574_hsa-miR-574-5p	51	0	70	81
hsa-mir-590_hsa-miR-590-5p	0	0	39	16
hsa-mir-625_hsa-miR-625-3p	0	0	43	0
hsa-mir-652_hsa-miR-652-3p	0	226	0	0
hsa-mir-708_hsa-miR-708-5p	0	239	0	0
hsa-mir-92a-1_hsa-miR-92a-3p	67	223	46	36
hsa-mir-92a-2_hsa-miR-92a-3p	46	210	50	37
hsa-mir-92b_hsa-miR-92b-3p	38	0	57	15
hsa-mir-93_hsa-miR-93-5p	60	954	191	52
hsa-mir-99a_hsa-miR-99a-5p	20	220	0	0
hsa-mir-99b_hsa-miR-99b-5p	0	393	0	0

Table 10.1 Counts of miRNA sequences detected in OSCC derived EVs with minimum of 1000 RPM

10.3. Label free mass spectrometry data tables

Protein names	D201	D202	D351	D352
Collagen alpha-2(I) chain	0	0	0	0
Apolipoprotein B-100	25.7024	25.91397	0	0
Spectrin beta chain, non-erythrocytic 1	0	0	0	0
Clathrin heavy chain	25.72328	25.73332	0	21.80266
Ribosome-binding protein 1	25.01465	24.64427	0	22.09045
Collagen alpha-1(V) chain	0	0	28.47158	28.53204
Collagen alpha-2(V) chain	0	0	23.07811	22.96476
40S ribosomal protein S16	0	22.00734	0	0
Collagen alpha-1(VI) chain	25.3867	25.51244	24.12171	25.83843
Aggrecan core protein	23.76101	23.58325	0	0
Elongation factor 1-delta	0	22.1774	0	0
TNFAIP3-interacting protein 1	0	0	0	0
Peroxiredoxin-1	23.70113	0	0	0
Integrin-linked protein kinase	23.25954	23.01716	0	0
40S ribosomal protein SA	0	23.59229	0	0
Nesprin-1	0	0	0	0
Ras-related protein R-Ras2	21.66622	0	0	0
Band 4.1-like protein 1	0	0	0	0
Heat shock 70 kDa protein 1B	26.15898	25.52561	0	0
HLA class I histocompatibility antigen, A-2 alpha chain	0	0	0	0
Fatty acid synthase	0	0	0	0
60S ribosomal protein L7	22.78863	0	0	0
Heterogeneous nuclear ribonucleoproteins C1/C2	0	0	0	0
Ubiquitin-60S ribosomal protein L40	24.48438	24.70783	0	0
Epithelial cell adhesion molecule	0	0	0	0
GTP-binding nuclear protein Ran	24.85296	24.47376	0	0
Myosin light polypeptide 6	23.97272	0	0	0
T-complex protein 1 subunit epsilon	22.16653	22.50516	0	0
Tax1-binding protein 1	0	0	0	0
Ras-related protein Rab-7a	0	23.30048	0	0
Latent-transforming growth factor beta-binding protein 1	0	0	0	0
Guanine nucleotide-binding protein G(I)/G(S)/G(T) subunit beta-2	0	0	0	0
Catenin delta-1	0	0	0	0
Collagen alpha-1(XII) chain	24.49467	24.49796	0	0
Collagen alpha-3(VI) chain	24.35286	24.71167	25.50027	25.69846
Ezrin	25.39999	24.00033	0	0
Thrombospondin-4	0	0	0	0
Multifunctional protein ADE2	21.85308	0	0	0
Unconventional myosin-Ib	0	23.7349	0	0
Receptor protein-tyrosine kinase	0	0	0	0

Alpha-1,4 glucan phosphorylase	23.10064	22.621	0	0
Protein transport protein Sec16A	0	0	0	0
Pre-mRNA-processing factor 19	0	0	0	0
Lactadherin	25.87462	25.95178	26.38096	26.17807
4F2 cell-surface antigen heavy chain	25.22008	25.25501	0	0
High mobility group protein HMGI-C	0	0	0	0
C-1-tetrahydrofolate synthase, cytoplasmic	0	0	0	0
Tubulin alpha-1C chain	27.20965	27.31363	0	0
Neutral alpha-glucosidase AB	0	0	0	0
Sodium-coupled neutral amino acid transporter 2	0	0	0	0
Laminin subunit beta-1	27.00378	27.19103	0	0
60S ribosomal protein L18	23.4086	0	0	0
60S ribosomal protein L28	21.83295	0	0	0
Ras-related protein Rab-11A	0	23.9872	0	0
Envoplakin	0	0	0	0
Kunitz-type protease inhibitor 2	0	0	0	0
Choline transporter-like protein 2	0	0	0	0
Amino acid transporter	0	0	0	0
Matrilin-2	0	0	0	0
Agrin	27.65963	27.96339	0	0
Syntenin-1	23.30605	23.46712	0	0
Disintegrin and metalloproteinase domain-containing protein 10	0	0	0	0
Laminin subunit alpha-5	27.73363	27.52223	0	0
D-3-phosphoglycerate dehydrogenase	0	22.20117	0	0
Charged multivesicular body protein 2a	0	0	0	0
EGF-like repeat and discoidin I-like domain-containing protein 3	0	0	0	0
WD repeat-containing protein 1	24.20769	24.05614	0	0
Core histone macro-H2A.1	24.58314	25.31731	0	0
Filamin-B	0	0	0	0
Isocitrate dehydrogenase [NADP] cytoplasmic	0	0	0	0
Serine protease 23	0	0	0	0
Myelin protein zero-like protein 1	0	0	0	0
L-lactate dehydrogenase A chain	0	0	0	0
Phosphoglycerate kinase 1	24.47574	24.58761	0	0
Adenylate kinase isoenzyme 1	0	0	0	0
Coagulation factor X	26.21442	26.23916	0	0
Collagen alpha-1(I) chain	0	0	0	0
Fibronectin	31.32876	31.38082	31.72212	31.75736
Transferrin receptor protein 1	0	23.43224	24.50531	24.65119
Annexin A1	0	23.14389	0	0
Glyceraldehyde-3-phosphate dehydrogenase	26.80403	26.83232	0	0
Heat shock protein beta-1	24.07227	24.36058	0	0

Guanine nucleotide-binding protein G(i) subunit alpha-2	24.77077	24.76537	0	0
Sodium/potassium-transporting ATPase subunit alpha-1	21.73851	0	0	0
Integrin beta-3	23.22133	23.24648	0	0
Integrin beta-1	23.97044	23.53991	0	0
Keratin, type I cytoskeletal 18	24.17104	24.28093	0	0
ATP synthase subunit beta, mitochondrial	0	0	0	0
Alpha-enolase	25.15538	24.97115	0	0
Nucleophosmin	0	0	0	0
L-lactate dehydrogenase B chain	23.71754	23.48873	0	0
Annexin A2	24.44556	24.56866	0	0
Tubulin beta chain	25.08614	26.29843	0	0
Profilin-1	0	0	0	0
Bifunctional glutamate/proline--tRNA ligase	0	0	0	0
Heat shock protein HSP 90-alpha	24.63511	24.738	0	0
Tyrosine-protein kinase Lyn	0	0	0	0
Thrombospondin-1	27.97388	28.25327	24.09772	23.51701
Heat shock protein HSP 90-beta	26.63215	26.70491	0	0
Collagen alpha-2(IV) chain	0	22.20009	0	0
U1 small nuclear ribonucleoprotein 70 kDa	0	0	0	0
Guanine nucleotide-binding protein G(k) subunit alpha	0	0	0	0
Glutathione S-transferase P	0	0	0	0
Tumor-associated calcium signal transducer 2	0	23.38706	0	0
Poly [ADP-ribose] polymerase 1	0	0	0	0
Histone H2A.V	24.79853	24.57911	27.20247	26.72025
Histone H2A type 1-J	23.42355	0	27.60936	25.84283
Histone H1.4	23.81157	23.74283	23.54333	23.20597
78 kDa glucose-regulated protein	23.31935	23.18728	0	0
Laminin subunit gamma-1	27.48108	27.23105	23.49045	23.20054
Heat shock cognate 71 kDa protein	26.90403	27.09295	24.86122	25.19648
Solute carrier family 2, facilitated glucose transporter member 1	0	0	0	0
Proliferating cell nuclear antigen	0	0	0	0
Proto-oncogene tyrosine-protein kinase Src	0	0	0	0
Versican core protein	24.05565	24.55877	0	0
Elongation factor 2	24.4612	24.43835	0	0
Nidogen-1	24.02471	23.68517	0	0
Alcohol dehydrogenase [NADP(+)]	0	0	0	0
Pyruvate kinase PKM	27.98338	27.94949	24.28503	0
Junction plakoglobin	21.84774	21.53635	0	0
Desmoplakin	23.36306	22.45513	0	0
CD44 antigen	0	0	0	0
Integrin beta-4	24.19551	24.1187	0	0
HLA class I histocompatibility antigen, A-31 alpha chain	23.29334	23.40133	0	0
Histone H1.5	22.62999	0	23.08328	22.99455

Histone H1.3	26.01663	24.21875	0	0
Histone H1.2	0	0	0	0
High mobility group protein HMG-I/HMG-Y	0	0	0	0
T-complex protein 1 subunit alpha	23.64053	22.67659	0	0
Nucleolin	0	0	0	0
Plasma membrane calcium-transporting ATPase 1	0	0	0	0
Filamin-A	27.12888	26.62073	22.36768	0
5-nucleotidase	0	0	0	0
Integrin alpha-6	0	0	0	0
Adenosylhomocysteinase	23.22535	23.381	0	0
Histone H2B type 2-E	0	0	0	0
Cofilin-1	25.15723	25.62293	0	0
Tenascin	0	0	0	0
Integrin alpha-3	0	0	0	0
Pentraxin-related protein PTX3	27.48554	28.37057	30.77109	30.58701
Moesin	0	23.35917	0	0
Elongation factor 1-gamma	22.85772	22.64469	0	0
14-3-3 protein theta	0	0	0	0
Ephrin type-A receptor 2	0	0	0	0
HLA class I histocompatibility antigen, B-41 alpha chain	0	0	0	0
HLA class I histocompatibility antigen, B-48 alpha chain	23.0239	22.92575	0	0
HLA class I histocompatibility antigen, Cw-12 alpha chain	0	0	0	0
Syndecan-4	0	0	0	0
14-3-3 protein beta/alpha	24.09523	23.34516	0	0
14-3-3 protein sigma	0	0	0	0
Desmoglein-3	0	0	0	0
Glypican-1	0	0	0	0
Catenin beta-1	0	0	0	0
Myosin-9	28.44932	28.46599	22.77024	22.39679
Myosin-10	0	0	0	0
Transgelin-2	24.05225	23.34489	0	0
T-complex protein 1 subunit zeta	0	0	0	0
26S protease regulatory subunit 6B	0	0	0	0
ATP-dependent DNA helicase Q1	0	0	0	0
60S ribosomal protein L5	0	0	0	0
Ras GTPase-activating-like protein IQGAP1	0	0	0	0
T-complex protein 1 subunit gamma	22.0013	22.27787	0	0
Vasodilator-stimulated phosphoprotein	0	0	0	0
T-complex protein 1 subunit delta	24.24858	23.63721	0	0
Ras-related protein Rab-5C	0	0	0	0
Coatomer subunit alpha	0	0	0	0
Monocarboxylate transporter 1	0	0	0	0
Laminin subunit beta-2	0	0	0	0

Histone H2B type F-S	0	0	0	0
Actin, cytoplasmic 2	29.96719	29.8804	26.61765	26.92082
Eukaryotic initiation factor 4A-I	23.47098	23.44443	0	0
40S ribosomal protein S20	0	0	0	0
Cell division control protein 42 homolog	0	0	0	0
Ras-related protein Rab-14	0	0	0	0
Ras-related protein Rap-1b	25.83584	25.58938	0	0
60S ribosomal protein L15	0	22.5316	0	0
Transforming protein RhoA	0	0	0	0
Heterogeneous nuclear ribonucleoprotein K	22.20958	0	0	0
14-3-3 protein gamma	0	0	0	0
40S ribosomal protein S8	0	0	0	0
14-3-3 protein epsilon	24.17585	25.47584	23.27242	0
40S ribosomal protein S4, X isoform	0	0	0	0
Histone H4	27.50059	27.52694	27.09587	26.85436
60S ribosomal protein L11	0	0	0	0
Peptidyl-prolyl cis-trans isomerase A	25.87185	26.0254	0	0
14-3-3 protein zeta/delta	24.78721	25.02707	0	0
Guanine nucleotide-binding protein subunit beta-2-like 1	0	0	0	0
Actin, alpha skeletal muscle	0	0	0	0
Putative elongation factor 1-alpha-like 3	26.71607	26.31772	0	0
Tubulin beta-4B chain	26.92717	26.92717	0	0
Histone H3.2	27.34121	27.22361	26.00084	25.93017
T-complex protein 1 subunit beta	0	23.63112	0	0
DNA-dependent protein kinase catalytic subunit	0	0	0	0
Brain acid soluble protein 1	0	0	0	0
Rho-related GTP-binding protein RhoG	0	0	0	0
Tumor necrosis factor-inducible gene 6 protein	0	0	26.16795	26.283
Fibulin-2	0	0	0	0
Basement membrane-specific heparan sulfate proteoglycan core protein	26.9927	27.00764	22.42083	25.14942
Ephrin-B1	0	0	0	0
Adenylyl cyclase-associated protein 1	21.86793	22.66336	0	0
Large neutral amino acids transporter small subunit 1	24.28912	24.57496	0	0
Caveolin-1	0	0	0	0
Fibromodulin	23.36252	23.56186	0	0
Galectin-3-binding protein	25.75142	25.69139	0	0
Neuroblast differentiation-associated protein AHNAK	0	0	0	0
Sequestosome-1	0	0	0	0
Laminin subunit beta-3	27.42021	27.4453	0	0
Laminin subunit gamma-2	27.73014	27.01945	0	0
Nuclear receptor coactivator 4	0	0	0	0
Desmoglein-2	0	0	0	0
Eukaryotic translation initiation factor 3 subunit A	0	0	0	0

Cytoplasmic dynein 1 heavy chain 1	0	0	0	0
Fibroblast growth factor-binding protein 1	22.66967	0	0	0
Major vault protein	26.22422	26.83461	0	22.573
Plectin	20.62123	20.21585	0	0
Non-POU domain-containing octamer-binding protein	0	22.64498	0	0
Transforming growth factor-beta-induced protein ig-h3	24.82978	25.25782	0	0
Fascin	22.6046	22.37616	0	0
Histone H2A type 2-C	28.31103	28.91767	28.69395	28.69508
Laminin subunit alpha-3	27.47723	27.43484	0	0
Histone H3	0	0	0	0
Golgi-associated plant pathogenesis-related protein 1	0	0	0	0
von Willebrand factor A domain-containing protein 1	0	0	0	0
Staphylococcal nuclease domain-containing protein 1	0	0	0	0
Cytoplasmic FMR1-interacting protein 1	0	0	0	0
Lipolysis-stimulated lipoprotein receptor	0	0	0	0
Misshapen-like kinase 1	0	0	0	0
Retinoic acid-induced protein 3	0	0	0	0
Programmed cell death 6-interacting protein	23.06511	22.54753	0	0
Histone H1x	0	0	0	0
Histone H2A type 1-C	0	0	0	0
Multivesicular body subunit 12A	0	0	0	0
Phosphatase and actin regulator 3	0	0	30.64349	30.55161
Histone H2B type 1-M	28.40625	28.25106	27.57542	27.62101
EMILIN-2	0	0	0	0
Protein tweety homolog 3	0	0	0	0
Tubulointerstitial nephritis antigen-like	0	0	0	0
Ras-related protein Rab-1B	24.28263	23.97176	0	0
EH domain-containing protein 1	0	0	0	0
Myoferlin	0	0	0	0
Prostaglandin F2 receptor negative regulator	0	0	0	0
Brain-specific angiogenesis inhibitor 1-associated protein 2-like protein 1	0	0	0	0
Collagen alpha-1(XVII) chain	22.56788	22.0142	0	0
Plakophilin-3	0	0	0	0
Talin-1	26.32459	26.4381	0	0
Junctional adhesion molecule A	0	0	0	0

Table 10.2 Log2 of label free intensity scores for proteins in EVs derived from mild dysplastic (D20) and severe dysplastic (D35) cells

Protein names	H3571	H3572	B221	B222
Collagen alpha-2(I) chain	0	0	25.74778	25.78576
Apolipoprotein B-100	24.59645	0	25.60916	25.50857
Spectrin beta chain, non-erythrocytic 1	20.98266	20.92477	0	0
Clathrin heavy chain	27.47676	27.66296	26.80501	27.20154
Ribosome-binding protein 1	23.91342	23.88092	0	0
Collagen alpha-1(V) chain	22.81613	22.58265	0	0
Collagen alpha-2(V) chain	0	0	0	0
40S ribosomal protein S16	22.91417	23.52886	0	0
Collagen alpha-1(VI) chain	25.53905	25.34313	25.6086	25.33067
Aggrecan core protein	0	0	23.9304	23.17521
Elongation factor 1-delta	22.90558	22.27378	0	0
TNFAIP3-interacting protein 1	23.61414	23.19877	0	0
Peroxiredoxin-1	24.85681	25.18639	0	0
Integrin-linked protein kinase	0	0	0	0
40S ribosomal protein SA	24.55491	24.69259	0	0
Nesprin-1	0	0	28.35477	27.88116
Ras-related protein R-Ras2	23.26112	23.04312	22.40678	22.21511
Band 4.1-like protein 1	22.03049	22.29964	0	0
Heat shock 70 kDa protein 1B	26.96521	26.91171	0	22.48375
HLA class I histocompatibility antigen, A-2 alpha chain	24.68448	24.68565	0	0
Fatty acid synthase	26.19669	26.34755	0	0
60S ribosomal protein L7	22.96408	23.01076	0	0
Heterogeneous nuclear ribonucleoproteins C1/C2	23.31424	23.32649	0	0
Ubiquitin-60S ribosomal protein L40	27.02739	27.01977	25.35269	25.00222
Epithelial cell adhesion molecule	22.8906	22.48353	0	0
GTP-binding nuclear protein Ran	25.86992	25.83641	24.17965	24.11807
Myosin light polypeptide 6	24.29214	23.67799	0	0
T-complex protein 1 subunit epsilon	24.3761	24.69285	0	0
Tax1-binding protein 1	24.60286	24.93674	0	0
Ras-related protein Rab-7a	24.30096	24.06069	0	0
Latent-transforming growth factor beta-binding protein 1	0	0	22.88575	23.05696
Guanine nucleotide-binding protein G(I)/G(S)/G(T) subunit beta-2	24.34279	24.48971	0	0
Catenin delta-1	22.80499	22.42949	0	0
Collagen alpha-1(XII) chain	24.11434	25.17874	24.73567	24.7305
Collagen alpha-3(VI) chain	23.97088	23.68785	24.79877	24.76172
Ezrin	24.4562	23.99524	24.41693	0
Thrombospondin-4	24.26234	24.18246	23.53908	23.71051
Multifunctional protein ADE2	22.44615	21.96406	0	0
Unconventional myosin-Ib	23.85984	23.48984	0	0
Receptor protein-tyrosine kinase	25.77548	25.94639	0	0

Alpha-1,4 glucan phosphorylase	0	0	0	0
Protein transport protein Sec16A	22.09713	21.6197	0	0
Pre-mRNA-processing factor 19	22.38311	22.25491	0	0
Lactadherin	24.83374	24.73159	0	0
4F2 cell-surface antigen heavy chain	27.56776	28.08507	0	0
High mobility group protein HMGI-C	24.54256	24.83128	0	0
C-1-tetrahydrofolate synthase, cytoplasmic	21.70083	21.99924	0	0
Tubulin alpha-1C chain	27.84308	27.93708	26.30933	26.13759
Neutral alpha-glucosidase AB	24.48031	24.07594	0	0
Sodium-coupled neutral amino acid transporter 2	25.03616	25.20494	0	0
Laminin subunit beta-1	28.69395	28.76468	25.36806	25.3656
60S ribosomal protein L18	24.05383	23.68817	0	0
60S ribosomal protein L28	21.92405	21.94271	0	0
Ras-related protein Rab-11A	24.15027	24.08894	0	0
Envoplakin	21.86676	21.68466	0	0
Kunitz-type protease inhibitor 2	24.15074	23.50506	0	0
Choline transporter-like protein 2	21.45186	21.21371	0	0
Amino acid transporter	25.12617	24.88758	0	0
Matrilin-2	24.90238	24.89855	0	0
Agrin	29.41127	29.40696	0	0
Syntenin-1	28.45838	28.48174	24.52349	24.48456
Disintegrin and metalloproteinase domain-containing protein 10	22.81039	22.93485	0	0
Laminin subunit alpha-5	29.96761	29.95782	24.31603	22.95752
D-3-phosphoglycerate dehydrogenase	0	0	22.72334	22.93135
Charged multivesicular body protein 2a	22.22406	22.26651	0	0
EGF-like repeat and discoidin I-like domain-containing protein 3	28.51454	28.57091	0	0
WD repeat-containing protein 1	23.9227	24.19061	0	0
Core histone macro-H2A.1	25.75055	25.73611	0	0
Filamin-B	24.77077	25.20023	0	0
Isocitrate dehydrogenase [NADP] cytoplasmic	22.45046	22.44559	0	0
Serine protease 23	24.31389	24.28574	0	0
Myelin protein zero-like protein 1	22.7915	22.45151	0	0
L-lactate dehydrogenase A chain	23.48038	23.41002	23.15208	22.87049
Phosphoglycerate kinase 1	25.46896	25.25184	25.30414	24.32711
Adenylate kinase isoenzyme 1	0	0	22.20437	22.63482
Coagulation factor X	25.15896	25.08103	25.08456	0
Collagen alpha-1(I) chain	0	0	28.97345	28.81754
Fibronectin	28.97076	29.07143	30.07304	30.51944
Transferrin receptor protein 1	25.47503	25.5013	0	0
Annexin A1	25.68798	25.75159	0	0
Glyceraldehyde-3-phosphate dehydrogenase	27.80833	27.65731	23.55754	0

Heat shock protein beta-1	24.70282	24.4318	0	0
Guanine nucleotide-binding protein G(i) subunit alpha-2	25.26374	25.46404	25.62182	25.25238
Sodium/potassium-transporting ATPase subunit alpha-1	24.98676	25.11898	24.84929	23.89791
Integrin beta-3	0	0	0	0
Integrin beta-1	25.11012	25.1047	23.829	23.67885
Keratin, type I cytoskeletal 18	24.38949	24.33831	0	0
ATP synthase subunit beta, mitochondrial	23.49424	24.04068	0	0
Alpha-enolase	25.83632	25.838	25.18711	25.27789
Nucleophosmin	23.64482	23.28334	0	0
L-lactate dehydrogenase B chain	24.09507	24.01929	0	0
Annexin A2	25.57707	25.7399	0	0
Tubulin beta chain	26.80082	26.92298	25.39575	25.65155
Profilin-1	24.80149	24.84795	23.3041	0
Bifunctional glutamate/proline--tRNA ligase	23.63079	23.53077	0	0
Heat shock protein HSP 90-alpha	24.99131	25.08042	0	23.87371
Tyrosine-protein kinase Lyn	22.83169	22.70493	0	0
Thrombospondin-1	29.6211	29.66731	26.11054	25.51812
Heat shock protein HSP 90-beta	27.39149	27.47127	26.16465	26.4186
Collagen alpha-2(IV) chain	22.74049	22.77102	0	0
U1 small nuclear ribonucleoprotein 70 kDa	22.83289	22.65412	0	0
Guanine nucleotide-binding protein G(k) subunit alpha	22.91554	22.02726	0	0
Glutathione S-transferase P	24.61201	24.57358	0	0
Tumor-associated calcium signal transducer 2	26.78382	26.67976	0	0
Poly [ADP-ribose] polymerase 1	25.17249	25.41451	0	0
Histone H2A.V	26.63132	26.24235	0	23.90591
Histone H2A type 1-J	25.33892	23.05089	0	0
Histone H1.4	25.27888	25.22424	0	24.18858
78 kDa glucose-regulated protein	23.6919	23.78377	22.90356	22.94482
Laminin subunit gamma-1	29.02773	29.00045	25.06275	25.57868
Heat shock cognate 71 kDa protein	28.28604	28.06466	27.16087	27.35658
Solute carrier family 2, facilitated glucose transporter member 1	26.48336	26.27272	0	0
Proliferating cell nuclear antigen	22.75485	22.98591	0	0
Proto-oncogene tyrosine-protein kinase Src	22.3888	22.24203	0	0
Versican core protein	22.70257	0	31.07947	31.29313
Elongation factor 2	26.54113	26.21091	0	21.28506
Nidogen-1	23.34611	0	0	0
Alcohol dehydrogenase [NADP(+)]	22.53101	22.68207	0	0
Pyruvate kinase PKM	28.78216	28.82429	24.57473	22.99127
Junction plakoglobin	25.92375	26.14297	0	0
Desmoplakin	21.72134	21.78141	0	0

CD44 antigen	24.45676	24.51473	0	0
Integrin beta-4	28.18494	28.2102	0	0
HLA class I histocompatibility antigen, A-31 alpha chain	27.11575	26.93495	0	0
Histone H1.5	24.57109	24.64471	22.25098	0
Histone H1.3	26.90598	26.63159	26.66262	25.02335
Histone H1.2	24.72458	24.66947	0	0
High mobility group protein HMG-I/HMG-Y	25.10238	25.01372	0	0
T-complex protein 1 subunit alpha	24.12084	23.68667	23.23371	0
Nucleolin	23.97885	23.92107	0	0
Plasma membrane calcium-transporting ATPase 1	21.90481	21.91783	22.03523	20.97358
Filamin-A	27.4243	27.07051	25.07423	24.66281
5-nucleotidase	25.79504	25.92352	0	0
Integrin alpha-6	25.50827	25.54575	0	0
Adenosylhomocysteinase	24.50567	24.40795	0	0
Histone H2B type 2-E	26.57012	26.52409	0	0
Cofilin-1	26.90001	26.94347	24.65687	24.83384
Tenascin	26.18221	25.77651	0	0
Integrin alpha-3	24.31997	24.49082	0	0
Pentraxin-related protein PTX3	27.22509	27.25647	0	0
Moesin	22.94113	23.39859	23.60128	0
Elongation factor 1-gamma	25.59571	25.85291	23.76253	23.16451
14-3-3 protein theta	24.281	24.21111	0	0
Ephrin type-A receptor 2	25.48965	24.97719	0	0
HLA class I histocompatibility antigen, B-41 alpha chain	26.63104	26.63575	0	0
HLA class I histocompatibility antigen, B-48 alpha chain	0	0	0	0
HLA class I histocompatibility antigen, Cw-12 alpha chain	23.1321	23.29348	0	0
Syndecan-4	24.67395	24.67417	0	0
14-3-3 protein beta/alpha	23.55532	24.92565	23.0462	22.45521
14-3-3 protein sigma	22.35318	22.41359	0	0
Desmoglein-3	23.92098	24.05573	0	0
Glypican-1	24.28122	24.06472	0	0
Catenin beta-1	22.78592	23.06558	0	0
Myosin-9	29.0714	29.03113	24.27006	23.80745
Myosin-10	24.64284	24.7601	0	0
Transgelin-2	24.20015	24.16745	0	0
T-complex protein 1 subunit zeta	24.44594	25.21022	0	0
26S protease regulatory subunit 6B	22.90575	23.28433	0	0
ATP-dependent DNA helicase Q1	24.32649	24.21156	0	0
60S ribosomal protein L5	23.95145	23.73562	0	0
Ras GTPase-activating-like protein IQGAP1	23.57635	23.89393	0	0

T-complex protein 1 subunit gamma	22.92691	23.9778	0	0
Vasodilator-stimulated phosphoprotein	22.58302	23.42944	0	0
T-complex protein 1 subunit delta	23.98163	23.89587	0	0
Ras-related protein Rab-5C	23.56848	23.43721	0	0
Coatomer subunit alpha	23.57369	23.9558	0	0
Monocarboxylate transporter 1	24.0525	24.13148	0	0
Laminin subunit beta-2	26.11973	26.16321	0	0
Histone H2B type F-S	24.29411	24.28651	0	0
Actin, cytoplasmic 2	30.17795	30.25631	29.29195	29.12263
Eukaryotic initiation factor 4A-I	25.46151	25.49314	23.05522	23.15936
40S ribosomal protein S20	23.68571	23.51196	0	0
Cell division control protein 42 homolog	23.67088	23.69954	0	0
Ras-related protein Rab-14	24.71177	24.69285	0	0
Ras-related protein Rap-1b	25.27675	25.20594	25.16242	24.7494
60S ribosomal protein L15	22.9186	22.78835	0	0
Transforming protein RhoA	20.86597	20.88762	0	0
Heterogeneous nuclear ribonucleoprotein K	23.31174	23.4789	0	0
14-3-3 protein gamma	23.70187	24.15012	0	0
40S ribosomal protein S8	23.41687	24.44297	0	0
14-3-3 protein epsilon	24.26749	24.50045	23.78945	0
40S ribosomal protein S4, X isoform	23.22747	23.14272	0	0
Histone H4	30.65523	30.71849	29.22023	29.41135
60S ribosomal protein L11	22.46107	21.99106	0	0
Peptidyl-prolyl cis-trans isomerase A	26.89053	27.02707	25.81448	26.16806
14-3-3 protein zeta/delta	25.51479	25.34432	0	0
Guanine nucleotide-binding protein subunit beta-2-like 1	24.20873	24.19069	0	0
Actin, alpha skeletal muscle	26.02711	25.64694	0	0
Putative elongation factor 1-alpha-like 3	26.88635	26.89192	26.29964	26.09834
Tubulin beta-4B chain	27.39966	27.6238	25.67128	26.27067
Histone H3.2	29.9986	29.93719	28.63291	28.4241
T-complex protein 1 subunit beta	24.37901	23.62522	0	23.03261
DNA-dependent protein kinase catalytic subunit	23.1584	22.89783	0	0
Brain acid soluble protein 1	23.72119	23.61661	0	0
Rho-related GTP-binding protein RhoG	23.33906	23.11717	0	0
Tumor necrosis factor-inducible gene 6 protein	0	0	0	0
Fibulin-2	0	0	24.87446	25.03946
Basement membrane-specific heparan sulfate proteoglycan core protein	29.19254	29.22073	29.07824	28.763
Ephrin-B1	23.19	23.26442	0	0
Adenylyl cyclase-associated protein 1	0	0	22.22973	0
Large neutral amino acids transporter small subunit 1	26.93225	26.70807	0	0

Caveolin-1	25.50609	25.62469	0	0
Fibromodulin	23.69094	23.68228	0	0
Galectin-3-binding protein	26.32095	26.27402	0	0
Neuroblast differentiation-associated protein AHNAK	21.86748	22.27002	0	0
Sequestosome-1	25.47599	25.03481	0	0
Laminin subunit beta-3	27.88361	28.06301	0	0
Laminin subunit gamma-2	28.44498	28.32989	0	0
Nuclear receptor coactivator 4	22.6051	22.64566	0	0
Desmoglein-2	24.33497	24.50561	0	0
Eukaryotic translation initiation factor 3 subunit A	22.69867	22.5354	0	0
Cytoplasmic dynein 1 heavy chain 1	22.75367	22.85308	0	0
Fibroblast growth factor-binding protein 1	24.26363	23.84019	0	0
Major vault protein	26.42824	26.47964	21.766	23.27483
Plectin	27.22748	27.68966	0	0
Non-POU domain-containing octamer-binding protein	22.58866	23.11924	0	0
Transforming growth factor-beta-induced protein ig-h3	23.53517	23.60332	0	0
Fascin	25.79558	25.00475	22.54868	0
Histone H2A type 2-C	30.93473	31.10681	29.29404	29.57322
Laminin subunit alpha-3	27.47939	27.59049	0	0
Histone H3	23.55497	23.4706	22.97701	23.17359
Golgi-associated plant pathogenesis-related protein 1	0	0	24.7902	24.55614
von Willebrand factor A domain-containing protein 1	23.63954	23.64548	0	0
Staphylococcal nuclease domain-containing protein 1	22.75185	22.87897	0	0
Cytoplasmic FMR1-interacting protein 1	22.2556	22.41227	0	0
Lipolysis-stimulated lipoprotein receptor	24.11521	24.11402	0	0
Misshapen-like kinase 1	22.585	22.83842	0	0
Retinoic acid-induced protein 3	26.63312	26.83858	0	0
Programmed cell death 6-interacting protein	27.32294	27.44829	23.25262	0
Histone H1x	22.69562	23.02692	0	0
Histone H2A type 1-C	24.53077	24.78387	25.54451	26.07672
Multivesicular body subunit 12A	23.72972	23.95465	0	0
Phosphatase and actin regulator 3	0	0	0	0
Histone H2B type 1-M	30.68937	30.66746	29.84634	29.4751
EMILIN-2	0	0	22.56769	22.62136
Protein tweety homolog 3	22.5968	22.18307	0	0
Tubulointerstitial nephritis antigen-like	25.53623	25.76946	26.30855	26.40991
Ras-related protein Rab-1B	24.75781	24.62968	0	0
EH domain-containing protein 1	23.30131	23.26399	0	23.91807
Myoferlin	25.47908	25.47568	0	0

Prostaglandin F2 receptor negative regulator	25.85875	26.16728	22.12405	0
Brain-specific angiogenesis inhibitor 1-associated protein 2-like protein 1	22.64705	22.63387	0	0
Collagen alpha-1(XVII) chain	25.41529	25.09527	0	0
Plakophilin-3	23.58474	23.8261	0	0
Talin-1	26.39226	26.17957	24.86561	24.05283
Junctional adhesion molecule A	23.96367	23.83123	0	0

Table 10.3 Log2 of label free intensity scores for proteins in EVs derived from carcinoma (H357) and metastatic deposit (B22) cells